High-field asymmetric ion mobility spectrometry (FAIMS) study for on-site monitoring of aromatic volatile organic compounds in groundwater and their degradation in the presence of ferrous iron and carbonate

Dissertation

zur Erlangung des akademischen Grades eines
Doktors der Naturwissenschaften
– Dr. rer. nat. –

vorgelegt von

Sasho Joksimoski

geboren in Skopje, R. Nordmazedonien

Fakultät für Chemie - Instrumentelle analytische Chemie
der
Universität Duisburg-Essen

2023

DOI: 10.17185/duepublico/81825
URN: urn:nbn:de:hbz:465-20240419-094156-9

Die vorliegende Arbeit wurde im Zeitraum von April 2017 bis Dezember 2021 im Arbeitskreis von PD Dr. Ursula Telgheder in der Abteilung Instrumentelle Analytische Chemie der Universität Duisburg-Essen durchgeführt.

Tag der Disputation: 05.09.2023

Gutachter: PD Dr. Ursula Telgheder
Prof. Dr. Stefanie Sielemann

Vorsitzender: Prof. Dr. Mathias Ulbricht

Acknowledgement

This thesis owes its existence to the help, support and inspiration of many people.

First and foremost, I would like to thank Prof. Dr. Torsten C. Schmidt for his kind recommendation to the IAC department at the University of Duisburg-Essen, which was the impetus for my Master and later PhD thesis.

I would like to express my deepest gratitude to my mentor, PD Dr. Ursula Telgheder, for her understanding, patience, stimulating suggestions and valuable advice, which were important for the development of this work. I am glad that I had the opportunity to work with her and to get to know her scientific, but especially her human qualities. In this respect, I would also like to thank Dr. Klaus Kerpen, whose support and guidance helped me a great deal. He was actively interested in my work and was always available to give me advice and support. I am very grateful for his time, patience, motivation, enthusiasm and the immense knowledge he shared with me.

I would also like to mention Dr. Florian Uteschil, Dr. Andriy Kuklya, Rukiyye Abis, and Robert Knirim, as well as the rest of my colleagues at IAC for their help in completing this work. A special thanks for the wonderful cooperation and help goes to our project partner, the company Fabricius Pro Terra GmbH.

My deepest gratitude goes to my family, my parents, my brother and his family, and especially to my mother- and father-in-law for their constant support and love throughout this journey.

And finally to my wonderful, supportive, loving wife without whom none of this would have even been possible.

Sasho Joksimoski
May 2023
Krefeld, Germany

Summary

Possibilities and limitations of remediation of VOC-contaminated groundwater and its analytical monitoring are the focus of this dissertation. Focal points are the development of a novel, continuous sample introduction system in combination with APPI-FAIMS for on-site monitoring of contamination, site-specific assessment analyses and introduction of a possible additional remediation step by oxygen implementation (e.g. with a permeable membrane) in iron- and carbonate-rich groundwater environments.

For this purpose, the possibility of using a low-cost, stand-alone, continuous real-time FAIMS system for on-site monitoring of groundwater was determined. The effects of high humidity and humidity variations on the signal in the analysis of aromatic VOCs were investigated for two different ion sources (APPI, APCI). To reduce the influence of humidity, a novel gas-water separation unit coupled to the FAIMS was implemented. Signal-specific values were determined from the maximum signal intensity at a given compensation voltage (CV_{max}) and a given dispersion field strength (DF) for selected aromatic VOCs, including BTEX from water. Successful calibration of the aromatic VOCs as a single analyte was performed with the gas-water separation APPI-FAIMS from spiked water samples. The limit of detection (LOD) of benzene, toluene, ethylbenzene, *o*-xylene and indane in water was 0.1, 0.9, 1.1, 0.3, 0.8 mg L^{-1} at 0% DF and 0.1, 0.9, 1, 0.4, 0.7 mg L^{-1} at 36% DF, respectively.

The effectiveness of the sample introduction system (i.e. the gas-water separation unit) and the repeatability of the APPI-FAIMS signal were confirmed by monitoring of aromatic VOCs in water/groundwater samples under laboratory conditions. Similarly, an aromatic VOCs sum-signal was used to monitor contamination intensity at a groundwater contamination site. The sum-signal was enabled due to the low humidity provided by the gas-water separation unit. This allowed effective charge transfer and minimized influence of humidity on the signal in the analysis of aromatic VOCs. The results were validated with HS-GC/MS.

The geochemical composition of the remediation site was investigated, including the iron concentration and the concentration of BTEX pollutants in the groundwater. In addition to BTEX, other groundwater pollutants such as indane were also determined.

Furthermore, a membrane-supported oxygen injection (OxyTech) was used as a non-standard remediation method and its effect on the redox conditions in the remediation well was investigated. In order to determine the short-term effects of the oxygen addition to anoxic groundwater on the contaminants, the previously described gas-water separation APPI-FAIMS method was applied for on-site aromatic VOC monitoring. The results were confirmed with HS-GC/MS. In addition, the general properties and oxygen permittivity of OxyTech (silicone) membrane were determined. Further aspects involving ferrous iron oxidation followed by subsequent, induced $^{\bullet}OH$ production and aromatic VOCs oxidation were carried out. This included the chemical potential involved in oxygenation in anoxic groundwater containing ferrous ions and carbonate/bicarbonate ions in high concentration. By using the coumarin detection method the formation of the

reactive •OH radicals during the oxidation of the iron ions was confirmed. The possible oxidation products from the aromatic volatile organic groundwater contaminants were detected and identified after liquid-liquid extraction and direct analysis by GC/MS.

Additionally, the oxidation capabilities of the system were confirmed on other water contaminants. Ibuprofen as a non-volatile organic water contaminant was also oxidized in presence of oxygen and ferrous ion in carbonate/bicarbonate rich water. In addition, the presence of one or more carboxyl groups was shown to play a special role in Fe-complex coordination and the formation of •OH radicals, as found when trisodium citrate dihydrate was used instead of sodium bicarbonate.

List of abbreviations and acronyms

APPI - atmospheric-pressure photoionization
APLI - atmospheric-pressure laser ionization
PI - photoionization
IMS - ion mobility spectrometry
FAIMS - high-field asymmetric ion mobility spectrometry
DMS - differential ion mobility spectrometry
VOC - volatile organic compound
AVOC - aromatic volatile organic compound
BTEX - benzene, toluene, ethylbenzene, xylenes
BTX - benzene, toluene, xylenes
EPA – Environmental Protection Agency
NAPL - nonaqueus phase liquids
DNAPL - dense nonaqueus phase liquids
LNAPL - light nonaqueus phase liquids
VUV - vacuum ultra violet
PA - proton affinity
GB - gas basicity
IE - ionization energy
P&T - pump-and-treat
SVE - soil vapour extraction
ISCO - *in-situ* chemical oxidation
ISCR - *in-situ* chemical hydratation
ZVI - zero-valent ion
NOM - natural organic matter
CHP - catalyzed hydrogen peroxide
MNA - monitored natural attenuation
ESI - electrospray ionisation
DF - dispersion field (%)
CV - compensation voltage (V)
CV_{max} - analyte specific CV where maximum of the intensity signal/peak is detected (V)
CV N^{-1} - reduced field strength calculated from CV (Td)
CV_{max} N^{-1}- analyte specific CV N^{-1} where maximum intensity of the signal/peak is detected (Td)
E/N - normalized field intensity
E/N_c - critical E/N (above this value K_0 notably depends on E/N)
CF - compensation field, or CV N^{-1} (Td)
Td - Townsend (unit of the reduced electric field)
$\Delta_r H°$ - standard enthalpy of reaction
FWHM - full width at half maximum (of the peak)
PTFE - polytetrafluoroethylene

LOD - limit of detection
TOC - total organic carbon
NPOC - non purgeable organic carbon
TC - total carbon
IC - total inorganic carbon
AAS - atomic absorption spectroscopy
ICP OES - inductively coupled plasma optical emission spectroscopy
DO - dissolved oxygen
SATP - standard ambient temperature and pressure
barg – unit of gauge (relative) pressure
TIC - total ion chromatogram
k - Reaction rate constant
7-HO-COU - 7-hydroxycoumarin (Umbelliferone)
COU - Coumarin
K_{sp} - solubility product constant
MTBE - Methyl tertiary butyl ether
PIPES - 1,4-Piperazinebis (ethanesulphonic acid)
I - ionic strength (molarity based)
K_a - dissociation constant of an acid
pK_a - negative (base 10) logarithm of K_a
log*K* - stability constant of complexes
EDTA - Ethylenediaminetetraacetic acid
HPLC - High performance liquid chromatography
ESI - Electrospray ionization
AOP - advanced oxidizing process
CVOCs - chlorinated volatile organic compounds
VP - vapour pressure
DTPA - Diethylenetriamine penta acetate
bpy - 2,2'-bipyridine
L - ligand
Δ_o - crystal field splitting power

Table of contents

1. General introduction

Groundwater is often and widely used as the primary source of drinking water, data in literature suggests half of the world's population uses groundwater as their primary drinking source. This is only in addition to irrigation purposes in agriculture, which makes groundwater essential part of the water cycle and of importance for the water economy. The total estimated percentage of groundwater is 97 to 99% of the total freshwater volume, including the global volume of freshwater in lakes, not considering the glaciers and polar caps. [1,2] This data serves more to point out the awareness of groundwater importance, and its value as a hidden asset. Fortunately, unlike other resources, groundwater is renewable and subjected to dynamic changes originating from the water cycle. [2] Precipitation is the main recharging mechanism, complemented by natural infiltration by surface water or artificial recharge. [3] Yet this does not mean that groundwater is not subject to overuse thereby causing drying of streams, lakes and wetlands. Groundwater quality is affected by many factors and one of them is the degree of confinement of the groundwater reservoirs (aquifers) (Fig. 1). Contamination from surface sources can be related to the degree of aquifer confinement. Non-confined aquifers are usually in direct contact with the vadose zone

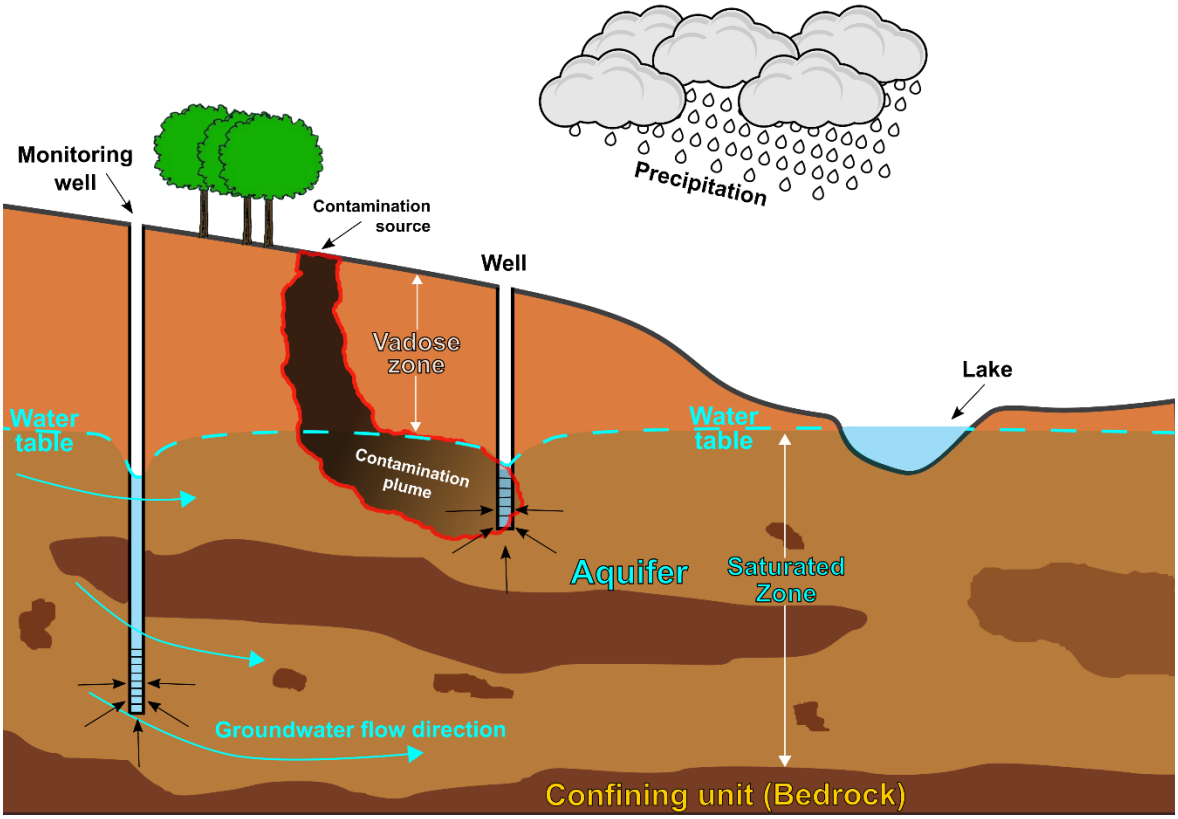

Fig. 1: Groundwater contamination from a surface contamination source of an unconfiant and semiconfiant aquifer.

and they form the water table which can change depending on the recharging amount and frequency. Non-confined aquifers are more easily susceptible to contamination than the confined ones. In comparison, semi-confined or confined aquifers are surrounded by rocks with lower permeability (e.g., volcanic rocks) or other confining materials such as clay, and generally have much lower concentrations of contaminants. [4,5]

Large-scale groundwater pumping is responsible for the emergence of arsenic, radium, salts and other naturally occurring contaminants due to increased well-drilling. Hydrogeological conditions can be a large part of naturally occurring contaminants like α- and β-particle radioactivity, increased presence of uranium, strontium, manganese, fluoride, arsenic etc. Contamination originating from anthropogenic sources can encompass surface runoffs, spills, sewage treatment plants, or underground storage tank leakages involving variety of compounds including fertilizers (nitrate), pesticides, herbicides, solvents, gasoline hydrocarbons including oxygenates and other volatile organic compounds (VOCs), even coliform bacteria. [5]

Monoaromatic gasoline constituents like benzene, ethylbenzene, toluene and xylenes (BTEX) are responsible for as much as 98% of all dissolved gasoline compounds that reach groundwater reservoirs making them "fingerprint" gasoline contaminants. [6] Older studies from EPA (Environmental Protection Agency) show toluene as the third most frequent VOC and fourth overall organic contaminant of drinking water wells in the USA. [4] Nevertheless, BTEX still remain a health hazard [7] despite the targeted decreasing of fossil fuel use in the future. The heavy reliance on benzene, toluene, xylenes (BTX) as raw materials in the industry, contribute to estimated production of more than 367 million metric tons in 2020. [8] This leads to increased possibility of leakages from the industry which we have encountered in our case. A great variety of techniques can be selected for efficient remediation of aromatic VOC contamination targeting both the unsaturated (vadose) and the saturated zone of the subsurface. In addition, contamination monitoring is a necessary step and plays an important part in estimating remediation efficiency and tracking of the contamination plumes given the recharging capabilities of groundwater. Groundwater movement, together with other characteristics of subsurface materials influences the spatial distribution of the contaminant greatly. Due to the hydraulic gradient, the different pore size and pore interconnectivity wide range of groundwater velocities are detected, from centimeters to tens of meters per day. [9] Field-deployable detection systems are therefore particularly practical for monitoring contaminants such as BTEX and provide the ability to monitor remediation progress over time. High-field asymmetric ion mobility spectrometry (FAIMS), i.e. differential ion mobility spectrometry (DMS), was first used by Eiceman et.al (2000) [10] for monitoring VOCs in the atmosphere. Screenings of groundwater contaminated with BTEX have mostly been performed using ion mobility spectrometry (IMS) after implementing an additional water separation step. [11]

The possibility of implementation of a continuous, improved gas-water separation system with APP-ionization in combination with stand-alone FAIMS system for detection of groundwater contamination from aromatic VOCs (mainly BTEX) was addressed.

An improved membrane oxygen inlet system (OxyTech) was characterised and utilized as an additional remediation step, moreover the chemical side from the possible effects of oxygen on the aromatic VOC contaminants was investigated and presented.

1.1. Aromatic volatile organic compounds as groundwater contaminants

Groundwater contamination with organic compounds, in general, involves dissolution of the contaminants into water i.e. into the aqueous phase. Dissolution can occur either from contamination liquids or residuals in the vadose zone or from the non-aqueous phase liquids (NAPL) in the saturated zone. NAPL is a term implying formation of a two phase system between the hydrocarbon liquid and the groundwater responsible for controlled, extended, dissolution of the hydrocarbons. It is different for

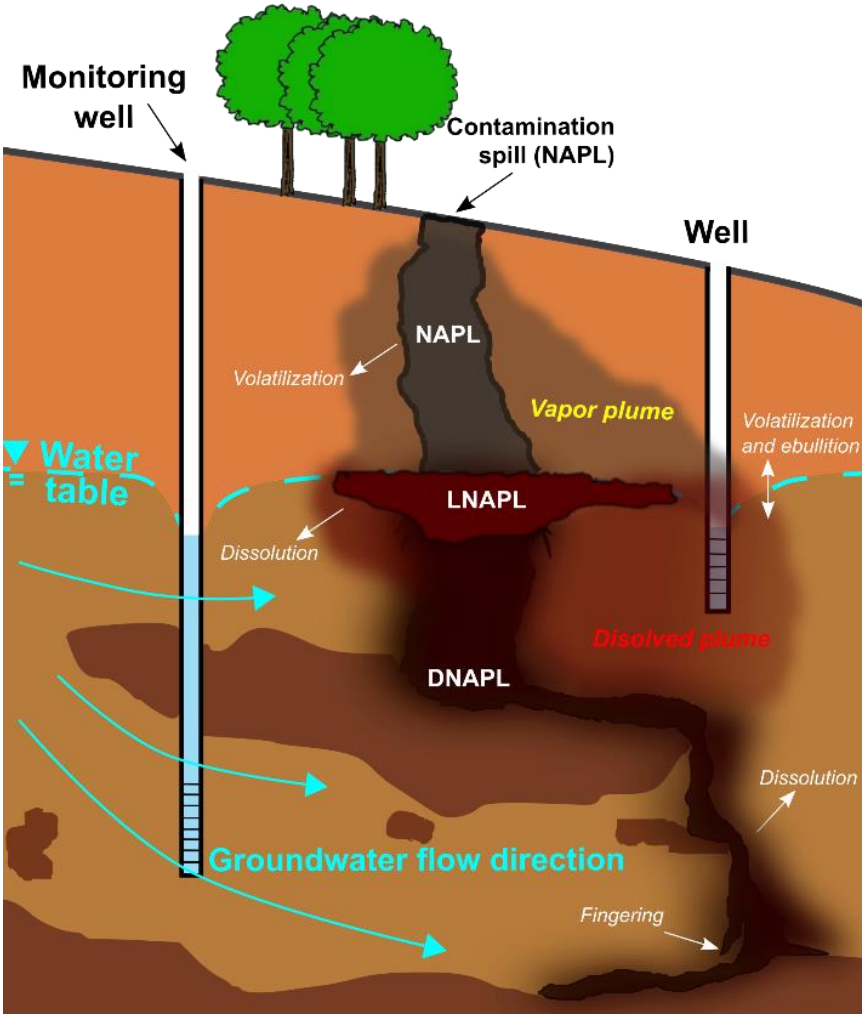

Fig. 2: Movement of LNAPL (BTEX) and DNAPL and subsequent development of vapor and dissolved organic plumes in the aquifer, modified from [12].

different organic contaminants and it can influence the retardation of a contamination to a great extent. NAPL are typically divided into two general categories, dense (DNAPL) and light (LNAPL). Dense nonaqueous phase liquids DNAPL have higher density relative to water. The density difference accounts for different types of movement through the subsurface compared to NAPLs (Fig. 2). [5]
Aromatic VOCs like BTEX (benzene, toluene, ethylbenzene, xylenes) and TMBs (trimethylbenzenes), which are the focus of this work, are classified as LNAPL considering their density is less than the density of water (Tab. 1). [9]

Tab. 1: Physical properties of the aromatic volatile organic compounds of interest.

Compound	**CAS No.**	**Mol. Weight**	**Density** [a]	**Henry's const.** [b]	**Solubility** [c]	**log K_{ow}** [d]
		g/mol	**g/cm^3**	**mol/(m^3 Pa)**	**g/kg H_2O**	**-**
Benzene	71-43-2	78	0.873	0.0018	1.77	2.13
Toluene	108-88-3	92	0.865	0.0015	0.519	2.73
Ethylbenzene	100-41-4	106	0.865	0.0011	0.161	3.15
***o*-Xylene**	95-47-6	106	0.876	0.0018	0.171	3.12
***m*-Xylene**	108-38-3	106	0.861	0.0014	0.161	3.2
***p*-Xylene**	106-42-3	106	0.858	0.0017	0.181	3.15
1,2,3-TMB	526-73-8	120	0.891	0.0029	0.07	3.6
1,2,4-TMB	95-63-6	120	0.872	0.0018	0.057	3.63
1,3,5-TMB	108-67-8	120	0.861	0.0013	0.05	3.42
Indane	496-11-7	118	0.96	4.30E-03	0.1	3.33

[a]- density at 25 °C [13]
[b] - calculated Henry constants at 25 °C [14] as cited in [15]
[c] - solubility in water at 25 °C (benzene 20 °C) [16] as cited in [17] and indane [16] as cited in [18]
[d] - log $K_{o/w}$ - octanol / water partition coefficient at 25 °C [16]

Due to their low water solubility Henry's law can be used to describe partitioning between liquid phase (water) and gas phase (air). It is obvious, gas phase or air would be more preferred to groundwater, considering the Tab. 1 and the determined Henry constant and solubility values for BTEX, TMB and indane. The inclination of the analytes for the gas phase makes them suitable for gas phase analyses. Gas chromatography separation in combination with different detectors is used as a standardized detection procedure. The favourable analysis of VOCs in the gas phase allowed for stand-alone IMS based detection [19] and possible considerations for *in-situ* VOCs monitoring in the vadose zone. [20]

1.2. The persistent problem of groundwater pollution and application of standard remediation techniques

There are a variety of successful remediation clean-up techniques for contaminated groundwater and soil. Appropriate assessment should be taken into consideration including factors such as local climatic conditions, site hydrogeology and most importantly, the properties of the involved contaminants including their interaction with the geological media. This usually requires a site-specific solution or combination of solutions to be applied since very seldom two contamination sites can be considered fairly identical. [9]
Generally, groundwater remediation technologies are divided into three main groups involving physical, chemical and biological treatments (Tab. 2).

Tab. 2: Established soil and groundwater remediation treatments [9].

Physical treatment	Chemical treatment	Biological treatment
- Free product recovery - Pump-and-treat - Soil vapor extraction - Air sparging - Groundwater circulation wells - Multiphase extraction - Induced fracturing - Soil heating	- Precipitation - Chemical oxidation and reduction - Permeable reactive barriers - Stabilization/solidification - Adsorption and ion exchange - Electrochemical processes - Chemical leaching and solvent extraction - Soil flushing	- Biosparging - Bioventing - Biostimulation - Bioaugmentation - Anaerobic biotransformation - Aerobic biotransformation - Biological fixation - Monitored natural attenuation

Despite groundwater treatment, in cases such as BTEX contamination, if the source of contamination is from the surface (Fig. 1) or the vadose zone, simultaneous treatment of the soil is also performed.

In continuation some remediation techniques relevant for treating of LNAPL i.e. BTEX are addressed.

1.2.1. Physical treatments of groundwater contamination

Since the beginning of the initial remediation treatments in the 1970s, physical treatments had the main role in cleaning up groundwater or soil contaminations. To this day, treatments like soil excavation, groundwater pump-and-treat method (P&T) or soil vapour extraction (SVE) are heavily favourable in comparison to other new and innovative technologies. [21]

Pump-and-treat (P&T) systems are the most used in active remediation treatment of groundwater contaminations in general. It is used as a stand-alone or in combination with other complementary technologies. The contaminated groundwater is extracted from the ground and treated on the surface to finally be discharged or re-injected into the groundwater. If a strategic and carefully designed capture zone of remediation wells is arranged, high efficiency removal of the migrating contaminants with P&T is possible. The disadvantages of P&T arise as the contaminant concentrations get lower. Then the removal efficiency also drops and long expensive remediation periods are required due to the phenomena of slow concentration tailing. The reason often lies in the mass-transfer limitations of the contaminant in aquifer (e.g. contaminant solubility, partitioning). Upon extraction of the groundwater different physical, chemical or biological treatments can be used. Adsorption, volatilization, stripping or variety of other techniques are used in the case of BTEX contamination. [9,22]

Soil vapour extraction (SVE) is an established physical remediation treatment with a lot of success for LNAPL contaminants like BTEX. In comparison to P&T the contaminants here are extracted from the unsaturated zone (i.e., soil). It is used *in situ* and it represents a vacuum extraction technology. The vapour pressure or the Henry's law constant of the contaminants have an important role in this case which makes it suitable for BTEX. [9] Apart from the contaminant properties, the efficiency of SVE can be affected by several factors including operating conditions like soil temperature, airflow rate (best results by increased soil permeability > 10^{-10} cm^2) and soil properties like the amount of water and natural organic matter in the vadose zone. These conditions influence the efficiency and its radius of influence (ROI). [23] SVE is usually combined with other remediation technologies for the saturated zone and it is cost-effective, but contaminants removal > 90% is hard to achieve. [9]

1.2.2. Chemical treatments of groundwater contamination

The goal in using chemical remediation techniques is to oxidize or reduce groundwater contaminants to fewer toxic components/pollutants. Oxidizing agents like potassium and sodium permanganate ($KMnO_4$, $NaMnO_4$), sodium persulfate (NaS_2O_8), ozone (O_3), hydrogen peroxide (H_2O_2) are applied for *in-situ* chemical oxidation (ISCO) as already established and widespread technique. *In-situ* chemical reduction (ISCR), on the other hand, is applied in specific cases (e.g. dehalogenation of chlorinated or brominated organics), involving reducing agents like zero-valent iron (ZVI). [9,24]

Given the broader range of ISCO applications and their suitability for BTEX as our groundwater contaminants, an overview of *in-situ* chemical oxidation processes and oxidants is provided. Careful consideration should be given to specific site conditions and oxidant properties prior to any ISCO application.

Permanganate (MnO_4^-) is a selective oxidant, having strong oxidation power (Tab. 3) with relatively simple reaction chemistry, implemented in the form of $KMnO_4$ and $NaMnO_4$. Organic contaminants are directly oxidized through electron transfer in comparison to other oxidants like H_2O_2 where activation and formation of radical intermediates is crucial for an enhanced oxidizing efficiency. MnO_4^- is highly reactive towards alkene and double bonds in comparison to saturated hydrocarbons. It is also relatively insensitive to pH changes. The permanganate oxidation reactions follow second order kinetics with reference to the contaminant and permanganate concentration. Permanganate is a good oxidizer for all BTEX compounds except for benzene. [24]

Tab. 3: Reactive species and standard reduction potential from [24], as cited in [25].

Reactive species	**Formula**	**Standard reduction potential (V)**
Hydroxyl radical	$^{\bullet}OH$	2.8
Sulfate radical	$SO_4^{\bullet-}$	2.6
Ozone	O_3	2.1
Persulfate anion	$S_2O_8^{2-}$	2.1
Hydrogen peroxide	H_2O_2	1.77
Permanganate anion	MnO_4^-	1.7
Perhydroxyl radical	$HO_2^{\bullet}$	1.23
Oxygen	O_2	1.23
Hydroperoxide anion	HO_2^-	-0.88
Superoxide radical	$O_2^{\bullet-}$	-2.4

Ozone (O_3) represents short-lived, strong oxidant which could be applied to the vadose and/or saturated zone independently for both gas phase and aqueous phase reactions. Similarly to hydrogen peroxide it can react with organic contaminants by direct oxidation and/or by activation (eq. 1 and eq. 2 respectively). Many reactive species are produced with the ‘‘activation’’ of ozone, but mostly are formed as hydroxyl ($^{\bullet}OH$) or hydroperoxide ($HO_2^{\bullet}$) radicals (eq. 2). [26]
Carbonate (CO_3^{2-}), bicarbonate (HCO_3^-), sulphate (SO_4^{2-}) and chloride (Cl^-) anions can also react with $^{\bullet}OH$ thus lowering the efficiency (scavenging) by producing intermediates including radicals and even react with aromatic contaminants as presented by Umschlag and Herrmann (1999). [27]

$$O_3 \rightarrow \underset{(slow)}{Direct\ selective\ oxidation} \rightarrow Products \qquad \text{eq. 1}$$

$$\underset{Ozone\ decomposition}{O_3 + OH^-} \rightarrow \underset{other\ reactive\ species}{\begin{matrix} HO^{\bullet} \\ HO_2^{\bullet} \end{matrix}} \rightarrow Products \qquad \text{eq. 2}$$

Ozone generally is a better oxidant than permanganate and can be used to transform or mineralize wide variety of organic contaminants including BTEX as well as support aerobic biodegradation after its decomposition to O_2. BTEX are slowly oxidized by direct reaction with ozone, but with the addition of activator like H_2O_2 and pH increase the degradation is rapidly accelerated. One of the major disadvantages of using ozone, as with other oxidants, is the oxidant requirement, i.e. the influence on the natural organic matter (NOM) content and the hydrogeological and geochemical properties of the aquifer. This can limit the stability and transport of ozone in the subsurface. In addition, ozone must be electrically generated on-site by electrical discharges in air or oxygen atmosphere and immediately introduced into the dedicated remediation site. This complicates its *in-situ* use due to the power supply dependence. [24]

Hydrogen peroxide (H_2O_2) represents a weak reductant and a strong oxidant slightly more powerful than chlorine but less than ozone (Tab. 3).

In order to increase its oxidizing ability hydroxyl radicals ($^{\bullet}OH$) are produced by H_2O_2 catalyzation processes in water. In this way H_2O_2 is able to produce a variety of other radicals/reactive species capable of oxidizing organic chemicals like BTEX (e.g., $O_2^{\bullet-}$, $HO_2^{\bullet}$, $O_2^{\bullet-}$, HO_2). Catalyzation processes, i.e., H_2O_2 activation processes, can occur via UV irradiation, ultrasound and metal catalysis and are referred as catalyzed hydrogen peroxide systems (CHP). Nevertheless, hydrogen peroxide can also oxidize many organic compounds directly. The direct H_2O_2 oxidation of organic compounds is considered to be slow and negligible in comparison to the activated i.e. the catalyzed one. [28]

The activation of H_2O_2 via Fe^{2+} and production of hydroxyl radicals is known as the Fenton reaction or Fenton's reagent [29] (eq. 3). Especially powerful contaminant oxidation happens at slightly acidic conditions pH 3 - 5 where ''Fenton's Chemistry'' occurs. [24]

$$Fe^{2+} + H_2O_2 \rightarrow Fe^{3+} + OH^- + HO^{\bullet} \qquad \text{eq. 3}$$

The pH is critical for radical production and reactivity, as deprotonation affects reaction pathways and standard reduction potential, reducing thermodynamic feasibility. [24]

The fate and reactions of hydrogen peroxide are particularly complex in *in situ* applications compared to eq. 3. CHP can roughly be categorized in initiation and free radical chain reactions; propagation and termination steps; radical scavenging; oxidation of organic contaminants; and competitive and non-productive reactions. [24]

$^{\bullet}OH$ radicals can be also produced by absorbance of UV radiation with an absorbance maximum at 220 nm (eq. 4), as an alternative to the previous Fe^{2+} activation or in combinations of more catalysts e.g. O_3, H_2O_2 and UV radiation. [9]

$$H_2O_2 + hv \rightarrow 2\,HO^{\bullet} \qquad \text{eq. 4}$$

The reaction efficiency could be also influenced from inorganic ions previously mentioned (carbonate, bicarbonate, chloride) or even hydrogen peroxide itself. [24]

1.2.3. Biological treatment of groundwater contamination

Biodegradation at groundwater contamination sites involves microbial/enzymatic reactions that result in transformation of toxic chemicals which are highly dependent on factors such as temperature, nutrients, and oxygen availability. The presence of multiple components of an NAPL contamination mixture can affect biodegradation or remediation of BTEX. For instance, biodegradation of benzene may be inhibited by toluene or other BTEX compounds of a NAPL mixture, similarly the

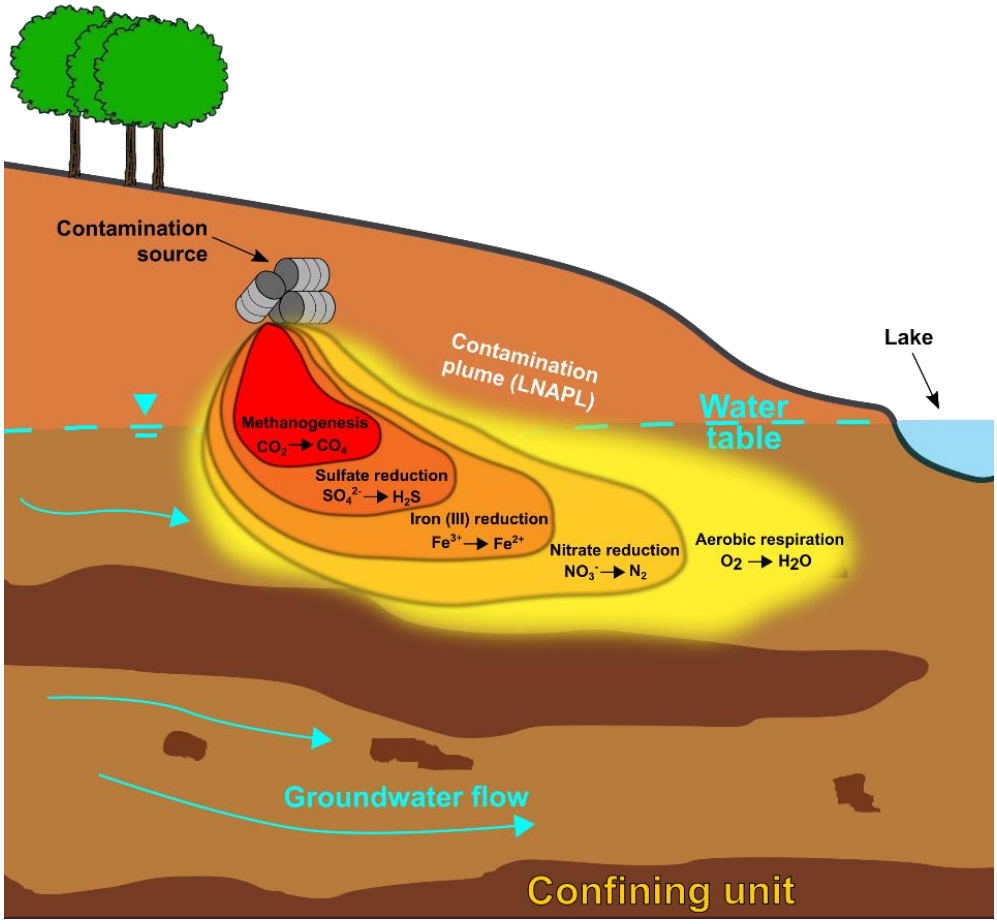

Fig. 3: Simplified development of different electron accepting conditions in a dissolved LNAPL contaminant plume from an underground contamination source.

sorption of benzene in the soil may be reduced by the sorption of toluene (competition mechanism). [5]

Microorganisms are included in the remediation of groundwater NAPL contamination intrinsically through processes such as aerobic respiration, denitrification, iron or manganese reduction, sulphate reduction and methanogenesis as shown in Fig. 3. [30]

Fig. 3 shows the order of main electron acceptors in a developed contamination plume. The conditions usually vary from highly aerobic, on the periphery of the plume, to anaerobic or oxygen depleted areas, thereby following the microbial preference according to the electron acceptor tower theory $O_2 > NO_3^- > Fe_3^+ > SO_4^{2-} > CO_2$. Accordingly, aerobic and anaerobic microorganisms would be preferred depending on the conditions, unless facultative cultures (mostly microbes utilizing NO_3^-) are present. Formation of different redox-influence-zones occur in underground areas where more thermodynamically favoured electron acceptors are not present or depleted, thereby allowing emergence of other microorganisms and less favourable redox conditions.

Oxygen, as the most thermodynamically favourable electron acceptor, provides the greatest energy gain for aerobic microorganisms (Tab. 4). In the specific case of aromatic hydrocarbons like BTEX the Krebs' cycle is accepted as a final metabolic destination with catechols (pyrocatechol) [31], protocatechuate or benzoate as usual converging products on the path of the aerobic degradation. [9] Successful anaerobic degradation of LNAPL or BTEX, has been already demonstrated in the form of nitrate respiration, sulfate reduction, methanogenic fermentation [5], as well as iron (III) reduction. [32] The presumed anaerobic degradation pathway of the BTEX converges to Benzoyl-CoA [33] and it is much slower compared to oxygen as an electron acceptor (aerobic degradation).

Therefore, support of the biodegradation processes is considered and utilized in some cases. [5,34]

The biological remediation or bioremediation is divided into *in-situ* and *ex-situ* biological treatments. Bioventing, biosparging, biostimulation and bioaugmentation are some of the *in-situ* biological treatments usually applied, of course, with monitored natural attenuation as the most prominent of all.

Monitored natural attenuation, or MNA, is also referred to as intrinsic bioremediation and relies on naturally occurring physical/chemical processes and microbial biodegradation, thereby controlling the migration of the contaminant, which requires permanent active monitoring. The advantages of MNA as a remediation method include low overall cost and waste generation, and the ability to avoid additional intrusive methods. Disadvantages could be the long remediation time, the need for long-term monitoring, and the further spread of the contaminant plume. [5]

Ex-situ bioremediation encompasses techniques like biopharming, composting, biopiles, slurry-phase bioreactors for treatment of contaminant soil which involve transfer or excavation of pollutants from the site for an away treatment. [5]

1.3. Analysis of contamination sites and remediation monitoring

1.3.1. Standard analytical techniques

Standardized, laboratory-based methods involve time-demanding, mistake prone, groundwater sampling procedures, conservation, transport and storage of samples. Subsequently, a standardized method, possibly HS-GC/MS is used for determination and quantification of benzene and derivatives in water. [35] Other methods e.g. liquid-liquid extraction GC/MS and HS-SPME-GC/MS can be also applied. [36–38] The use of GC in combination with flame ionization detector (FID) as an alternative should be also mentioned.

Monitoring of groundwater remediation requires increased sampling frequency and it can be time-consuming and rather costly.

The use of ion mobility-based systems such as FAIMS to detect and monitor volatile organic compounds (VOCs) in water could provide more reliable monitoring results for contaminated sites due to real-time measurements and reduced sample manipulation, or reduce costs by reducing the frequency of standard sampling procedures required.

Tab. 4: Preferred microbial terminal electron acceptors and the reduced counterpart.

	Terminal electron acceptor	**Reduced counterpart**	**Redox reaction[a]**	**ΔG[a] kJ/mol**
Aerobic respiration	Oxygen (O_2)	Carbon dioxide (CO_2)	$\frac{1}{4}O_2 + H^+ + e^- \rightarrow \frac{1}{2}H_2O$	-220.9
Nitrate reduction	Nitrate (NO_3^-)	Ammonium (NH_4^+) Nitrogen (N_2) Nitrous oxide (N_2O)	$\frac{1}{5}NO_3^- + \frac{6}{5}H^+ + e^- \rightarrow \frac{1}{10}N_2 + \frac{3}{5}H_2O$	-210
Iron reduction	Ferric iron (Fe^{3+})	Ferrous iron (Fe_2^+)	$Fe^{3+} + e^- \rightarrow Fe^{2+}$	-100
Sulphate reduction	Sulphate (SO_4^-)	Bisulfide (HS^-)	$\frac{1}{8}SO_4^{2-} + \frac{19}{16}H^+ + e^- \rightarrow \frac{1}{16}H_2S + \frac{1}{16}HS^- \frac{1}{2}H_2O$	-20
Methanogenesis	Carbon dioxide (CO_2)	Methane (CH_4)	$\frac{1}{8}CO_2 + H^+ + e^- \rightarrow \frac{1}{8}CH_4 + \frac{1}{4}H_2O$	-15

[a] – from [5]

1.3.2. IMS based techniques

Compared to the previously mentioned gas phase separation methods and MS detectors, the IMS-based systems combine separation and detection in one, resulting in specific advantages and disadvantages.

IMS systems are portable, small in size, relatively inexpensive, can be used under ambient pressure, are fast-responding, and are very sensitive, so they can be used in locations where a continuous monitoring system is needed. Nevertheless, there are several difficulties related to selectivity and signal complexity (e.g. when using radioactive ionizing sources), and most importantly, the relatively low resolving power compared to other separation techniques, such as gas chromatography. Complex gas-phase reactions due to carrier gas inconsistencies (e.g. impurities) such as the presence of water (humidity) can significantly alter the results. [39]

1.3.2.1. Terms and principles of ion mobility spectrometry techniques

All detection systems based on ion mobility spectrometry, in their simplest form are divided in three successive main parts. Ionization part, where ionization of the analytes in the carrier gas is performed, separation part and detection part. The differences between IMS and FAIMS are mainly differences in the separation part.

1.3.2.1.1. Ion separation in IMS

In IMS, ions are separated by shape and charge, according to their ion mobility (K), at ambient pressure with relatively low electric fields of 100 to 300 V cm^{-1}. [40,41] Characterization of chemical substances is based on the velocity of their gas-phase ions in the drift region on a millisecond scale. [40,41]

The drift region is representing the distance from the injection region i.e. the ion gate (shutter) to the detector plate, and it is the part where the ion-swarm-separation occurs. The velocities (V_d) of different ion-swarms through the drift region are proportional to the strength of the electric field gradient ($V_d = f(E)$) as shown in Fig. 4 and described by eq. 5. [41]

The ion mobility coefficient (K) can be seen as a proportionality coefficient between the drift velocity (V_d) and the electrical field gradient (E) under certain IMS conditions for different kinds of ions, thus acting as an ion characteristic parameter.

This characteristic parameter is responsible for the separation of the different ion swarms by mass, shape and charge in the drift region. This is confirmed by the fact that ions with different functional groups or geometrical arrangements but with the same molecular mass have different K values as witnessed by isomer separation. [41]

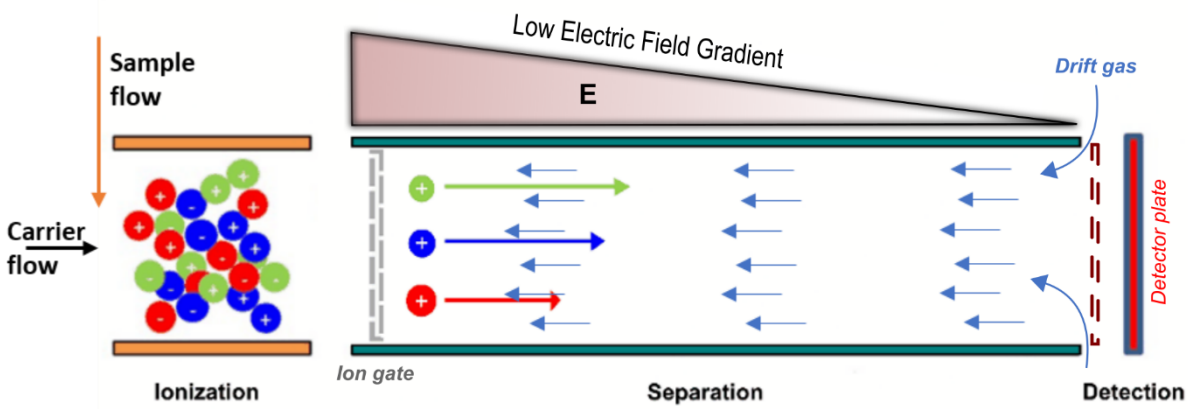

Fig. 4: Basic scheme of a drift time ion mobility spectrometer (DT IMS) showing the three main areas of ionization, separation and detection.

$$V_d = K\,E \qquad \left[\frac{cm}{s}\right] \qquad \text{eq. 5}$$

$$K = \frac{V_d}{E} \qquad \left[\frac{cm^2}{V\,s}\right] \qquad \text{eq. 6}$$

Where:
K - ion mobility coefficient ($cm^2\ V^{-1}\ s^{-1}$);
E - voltage gradient i.e. electric field gradient ($V\ cm^{-1}$);
V_d - drift velocity of ion/ ion swarm ($cm\ s^{-1}$).

Other operating conditions (e.g. moisture, temperature, pressure, unwanted neutral molecules) can greatly influence the K value and should always be closely observed. Cluster formation between the ions and the neutrals present in the carrier gas contribute to different mobilities for the same ion, as does the polarity of the drift gas. [42] By controlling the operating parameters, models can be constructed for the mobility coefficient as a function of the properties of the ion, eq. 7 describes one of these models, where *e* is the charge of an electron; N is the number density of neutral-gas molecules at the pressure of measurement; α is the correction factor; μ is the reduced mass of the ion-neutral collision pair defined as mM/(m+M); k is the Boltzmann constant; T_{eff} is the effective temperature of the ion determined by the thermal energy and the energy acquired in the electric field; and Ω is the effective collision cross-section of the ion in the supporting atmosphere. [41]

$$K = \frac{3e\,(1+\,\alpha)\,\sqrt{2\pi}}{16N\,\sqrt{\mu k T_{eff}}}\,\frac{1}{\Omega\,(T_{eff})} \qquad \text{eq. 7}$$

Calculated mobility coefficients are normalized to temperature of 273.15 K (Kelvin) and pressure of 760 Torr (i.e. STP - standard temperature and pressure) for better comparability of data at different N (eq. 8). The so-called reduced ion mobility (K_0) can alternatively be calculated using the Loschmidt number ($N_0 = 2.687 \cdot 10^{25}$ m^3) at STP. [43]

$$K_0 = K\,\frac{273.15}{T}\,\frac{P}{760} = K\left(\frac{N}{N_0}\right) \qquad \text{eq. 8}$$

1.3.2.1.2. Ion separation in DMS and FAIMS

Field asymmetric ion mobility spectrometry (FAIMS) and differential ion mobility spectrometry (DMS) differ from conventional ion mobility spectrometry (IMS) by affecting the transport properties of the ions through implementation of time dependent high and low electric fields in the separation part.

The ion mobility coefficient (K) in DMS and FAIMS experiences high (> 1000 V/cm) and low electric field conditions i.e. E_{max} and E_{min} respectively and changes accordingly (Fig. 5). [44] This causes significant net ion trajectory differences due to multiple, successive, asymmetric periods (eq. 9).

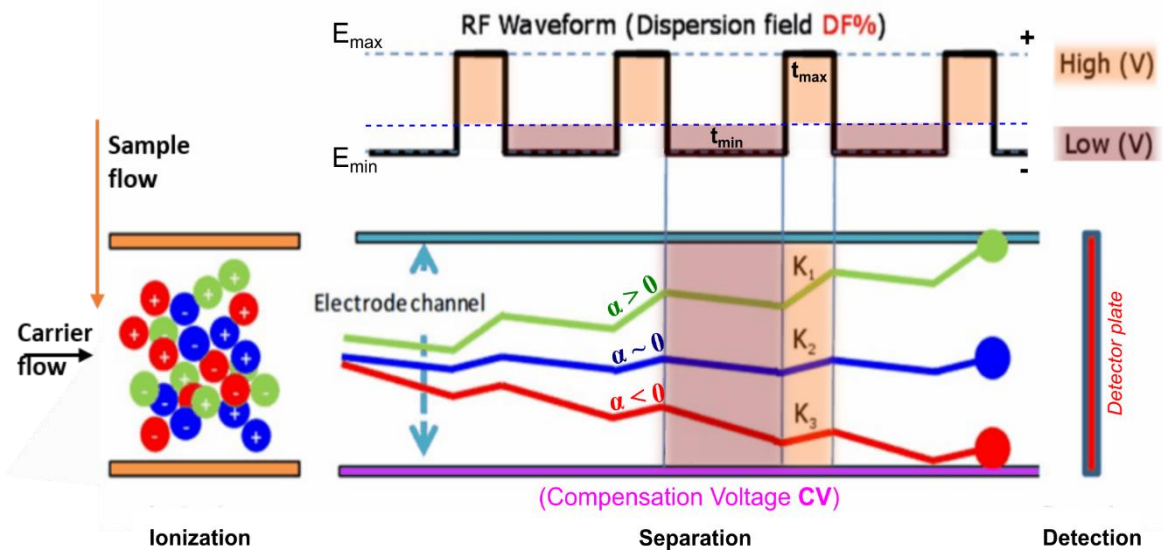

Fig. 5: Basic scheme of a high-field asymmetric ion mobility spectroscopy.

In this way, different ions with similar mobility coefficients at low electric fields can be resolved and separated based on their different behaviour at high electric fields. [41]

$$K(E) = K_0 \left[1 + \alpha \left(\frac{E}{N}\right)^2 + \alpha \left(\frac{E}{N}\right)^4 + \cdots\right] \quad \text{eq. 9}$$

$$K(E) = K_0 \left(1 + \alpha(E)\right) \quad \text{eq. 10}$$

Equations eq. 9 and eq. 10 represent this change of K in FAIMS/DMS for higher E/N (electric field to gas density ratio), K_0 is the reduced mobility of the ion in weak electric field and α is the coefficient of expansion independent from E/N. [45] The relative variation of K_0 depending on E/N is represented by the alpha function (Fig. 6). [43] The coefficient K has non-linear dependence in high electric fields and it can be considered to be ion specific.

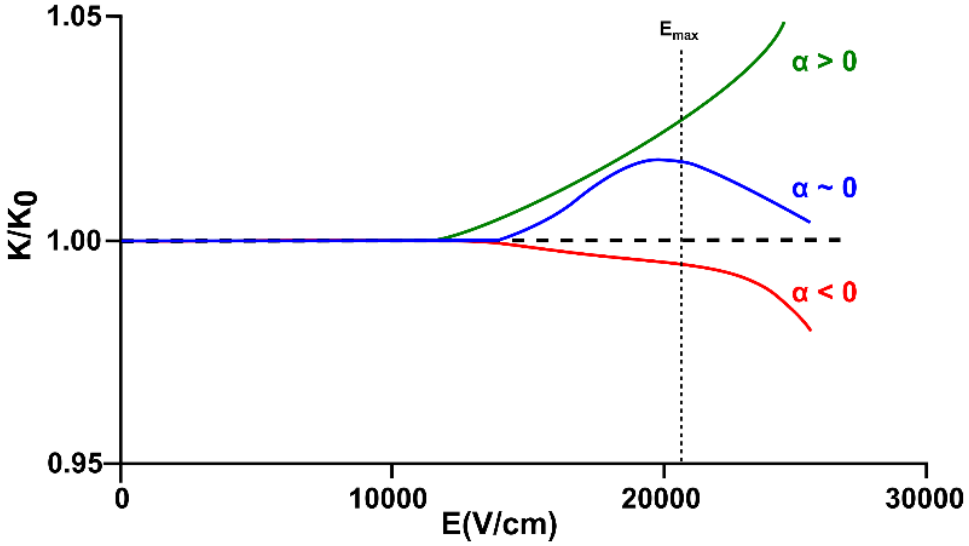

Fig. 6: Relation between ion mobility and the electric field intensity; adopted from [45].

According to eq. 10 when α(E) > 0, K increases with the increasing field strength (E), when α(E) ≈ 0 the mobility K does not appear to change with the increasing of E, and for α(E) < 0 the K has a decreasing trend with increasing of field strength. [45,46] The dependency is shown in Fig. 6.

This behaviour of K under higher electric fields contributed to the establishment of three major ion types. Type A (green) ions increase their mobility with increasing field strength. Type B (blue) ions initially increase mobility proportionally with field strength followed by decreasing after certain E_{max}, where Type C ions (red) show a decrease in ion mobility with increasing field strength. [46] Taking into account eq. 7, the behaviour of ions under such high-energy fields can be explained as follows:

In the case where $\alpha(E) < 0$, it is assumed that the ion collision cross-section (Ω) do not change significantly for rigid-sphere interactions and therefore with increasing of the effective temperature (T_{eff}) or energy (E) the K value will decrease. Meaning, with increasing E, ions will increase the colliding frequency with neutral molecules, thus contributing to decreased K (E) i.e. decreased drift velocity (V_d). [45]

On the other hand, for $\alpha(E) > 0$ the mechanism of clustering and de-clustering of ions is proposed (Fig. 7). During high energy parts of the cycle (Fig. 5), ions are de-clustered from other polar molecules due to increase of kinetic and effective temperature (T_{eff}). This is adding to the decrease of Ω which is overcoming the increase of the effective temperature. In this way, according to eq. 7 the increase of K with the increase of E is achieved. [45,46]

In the case when $\alpha(E) \approx 0$ the same mechanism of clustering and declustering of ions with polar neutral molecules is adopted. But in this case the change of Ω and T_{eff} in eq. 7 does not produce any net difference, thus the K appear not to change significantly with increasing electric field (Fig. 5 - blue ion trajectory). [45,46] Other mechanisms like elastic polarization ion interaction, resonant charge transfer and change in shape due to RF field and effective temperature were also proposed to describe the behaviour of ions under high electrical fields. [47]

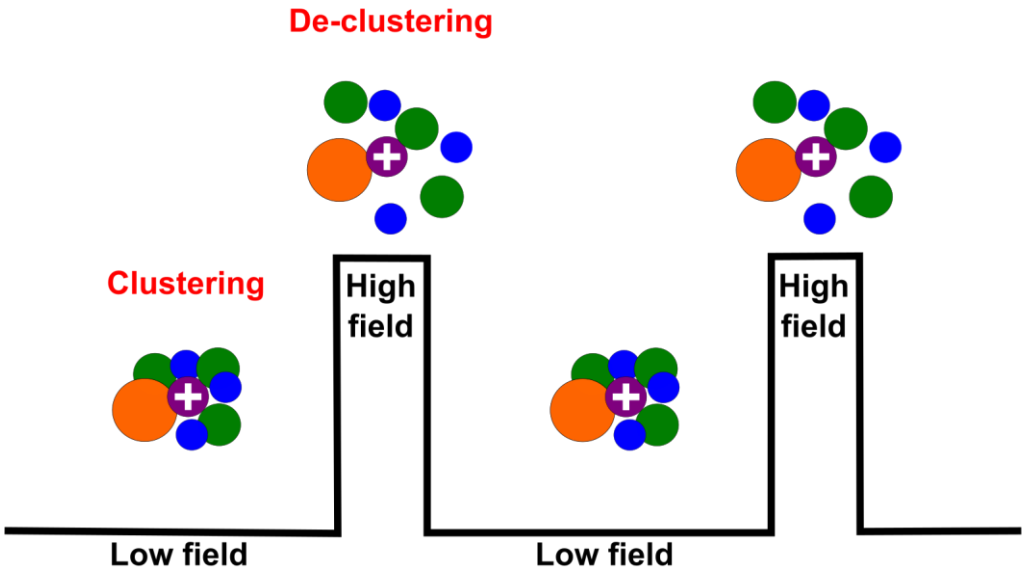

Fig. 7: Clustering/ de-clustering (type A model i.e. for $\alpha > 0$) at low and high electric fields respectively [47].

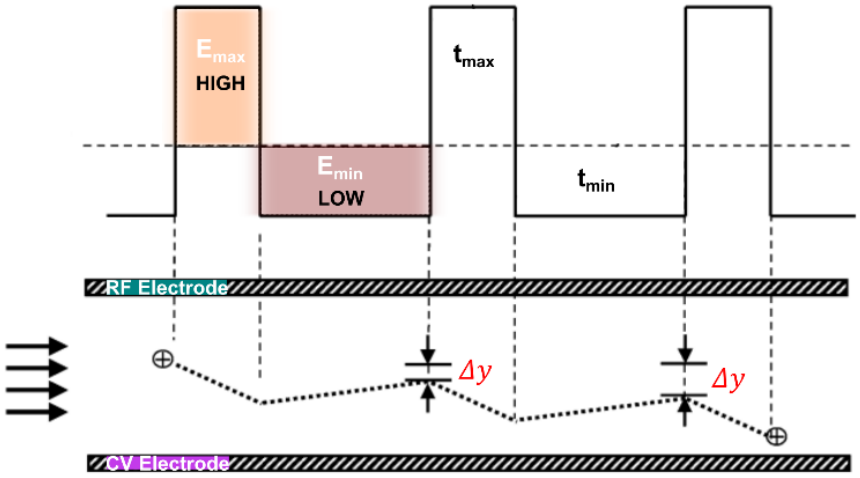

Fig. 8: Displacement of an ion (**Δ*y***) in the separation region between the asymmetric field of the RF-electrode and the compensation field of CV-electrode, adopted from [48].

The separation region i.e. the drift region consists of two parallel plates (electrodes) between which a gas is passing through, carrying the ionized analytes to the detector. The upper RF electrode (Fig. 8) applies the asymmetrical electric field and the lower electrode is held at ground potential (CV electrode). This asymmetric wave from the RF electrode has different duration t_{max} and t_{min} for E_{max} (high) and E_{min} (low), respectively. These asymmetric electric field waveforms with different polarities are such that the time-averaged electric field of the two is equal to zero (eq. 11). [48]

.

$$E_{high}\, t_{max} + E_{low}\, t_{min} = 0 \qquad \text{eq. 11}$$

The separation of ions is done mainly in high-field electric periods (t_{max}) (Fig. 8). [45,46] As mentioned earlier, a shift of ions toward one of the two electrodes occurs when the difference in K values for the same ion in high and low electric fields (E) and the respective time periods t_{max} and t_{min} contributes to net path difference (Δy) (eq. 12).

$$\Delta y = K_{high}\, |E_{high}|\, t_{max} - K_{low}\, |E_{low}|\, t_{min} \qquad \text{eq. 12}$$

$$\Delta K = K_{high} - K_{low} \qquad \text{eq. 13}$$

This *Δy* difference increases with repetitive high-low energy cycles and when a certain path deviation is achieved, the ions are neutralized on one of the electrodes (Fig. 8). Only ions with certain K_{high} i.e. ΔK (eq. 13) will be able to pass through the separation region and be detected from the Faraday plate in the detection region. [41] In order for other ions to be detected, additional compensation voltage (CV) on the bottom electrode is superimposed to correct for the transverse displacement (*Δy*). The compensation voltage (CV) is characteristic value for ion entities in the same way K_{high} i.e. ΔK are. Meaning, for a certain CV value a certain ion entity will be able to reach the detector.

Buryakov et al. (1993) was one of the first papers presenting the DMS/FAIMS technology and its separation principles, later followed by the monograph from Shvartsburg (2009). [43,49]

1.3.2.2. Miniaturization of FAIMS (Multichannel FAIMS microchip)

A miniaturized version of the DMS/FAIMS from Owlstone Nanotech Inc. (Cambridge, UK) was used for separation and detection of aromatic VOC i.e. BTEX in our case. As previously shown for DMS/FAIMS, the same working principles based on ion mobility (K) differences in low and high fields are utilized for ion separation (Fig. 9). It has a short separation region (L= 300 μm), an inflow, serpentine channel area of 1.2 mm^2 (Fig. 9b) and is often referred to as FAIMS chip or FAIMS ion filter.

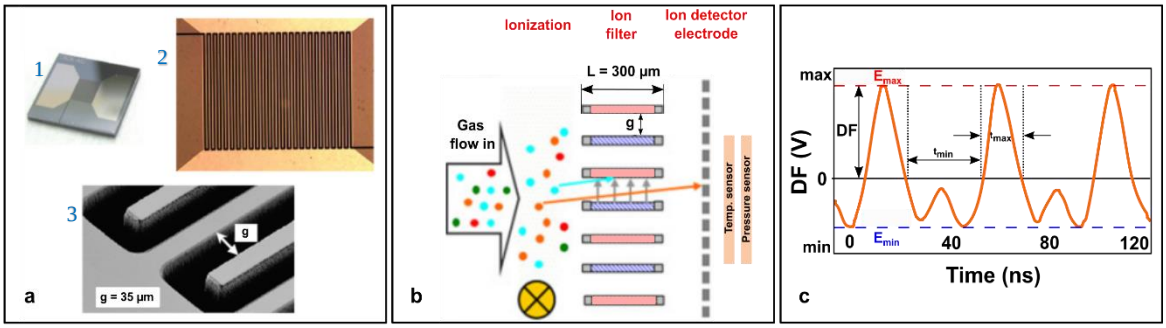

Fig. 9: a) (1) Owelstone's FAIMS chip, (2) inlet (front) perspective of the FAIMS' serpentine channel, (3) entrance gap from the chip done with an electron micrograph; b) Simplified schematics of the chip's cross section showing ionization, separation and detection regions. ; c) Actual waveform profile from the FAIMS chip; adopted from [50,51].

After an ionization step the carrier gas and the electrically biased FAIMS casing are directing the ions through the serpentine channel area, as the beginning of the ion separation field, consisting of 27 pairs of electrodes (like the one from Fig. 5) imposing a strong electric field (E/N) also called a dispersion field (DF) (Fig. 9c). DF is an electric field generated from a wave form, defined from zero to maximum peak voltage (E_{max}).

E_{max} is the maximum possible electric field applied (60 kV/cm in our case) i.e. 100% DF. The DF ranges from 0 to 100% or 0 - 243 Td (Townsends), when normalized (E/N_0) for 25°C, 101.3 kPa. [51]
Additional superimposing of the sweeping compensation voltage (CV) allows changes in ‘‘ion filtering’’ to occur. Changes in DF (i.e., E/N) and CV result in analyte-specific signal intensity scatter (DF/CV matrices) that are used to determine optimal separation conditions, which are then used for continuous monitoring. Changes in DF (i.e. E/N) and CV result with an analyte-specific signal intensity dispersions matrices (DF/CV matrices), that are used to determine the optimal separation parameters, which are then used for monitoring purposes.
Individual analyte signals can be defined trough CV_{max} (V) values at specific DF (%). CV_{max} is basically a CV value at which the intensity peak of an analyte is at its maximum. CV_{max} changes with changing DF.

The actual FAIMS chip can switch the polarity enabling positive and negative ion modus and it is approximately 10^2 - 10^4 time faster than macroscopic FAIMS, but with lower resolving power.

1.3.3. Ionization methods

α-ionization from ^{241}Am, β-ionization from ^{63}Ni or tritium (^{3}H) and the variety of VUV ionizing lamps (Kr, Xe, Ar) count for the most widely and commercially used ionization techniques in IMS/FAIMS, both with their advantages and disadvantages. Other ionization methods like ESI (electrospray ionization) or corona discharge are also utilized.

1.3.3.1 ^{63}Ni β- ionization

^{63}Ni-*β*-ionization was used as ionization source with radioactive activity of 370 MBq, producing electrons with mean ionization energy of 17 keV. Such high energy electrons ionize the supporting atmosphere thereby producing ions and secondary electrons both responsible for analyte ionization. [40] The ions produced are called reactant ions and are essential to the ionization of a sample. Positive and negative reactant ions (RIP and RIN respectively) act as reservoirs for analyte ionization in positive or negative operating mode and are of great significance. The successive production of RIP and RIN is explained elsewhere. [40] The RIP peak is mainly constituted of hydrated protons: $H^+(H_2O)_n$, as well as $NH_4^+(H_2O)_n$, $NO^+(H_2O)_2$ and other hydrated or not hydrated ions which could be witnessed in a lesser degree. The RIN peak consists of $O_2^-(H_2O)_n$, in addition to various adducts and ions like CO_3^- and O_4^-. When an analyte/sample is introduced into the ionization section the produced reactant ions are contributing to its ionization via collisions and cluster-formation resulting in formation of so-called product ions. The ionization process is governed through the

gas-phase proton affinity (gas basicity) and electron affinity of the analytes. Stabilization of the positive/ negative product ions may occur through displacing of molecule cluster, usually water molecules. [52]

Use of radioactive sources in analyte ionization has some disadvantages compared to UV-ionization. The biggest one is the requirement of special permissions, licenses and disposal procedures, which complicates its overall use. In this case, the focus is on UV ionization because of its favourable selectivity toward aromatic VOCs.

1.3.3.2 Atmospheric-pressure photoionization (APPI)

Ultraviolet photoionization (UV-photoionization) or, more precisely, vacuum ultraviolet ionization (VUV) (< 200 nm) differs from the ^{63}Ni-ionization source, mainly in the energy of the emitted photons (Xe-lamp 8.4 eV; Kr-lamp 10.6 eV; Ar-lamp 11.2 eV) compared to the high energy of the emitted electrons. Therefore, the use of photons to ionize gas-phase molecules contributes to higher ionization selectivity. [52,53] Photoionization occurs either by direct ionization of the analytes or indirectly by chemical ionization, usually through the addition of photoionizable dopants. The VUV lamps generate photons with ionization energy that is higher than the ionization potentials of most of the analytes, but lower than those of the supporting atmosphere, carrier or drift gases (N_2, O_2, He). The ionization of certain analytes can be ensured, and at the same time, the additional interference from background can be significantly reduced. [52]

Photoionization occurring under atmospheric conditions is referred to as atmospheric photoionization (APPI). In this work, so-called photoionization detector lamp (Kr-lamp) with MgF_2 window (transparency limit of 11.1 eV) [54] is used in atmospheric conditions as an ionization source for aromatic compounds i.e. BTEX. Most of this monoaromatic compounds have ionization energies (IE) between 8 and 9.5 eV and therefore the use of Kr-discharge lamp (IE = 10.0 and 10.6 eV) provides a certain selectivity during the ionization process, which makes it a suitable ionizing source for the nonpolar aromatic compounds.

Positive and/or negative ions are produced during the photoionization. These ions can be detected in separate modes or even simultaneously like in our case with the FAIMS from Owlstone Nanotech Inc. [50].

Some features of APPI can be seen as an advantage over radioactive ionization sources, for instance the higher selectivity and especially the fact that APPI is a non-radioactive ionization source.

The general disadvantages of APPI are the limited operating life, the maintenance requirements (cleaning of the lamp window) and in some cases the insufficient photon intensity of the VUV-lamps. [53]

It should be mentioned that lasers are also widely used as atmospheric-pressure photoionization sources (e.g., APLI), but their use in field applications is hampered by size and cost.

1.3.3.2.1. Photoionization – Positive mode

The ion formation in positive mode is characterized by the presence of two main types of ions which can coexist in the same time. The $M^{\bullet+}$ radical cation and the protonated molecule $[MH]^+$ are produced by photoionization of the molecule of the analyte, and with additional ion-molecule reactions after the photoionization as shown by the following two equations (eq. 14 and eq. 15):

$$M + \mathrm{h}v \rightarrow M^{\bullet+} + e^- \qquad \text{eq. 14}$$

$$M^{\bullet+} + S \rightarrow [MH]^+ + [S - H^{\bullet}] \qquad \text{eq. 15}$$

The formation and the amount of produced product ions in positive mode ($M^{\bullet+}$ and $[MH]^+$) depends, among other parameters, on the ionization energy as well as on the proton affinity of both, the analyte (M) and the neutral molecules (S). Higher proton affinity of the $M^{\bullet+}$ radical cation (in comparison to a neutral molecules) would favour the formation of the protonated product molecule $[MH]^+$ by hydrogen abstraction (eq. 15). [55] The presence of such $[MH]^+$ ions was already demonstrated. [52]

The fate of the photoelectrons like in eq. 14 is determined upon collision with other ions or molecules with electron affinity. [55]

1.3.3.2.2. Photoionization – Negative mode

Electron affinity is responsible for producing negative analyte ions in negative ion mode (eq. 16). The radical anion ($M^{\bullet-}$) can be produced when the analytes have higher electron affinity than the surrounding carrier gas, thus capturing the available thermal electrons produced by the photoionization.

$$M + e^- \rightarrow M^{\bullet-} \qquad \text{eq. 16}$$

Other ionizing pathway involves production of $O_2^{\bullet-}$ anion radical via charge exchange reactions thereby, if the electron affinity of the analyte is higher than that of O_2 (0.45 eV) [16] the ionization of analyte (M) can take place (eq. 17, eq. 18).

$$O_2 + e^- \rightarrow O_2^{\bullet-} \qquad \text{eq. 17}$$

$$M + O_2^{\bullet-} \rightarrow M^{\bullet-} + O_2 \qquad \text{eq. 18}$$

Additional possibilities for analyte ionization are presented in eq. 19 and eq. 21. In cases when the analyte has low proton affinity (PA) i.e. higher acidity compared to the neutral molecules/solvent (S) (eq. 19), or when other ionizing species such as $O_2^{\bullet-}$ cause deprotonation of analyte to take place (eq. 21). Another prerequisite for the ionization described by proton abstraction in eq. 20 and eq. 21 is the lower PA of the neutral molecule/solvent (S) and the analyte (M) compared to $O_2^{\bullet-}$. Quantitatively, (S) and (M) should not have higher acidity than that of $HO_2^{\bullet}$ (Δ_{acid} G = 1451 kJ mol^{-1}) for negative ionization to occur due to proton abstraction. [52,52,56]

$$M + [S-H]^- \rightarrow [M-H]^- + S \qquad \text{eq. 19}$$

$$O_2^{\bullet-} + S \rightarrow [S-H]^- + HO_2^{\bullet} \qquad \text{eq. 20}$$

$$M + O_2^{\bullet-} \rightarrow [M-H]^- + HO_2^{\bullet} \qquad \text{eq. 21}$$

1.3.3.2.3. The dopant effect

APPI or PI in general, as ionizing methods, provide relatively low ionization efficiency which affects the intensity of the signals. One of the reasons for such low ionizing efficiency is the fact that UV radiation is absorbed by the surrounding molecules/carrier gas. This reduces the number of directly ionized analyte-molecules, thus contributing to lower intensity of signal which affects the overall performance. [52]

Utilization of dopants is one of the solutions for increasing the number of ionized molecules of the analyte. Dopants are usually introduced in much higher concentration in the system in order to maximize the ionization energy from the emitted photons. They are directly ionized and serve as intermediates (reactive ions) for the indirect ionization of the analytes. The supposed mechanism of the dopant-assisted photoionization in positive ion mode can occur via protonation (eq. 23, eq. 24) and charge transfer (eq. 25), after the initial photoionization of the dopant ($h\nu_{lamp} > IE_D$) (eq. 22).

$$D + h\nu \rightarrow D^{\bullet+} + e^- \qquad \text{eq. 22}$$

Equation eq. 22 represents the formation of radical cation from the introduced dopant (D), followed by ionization (via protonation) of the neutral molecule/solvent (S)

by the dopant (eq. 23), and finally by ionization of the analyte (M) through the protonated solvent $[SH]^+$ (eq. 24).

$$D^{\bullet+} + S \rightarrow [SH]^+ + [D-H]^{\bullet} \quad \text{eq. 23}$$

$$M + [SH]^+ \rightarrow [MH]^+ + S \quad \text{eq. 24}$$

The PAs (proton affinities) of all participants (see eq. 23 & eq. 24) should meet some requirements for these proton transfer pathways to take place. That is, the PA of the solvent should be greater than that of the dopant but less than that of the analyte (M) or $PA_M > PA_S > PA_D$. If this is not the case and the mentioned PA requirements are not met, protonation of the analyte i.e. ionization cannot take place.

Another, more likely and more common form of ionization of the analyte by the dopant is through a charge transfer reaction (eq. 25). For a charge exchange ionization between the dopant and the analyte to occur only one requirement is necessary. The IE (ionization energy) of the dopant must be higher than that of the analyte ($IE_D > IE_M$).

$$D^{\bullet+} + M \rightarrow M^{\bullet+} + D \quad \text{eq. 25}$$

Charge transfer is also favoured by solvents (i.e. carrier gases) with low proton affinity like nitrogen (used in our case). Other solvents with higher PA are favouring the proton transfer. [52]

The dopant effect takes an important place in IMS/FAIMS based techniques, especially when higher sensitivity is required. To take advantage of the dopant effect and obtain reproducible and reliable results with IMS/FAIMS, the humidity in the sampling gas should be effectively decreased and kept at a constant minimum. This is in general the case when IMS or FAIMS are used as detectors. [39]

In general, humidity plays a crucial role in ion mobility spectrometry, especially when used for on-site monitoring. At these sites, it is almost exclusively a matter of monitoring the air or gas phase. The difficulty in monitoring water and groundwater therefore increases dramatically. Various methods of water separation can be used, of which continuous sampling systems are the most suitable. However, such systems use membranes (e.g. PDMS) that have a high affinity for the analytes, i.e. they require a longer response and cleaning times.

In this work, an effective, continuous, gas-water separation system (microporous PTFE membrane and a drying unit) is presented along with the effects

of humidity on the signal of different aromatic VOCs for ^{63}Ni- and APP-ionization in combination with FAIMS as ion filter.
In addition, the feasibility of a low-cost, stand-alone APPI-FAIMS for on-site monitoring of groundwater contamination by aromatic VOCs using the same gas-water separation system for effective water extraction was investigated and validated.

Other aspects of groundwater contamination remediation were also addressed in this work, as described in the scope of the thesis, part (2) below. Previous field observations showed that contaminant concentrations in groundwater wells may decrease with the slow addition of oxygen. The possibility of oxygen activation and Fenton-like chemistry without the presence of a typical activator (e.g. H_2O_2) was investigated. For this reason, a novel slow permeable silicone membrane and a specific contaminated groundwater site that could allow such additional remediation were characterised.

2. Scope of the thesis

Various aspects of groundwater contamination with aromatic VOCs (or AVOCs) are the subject of this work, such as the development of a novel, cost-effective FAIMS-based monitoring method and the investigation of the potential impact of a site-specific, oxygen-assisted remediation process.

One of the priorities is investigating the potential of using stand-alone field asymmetric ion mobility spectrometry in combination with atmospheric-pressure photoionization as an ionization source (APPI-FAIMS) for on-site, real time, continuous monitoring of groundwater pollution with aromatic VOCs i.e. BTEX. First of all, the reference values of the pollutants involved should be determined in both cases of FAIMS ionisation (^{63}Ni and APP ionisation) at a specific dispersion field strength previously optimised for the analytes of interest. High priority was given to the development of an effective, continuous separation of water from the AVOC at a constant negligible moisture content. Subsequently, the limits of the separation process are to be determined, including the minimum moisture content achieved and its robustness and stability; the degree of interaction of the separation unit with the analytes of interest and its influence on the analyte signal; the response and cleaning time of the unit; the potential of quantitatively reliable charge transfer to possibly produce a characteristic groundwater AVOC sum signal; the optimization of the operating parameters, etc.

The method should be tested under laboratory conditions and possibly validated in an on-site application. Validation of the results shall be carried out using a standard analytical technique (e.g. GC/MS).

Ideally, this monitoring method should be used for the determination of possible oxidation of aromatic VOCs by slow addition of oxygen in an anoxic groundwater conditions in presence of relatively high ferrous iron concentrations.

A relevant geo-chemical characterisation of the contamination site, including the involvement of the standard physical remediation treatments like P&T and SVE should be taken in consideration. The oxygen permeability of a special silicone membrane (OxyTech) should be determined in connection to the applied oxygen pressure.

Furthermore, the involvement of oxygen in the groundwater remediation as an initiator of *in-situ* chemical oxidation will be investigated. The possible formation of reactive species upon ferrous oxidation is to be confirmed and determined. The possible successful involvement of oxygen in the remediation process using OxyTech membrane shall be confirmed, and the influence of iron, carbonate/bicarbonate ions and other groundwater parameters on the mechanism and efficiency of the process should be investigated. The determination of possible oxidation products, the reaction mechanism and the possible remediation effect is seen as an additional advantage.

3. Implementation of FAIMS for monitoring of aromatic volatile organic compounds in groundwater

3.1. Introduction

This chapter contains most of the results that have been previously peer-reviewed and successfully published. [39]

The contamination of groundwater with aromatic volatile organic compounds (VOCs) such as benzene, toluene, ethylbenzene, xylenes (BTEX) still represents a continuous environmental issue, mostly due to leakages of fossil fuels into the soil. [57] Depending on the severity of the soil contamination, years of remediation can be involved, during which, regular contamination monitoring is done. Standardized, laboratory-based methods for analysis usually require groundwater sampling, conservation, transport and storage of samples. Subsequently, a standardized method like HS-GC/MS is used for the determination and quantification of benzene and derivatives in water. [35] Other methods e.g. liquid-liquid extraction GC/MS and HS-SPME-GC/MS can be also applied. [36–38] Monitoring of groundwater remediation requires increased sampling frequency, it can be time-consuming and rather costly.

The presence of water in the sample flow represents a major problem in IMS/FAIMS based techniques. However, it is even more emphasized considering BTEX contaminated water was sampled instead of the usual monitoring of air. The presence of humidity (water) in the system makes quantification and possible analyte identification very difficult or virtually impossible. [58]

FAIMS is used for separation of molecular ions in a gas-phase at atmospheric-pressure based on their nonlinear ionic mobility (K) under high electric field strength i.e. dispersion field (DF) as explained in part 1.4.2. [43,49] Similar to other IMS based techniques, FAIMS as a stand-alone device demands an effective separation of the analytes from the water-phase beforehand. Even small humidity amounts can make quantification and possible contaminant identification difficult or virtually impossible depending on the ion source and analytes involved. [58] This was previously shown for ^{63}Ni-ionization and atmospheric-pressure photoionization (APPI) in combination with FAIMS. [34,59] Langejuergen et al. succeeded in obtaining a reliable quantitative signal and separation for BTX under high humidity conditions using a High-kinetic-energy IMS with corona discharge ionization. [60]

Various continuous and non-continuous sample extraction methods and/or separation methods were used in combination with IMS/FAIMS to decrease the humidity and avoid complex gas phase reactions by improving the sensitivity and signal stability. [49,61,62] PDMS membrane extraction in combination with IMS was previously used for detection/ determination of chlorinated hydrocarbons [63], methyl tert-butyl ether [64] and other ethers in water. [65] Pseudo-continuous, outside-to-inside, tubular, membrane extraction units for the determination of BTEX in water by ^{63}Ni- and APPI-IMS were also investigated. [19,66]

In order to minimize moisture, a continuous gas-water separation module will be developed in the present work. This consists of a microporous, tubular Teflon

separation membrane (SU) and a drying unit (DU). The module is connected to a multichannel FAIMS filter sensor. [50] Both, ^{63}Ni- and APPI-FAIMS were used as detectors in combination with the gas-water separation unit. The effect of humidity on the detected APPI signal was investigated for different aromatic VOCs, and continuous on-site monitoring of aromatic VOCs in groundwater with gas-water separation APPI-FAIMS was performed using a specific aromatic VOCs sum-signal at low humidity. The method should provide a relative simple way for direct and reliable monitoring of aromatic VOCs contamination in groundwater.

3.2. Experimental

3.2.1. Chemicals

For the experiments the following chemicals were used: benzene >99% (AppliChem GmbH, Germany); toluene >99.5%; p-xylene >99.5%; 1,2,4 trimethylbenzene >98%; 1,3,5 trimethylbenzene >98% and indane >95% (Sigma-Aldrich, Germany); ethylbenzene ≥99%; m-xylene ≥99.9%; o-xylene >99.5% (Fluka Analytical, Switzerland). For the preparation of standard solutions, Milli-Q water was used from a Milli-Q Plus water purification system (Millipore, USA). The laboratory stock solutions used for the calibration of the APPI-FAIMS and HS-GC/MS analysis were mixed in 1L Schott bottle for at least 24 hours at 25 ±1 °C in an overhead shaker (Reax 20 from Heidolph, Germany) and discarded after sampling.

3.2.2. Gas-water separation unit

The gas-water separation unit consisted of a membrane separation unit (SU) constantly heated at 30 °C and a drying unit (DU). A Gore-Tex® microporous tube membrane (length=18 cm, OD=1.6 mm ID=0.8 mm) served as a membrane separation unit (SU). A self-made drying unit (DU) (length=8 cm, OD=1 cm, ID=0.8 mm) packed with Sicapent (water absorption capacity ≥50%) from Elementar - Germany, containing a moisture indicator, was utilized for removing the remaining moisture after the SU.

A PPM1 Trace Moisture Analyzer (Edgetech Instruments, USA was placed in position 1 and 2 within the gas flow (Fig. 11) before and after application of the DU (decoupled from the make-up flow) recording the initial humidity drop. Monitoring of the humidity for the results presented here was carried out at position 3. The average breakthrough time of the DU was ~4 h.

The detection of *p*-xylene generated by a permeation tube at 50°C was used to determine the influence of the DU on the analyte signal.

3.2.3. FAIMS and GC/MS Instrumentation

Two identical FAIMS systems from Owlstone^{TM} Ltd. (Cambridge, UK), with the same functional block including a microfabricated FAIMS chip, but different ionization mechanisms were used:

FAIMS chips: Electrode gap 34.5 (±0.2) µm; dispersion field (DF) range 0-100% i.e. 0-243 Td (25 °C, 101.3 kPa), waveform frequency of 27.15 MHz, duty cycle 33%, under superimposed compensation voltage (CV) sweep range ±6.0 V and Faraday-cup as a detector.

a) The Lonestar system: equipped with a cylindrical ^{63}Ni foil (8 mm diameter and 10.5mm length) with an activity of 555 MBq to provide radioactive ionization source. Compensation voltage (CV) parameters: sample number 512, over-sweep length 950 ms, sampling time 2 ms; static bias ±42 V, detector bias ±43 V; with constant sensor temperature of 60±1 °C.

b) APPI-FAIMS System (PAD Development Kit): equipped with RF PID krypton lamp 10.6 eV from Heraeus, Germany (PKR 106, MgF_2 window material) providing UV ionization. Compensation voltage (CV) parameters: sample number 512, over-sweep length (CV sweep time per mode) 500 ms, sampling time 2 ms; static bias (casing bias surrounding the chip) ±60 V, detector bias ±60 V, with constant sensor temperature of 60±1 °C.

The Lonestar system was used here only to show the effect of the gas-water separation system on the analyte signal and to better determine the breakthrough time of water.

Data collection for the FAIMS analysis was done in two ways:

1) Dispersion field/compensation voltage matrices (i.e. DF/CV intensity plots) and

2) CV matrix sweep at fixed DF (36%) for continuous signal intensity monitoring. The signal was recorded in 1 min average if not stated otherwise.

CV_{max} values are normalized with regard to pressure/temperature effect and shown as reduced field strength values (CV_{max} N^{-1}) in Td at 25 °C and 101.3 kPa for 35 µm electrode gap.

A gas calibrator (GC/T 400, Schumann-Analytics, Germany) with home-made PTFE permeation tubes filled with the analytes was used as reference. The nitrogen carrier gas flow (5.0; 99.999 % Air Liquide, Germany) was set to 1 L min^{-1}.

For the validation experiments a GC/MS system was used (GC: Trace GC (ThermoQuest); MS: Finnigan PolarisQ (US), EI, 70 eV; Full scan mode: 50-200 m/z; Column: Stabilwax®-DA (Restek, Germany) 60 m, 0.32 mm ID, 1 µm film thickness). The temperature program was set to 50 °C to 120 °C with 7 °C min^{-1}, 120 °C to 220 °C with 30 °C min^{-1}, 220 °C for 2 min. Hydrogen (>99.99999%; hydrogen desktop generator WM H2.500, F-DGSi France) was used as carrier gas with a gas flow of 1.7 mL/min. The injection of the sample was carried out by automatic injection PAL Combi-xt (CTC Analytics AG, Switzerland). The 20 mL headspace screw vials (amber) were filled with 15 mL of the sample solution and heated to 70 °C for 5 min in an agitator. Static headspace (HS) (300 µL) and a split ratio of 1:30 was used. The transfer line

temperature was set to 250 °C. The identification of the signals obtained by the analysis of groundwater was confirmed by analytical standards.

Contaminated water was pumped by a HPG pump (Platinblue - Knauer, Germany) through the SU. The total flow rate, pressure, and inline temperature were monitored continuously during the measurements using built-in sensors from the FAIMS analyzers. Flows were additionally controlled by FM, FP-407 flow meter (Applied Instruments, The Netherlands).

External calibration of toluene in water (22 - 23 °C) was performed at 36% DF strength (21.6 kV or 87.7 Td at 25 °C). Additional calibration without applied voltage (0% DF) was carried out in identical manner as for 36% DF. LOD and LOQ [67] were determined by averaged signal acquisitions ≥1 min. The S/N ratio was calculated as the sum of the mean blank signal and three times of its standard deviation.

Contaminated groundwater was sampled from a BTEX contamination site in Germany and divided into four identical samples under laboratory conditions. The samples were stored (6 °C) without conservation and periodically analyzed by APPI-FAIMS at 17 °C (sample temperature). For control/validation of the FAIMS results a static headspace GC/MS analysis of the same samples, in doubles, was performed.

3.3. Results and discussion

3.3.1. Generation of FAIMS signals for the detection of aromatic VOCs (permeation tubes)

DF/CF intensity matrices were generated from the analysis of analyte-filled permeation tubes for establishing the specific ‘‘signal fingerprints’’ of the pure aromatic VOCs with ^{63}Ni- and APP-ionization (Fig. 10 10). The fingerprints were taken in positive mode under increasing DF and sweeping CV. CV (compensation voltage [V]) is replaced by the term CF (compensation field [Td]) similar to DF (dispersion field [Td]), both corrected for the atmospheric temperature and pressure effect, resulting in the so-called reduced field strength, as proposed from Nazarov et al. (2006). [47]

When DF is increased, above 40 Td (or 16.5% DF), differences in ion signals appear due to the nonlinear behaviour of their ion mobility (K) in high electric fields. [68] If a constant DF, above 16.5% is applied, an aromatic VOC signal is generated with an intensity maximum at certain CF. This CF value could serve as an analyte-specific parameter (CV_{max} N^{-1}). For better comparison under different experimental conditions, the specific CV_{max} N^{-1} values are used as the standard FAIMS scaling, derived from CV_{max} as explained previously. CV_{max} is corrected for standard ambient temperature and pressure (SATP), i.e. 25 °C and 101.3 kPa.

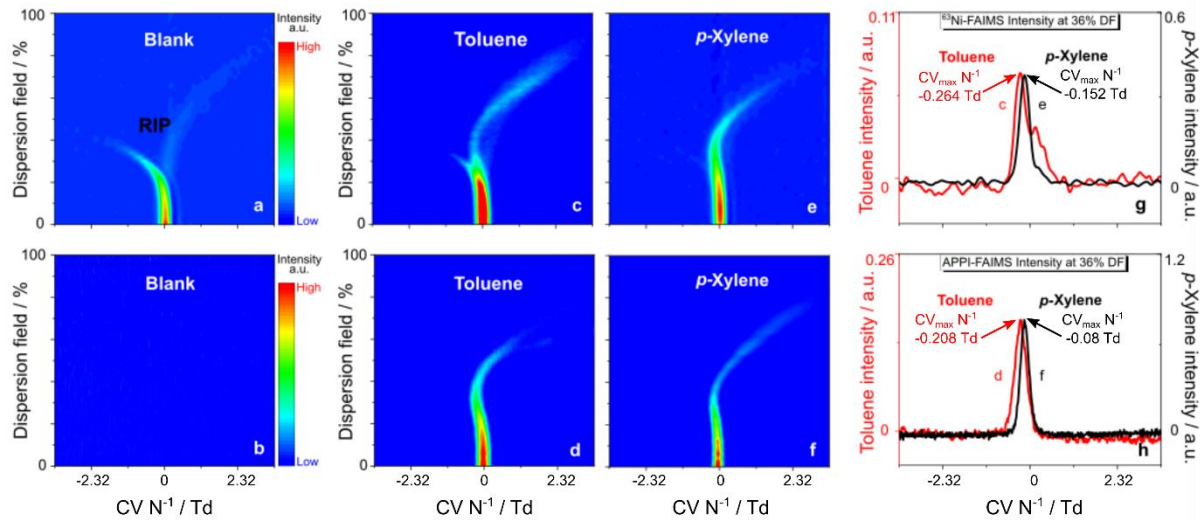

Fig. 10: Typical signal fingerprints of blank (N_2), toluene and *p*-xylene from permeation tubes incubated at different temperatures (i.e. with different signal intensities). (**a**,**c**,**e**,**g**) With ^{63}Ni- FAIMS (upper row) and (**b**,**d**,**f**,**h)** with APPI-FAIMS (lower row) in positive mode. (**d** and **h**) Overlay of extracted dimer signals at 36% DF Note: Flow 1L min^{-1} at SATP.

In all experiments performed, 36% DF, or a field strength of ~87.7 Td (25 °C) was used as the ion filtering field, with a good compromise between ion selectivity and sensitivity of the method as further explained. The overlay of the signals for toluene and *p*-xylene obtained by ^{63}Ni- and APP-ionization at 36% DF, showed differences in CV_{max} N^{-1} consistency and specificity considering different ionization mechanisms and FAIMS chips used. Although the field strength of the matrix-extracted DF was well beyond the critical E/N_c of 40 Td (16.5% DF), the separation of toluene and *p*-xylene ions at the chosen field strength ~88 Td (36% DF) in Fig. 10g,h was rather poor.

Signal intensity and CV_{max} N^{-1} inconsistencies occur mostly through pressure, temperature or humidity changes especially with on-site implementation of the FAIMS system. Small atmospheric temperature variations are considered negligible in comparison to the overall rise of T_{eff} in the sensor due to increased number of ion-neutral (N_2) collisions in fields with high electric strength. [69]

According to Wilks et al. (2012) increased residence time under a high electric field (E/N) increases the neutral-ion collisions, thus increasing the T_{eff} of the ion accordingly. T_{eff} is of great importance because it summarizes the effect of the gas temperature (T) with the electric field and pressure (E/N) in the sensor into a single variable (eq. 26), thus simplifying the influence on the rate constant. [70,71] The efficiency factor ζ corrects for the loss of energy input from the field applied, as the situation gets complicated for polyatomic ions and/or neutrals. [72]

$$\frac{3}{2}kT_{eff} = \frac{3}{2}kT + \frac{1}{2}\zeta M{N_0}^2{K_0}^2\left(\frac{E}{N}\right)^2 \qquad \text{eq. 26}$$

The increased T_{eff} at high (E/N) could also minimize atmospheric influence and potentially affect the undesired analyte-water cluster formation by desolvation. This could contribute to more consistent CV_{max} N^{-1} values and analyte-to-signal response of the monomer ions used in monitoring purposes.
Nevertheless, humidity can have a significant impact on the ionization of analytes prior to the application of the separating DF field. This has already been addressed for the case of ^{63}Ni-ionization of BTEX (with DMS) by Kuklya et al. (2014). [59] The humidity aspect of ^{63}Ni- and especially APP-ionization of BTEX and indane with FAIMS is investigated, and a solution prior to analyte ionization is implemented and presented as follows.

3.3.2. Implementation of the gas-water separation unit

The IMS technique was essentially developed for the investigation of analytes in dry gas phase. Therefore, it is necessary to separate the analyte from the water in aqueous solutions. For this reason, a system for gas-water separation of aromatic VOCs was developed within the framework of this work. The experimental setup is shown in Fig. 11. The continuous gas-water separation system was constructed from two separate, successive units: a tubular gas-separation unit (SU) and a drying unit (DU). The SU contributed to the separation of the aromatic VOCs from the water phase while the DU provided fast and efficient water extraction to constant low values.

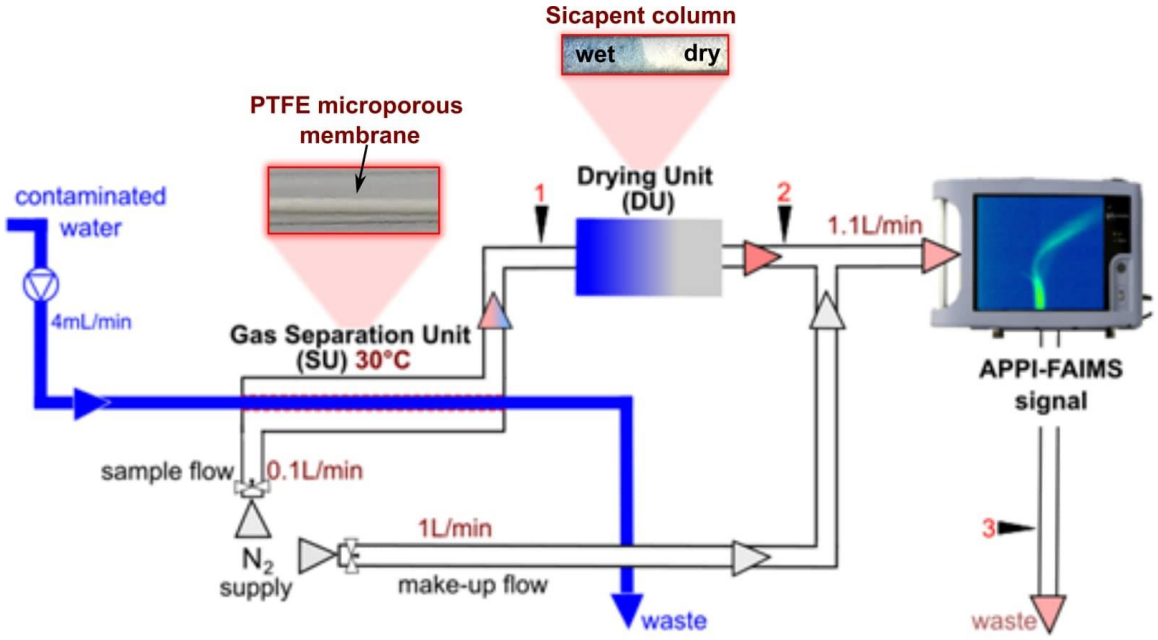

Fig. 11: Scheme of the experimental setup: Gas-water separation unit including SU and DU coupled with FAIMS unit; Sample points 1 and 2 are used to determine humidity before (> 300 ppm_v) and after DU (≤ 1.6 ppm_v); point 3 is used as a permanent humidity control point. Water and gas flow remained the same only if not stated otherwise.

3.3.2.1. Separation unit (SU)

PDMS and silicone as hydrophobic and organophilic polymers can be successfully used as effective separation of non-polar VOC like BTEX from water (like previously mentioned 3.1.). Silicone or PDMS can be advantageously used as an extraction and enrichment medium for the non-polar analytes from water. In this case the drying unit could probably be considered sufficient, but the aromatic VOC enrichment, in general, can cause the residual analyte signal to appear longer and to significantly increase the cleaning time of the PDMS/silicone membrane.

Instead, Gore-Tex®, Dupond's expanded PTFE (polytetrafluoroethylene), was used, thus avoiding longer cleaning and providing faster response times. VOC analytes including water can pass unhindered from one side of the membrane to the other [73], thus separating the gas-phase from the water-phase, but still having a high humidity

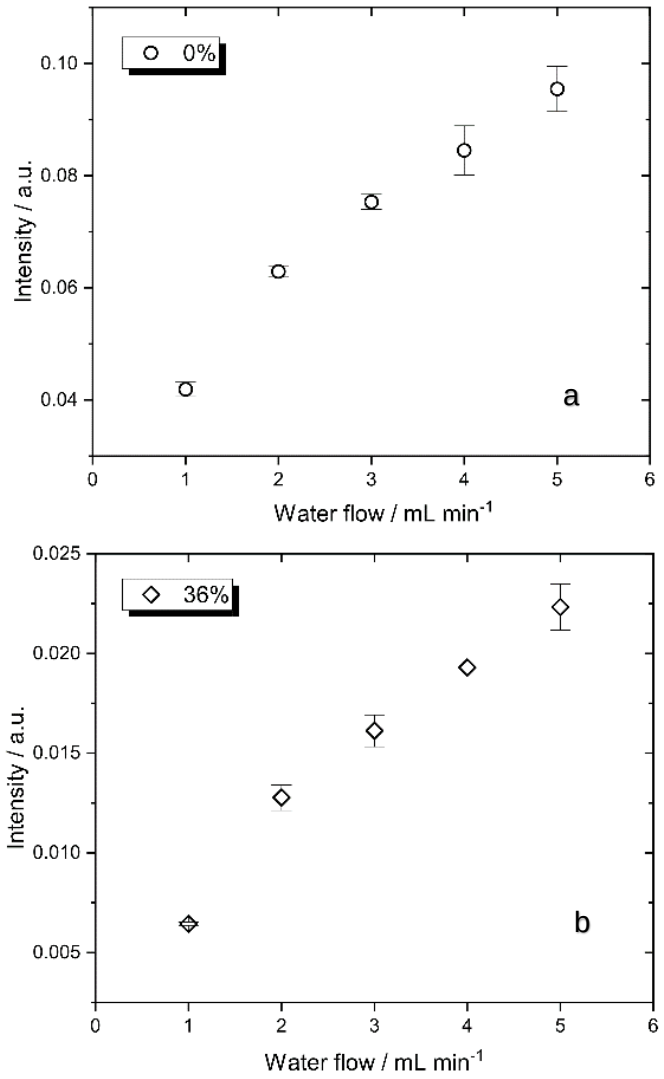

Fig. 12: Change of the toluene signal intensity (APPI-FAIMS) with the change of the water flow in the separation unit (SU) at 0% and 36% DF.

content (>300 ppm_v). This microporous Teflon membrane has higher polarity than the PDMS membrane and, combined with the drying unit, had a relatively acceptable cleaning times, as later shown for toluene.

The primary objective of the membrane was to enable a continuous, constant flow of contaminated groundwater and thus relative constant pervaporation of the aromatic VOCs. The whole gas-water separation system was used for better evaluation of the tubular-separation membrane (SU), all other parameters were kept constant. The temperature of the SU was maintained at 30 °C, slightly above the ambient temperature, to avoid major temperature fluctuations affecting the pervaporation.

Experimental conditions such as the effect of water flow rate in the membranes on the analyte signal were studied. This resulted with an expected increase in intensity with increase of contaminated water flow, as shown for cases when electrical field was not applied (Fig. 12a) or in an increased field strength (Fig. 12b). The intensity increase is smaller at higher water flow rates. Considering the results, the flow rate was adjusted to 4 mL min^{-1} for further investigations, as this provided a relatively good increase in signal sensitivity.

The effect of membrane length was investigated and shown in Fig.13. It was observed, more than 50% increase in length of the Teflon membrane resulted in approximately 20% increase of signal intensity when toluene was used as model

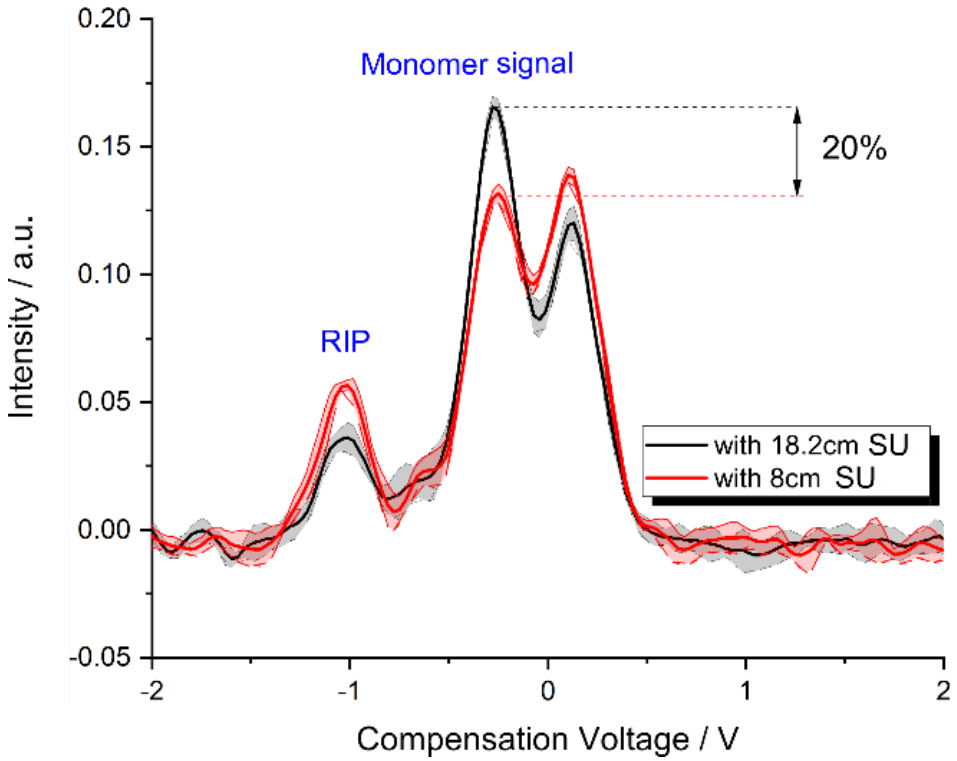

Fig. 13: Increase of toluene monomer signal at 36% DF (^{63}Ni-FAIMS) with the increase of SU length (the average black signal originates from 18.2 cm long SU; the average red signal originates from 8 cm long SU).

contaminant in water (using ^{63}Ni-FAIMS). These results have shown that the sensitivity of the system can be further increased indirectly if necessary; the decrease in RIP intensity is evident with increasing presence of toluene molecules due to the longer membrane. For clarification, in both cases, the results were produced at low humidity (< 1.6 ppm_v) in combination with the drying unit.

3.3.2.2. Drying unit (DU)

The main purpose of the drying unit (DU) is to further effectively decrease the humidity in the sample flow which is coming from the SU (i.e., PTFE membrane). The drying substance (P_2O_5) from the DU should also be inactive towards the analytes and should not affect the signal of the analytes in any way.

No signal originating from P_2O_5 i.e. the DU was detected under the applied conditions for blank measurements due to the very low vapour pressure of P_2O_5 when in dry or humid conditions. To test the interaction of the analytes with the DU, *p*-xylene was selected as an aromatic VOC representative. In Fig. 14 the continuous signal monitoring of *p*-xylene (at CV_{max} N^{-1} = -0.08 Td) with and without the presence of DU shows no difference in signal intensity. After the DU is applied, only a slight delay of the signal is detected. Around 2% difference in signal intensity was observed after replacing a saturated DU with a new dry DU.

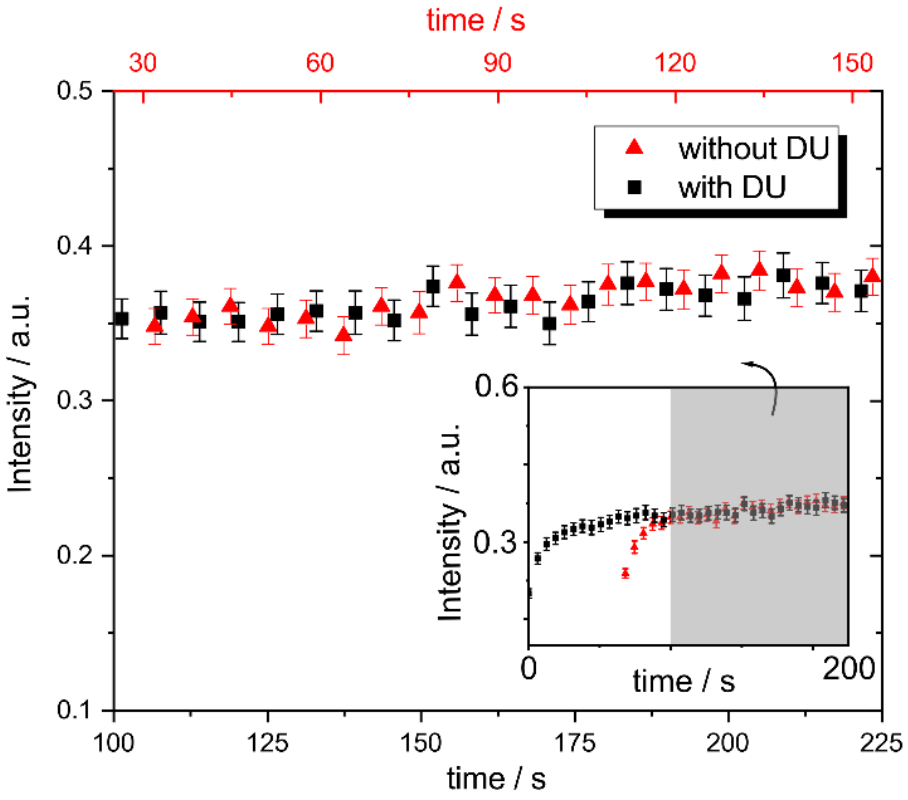

Fig. 14: Influence of the drying unit (DU) on the *p*-xylene signal originating from a gas calibrator at 36% DF (i.e. *p*-xylene permeation tube -0.08 Td).

Changes in flow due to small leakages for the different DU is also seen as a contributor to the minor inconsistencies.

By placing a trace moisture analyzer in position 2 or 3 within the gas flow before and after application of the DU (Fig. 11) the average breakthrough time of the DU was determined. Multiple measurements like in Fig. 15 have confirmed a breakthrough time of 4 h (Fig. 15b) for 8 cm long DU (see 3.2. Experimental). In most cases, a longer breakthrough time was found to depend mainly on the packing of the homemade DU column. Humidity decreases from >300 ppm_v to <1.6 ppm_v was detected from the DU, when measurements in position 1 and 2 were compared. A lower humidity then 1.6 ppm_v was suspected and later confirmed.

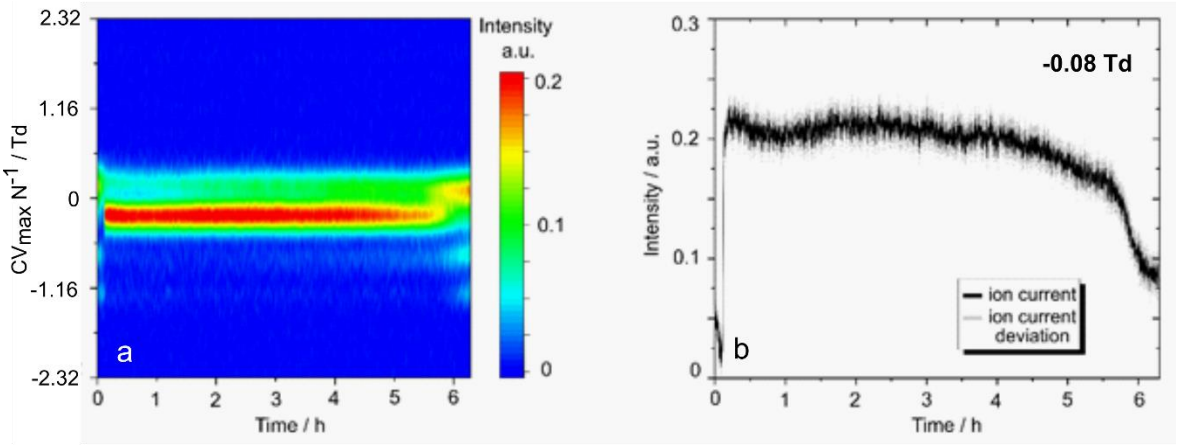

Fig. 15: Breakthrough time of a drying unit (DU) with ^{63}Ni-FAIMS for *p*-xylene signal from water. (**a**) Continuous heat map signal from *p*-xylene in water at 36% DF (88 Td); (**b**) Extracted signal at 36% DF and CV_{max} N^{-1} of *p*-xylene (-0.08 Td).

The implementation of the gas-water separation system for the analysis of aqueous samples successfully reduced the humidity in the sample flow to ≤ 1.6 ppm_v without interacting with the nonpolar VOCs, thereby matching the reference conditions from the gas calibrator and the specific CV_{max} N^{-1} of BTEX and indane at 36% DF.

All of this has proven critical to the application of the gas-water separation system for on-site detection of aromatic VOCs in groundwater.

3.3.3. Establishing of analyte-specific FAIMS-signals from aqueous solutions for BTEX and indane at 36% DF

The determined CV_{max} N^{-1} values from the reference permeation tubes were in agreement with the analysis of separate aqueous samples containing an aromatic VOC at low humidity (< 1.6 ppm_v) when the gas-water separation unit was used. The same experiments were performed for both cases, with ^{63}Ni- and APPI-FAIMS, and

Tab. 5: List of determined CV_{max} (V) and calculated $CV_{max}\ N^{-1}$ (Td) for aromatic VOCs at low humidity (< 1.6ppm$_v$) by using reference permeation tubes and the gas-water separation system for BTEX and indane by ^{63}Ni-FAIMS.

	***o*-Xylene**	***p*-Xylene**	***m*-Xylene**	**Benzene**	**Ethylbenzene**	**Toluene**	**Indane**
CV_{max} (V)	-0.16	-0.16	-0.102	-0.483	-0.16	-0.278	-0.072
$CV_{max}\ N^{-1}$ (Td)[a]	-0.186	-0.186	-0.118	-0.560	-0.186	-0.322	-0.084

a) Reduced field strength values ($CV_{max}\ N^{-1}$) calculated from CV_{max} with 35 µm electrode gap at 25 °C and 101.3 kPa

Tab. 6: List of determined CV_{max} and calculated $CV_{max}\ N^{-1}$ (Td) for M^+ at low humidity (< 1.6ppm$_v$) by using reference permeation tubes and the gas-water separation system for BTEX and indane by APPI-FAIMS.

	***o*-Xylene**	***p*-Xylene**	***m*-Xylene**	**Benzene**	**Ethylbenzene**	**Toluene**	**Indane**
CV_{max} (V)	-0.084	-0.069	-0.037	-0.366	-0.084	-0.178	-0.061
$CV_{max}\ N^{-1}$ (Td)[a]	-0.097	-0.08	-0.043	-0.425	-0.097	-0.208	-0.07

a) Reduced field strenght values ($CV_{max}\ N^{-1}$) calculated from CV_{max} with 35 µm electrode gap at 25 °C and 101.3 kPa.

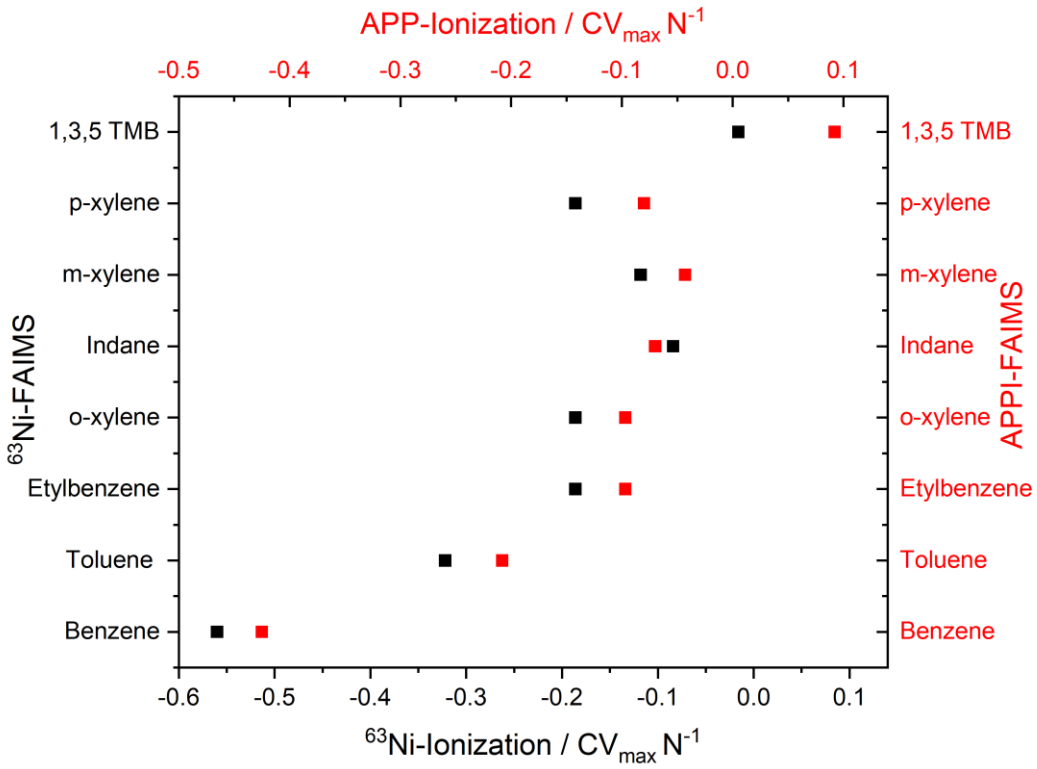

Fig. 16: Comparison of the $CV_{max}\ N^{-1}$ for FAIMS with ^{63}Ni- and APP-Ionization.

the results can be seen in Tab. 5 and Tab. 6, respectively. The differences between the values in the two tables were likely due to a kind of systematic bias, e.g., variations in the applied electric field strength, device construction or other unknown post ionization reactions of the analytes.

These differences are shown in Fig. 16. All the $CV_{max}\ N^{-1}$ values including BTEX, 1,3,5 trimethylbenzene (1,3,5 TMB) obtained by APPI-FAIMS (red) were more positive compared to those obtained by ^{63}Ni-FAIMS (black). Only in the case of indane a deviation in this trend is observed which we cannot fully explain. The formation of adducts or clusters due to the different ionization techniques cannot be excluded.

3.3.4. Detection of aromatic VOC by coupling of gas-water separation unit with ^{63}Ni- and APPI-FAIMS at different humidity

The preferred mode of ionization is dictated by the properties of the analytes, dopants, solvents and matrices involved. These properties include gas-phase acidity/basicity (GB), ionisation energy (IE), electron affinity (EA), and other gas-phase thermodynamic properties including proton affinity (PA). [52,56] Gas basicity i.e. proton affinity are the main properties responsible for the outcome of the ^{63}Ni ionization of the analytes. Higher PA or GB values favour analyte ionization because these analytes are more likely to be ionized and avoid ion suppression. The opposite is observed when photoionization is involved. The analytes with high ionization energy (IE) are likely to be involved in charge transfer reactions with other analytes with lower IE if no pre-separation step is provided.

Tab. 7 shows PA, GB and IE data from some of the groundwater relevant contaminants. PA and GB for certain compounds were not reported.

Tab. 7: Proton affinity (PA), gas basicity (GB) and ionization energy (IE) of the aromatic VOCs of interest.

Compound	PA[74]	GB[74]	IE (evaluated)[75]	IE (PE)
	kJ/mol	kJ/mol	eV	eV
Benzene	750.4	725.4	9.25	9.25[76]
Toluene	784	756.3	8.83	8.79[76]
Ethylbenzene	788	760.3	8.77	8.77[77]
***o*-Xylene**	796	768.3	8.56	8.45[78]
***m*-Xylene**	812.1	786.2	8.55	8.56[77]
***p*-Xylene**	794.4	766.8	8.44	8.44[79]
1,2,3-TMB	/	/	8.42	8.42[77]
1,2,4-TMB	/	/	8.27	8.27[77]
1,3,5-TMB	836.2	808.6	8.4	8.42[77]
Indane	/	/	8.6	8.5[80]
H_2O	691	660	12.62	12.62[81]

$IE_{(evaluated)}$ as shown in [75]; $IE_{(PE)}$ - after the same photoelectron spectroscopy method from different sources [76], [77], [78], [79], [80], [81] as cited by [75].

3.3.4.1. The influence humidity on the detection of aromatic VOC with ^{63}Ni-FAIMS under atmospheric conditions

A common feature of all radioactive sources is their high-energy of ionization. In a stand-alone version, this is significant because this energy is capable of ionizing all kinds of molecules, including the surrounding atmosphere, (carrier gas) and initiate formation of RIP and RIN leading to complex ion-molecule reactions involving PA. The mechanism for formation of positive and negative reactant ions (RIP and RIN respectively) has been addressed previously and is discussed in detail in other publications. [40] In the case of BTEX a MH^+ ion or more probable $MH^+(H_2O)_n$ cluster ion, depending on the inline humidity, is produced and detected in the positive ionization mode.

The detection of the BTEX signals is dependent on the proton affinity of the analytes. In Fig. 17 this PA concept can be better observed. Namely, at relatively high humidity (> 300 ppm_v) in the total flow, differences in signal/peak between a sample with and without toluene cannot be observed independent from the concentration (see Fig. 17a,b,d,e). When the signal at 36% DF was extracted the same peak at -0.66 Td was noticed in both cases. Only with the application of the DU and lowering the humidity (< 1.6 ppm_v) a toluene signal from the aqueous sample has been observed (Fig. 17c,f).

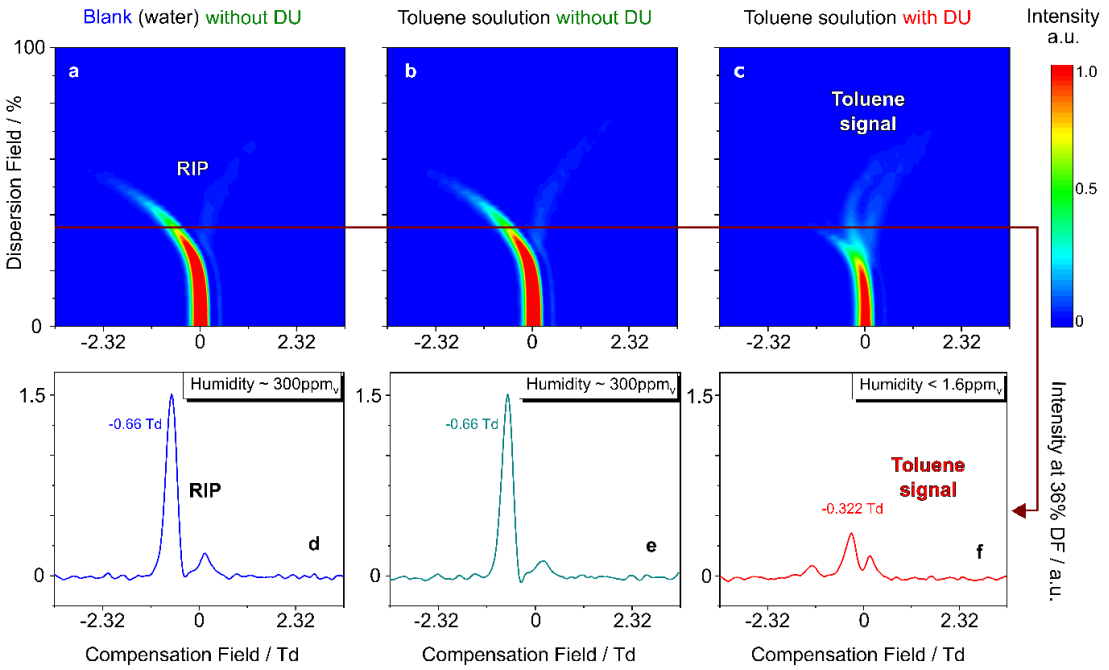

Fig. 17: Humidity influence on ^{63}Ni β-ionization with FAIMS. (**a,b,c**) DF/CF heat maps of blank (water) and toluene solution with (<1.6ppm_v) and without (>300 ppm_v) DU. (**d,e,f**) extracted intensity signals at 36% DF (88 Td) for a,b and c successively.

The main reason for this is the high PA of the water compared to toluene. This statement is somewhat misleading, since the PA of water is 691 kJ mol^{-1} and of toluene 784 kJ mol^{-1} (Tab. 7). However, it should be pointed out, the PA of water increases with the growth of the water cluster in proportion to the increase in humidity. For instance, a water dimer $H^+(H_2O)_2$ has an effective PA of 827 kJ mol^{-1} and $H^+(H_2O)_3$ of 911 kJ mol^{-1}. [82] Therefore, the ionization of the toluene under these conditions is hindered.

The presence of proton bound water dimer and larger clusters is confirmed in Fig. 18. A constant background signal (also in presence of N_2 carrier gas), appeared from the beginning, when the humidity is < 1.6 ppm_v (Fig. 18a). At the same time, the intensity of the presumed RIP signal, which consists mainly of proton-bound water clusters (b), also increased with increasing humidity. Even more interesting is the observation of the RIP shift from about -1.16 to -0.6 Td, which occurs during the same time (b and c). This also explains the peak value in Fig. 17 at -0.66 Td, which occurs at high humidity due to a large water cluster.

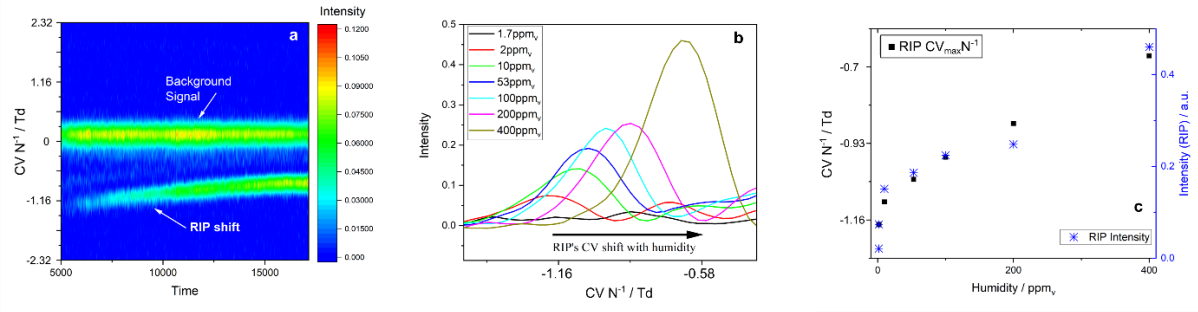

Fig. 18: RIP signal by ^{63}Ni-FAIMS with increasing humidity: (**a**) continuous heat map at 36% DF (88 Td). (**b**) Extracted RIP signals from (a) at different humidity (1.7-400 ppm_v). (**c**) CV_{max} N^{-1} and intensity increase for RIP at increasing humidity.

The positive RIP shift toward more positive CV_{max} N^{-1} values (c) implies that the water cluster is ‘‘growing’’ with the increase in humidity, despite the applied DF. This is in contrast to the humidity increase in other previously investigated FAIMS/DMS systems. For instance, Kuklya et al. (2015) showed that the ion clustering/declustering effect, with a planar DMS, contributed to negative RIP shift toward more negative CV_{max} N^{-1} values with increasing humidity.

The mentioned DMS from Scionex Corp. USA used a slightly lower reduced field strength (81 Td), but comparable to the field strength applied in the experiments presented here (88 Td). Nevertheless, the overal design and miniturized size of the FAIMS chip showed a different effect on ion-clustering, considering the shorter separation region (50 times), the increased high/low field frequency (7-14 times) and total gas flow (~4.4 times). [50,59] The results have shown that the typical ion clustering/declustering effect depends on the design parameters of the FAIMS/DMS systems when polar analytes (e.g., water) are involved.

The observed shift was also noticed with polar analytes such as acetone and it questions the separation efficiency of miniaturized FAIMS/DMS systems when more polar analytes are used.

This was not the case with BTEX. Non-polar analytes such as BTEX form weaker dimers and water clusters compared to clusters formed only from polar molecules such as water. For example, the standard enthalpy ($\Delta_rH°$) of the proton-bound water dimer reaction is about twice that of the benzene proton-bound water cluster reaction, and tree times that of the proton bound benzene dimer reaction. [83–86] Therefore, BTEX and TMBs have nearly constant CV_{max} N^{-1} values under high electrical fields at different humidity, as confirmed for planar ^{63}Ni-DMS. [59] Wang et al. (2015) established the same for APPI-FAIMS. [34]

The use of the gas-water separation unit for ^{63}Ni-FAIMS detection of non-polar analytes from water enabled, most importaintly, the ion-suppresion from water to be totally avoided, which also implied less interaction of polar water molecules with protonated analyte ions. The humidity fluctuations were prevented and the specific CV_{max} N^{-1} values were reliable and constant, permitting quantitative measurements.

In Fig. 19 summarizes the effects of the gas-water separation unit for four other aromatic VOCs (ethylbenzene; *o*- and *m*-xylene; 1,3,5-trimethylbenzene). At the beginning, after an initial blank phase, the aqueous solution with a sole contaminant was pumped through the gas-water separation unit. Constant monitoring of the aromatic VOC signal was done simultaneously and beyond the water-breaktrough point of the unit as shown in Fig. 19b,d,f,h. Increasing humidity after the breakthrough of the gas-water separation unit caused an immediate change in the previously stable ^{63}Ni-FAIMS signals, as further explained.

Ethylbenzene, *o*-xylene, *m*-xylene and 1,3,5-TMB showed relatively constant signal intensity until the breakthrough of DU occurred, only in the case of *o*-xylene (d), due to humidity variations, inconsistencies were detected. Generally, after the breakthrough of the DU the signals gained on complexity (Fig. 19a,c,e,g) and the signal specificity was lost. This is consistent with the relatively rapid formation of water dimers after the breakthrough i.e. the high sensitivity of ^{63}Ni-ionization to the presence of small amounts of water. It is obvious that for ethylbenzene and *o*-xylene, as for toluene, the $PA_{\text{water dimer}} > PA_{\text{ethylbenzene / } o\text{-xylene}}$ wich results with an immediate intensity decrease (signal suppresion).

Of particular interest is the increase of intensity shortly after the breakthrough for the cases of meta-substituted monoaromatic compounds (*m*-xylene and 1,3,5-TMB; Fig. 19f,h). This phenomenon confirms the “growing” of the water cluster and the positive RIP shift.

According to Goebbert and Wenthold (2004) the registered PA of the proton-bound water dimer is 808 kJ mol^{-1}, which is lower than PA of *m*-xylene (812.1 kJ mol^{-1}) and of 1,3,5-TMB (836.2 kJ mol^{-1}), thus enabling possible further ionization to occur in both cases. [87] The formation of proton-bound water dimers increases steadily with inline humidity as shown by the increase of the specific signal intensity from *m*-xylene and

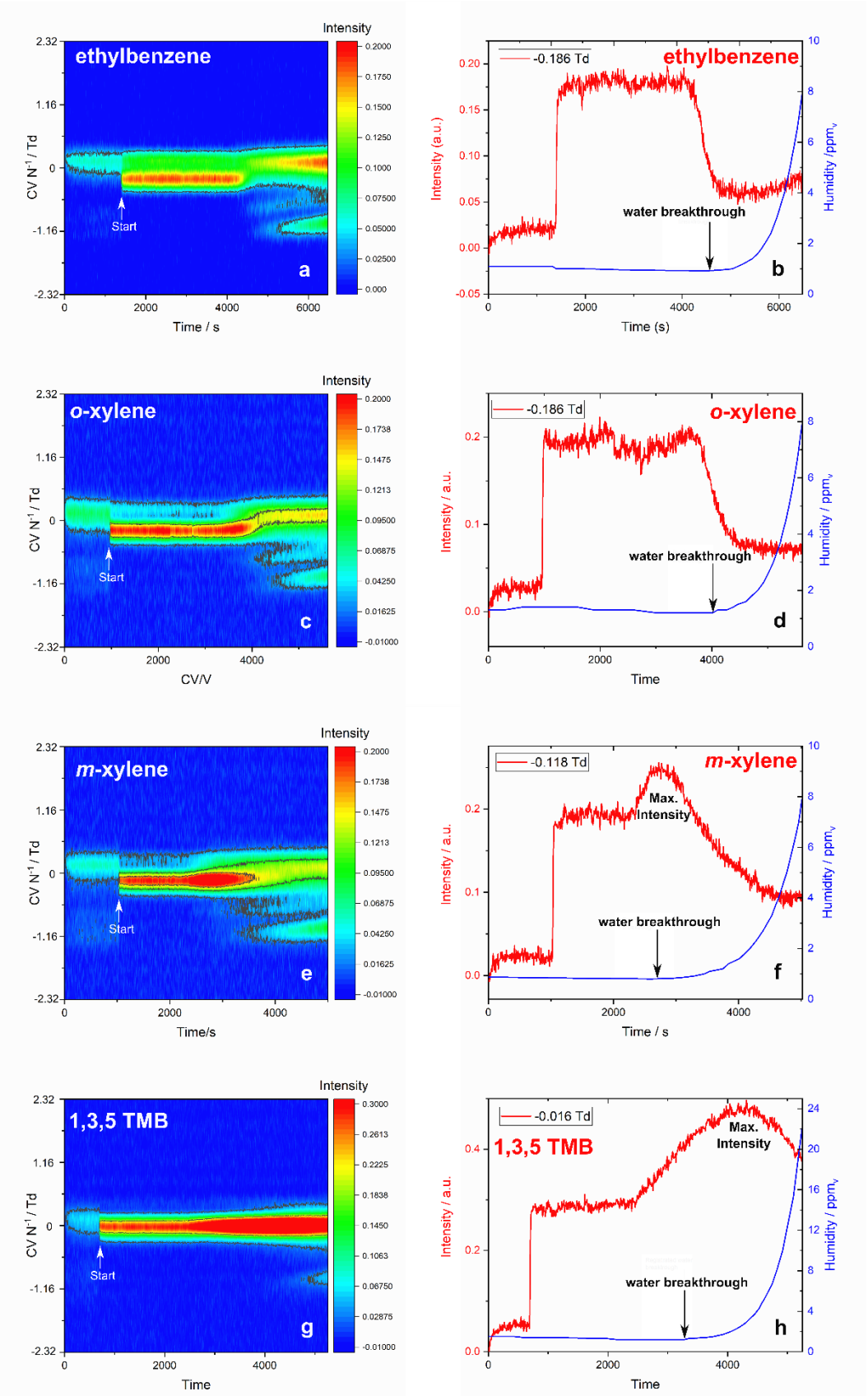

Fig. 19: Continuous monitoring of aromatic VOCs in water with ^{63}Ni-FAIMS before and after water breakthrough of the DU. **b,d,f,h** are extracted analyte specific signals from the continous intensity heat maps **a,c,e,g**; **a,b**) ethylbenzene CV_{max} N^{-1} = -0.186 Td (15.2 mg L^{-1}). **c,d**) *o*-xylene CV_{max} N^{-1} = 0.186 Td (15.2 mg L^{-1}). **e,f**) *m*-xylene CV_{max} N^{-1} = -0.118 Td (14.7 mg L^{-1}). **g,h**) 1,3,5 trimethylbenzene (mesitylene) CV_{max} N^{-1} = -0.016 Td (14.9 mg L^{-1}).

1,3,5-TMB immediately after the water breakthrough (Fig. 19e,g). The intensity maximum of the FAIMS-signals, in both cases, simultaneously represents the moment of maximum concentration of the water dimer in the system, since the ionization of *m*-xylene and 1,3,5-TMB is assisted by the participation of the water dimer, which increases the ionization efficiency.
After reaching a maximum intensity, a similar steady loss of intensity as for the other aromatic VOCs is observed in both cases. Therefore, the further growth of the water cluster, most likely was responsible for the ion suppression of the *m*-xylene and 1,3,5-TMB. The presence of water trimer and larger clusters ($H^+(H_2O)_n$ where n>2) are suspected to be formed as the humidity continuously increases, confirming our previous results (Fig. 19). The possible growth of the water cluster, and the positive CV N^{-1} shift, end in the moment when the strength of the applied reduced electric field (E/N = 88 Td) is greater than the enthalpy of formation of the end cluster ($H^+(H_2O)_n$).

In some cases, the proton affinity (PA) of the water clusters has been reported as an effective proton affinity, with PA values increased by accounting for the association enthalpy of the water molecules. [82] We found the reported value of $PA_{water\ dimer}$ from Goebbert and Wenthold (2004) (808 kJ mol^{-1}) [87] more useful in explaining the intensity phenomena involving *m*-xylene and 1,3,5-TMB. The reported effective $PA_{water\ dimer}$ (827 kJ mol^{-1}) is larger than $PA_{m\text{-xylene}}$ and does not explain the initial intensity increase of *m*-xylene after the breakthrough of DU.

In summary, even slight changes in humidity, when ^{63}Ni-ionization is involved, can lead to significant signal inconsistencies depending on the aromatic VOC. The strong influence of water vapour could be successfully minimized with the drying unit (DU) by effectively separating water from the sample gas flow.

3.3.4.2. The influence of humidity on the detection of aromatic VOCs with APPI-FAIMS under atmospheric conditions

Compared to radioactive ionization, APPI is selective and allows for direct ionization of aromatic VOCs as the primary ionization process generating molecular ions or protonated molecular ions, minimizing other additional unwanted ion reactions in the ionization chamber. Considering $IE_{carrier\ gas} > h\nu_{\ krypton\ lamp} > IE_{\ avoc}$ formation of mostly $M^{\bullet+}$ from the aromatic VOCs (eq. 14) is expected, especially when low humidity conditions are present.This version of APPI-FAIMS has an on-axis design i.e., the Kr-lamp is positioned in the same direction as the ion flow to the detector.

However, a different phenomenon was observed at high humidity when APP-ionization was used (Fig. 20). When an aqueous toluene solution was analysed (36% DF) without DU, the direct ionization of toluene performed under high humidity conditions, resulted in two peaks (e). The peak at $CV_{max}\ N^{-1}$= -0.208 Td was similar to the toluene peak detected from the reference permeation tubes. An increase in the intensity of both peaks (e) was observed by increasing the toluene concentration.
On the other hand, only one peak, the toluene monomer (f), was observed when the DU was applied and the humidity fell below 1.6 ppm_v. The toluene intensity (at -0.208

Td) can improve more than six-fold with the application of the DU (i.e. gas-water separation unit). This was likely related to the difference in initial humidity/condensation in the FAIMS system prior to the application of the DU. Usually such large intensity differences are not observed in the lower humidity range (1.6 - 50 ppm_v) in contrast to ^{63}Ni-ionization. The implementation of the DU resulted in a reliable, quantitative toluene signal as further shown.

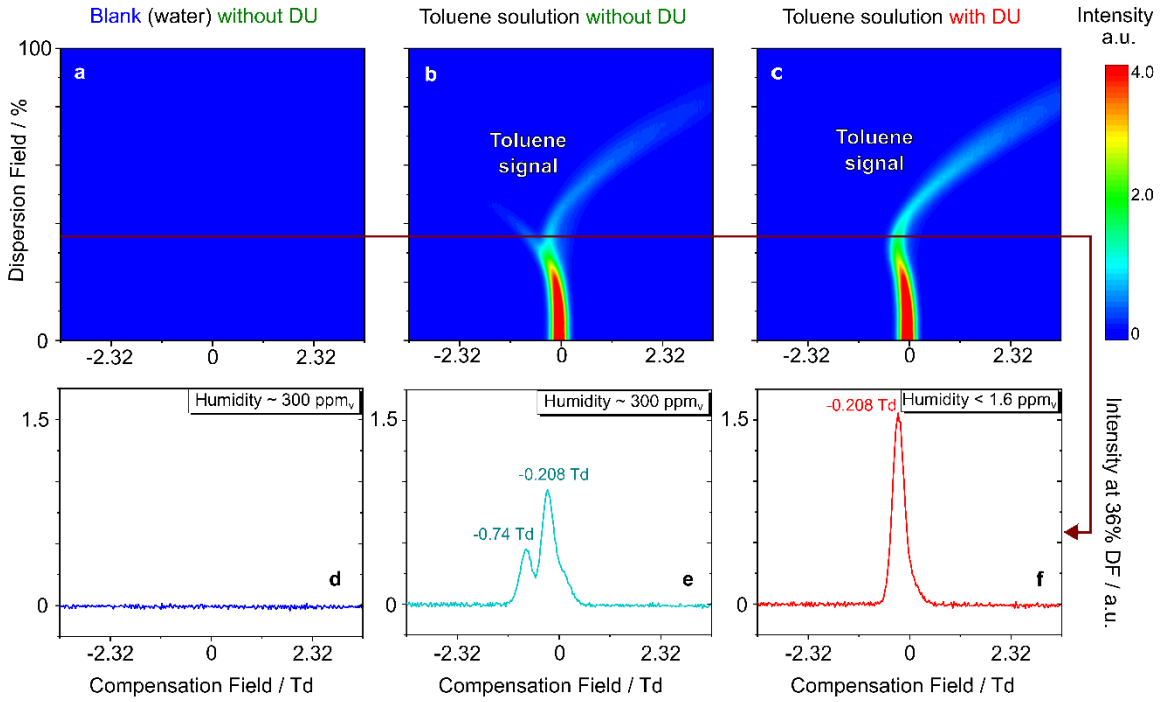

Fig. 20: Humidity influence on APPI-FAIMS. (**a,b,c**) DF/CF heat maps of blank (water) and toluene solution (β=200 mg L^{-1}) with (<1.6 ppm_v) and without (>300 ppm_v) DU. (**d,e,f**) extracted intensity signals at 36% DF (88 Td) for a,b and c successively.

In the presented work the toluene monomer M^+ was the dominant signal at 88 Td (36% DF) when the gas-water separation system reduced the humidity and thus its influence. Dimer formation was a minor issue only at high aromatic VOC concentrations. Klee et al. (2013) [88] observed the same dimer depletion and increased monomer abundance with rising electrical fields. Pressure, the effective ion temperature (T_{eff}) and the reduced electric field strength in the sensor are mainly responsible for increased M^+/M_2^+ ratio by affecting the dimer dissociation rate. [70–72] In the same manner, increased T_{eff} could prevent possible ion-adduct formation, contributing to more consistent CV_{max} N^{-1} values. Humidity on the other hand can influence both, pre- and post-ionization dynamics within the APPI-FAIMS analysis despite the selectivity of APPI towards aromatic VOC.

Fig. 21 shows the change in signal for four different aromatic VOCs with the change in humidity in the system. The first half of the measurements was carried out with a blank (water), then a water spiked with analytes was analysed.

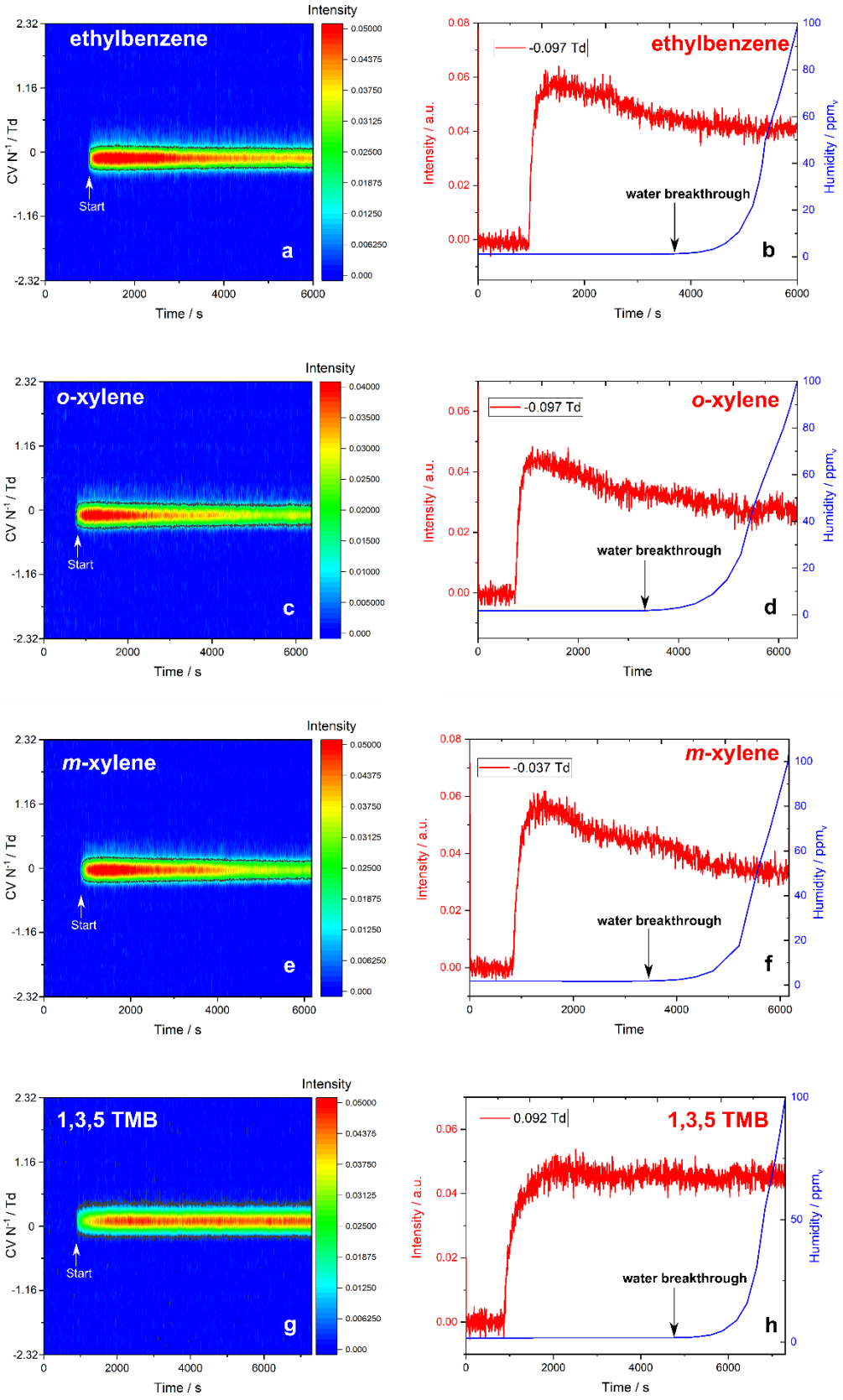

Fig. 21: Continuous monitoring of aromatic VOCs in water with APPI-FAIMS before and after water breakthrough of the DU. **b,d,f,h** are extracted analyte specific signals from the continous intensity heat maps **a,c,e,g**; **a,b**) ethylbenzene CV_{max} N^{-1} = -0.097 Td (14.8 mg L^{-1}). **c,d**) *o*-xylene CV_{max} N^{-1} = 0.097 Td (15 mg L^{-1}). **e,f**) *m*-xylene CV_{max} N^{-1} = -0.037 Td (14.7 mg L^{-1}). **g,h**) 1,3,5 trimethylbenzene (mesitylene) CV_{max} N^{-1} = 0.092 Td (15.2 mg L^{-1}).

Monitoring of the analyte signal was performed according to the previously established specific CV_{max} N^{-1} for APPI-FAIMS. The breakthrough of the DU enabled exponential change of humidity in the system to 100 ppm_v. It was evident that the effect of humidity had far less influence on the signal intensity of the analytes (Fig. 21) as for ^{63}Ni-ionization (Fig. 19). The decrease of signal intensity in the cases of ethylbenzene, *o*-xylene and *m*-xylene was primary due to volatilization of the analytes from water or possibly due to the effect of high humidity (up to 100 ppm_v), which was not the case with 1,2,3, -TMB (g,h). Humidity has shown different effects for different aromatic VOC. This is further shown in examples of the detection of toluene, benzene, *p*-xylene and indane with a humidity increase up to 500-600 ppm_v.

3.3.5. The different influence of humidity on the APPI-FAIMS signal of aromatic VOCs

After highlighting the challenges of FAIMS detection considering different ionization methods, APPI-FAIMS was preferred mainly because of the lower complexity of the acquired signal and its higher selectivity towards the analytes of interest. More importantly, the complicated procedures for possessing and transporting the radioactive source for on-site measurements were also avoided.

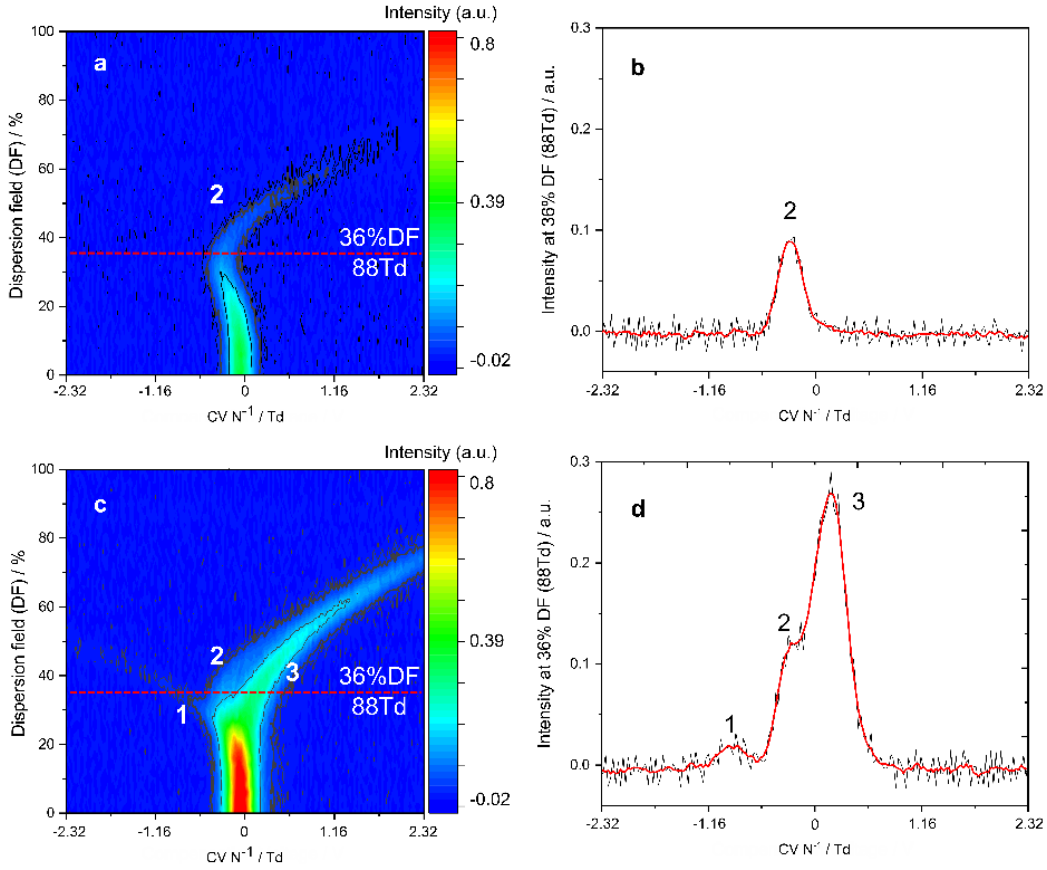

Fig. 22: DF signal fingerprints of toluene (10 mg L^{-1}) in positive mode at different humidity: (a) humidity <1.6 ppm_v with a drying unit (DU) and (c) humidity >300 ppm_v after DU breakthrough. (b,d) Signals at 36% DF (or 88 Td) from (a) and (c) respectively.

The increased humidity did not affect all aromatic VOCs in the same way. Fig. 22 shows the influence of humidity i.e. the impact of the drying unit (DU) from the gas-water separation system on the toluene signal. For this purpose the DU was arranged as shown in Fig. 11, reducing the sample flow humidity to <1.6 ppm_v, obtaining M^+ signal (2) by analysis of a toluene spiked aqueous sample (Fig. 22a). The toluene monomer signal (2) in Fig. 22b was extracted from Fig. 22a at 36% DF (88 Td). For the signal, $CV_{max}\ N^{-1}$ = -0.208 Td, which is specific for the toluene monomer.
With the DU breakthrough the humidity increased (>40 ppm_v) thereby increasing the overall toluene signal intensity (Fig. 22c). In the same time the complexity of the DF matrix increased with the appearance of additional peaks (1) and (3) at the same 36% DF (Fig. 22d). With further increase of the humidity (>400 ppm_v) a decrease of all signals was observed with time, implying suppression of the PID Lamp ionization energy (10.6 eV) by water (IE = 12.65 eV). When the signal intensities at 0% DF (''PID-mode'') were considered (e.g. in Fig. 22a,c), almost 30% increase in toluene signal area at ~400 ppm_v humidity in comparison to 0.3 - 1.6 ppm_v humidity was noted. This suggests that humidity has a different ionization effect on toluene ionization compared to other aromatic VOCs (Fig. 21). Other non-FAIMS systems such as photoionization detectors (PIDs) may also be affected.
A signal increase in intensity was observed together with increased signal complexity for the 40 - 400 ppm_v humidity range at 36% DF. Above 400 ppm_v humidity the ionization suppression of water becomes more relevant, even with high toluene concentrations in the carrier gas.

The same increasing / decreasing, dual role of humidity on intensity, was noticed for the detection of benzene in water. Benzene and toluene are considered less hydrophobic (considering K_{ow} (see Tab. 1)) to the remaining BTEX, indane and TMBs, which did not show the same signal complexity and intensity increase in the 2 - 400 ppm_v humidity range (see Fig. 25). The increase of the toluene signal intensity/ complexity within the humidity range of 40 - 400 ppm_v was contributed to several effects such as stabilized ion charge due to possible toluene-water cluster formation and increased collision frequency responsible for increased transmission efficiency through the electric field, especially at higher toluene concentrations. Such ion-dynamics influence the M^+/M^{2+} ratio and possibly support the detection of toluene-water clusters or even dimer clusters which are not likely to be detected at 88 Td. The result involves positive $CV_{max}\ N^{-1}$-shift / broadening of the signal (2). The appearance of peak (3) (Fig. 22d) at higher $CV_{max}\ N^{-1}$ in comparison to the monomer peak (2) confirms the detection of ions with masses > M^+, indicating the possible presence of toluene-water clusters.
The toluene-water clusters are likely to survive the reduced electric field because of their high concentration and relatively stronger interactions with water molecules compared to other aromatic VOCs.

Peak (1) from Fig. 22d (humidity >300 ppm_v) was assigned to the ionized water cluster. When comparing the signals (1) and (2) in Fig. 22 (a,c) it is evident, on the hand of the lower $CV_{max}\ N^{-1}$ value, that signal (1) is generated by an ion species smaller in mass, with a type A ion behaviour ($\alpha(E/N) > 0$), whereas signal (2) generated by the

toluene monomer M^+ (when humidity <1.6 ppm_v) behaves as type B ion (α(E/N) ~ 0) typical for aromatic hydrocarbons in the 78 - 202 Da mass range. [43]

In order to confirm that indirect ionization of water occurs with APPI-FAIMS in presence of toluene and high humidity, water was pumped through the gas-water separation unit until breakthrough of the DU occurred (Fig. 23a). As shown, no direct

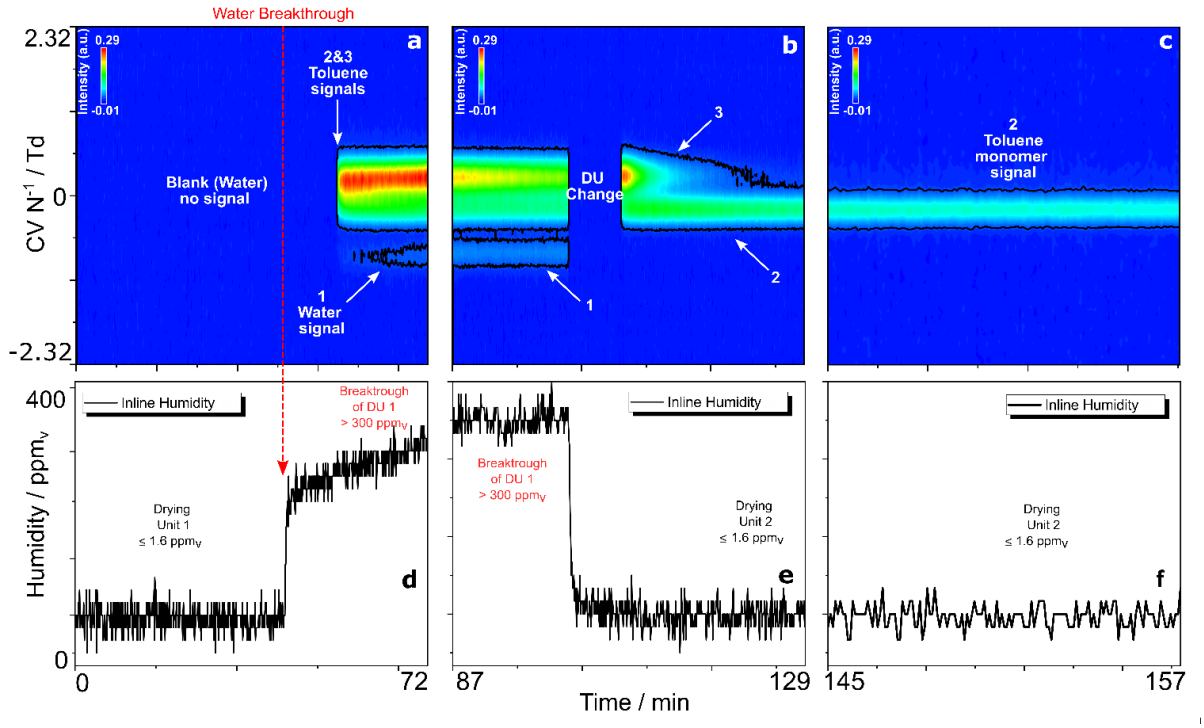

Fig. 23: (**a,b,c**) Monitoring of the influence of humidity on the toluene signal (10.4 mg L^{-1}) in water at 36% DF. (**d,e,f**) Continuous observation of the carrier gas humidity by build-in FAIMS humidity sensor and trace moisture analyzer (ppm_v).

water ionization occurred (by continuous monitoring at 36% DF), although the humidity increased sharply with the water breakthrough of DU. Only after toluene was added to the water (10.4 mg L^{-1}) the signal of the ionized water cluster appeared (1). This is due to possible toluene water interaction addressed in 3.3.4.

With increasing humidity (Fig. 23b), the signal intensity of toluene slowly decreased, but at the same time the intensity of signal (1) increased along with a small positive CV_{max} N^{-1} shift. The positive CV_{max} N^{-1} shift of the proposed water cluster with humidity is comparable to the behaviour of other polar molecules with increasing humidity, as shown for UV-FAIMS by Wang et al. [9] and previously discussed for ^{63}Ni-ionization of ”growing” water clusters in the FAIMS chip.

By changing the DU-1, responsible for the water breakthrough with a new, fully dry DU-2, shown in Fig. 23b,e, the humidity was reduced to below 1.6 ppm_v and the shape of the toluene signal changed (Fig. 23c).

Signal (1), the assumed water-cluster signal, (similar to peak (1) in Fig. 22d) was no longer detectable due to decrease in humidity (Fig. 23c,e) as well as signal (3)

associated with the effect of humidity. Only the specific signal assigned to the toluene monomer M^+ (2) at $CV_{max}\,N^{-1}$ = -0.208 Td remained.

The implementation of the DU kept the humidity relatively constant at low values. Therefore, signal (2) remained constant and enabled quantitative response of toluene in water as confirmed by toluene calibration done in 3.3.6.

Similar development was observed for the detection of benzene (Fig. 24). Here the supposed water cluster signal (1) was with lower intensity, probably because of the

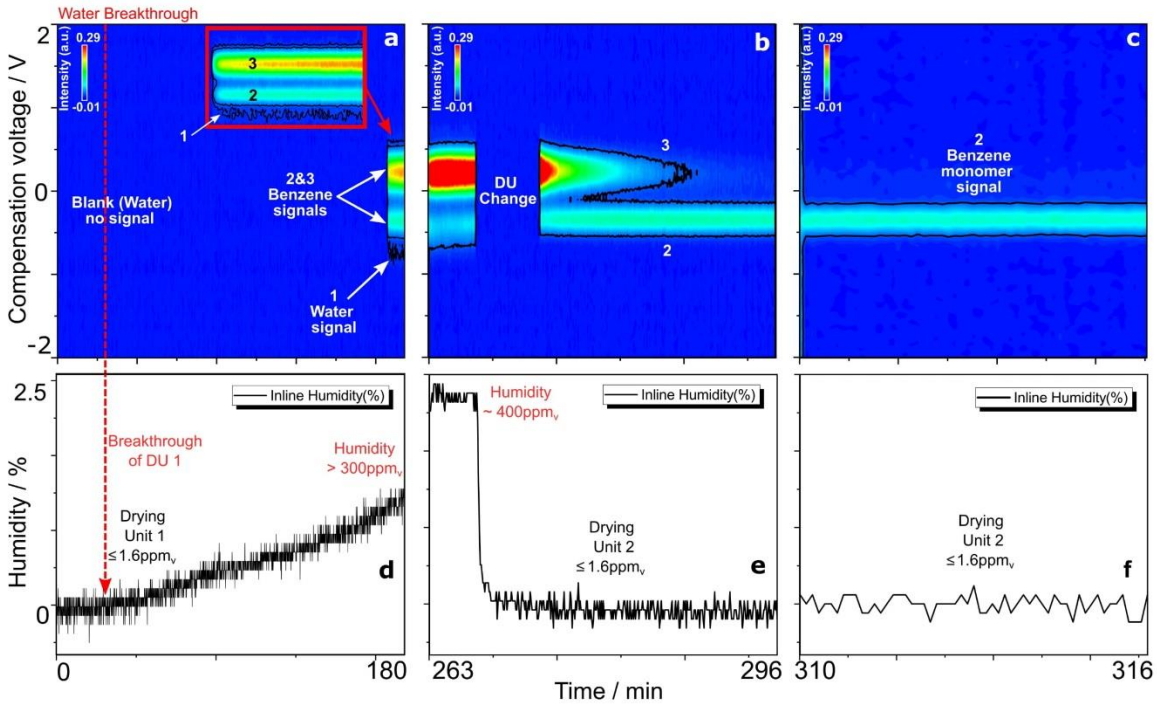

Fig. 24: (**a,b,c**) Monitoring of the influence of humidity on the benzene signal (β = 10.47 mg L^{-1}) in water at 36% DF. (**d,e,f**) Continuous observation of the carrier gas humidity by build-in FAIMS humidity sensor and trace moisture analyser (ppm_v).

formation of phenyl radical which had a higher PA and the involvement of protic solvents such as water which form large clusters and have an increased possibility for hydrogen abstraction from toluene and benzene, as addressed in 3.3.5.1.

The signal complexity of benzene increases, as with toluene, by producing an additional signal (3) originating from benzene, most probably due to the enhanced interaction with water.

In comparison to toluene and benzene no additional signals were observed with the humidity increase for the detection of aromatic VOCs such as ethylbenzene, xylenes, TMBs and indane. For the detection of *p*-xylene a relatively small, steady increase of the M^+ signal corresponding to the humidity increase was noticed, probably due to the before mentioned stabilization of the ion charge (Fig. 25a).

In contrast, the signal related to indane was not influenced even at high humidity (up to 416 ppm_v), as shown in Fig. 25b.

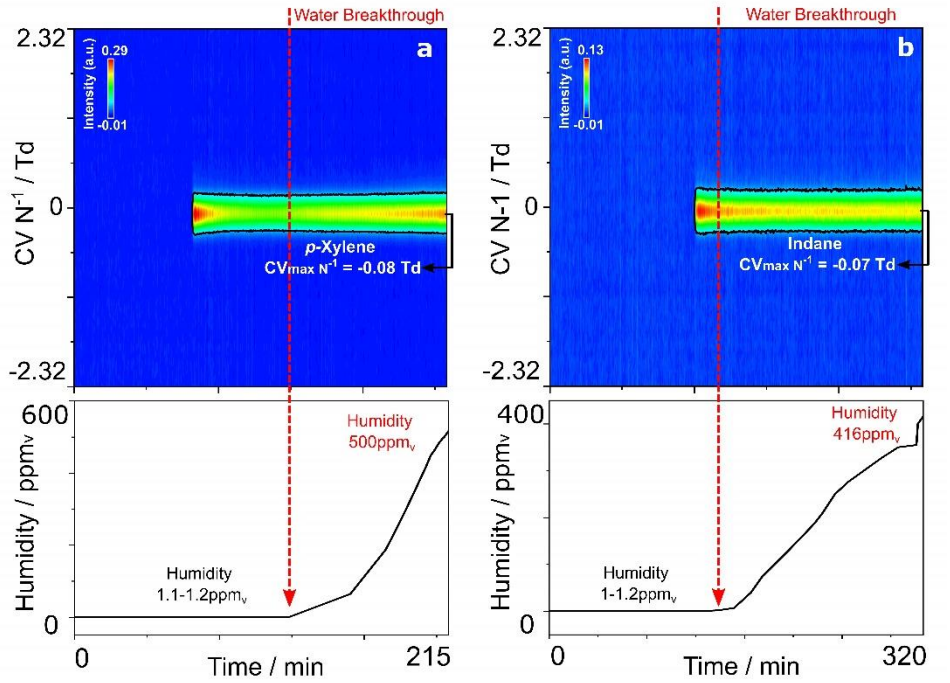

Fig. 25: Humidity influence on (**a**) p-xylene (β = 22 mg L^{-1}) and (**b**) indane (β = 12.4 mg L^{-1}) signals at 36% DF before and after water breakthrough of the drying unit (DU).

In order to minimize the different effects of humidity on various aromatic VOCs, the DU (humidity ≤ 1.6 ppm_v), as a part of the gas-water separation system, was applied for further analyses and on-site applications.

3.3.5.1. Crucial factors for the overall intensity increase and ionization of water clusters with APPI-FAIMS at high humidity conditions

The increased formation of toluene-water clusters or possibly toluene dimers prior to entering in the ionization region (pre-ionization) can later produce an overall increase in signal intensities. The increase of the ionization efficiency is due to decrease in IE of the formed toluene-water clusters [89] or toluene dimers (IE=8.34 eV). [90] As Li and Bernstein [89] showed, the apparent IE of $M(H_2O)_n$ can decrease with the increasing number of water cluster molecules (n) for toluene (Fig. 26), thus increasing ionization efficiency and the overall signal intensity of toluene.

Subsequent photo-fragmentation of the ionized toluene-water cluster ($M^+(H_2O)_n$) can occur before ions arrive to the FAIMS chip, knowing the krypton lamp characteristics [91,92] and its placement in the direction of the carrier gas/ion-flow. In this way the supposed water cluster signal (1) can be separately generated (generation time 60 ns) [89] and detected by FAIMS, especially at higher humidity and analyte concentrations. Cluster fragmentation can also occur by the influence of the reduced electric field.

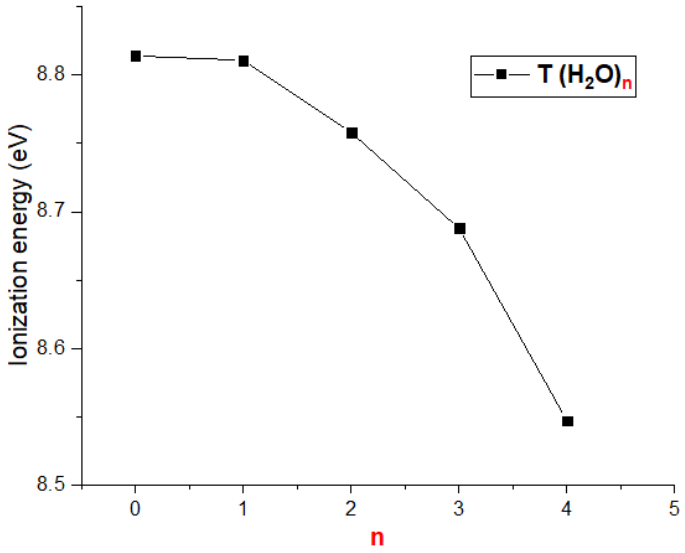

Fig. 26: Apparent ionization energy (IE) of toluene-water clusters [89].

In this case, the fragmentation of the toluene-water cluster can have two described outcomes. [89]

Firstly, when $M^+(H_2O)_n$ is fragmented to e.g. $M^+(H_2O)_{n-1}$ without producing a protonated water cluster/s for cases n < 3. Secondly, for the case when n ≥ 3, favourable for formation of protonated water clusters $H^+(H_2O)_n$ and a stable benzyl radical. [89]

Similar intracluster proton transfer reactions were observed for benzene with formation of phenyl radical (through hydrogen abstraction) but for clusters n ≥ 4 due to the higher PA of the phenyl radical compared to benzyl radical. [93] The higher PA of the phenyl radical could explain the apparent decrease of water-cluster ionization for benzene.

Other post-ionization factors that may contribute to the increased intensity due to increased humidity include the likely charge stabilization effect on the toluene and benzene ions through formation of proton-bound water clusters $MH^+(H_2O)_n$, that promote the transmission/detection of ions in the FAIMS.

It is also worth mentioning the possibility of hydrogen abstraction/proton transfer from benzene or toluene when a protic analyte such as water is involved at high concentrations after APP-ionization of the analytes, as shown in Nazarov et al. (2006) [56] and Syage et al. (2004). [97]

Probably the biggest factor contributing to the detection of toluene-water clusters at high reduced field strengths is the miniaturization of the FAIMS. The filter and separation region is 300 µm long with a resulting nominal residence time for the ions of 68 ns. The effective extraction of humidity due to the use of DU avoids the possible interaction with the analytes before and after ionization. This provides a rather simple way to generate a reliable quantitative determination in the form of a specific VOC sum signal.

3.3.6. Calibration of aromatic VOCs in aqueous samples

The intensity signal from the toluene monomer at low humidity (<1.6 ppm_v) (Fig. 23c) was used for the calibration determination of toluene in aqueous samples using the experimental setup shown in Fig. 11 at 88 Td (36% DF) represented in Fig. 27 and Fig. 28. If the calibration is based on peak area instead of intensity, similar results and correlation coefficients are obtained; for practical reasons, the latter method was chosen for on-site monitoring. An additional calibration at 0% DF (in “PID mode”) was also performed. The results of the calibration are shown in Tab. 8.

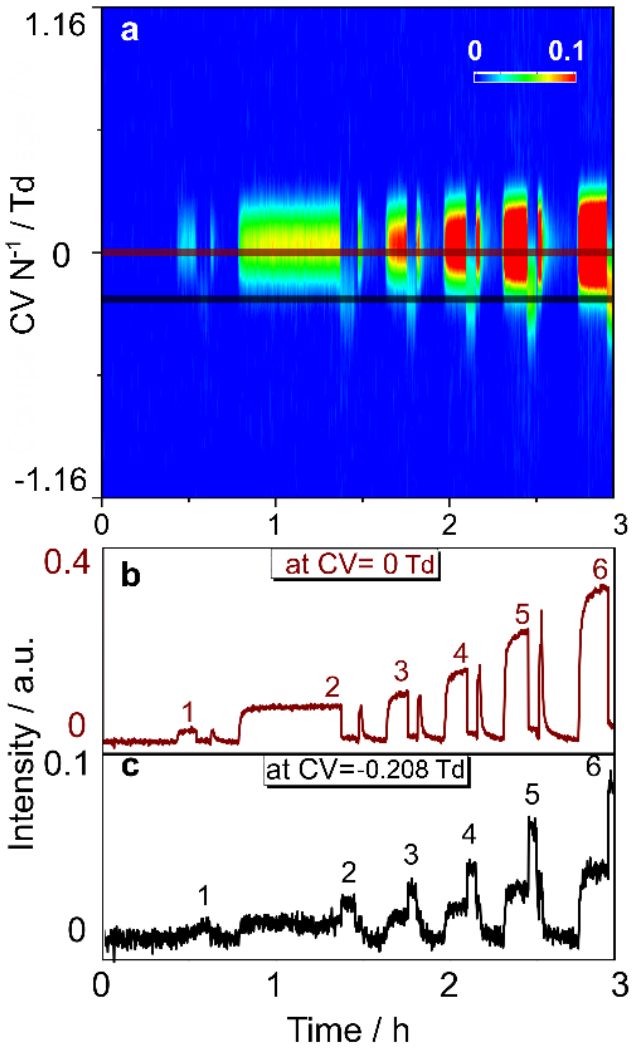

Fig. 27: (a) Calibration heat map of toluene in water with APPI-FAIMS and extracted intensity signals at (b) 0 and (c) 36% DF.

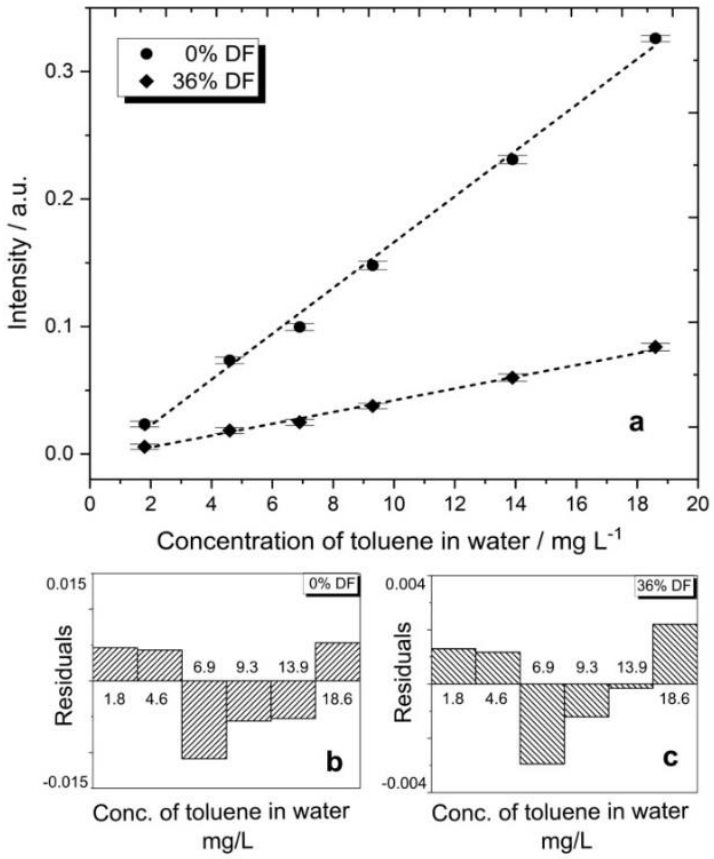

Fig. 28: (a) Calibration curves of toluene in water at 0% DF and 36% DF for setup like in Fig. 11 (SU length 18 cm); (b,c) residual plots of the calibration curves.

Fig. 28 shows the calibration of toluene in water encompassing a) heat intensity map and b) the corresponding extracted intensity signals for six points of calibration at 0 and 36% DF. As expected the peak at 0% DF is more sensitive at low humidity, but does not provide the ability for identification based on $CV_{max}\,N^{-1}$.

Tab. 8: Toluene calibration data from Fig. 28.

Dispersion field	Intercept	Slope	r^2	S/N[a]	LOD[b]	LOQ[b]
(%)					mg L^{-1}	mg L^{-1}
0	-0.145	0.018	0.996	1.47	0.89	3
36	-0.0045	0.0047	0.996	3.16	0.92	3.1

a) blank + $3SD_{blank}$.

b) [94] (see Experimental).

The decrease in sensitivity when a high field was applied was expected due to the difference in ion transmission efficiency between 0% and 36% DF, which is approximately 3.8 times higher at 0% DF for the detection of toluene. Linearity of the

calibration curves (Fig. 28a) was confirmed in both cases (for 0% and 36% DF) according to Mandel's fitting test. [95] The memory effect of the gas-water separation system depended mostly on the SU and on the analyte concentration in water.

The memory effect of the microporous Teflon membrane (SU) is considered to be much lower than that of the previously mentioned tubular PDMS membranes. Multiple successive calibrations were performed from low-to-high concentrations of toluene, then high-to-low and again for low-to-high concentrations with the same drying column and toluene solution. The calibration curves have shown very good repeatability; with a relative standard deviation (RSD) of the calibration slope of 2.6% (0% DF) and 5% (36% DF), for seven calibrations over a period of three days and three different toluene solutions. The relative standard deviation for the six separate calibration points (APPI-FAIMS at 0% DF) showed 2.79% difference in average.

Regarding the memory effect, when high concentrations of toluene were detected in the water (35 mg L^{-1}), less than 10 min was sufficient to clean the gas-water separation unit including the drying unit (Fig. 29). Indane and TMB were found to have a longer cleaning time compared to toluene and benzene [16], partly due to their lower vapor pressure, but always depending on the concentration of analytes in the water/groundwater.

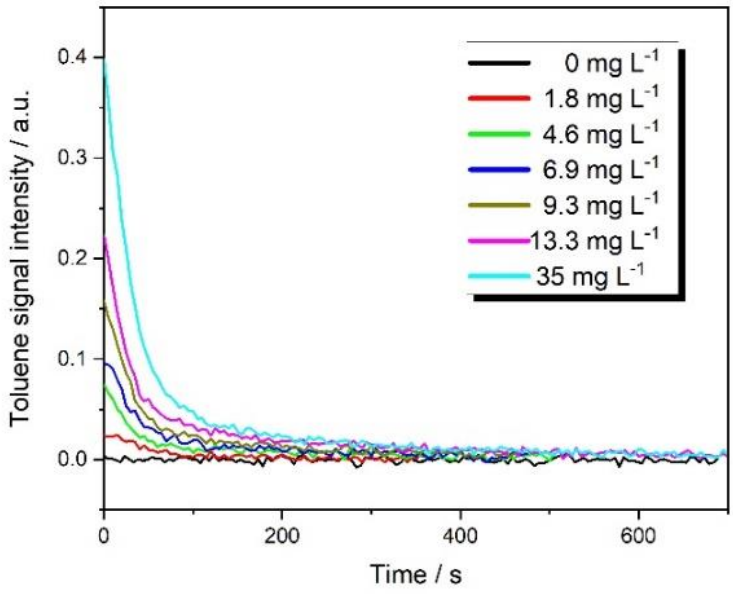

Fig. 29: Cleaning time of the Gore-Tex® microporous tube membrane (SU) and the drying unit (DU) for different toluene concentrations by APPI-FAIMS at 0% DF.

Calibration curves for selected aromatic VOCs are shown in Fig. 30 and the corresponding limit of detection values (LOD) are shown in Tab. 9.

As can be seen, the highest sensitivity to Kr-lamp photoionization under atmospheric conditions was observed for the determination of benzene, although it has the highest IE compared to the other aromatic VOCs.

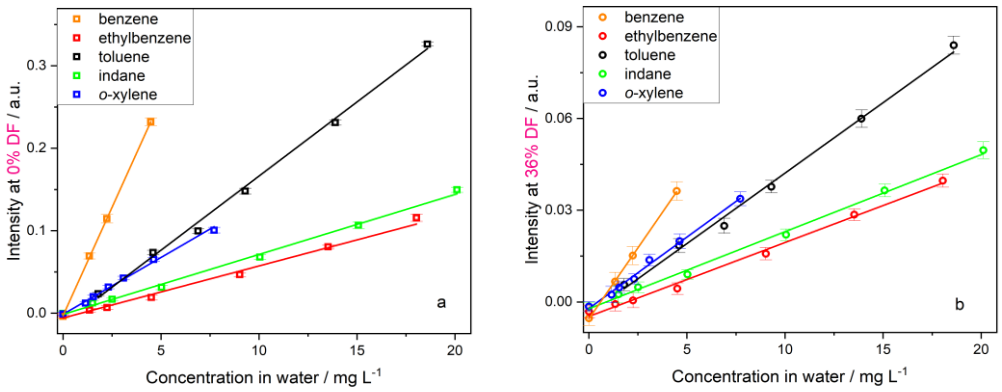

Fig. 30: Calibration of aromatic VOC from water (20-23°C) by APPI-FAIMS when (a) no electric field was applied (0% DF) and (b) with 88Td (36% DF); water flow 4mL/min, carrier flow 1L/min (N2) and sample flow 0.1L/min (N2) at T(SU) = 30°C.

With the increase of the benzene concentration in water, the concentration in the gas phase increased accordingly over a short linear region extending only to ~ 5 mg L^{-1}. A further increase in concentration resulted in an abrupt increase in sensitivity; this phenomenon was also described by Walendzik et al. (2005) for the detection of benzene by photoionization using IMS. [11] Beside the benzene concentration in water the increased sensitivity was connected to the intensity of the Kr-lamp.

Tab. 9: Calibration data for the selected aromatic VOC as shown in Fig. 30.

Aromatic VOCs	**0% DF**			**36% DF**		
	LOD	r^2	S/N [a]	LOD	r^2	S/N [a]
	mg L^{-1} [b]		mg L^{-1}	mg L^{-1} [b]		mg L^{-1}
Benzene	0.07	0.999	0.09	0.09	0.999	0.78
Ethylbenzene	1.1	0.992	1.8	0.9	0.995	3.27
o-Xylene	0.3	0.996	0.355	0.35	0.995	1.09
Indane	0.78	0.996	1.3	0.73	0.997	1.99

a) Averaged blank signal + 3 * SD_{blank}
b) [94] (see Experimental part 3.2.)

A likely reason for the increased sensitivity of benzene was the clustering of benzene molecules before ionization. The formation of benzene dimers prior to

photoionization can significantly increase the ionization efficiency due to the reduction of the IE (IE $_{Benzene}$ 9.25 > IE $_{Benzene\ dimer}$ 8.65). [90] The possible photo-fragmentation and high field strength (high T_{eff}) enable the dominant presence of the benzene monomer signal positively influencing the sensitivity. This aspect should be considered upon possible on-site application of APPI-FAIMS. A low benzene concentration in groundwater was an advantage in this regard. However, at high concentrations, benzene with its high IE could act as a dopant and be more sensitive to changes in groundwater contamination with aromatic VOCs. Therefore, prior determination of the groundwater contamination profile using standard analytical techniques is important.

3.3.7. Specific aromatic VOCs sum-signal in low humidity conditions

The established low humidity conditions in presence of DU are of great importance when quantitative or semi-quantitative monitoring of contamination is required. Sielemann et al. (2000), in a similar application of UV-IMS, concluded that it is difficult to quantify a single substance in a binary mixture when there are interactions between different ions. [96] In the meantime, some success has been achieved (Langejuergen et al. (2014) [60]). Nevertheless, in our case, the inclusion of a low-cost stand-alone FAIMS system with resolution limitations addresses the practicality of implementing a so-called sum-signal generated by dopant effects and its reliability.

Here it will be shown how the absence of water (< 1.6 ppm_v) positively influences the charge transfer between the multiple aromatic VOCs in the FAIMS and the production of stable and reliable specific contamination signal, further addressed as

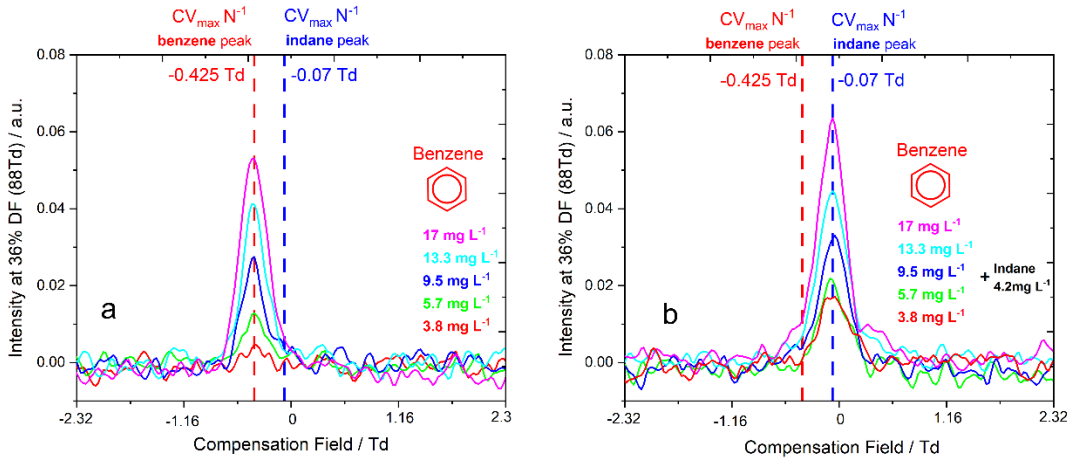

Fig. 31: Effective charge transfer for benzene and indane under low humidity conditions (< 1.6 ppm_v). a) Increasing benzene concentration and the appropriate signal from gas-water separation APPI-FAIMS. b) Increasing signal of benzene from Fig. 31a with the addition of 4.2 mg L^{-1} indane.

specific sum-signal, which can be possibly used in semi-quantitative monitoring purposes. Fig. 31 shows the effective charge transfer between two compounds (benzene and indane) that have ~200 to ~100 collisions in the low and high field per cycle in the FAIMS chip, respectively, according to Wilks et al. (2012). [51]

Since the ionization energy of indane is less than the IE of benzene, indane acts as a charge receiver and utilizes the dopant effect due to the probable collision-induced benzene charge transfer to generate a suitable response signal from water. It was obvious that the effectiveness in secondary ionization of indane increased proportionally with the increase of benzene concentration. This resulted in formation of a specific sum-signal that showed increased intensity (16.8%) compared to the highest benzene concentration and shifted to a specific CV_{max} N^{-1} value as indane (-0,07 Td) (Fig. 31).

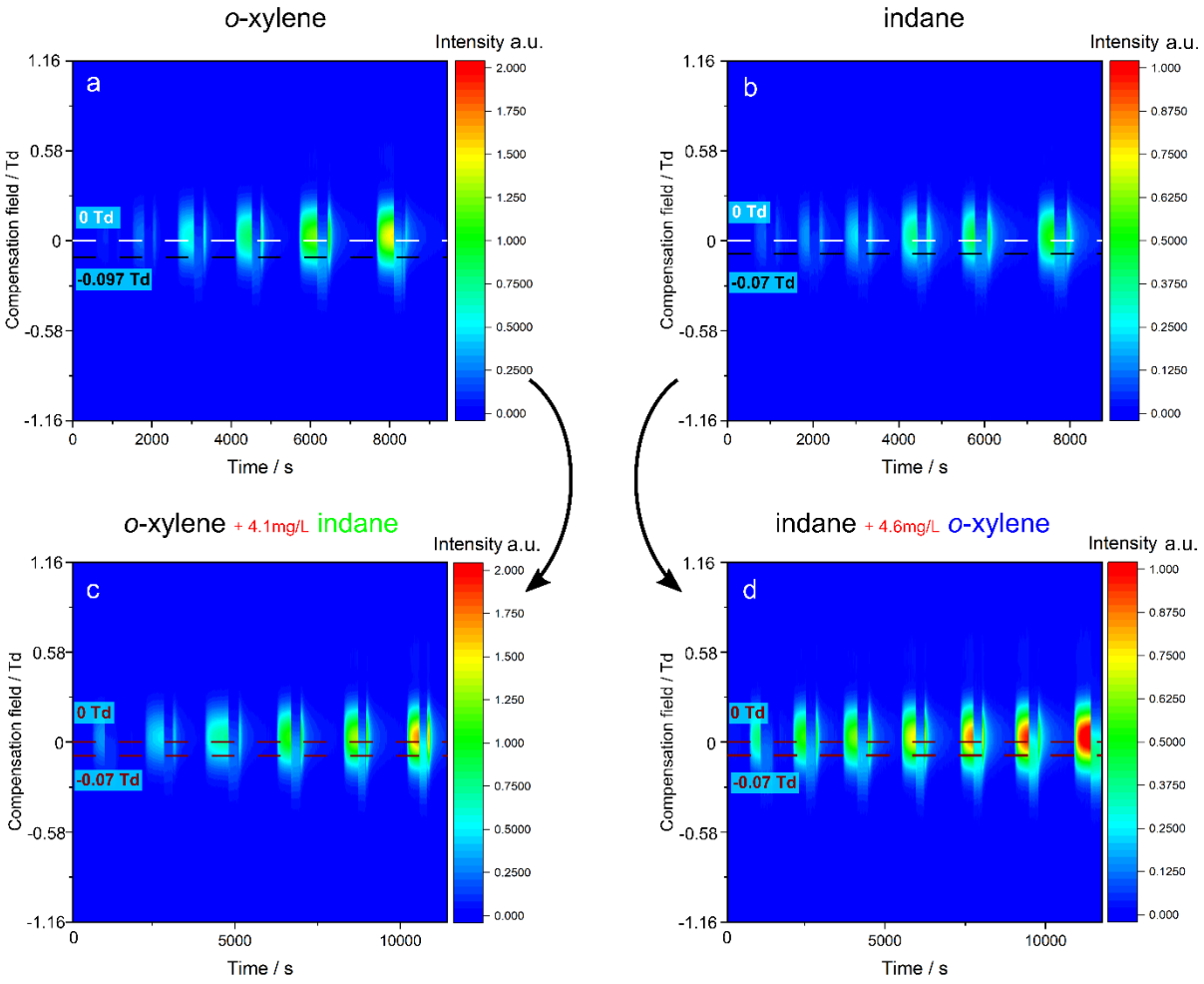

Fig. 32: **a**) Continuous calibration of *o*-xylene at 0% DF (0 Td) and 36% DF (-0.097 Td). **b**) Continuous calibration of indane at 0% DF (0 Td) and 36% DF (-0.07 Td). **c**) Continuous calibration of *o*-xylene spiked with 4.1 mg L^{-1} indane at 0% DF (0 Td) and 36% DF (-0.07 Td). **d**) Continuous calibration of indane spiked with 4.6 mg L^{-1} *o*-xylene at 0% DF (0 Td) and 36% DF (-0.07 Td).

Different binary systems were tested and gave similar results to those obtained for the detection of *o*-xylene and indane (Fig. 32). The linearity of the external calibrations is maintained in all cases where a second analyte has been added. (e.g., Fig. 33). The CV_{max} N^{-1} shift in this case was not as obvious as in the previous example because of the insufficient CV_{max} N^{-1} resolution and relatively small difference (0.027 Td) of *o*-xylene and indane signal. The calibration curve of the extracted intensity signals from the compensation field heat maps Fig. 32 is shown in Fig. 33.

It was confirmed that the concentration ratio between the analytes in the binary water solution does not affect the linearity of the calibration curve. The addition of *o*-xylene had decreased the correlation coefficient of the indane calibration curve. The LOD calculated by using the calibration line method did not improve [67], but after addition of indane 23% improvement was observed strictly by the improvement of r^2. The S/N-determined LOD for both cases has improved (decreased) significantly.

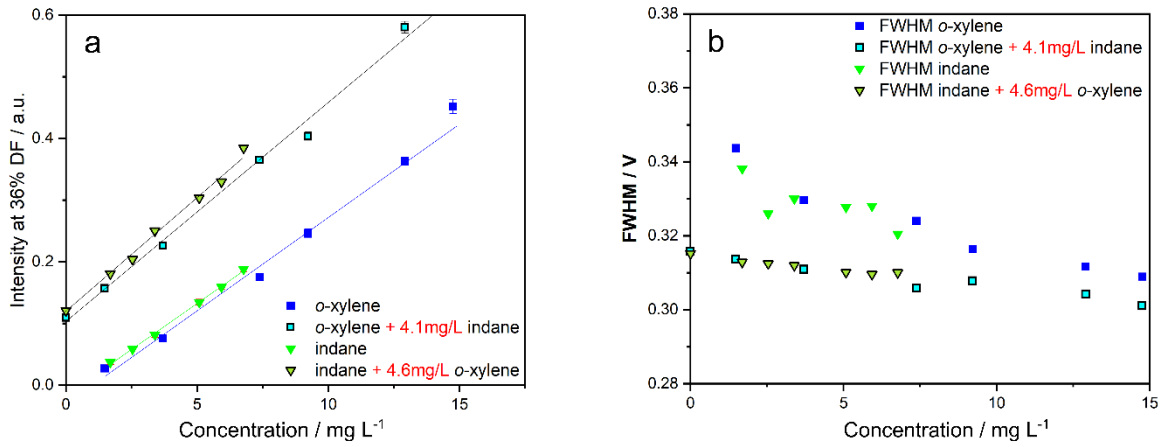

Fig. 33: **a**) Calibration curves from Fig. 32 (-0.07 Td) depicting the mutual dopant effect (with r^2 > 0.988 in all cases); **b**) Full width at half maximum (FWHM) for the peak signals from Fig. 33a.

Spiking the sample leads to an increase in concentration and to an enlargement of the signal intensity by about 0.1 a.u. on average. However, it is remarkable that the differences in the FWHM of the spiked and non-spiked samples are very marginal and thus negligible (Fig. 33b). Therefore, the possibility of simultaneous existence of two dominant ionized entities was discarded. Increased FWHM at lower concentrations was more seen as a part of the emphasized noise effect. Peak widening was not detected with any other combination of analytes. In this way, with an effective charge transfer in absence of water interference, formation of reliable, semi-quantitative characteristic sum-signal is possible. This sum-signal could be essential in groundwater monitoring purposes.

In Fig. 34 a characteristic sum-signal of benzene, ethylbenzene and indane in water is monitored. After the initial intensity peak (b) due to change of the aqueous solution a relative constant intensity was maintained. There was no peak broadening registered. The FWHM of 35.6 Td was well into the same FWHM range from Fig. 34c.

The CV_{max} N^{-1} of the sum-signal from the three contaminants was established at -0.07 Td (for 36% DF) and related to indane. Indane served as a charge acceptor for the rest of the ions because of its lower IE (IE benzene > IE ethylbenzene > IE indane) (see Tab. 7). This was one more evidence of the effective charge transfer in the FAIMS and the possibility of producing specific sum-signal with quantitative character after successful extraction of water with the gas-water separation unit (< 1.6 ppm_v).

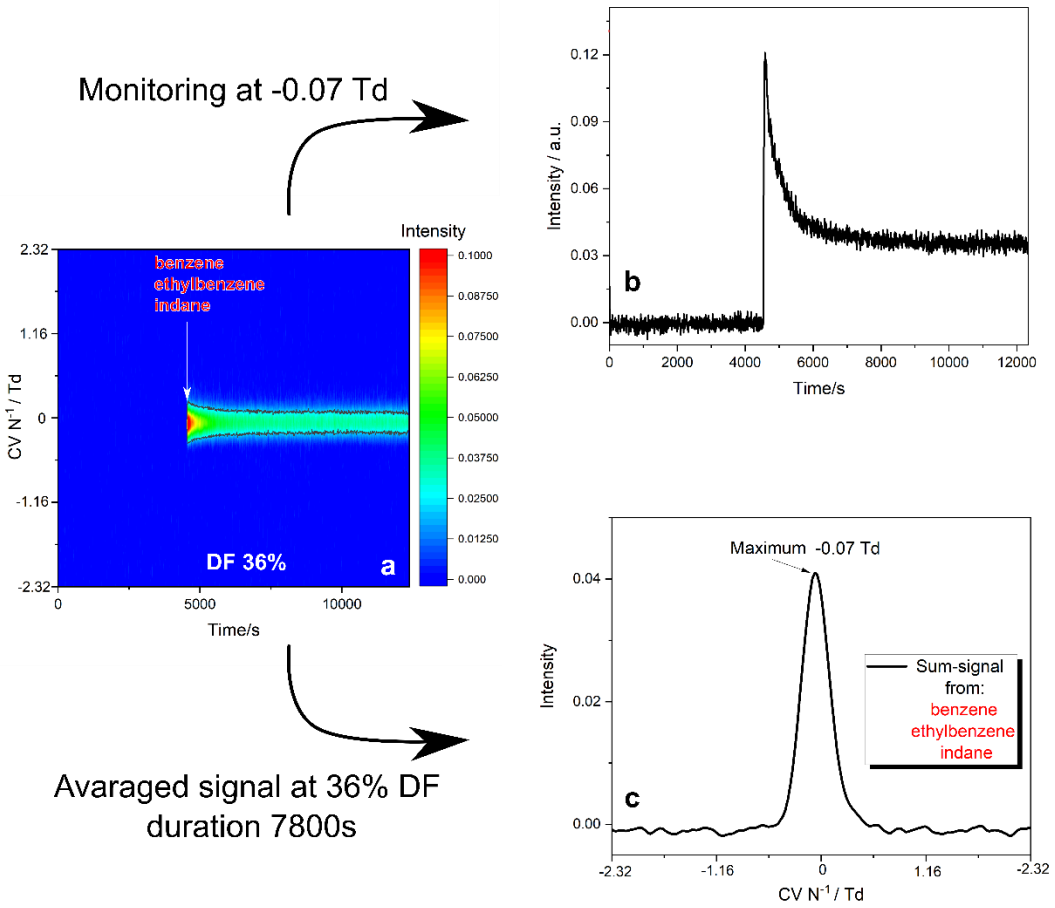

Fig. 34: Dopant effect involved in the production a specific sum-signal from three aromatic VOCs (benzene ß= 3.1 mg L^{-1}, ethylbenzene ß= 3.1 mg L^{-1} and indane ß= 3.4 mg L^{-1}). a) Signal monitoring at 36% DF. b) Extracted signal at 36% DF and CV_{max} N^{-1} = -0.07 Td. c) Specific sum-signal/ sum-peak for the whole monitoring duration.

3.3.8. Monitoring of aromatic VOCs in contaminated water by gas-water separation APPI-FAIMS under laboratory conditions

To further investigate the capabilities and limitations of the gas-water separation APPI-FAIMS system for monitoring real samples, a VOC-contaminated groundwater sample was collected, stored, and sampled under laboratory conditions at different time periods. The objective was to successfully monitor contaminant depletion / degradation in groundwater samples by using the generated sum intensity / sum area signal of the aromatic VOCs at 0% and 36% DF (Fig. 35a,b,c,d). At the same time, the control of the contamination status of the groundwater samples was carried out by HS-GC/MS in parallel with APPI-FAIMS (Fig. 35e,f,g,h). The HS-GC/MS results as total signal intensity/total signal area were compared with the sum signals (area/intensity) obtained by APPI-FAIMS at 0% and 36% DF. The signal depletion was well correlated in both cases. HS-GC/MS showed a nearly linear negative trend with storage time, and direct analysis of the groundwater samples by gas-water separation APPI-FAIMS successfully reflected this depletion trend.

Effective ion charge transfer in the FAIMS detector resulted in a peak at 36% DF (turquoise) with a CV_{max} N^{-1} of -0.07 Td, identical to the CV_{max} N^{-1} of indane, which

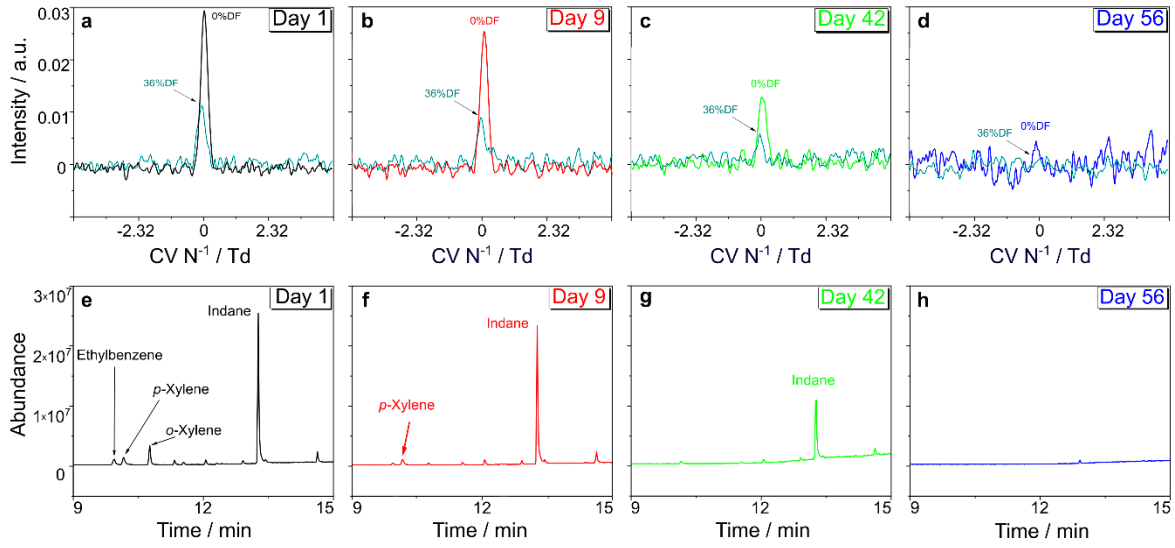

Fig. 35: (a,b,c,d) Monitoring of contaminated groundwater sample by APPI-FAIMS at 0% and 36% DF (data acquisition: 1 min signal average). (e,f,g,h) Analysis of the same samples by HS-GC/MS in laboratory conditions.

possibly served as the main charge receptor. This is consistent with IE of the identified compounds, which contribute to the sum-signal of indane (or *p*-xylene) via the dopant effect. [97] Due to changing analyte concentration ratios the ionization dynamics could influence the analytical sum-signal. This kind of change was noted at day 9 for the sum intensity signal at 36% DF. Depletion of analytes (ethylbenzene, xylenes) responsible

for the dopant effect (cf. Fig. 35e,f) caused ~10% larger intensity decrease at day 9 in comparison to HS-GC/MS control by influencing the ‘‘indane’’ ionization. Such specific signal changes can also be useful indicators in monitoring observations.

The decreasing signal intensity/area of aromatic VOCs in the real groundwater samples (Fig. 35) was again overlaid in Fig. 36. The intensities of the signals correlated well with the almost linear loss of total peak area and intensity of the real samples analysed with HS-GC/MS as control. Fig. 36 shows even better the dependence of the sum-signal from the decrease of dopant contaminants for day 9 compared to day 1.

Low concentrations of VOCs in water were more difficult to track due to the lower signal intensity, i.e., higher signal-to-noise ratio, and resulted in an overestimation of intensity for 0% DF on day 56. One way to overcome this problem and increase sensitivity at 36% DF was to increase the membrane separation unit (SU), i.e., the water-gas exchange area.

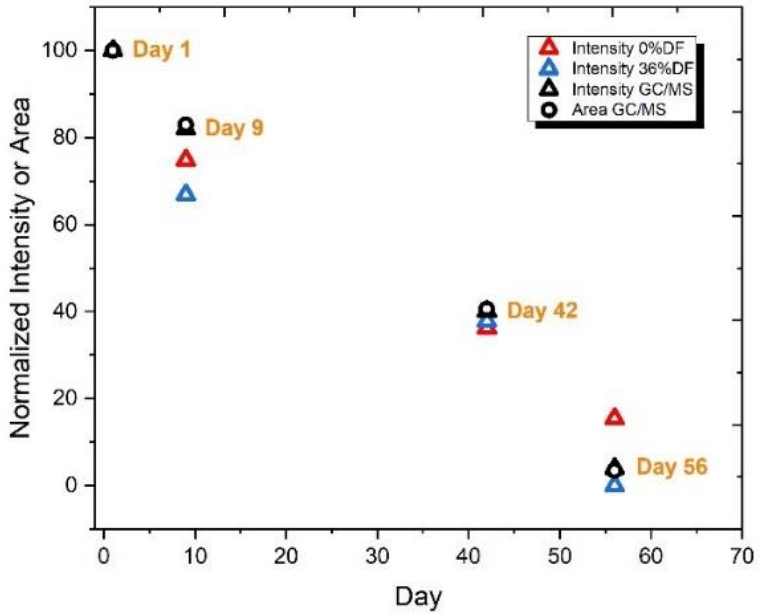

Fig. 36: Monitored intensity and area signals of APPI-FAIMS at 0% DF (red) and 36% DF (blue); Total area and intensity of HS-GC/MS control measurements (black).

Generally, the feasibility of the method was proven when the humidity in the system was lowered and kept stable in a very low range. Similar to this successful laboratory application of the gas-water separation APPI-FAIMS, an on-site monitoring was performed and addressed in the following chapter (4).

3.4. Conclusion

Using APPI-FAIMS, it was found that the effects of humidity on the AVOCs during APP-ionization and post-ionization increase the complexity, but more importantly the intensity, of the signals obtained to varying degrees compared to the use of ^{63}Ni-FAIMS. The high humidity presence (~ 400 ppm_v) had a major impact, especially on the ionization efficiency of toluene and benzene, which were found on the contamination site. The toluene ionization efficiency in the presence of high humidity increased to about 30%. This was due to the toluene-water cluster $M^+(H_2O)_n$ fragmentation, which, similar to the analysis of benzene, contributed to increased ionization efficiency. The fragmentation was also the cause for the detection of water clusters. This was observed for the non-polar analytes that had stronger interaction with water molecules (e.g. benzene, toluene).
When analysing indane, TMBs and other non-polar contaminants, the values were signifcantly lower and in some cases (e.g., TMB) no signal change was observed with increasing humidity. Xylenes such as *p*-xylene also showed an increase in signal intensity with increasing humidity, but to a much lesser extent than benzene and toluene.

Finally, an increase in humidity (> 400 ppm_v) decreased the sensitivity of APPI-FAIMS for all analytes. The implementation of the gas-water separation system in combination with APPI-FAIMS reduced the different effects of humidity on various aromatic VOCs providing stable conditions for acquiring reliable signals. This also minimized the effect of humidity on the charge-transfer reactions between multiple analytes, minimized the increase in intensity by some analytes (toluene and benzene), and greatly simplified the ion-chemistry in the FAIMS, resulting in the formation of a specific aromatic VOC sum-signal, thus enabling successful on-site, monitoring of the contamination trend in groundwater. The semi-quantitative response of specific aromatic VOC sum-signal was confirmed for several analyte combinations.

The gas-water separation unit included a PTFE tube as a separation unit (SU) and a P_2O_5 filled glass column (DU) separately coupled to both FAIMS detectors. The gas-water separation unit successfully decreased and maintained the humidity content to < 1.6 ppm_v, which has also enabled an appearance of a quantitative signal for ^{63}Ni-FAIMS. In the same time the unit showed relatively fast cleaning times (2 - 3 min) for higher AVOCs concentrations, nevertheless it was greatly dependent on the analyte. The gas-water separation APPI-FAIMS provided successful single contaminant calibration for the principal contaminants involved in the groundwater contamination. The limit of detection (LOD) of benzene, toluene, ethylbenzene, *o*-xylene and indane in water was 0.1, 0.9, 1.1, 0.3, 0.8 mg L^{-1} at 0% DF and 0.1, 0.9, 1, 0.4, 0.7 mg L^{-1} at 36% DF, respectively.

4. Investigations on the impact of groundwater remediation by the use of OxyTech® membrane

4.1. Introduction

In-situ remediation and monitoring of groundwater contamination is increasingly replacing classical pump-and-treat systems, as these can often no longer be operated economically due to lower contaminant concentrations. As the contaminant concentration in groundwater decreases, the efficiency of the pump-and-treat process decreases significantly. [9] Therefore, additional remediation methods are also employed to meet the imposed environmental requirements dictated by sensitive advanced analytical methods for integral groundwater remediation under the given circumstances. A variety of remediation techniques are developed and implemented in support of natural attenuation (part 1.2). The pathways and rate of natural attenuation are affected by contamination concentration, subsurface geochemistry, hydrogeology and availability of electron acceptors like oxygen, which can be used upon designing a more effective remediation process.

With the presence of oxygen, microbial aerobic metabolism takes place as the most thermodynamically favourable process (see Tab. 4). The aerobic degradation of organic compounds (e.g. BTEX) can be supported and accelerated by adding oxygen to the anoxic aquifer. [98] A small prerequisite for the success of this method is the presence of microorganisms that can metabolize the pollutant in aerobic conditions like *Pseudomonas* sp.. [31] Anaerobic species *Geobacter metallireducens* or *Geobacter sulfurreducens* can also enable oxidation of the organic contaminants with Fe^{3+} and SO_4^{2-} respectively, as electron acceptors instead of O_2. [99] Meckenstock et al. (2016) summarized the corresponding reactions of the anaerobic microbial degradation of benzene (eq. 27 & eq. 28). [100]

$$C_6H_6 + 30\ FeOH_3 \rightarrow 6\ HCO_3^- + 30\ Fe^{2+} + 18\ H_2O + 54\ OH^- \qquad \text{eq. 27}$$

$$C_6H_6 + 3\ H_2O + 3.75\ SO_4^{-2} \rightarrow 6\ HCO_3^- + 3.75\ HS^- + 2.25\ H^+ \qquad \text{eq. 28}$$

It should be added, after exhausting Fe^{3+} as electron acceptor, sulphate-reducing conditions are favoured. The formation of H_2S has a rather insignificant effect when dissolved in water (weak acid), but as a gas it is very dangerous and undesirable. Establishing a Fe^{3+} - Fe^{2+} cycle (e.g. microbial reduction with chemical oxidation of Fe^{2+}) should be of great benefit, similar to a miniaturized form of an oxic-anoxic Fe-boundary model as presented from Hering and Stumm (1990) [101] i.e. Davison (1985). [102]

Chemically based oxidation of the Fe^{2+} and possibly of the contaminants in presence of O_2 in anoxic conditions is a neglected aspect which will be especially discussed in part 5.3.

The use of silicone membranes for oxygen injection in anaerobic groundwater areas is not a new method and it was already used to enhance *in situ* remediation of BTEX contamination, as in the example by Gibson et al. (1998). [103] In this case of Gibson et al. (1998) the purpose of applying a silicone membrane was to enable a constant O_2 diffusion and invert the conditions in the groundwater from anaerobic to aerobic, thereby increasing the oxidation kinetics of the contaminants by simply increasing the bioconversion rate. When aerobic microorganisms are involved, an overall three-fold increase of BTEX biodegradation was claimed after completely oxygenizing the groundwater contamination site.

However, there are issues involving increased oxygen diffusion rate and its effect on groundwater permeability. Indeed, a rapid increase in oxygen content in an anoxic aquifer can lead to deposition of oxidized Fe and Mn, thereby impairing permeability. This is especially the case when air sparging is used in the removal of LNAPL. Fe^{2+} and Mn^{2+} in the aquifer can be oxidized to insoluble species during air sparging, i.e. in presence of O_2, resulting in occlusion of soil pores and reduction of groundwater flow. [9] Similary, biological oxidation of ferrous iron may also occur (e.g. genus *Gallionella*). [99]

Various monitoring systems are used in conjunction with groundwater remediation, and even in-situ microcosm vessels [104] are used to provide real conditions in order to understand and control the dynamic of the groundwater biodegradation potentials and rates.

In this work, the possibility of implementing a similar silicone membrane (OxyTech) with slow O_2 diffusion rate to avoid inverting of the redox conditions of the groundwater well was investigated. A stand-alone gas-water separation APPI-FAIMS (as shown in 3.3) was used simultaneously to monitor contamination with aromatic VOCs. In this and the next part (5.3), the possible remediation contributions of the soil lance for slow O_2 gas injection were addressed.

The method is expected to offer a cost-effective alternative/addition to conventional methods, especially for minor contamination.

The immersion of a silicone membrane is considered an environmentally friendly remediation method compared to other applied techniques. Such simple, deployable, cost-effective, in-situ remediation method with on-site monitoring of the VOCs groundwater contamination plume is considered attractive for commercial purposes.

In this part the contamination profile is determined with the characteristics of the groundwater chemistry and geological profile of the contaminated site. The biological and chemical aspects of oxygen-assisted remediation by the membrane are discussed in cases involving BTEX and non-polar, aromatic VOCs, as well as the characterization of the membrane. Finally, the on-site membrane deployment included gas-water separation APPI-FAIMS monitoring of the specific aromatic VOC sum-signal, and

separately included multi-parameter monitoring to better understand the conditions encountered during OxyTech-assisted remediation.

4.2. Experimental

Aromatic VOCs analytes described in 3.2.1. and indane were used to establish external calibration. For the preparation of standard solutions, Milli-Q water was used from a Milli-Q Plus water purification system (Millipore, USA). The laboratory stock solutions were mixed in 1L Schott bottles for at least 24 hours at 25 ±1 °C in an overhead shaker (Reax 20 from Heidolph, Germany) and discarded after sampling. The external calibration, BTEX identification, and control measurements were performed with HS-GC/MS like previously explained in 3.2.3. including the same parameters, column and devices.

Buffer solutions used for calibration of pH electrode: pH 7.00 (20 °C) phosphate mixture and pH 4.00 (20 °C) citric acid/NaOH/NaCl from Bernd Kraft, Germany. pH 9 (20 °C) VWR chemicals, USA. HCl (~37%) from Fisher, USA for glassware cleaning.

For the quantification of ferrous and total iron: 1,10-Phenanthroline ≥ 99% from Sigma Aldrich, Germany; $NH_2OH \cdot HCl$ (Hydroxylamine Hydrochloride) >99%, NaF_2 as masking agent (sodium fluoride) and Acetate Buffer Solution pH 4 from VWR chemicals, USA.

Buffer capacity i.e. total alkalinity was done according to DIN EN ISO 9963-1 [105]: for titration 0.1M HCl (~37%) from Fisher and 1N NaOH from Bernd Kraft, Germany; T,O_2, pH and conductivity were performed on-site with portable WTW multi 3420 Optical Oxygen Sensor FDO 925 and with Hach HQ30d portable multi metre, also used for the on-site multiparameter analysis.

ICP-OES (5800 ICP-OES from Agilent, USA) was used to determine total Fe, Mg, Mn and Ca.

TOC detection (TOC-L with TNML for total nitrogen from Shimadzu, Japan) was carried out after one day storage of the samples at 6 °C. Dilution 1:1 with Milli-Q water (Millipore, USA) was done when necessary (high total inorganic carbon (IC)).

4.2.1. Quantification of Fe^{2+} and Fe^{3+}

A large number of analytical methods can be applied for the determination of iron. The most important, involving the oxidation state, is based on the reaction of Fe^{2+} with 1,10 phenanthroline. [106] The absorbance of the solution was taken at 510 nm with Spectrophotometer Hach Lange Xion 500 LPG385 from Dr. Lange, Germany. Iron (II) chloride tetrahydrate ≥98% from Bernd Kraft, Germany was used for calibration. The calibration was performed under laboratory conditions, but the Fe^{2+} and Fe_{total} determinations were also carried out in the field.

The determination of total Fe under laboratory conditions were performed by AAS (Contraa 300, Analytik Jena GmbH, Germany) and ICP-OES (5800 ICP-OES from Agilent, USA). Previously the samples bottles (plastic - PP) were cleaned with 10% HNO_3 and distilled water. Samples were not filtered (when colourless, turbidity <

1.5 FNU), but conserved to pH < 2 with 0.5 mL HNO_3 (63%) on 100 mL groundwater sample. The samples were taken in PP-vessels stored at 6° C and diluted 1:1 (due to high concentration of Ca) prior to analysis.

4.2.2. *Geobacter metallireducens* detection and cultivation

High-Resolution Microscope Camera AxioCam ICc 3 (from Artisan Technology Group, USA) was used. Sensor: Sony ICX 262 AQ, Interlaced Readout, RGB Filter Mask. CCD Basic Resolution: 2080 x 1540 = 3.3 Megapixels. Pixel Size: 3.45 µm x 3.45 µm. Signal Amplification: 20 dB Analog. Digitization: 3 x 8 Bits/Pixel or 3 x 12 Bits/Pixel.

Geobacter metallireducens was cultivated in serum bottles on medium as described in [107]. Traces of O_2 were not removed with hot reduced copper filings, only nitrogen gas (5.0; 99.999% from Air Liquide was used. Instead of acetate, toluene (10 mg L^{-1}) was used as sole electron donor and Fe (III)-citrate as an electron acceptor (5 mg L^{-1}). Schott bottles (250 mL) with viton stoppers and the medium (pH 7). The prepared solutions were stored at 24 - 25 °C in the dark. Bacteria counting with Thoma cell counting chamber.

4.2.3. Application of the OxyTech membrane for groundwater remediation

OxyTech® membrane was received from Fabricius Pro Terra, Germany. It was reinforced with nylon fibres (average OD= 10 µm) and represented a tubular silicone membrane with OD= 1cm, ID= 0.8 cm i.e. 1 mm thick (see Fig. 44).

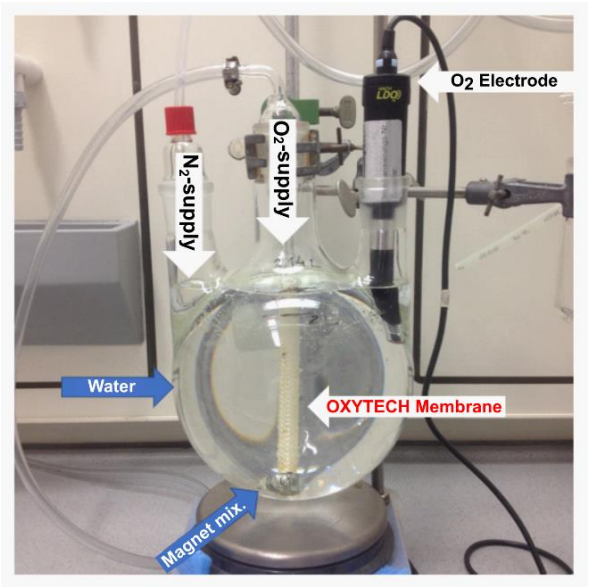

Fig. 37: Experimental setup for determining the oxygen permeability of the OxyTech® membrane.

Fig. 37 shows the experimental setup involved in the determination of the permeability of the membrane for the 10 cm long OxyTech membrane, performed at different membrane pressures with oxygen gas (O_2) 5.0 from Air Liquide, France. Nitrogen gas 5.0; 99.999% from Air Liquide, France was bubbled at 22 - 24 °C until the oxygen content was under the detection limit (< 0.01 mg L^{-1}). The membrane vessel was sealed and the membrane was set under desired pressure (0.6 - 2 bar). Minimum of five measurements were carried out for every applied pressure. After initial 200 min the permeability was compared for different pressures and in the range 2 - 6 mg L^{-1} O_2 or less, depending on the pressure. Measurements in which the OxyTech membrane was not under pressure were considered "blank" values and subtracted from the rest of the results.

4.2.4. On-site parameters and site characteristics

A special 2 L measurement unit (home-made from duran glass) was used for continuous measurement of conductivity, temperature, pH and oxygen content, in the same time the water volume pumped out was documented. The redox measurements were performed in a different vessel on-site with Ag, AgCl / 3M KCl electrode from Metrohm, Germany and 5 x 4 cm Pt-plate with multimeter 34401A from Hewlett Packard, USA.

4.2.5. On-site continuous aromatic VOCs monitoring by gas-water separation APPI-FAIMS

Contaminated groundwater from a contamination site in Germany was pumped out with an immersion pump (~300 mL/min), while maintaining a constant groundwater level within ±4 cm. The gas-water separation APPI-FAIMS System (as described in 3.2.3.); equipped with RF PID krypton lamp 10.6 eV from Heraeus, Germany (PKR 106, MgF_2 window material) providing UV ionization. Compensation voltage (CV) parameters: sample number 512, over-sweep length (CV sweep time per mode) 500 ms, sampling time 2 ms; static bias (casing bias surrounding the chip) ±60 V, detector bias ±60 V.

Gas-ware separation APPI-FAIMS measurements were performed on site continuously at 0% and 36% DF with setup like in Fig. 11. Nitrogen gas flow from a 10 L gas bottle (5.0; 99.999% from Air Liquide, France) was set up with needle valves, sensor pressure was 0.03 barg and the constant sensor temperature 60±1 °C. Control samples were taken periodically during this measurement period and preserved according to EN ISO 5667-3:2012 [108] for control with static headspace HS-GC/MS in the laboratory. The same HS-GC/MS system and autosampler procedure as in part 3.2.3. was used for providing control measurements.

4.3. Results and discussion

4.3.1. Initial assessment of the contaminated groundwater site

The selected groundwater contamination site was located in an industrial region in Ruhr area. The presence of a production and storage vicinity was accompanied with a transport pipeline for the produced aromatic volatile organic substances (AVOCs). Classical remediation methods were already used at the moment of initial sampling. This involved pump-and-treat of the groundwater in combination with soil vapour extraction of the vadose zone, which to a certain degree are especially successful in treating contamination with aromatic volatile organic compounds (see. 1.2.1.).

The likely determined point contamination source was not exactly pinpointed and possibly involved a larger industrial area. Nevertheless, the groundwater sampling and monitoring was performed in groundwater remediation wells placed next to the P&T and SVE remediation sites.

The geochemistry of the contamination site is greatly influenced by the minerals present i.e. the mineral characteristics of the aquifer. Marl or marlstone has a relatively high calcite or $CaCO_3$ percentage as well as a fair amount of clay content. In our case the saturated zone consisted of grey marlstone and yellow / brown sandy soil in the approximate first 3 metres of the boring site which characterizes mostly the vadose

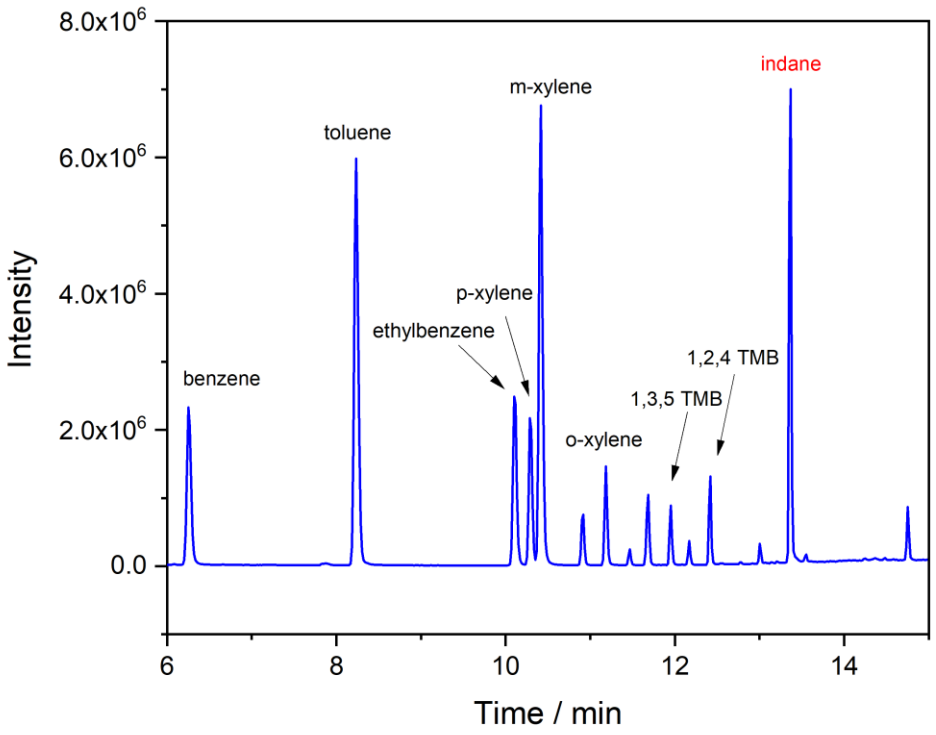

Fig. 38: Initial sampling of the contaminated groundwater and subsequent HS-GC/MS analysis (TIC).

zone of the contamination site. This implies, as further shown, that the groundwater in this region is a bicarbonate type of water containing Ca and Mg ions. The range of electrical conductivity of 900 - 1400 µS cm^{-1} determined in several remediation wells confirmed the previous finding. This range corresponded to the range of electrical conductivity of mineral waters described in the literature and its relationship to the rock type from which the water was extracted, in this case mostly marl and limestone. [109]

The contamination profile was reported previously and it included periodical monitoring of BTEX and trimethylbenzenes (TMBs). When additional samples were taken from the P&T site, the contamination profile showed additional volatile organic contaminants with a particularly intense peak, as shown Fig. 38. The presence of indane (red) was confirmed as a contaminant in the groundwater (MS database and analytical standards), as was the case for all other previously identified contaminants. The identified analytical signals from the contamination site summed up to more than 93% of the total analytical area signals generated, only less than 7% were not determined. The concentrations of the identified aromatic VOCs in the groundwater are shown in Tab. 10.

Tab. 10: The determined concentrations of aromatic VOC in groundwater (external calibration) using HS-GC/MS, with the LOD of the method and the correlation coefficient (r^2) of the calibration.

AVOC	**Conc. in groundwater** (mg L^{-1})	**LOD**[b] (mg L^{-1})	**LOQ**[b] (mg L^{-1})	**r^2**
Benzene	**7.7** ±0.8	0.35	1.1	0.989
Toluene	**7.7** ±0.6	0.25	0.84	0.994
Ethylbenzene	**2.5** ±0.5	0.3	1	0.99
***p*-Xylene**	**2** ±0.4	0.29	0.97	0.99
***m*-Xylene**	**5.8** ±0.5	0.24	0.83	0.994
***o*-Xylene**	**1.1** ±0.3	0.34	1.1	0.988
1,3,5 TMB	**0.5** ±0.3	0.36	1.2	0.986
1,2,4 TMB	**0.8** ±0.2	0.35	1.2	0.989
Indane	**7.5** [a]	0.1	0.34	0.997

[a] - estimated at a later time period after the identification of indane was done

[b] - Limit of detection and limit of quantification [67].

The pH of the collected samples at multiple monitoring points varied from 6.2 to 7, the temperature between 13 and 14 °C. The alkalinity calculated as mM HCO_3^- equivalent was rather high ~ 10 mM or 490 - 584 mg L^{-1} HCO_3^- depending on the sampling place. Hence, a carbonate aquifer system was assumed, where

marl/marlstone is the predominant mineral type of the saturated zone rich in carbonate, with high alkalinity (basicity) and Ca^{2+} as the predominant cationic species. As can be seen from the speciation diagram of a carbonate system (i.e. Bjerrum plot), bicarbonate ions are the dominant species at pH 7 [110], so they were suspected to be the dominant ion speciation form in the groundwater.

On-site determination of ferrous ion by reaction with 1,10-phenanthroline was also carried out. The absorbance was determined at 510 nm. The advantage of this method is that Ca ions do not interfere significantly with the reaction of Fe^{2+}. Carbonate can affect the response but at high concentrations which later will be seen as relevant. [106,111]

Fe^{3+} can also increase the absorbance at 510 nm as a result of complex formation with 1,10-phenanthroline in a range > 5 mg L^{-1}, but its effect is relative to Fe^{2+} concentrations. [106,112]

At this contamination site, aqueous Fe, i.e., total Fe, was present in the groundwater predominantly as Fe^{2+} (Fig. 39, Tab. 11), indicating anaerobic, reducing conditions in the aquifer. The concentration of Fe_{total} was also confirmed by application of AAS (atomic absorption spectroscopy) and ICP-OES (inductively coupled plasma – optical emission spectroscopy), thereby avoiding possible interferences from the phenanthroline method. ICP-OES was used to determine the amount of Fe_{total}, and indirectly of Fe^{2+}. Ferric species are mostly insoluble and deposited in the aquifer, e.g. ferric oxide (Fe_2O_3). [5]

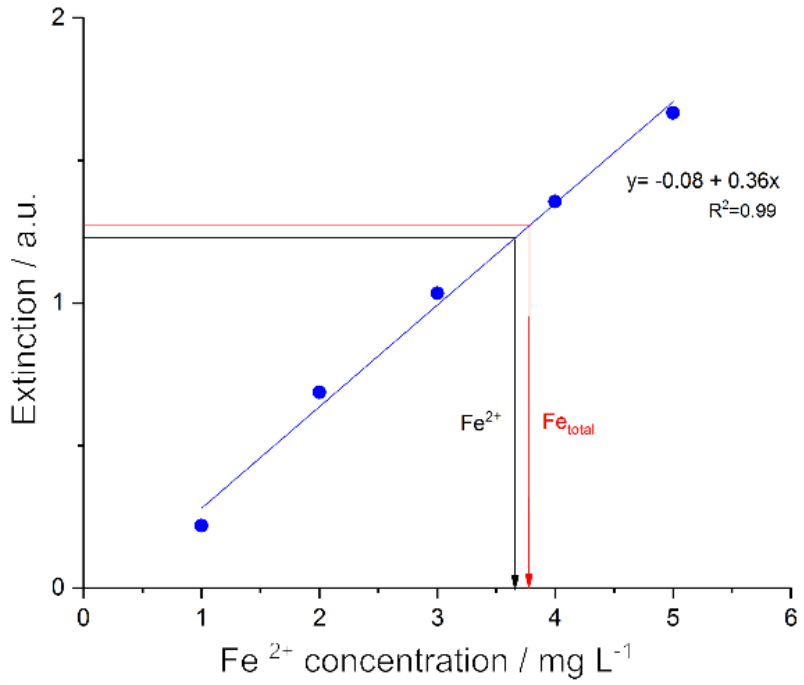

Fig. 39: On-site spectrophotometric determination of Fe^{2+} and Fe_{total} (at 510 nm) with 1,10-phenanthroline similar to [111] and [112].

Tab. 11: On-site concentration of dissolved iron in groundwater from Fig. 39.

Iron	Concentration (mg L^{-1})
Fe^{+2}	3.7 ±0.4
Fe $_{total}$	3.8 ±0.4

Furthermore, the concentration of Ca and Mg was additionally determined by ICP-OES with the following concentrations: for Ca^{2+} = 170 - 280 mg L^{-1} depending on the sampling place (collector or monitoring well respectively), as well as for Mg^{2+} (16.7 - 28 mg L^{-1}) and additionally Mn^{2+} (0.1 - 0.2 mg L^{-1}). The possible presence of iron reducing bacteria in these conditions was seen as more than favourable and therefore stimulation of their growth was considered, knowing aromatic hydrocarbons are susceptible to aerobic and anaerobic biodegradation. For ferrous concentrations >20 mg L^{-1} bioremediation is not recommended. [5]

4.3.2. Possibility of indigenous microbial remediation

The *ex-situ* application of microcosms to determine microbial remediation effects is widespread despite the amount of work involved. Similar to Albrechtsen and Christensen (1994) the goal was to estimate the significance of the microbial processes and its effectiveness, indirectly, through the reduction of Fe^{3+} from anaerobic metal-reducing bacteria. [113]

The microflora in the sampled contamination region has generally shown very low presence, nevertheless it varied from the sampling place. Only rod-shaped bacteria were identified in some of the real samples and nitrogen, as total nitrogen, crucial for microbial activity and growth, was found in groundwater at concentrations of around 1 mg L^{-1}. Since no actual sediment samples were available, the microbial culture was supplemented with *Geobacter metallireducens* as a typical representative.

Geobacter (*Geobacteraceae spp*.) is a genus of rod-shaped proteobacteria with capabilities in bioremediation. Its use in oxidation of radioactive metals and petroleum components (including VOCs) under anaerobic conditions and the use of a metal as an elecron acceptor is well known. [114] Therefore, *Geobacter metallireducens* was used as a typical representation (Fig. 40a) to investigate the possibilities in involevment of the OxyTech membrane and the *Geobacter spp.* possibility of monitoring the process of bacterial activity, ex-situ, through the reduction of Fe^{3+} to Fe^{+2} was considered. Hence In *Geobacter metallireducens* inoculation of a medium described as in [107] with toluene as carbon source and iron (III) citrate as an electron acceptor was performed.

An indirect method (the increase of Fe^{+2} conc.) was used for determining the efficiency of toluene conversion by using microcosms. The changes were negligible for a period of 91 days knowing the LOD of the phenanthroline method (0.094 Fe^{2+}/ mg L^{-1}) was higher than the determined average Fe^{2+} concentration (Fig 40).

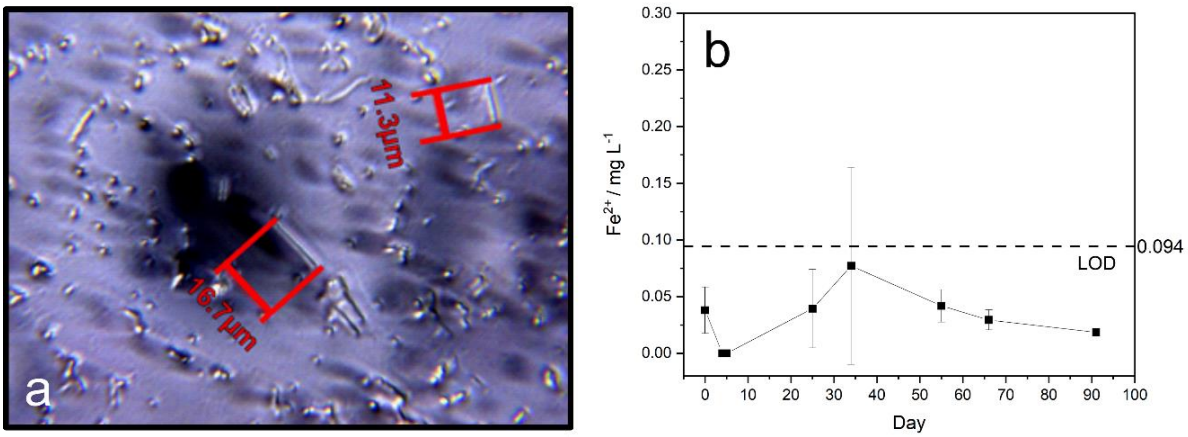

Fig. 40: **a**) *Geobacter metallireducens* after inoculation. **b**) Trend of possible iron (II) production from toluene as electron donor and iron (II) as electron acceptor in iron (III)-containing medium.

The use of microcosm experiments, as in this case, has highlighted the difficulties encountered in using laboratory methods to elucidate environmental processes.

The use of microflora for initial contaminant degradation in cases where carbon is used as an electron source may also lead to an underestimation of degradation potential under laboratory conditions compared to field conditions. [115] One of the possible reasons for negligible Fe^{3+} reduction was addressed by Lovley et al. (1988) and it considered iron citrate as the sole electron acceptor. When iron citrate was replaced with amorphic Fe^{3+} oxide *Geobacter metallireducens* grew faster and reduced the added Fe^{3+} to Fe^{2+}. [107]

Even in the case of aerobic bacteria Lang et al. (1996) has shown that there are problems when it comes to metabolizing xylenes and especially *o*-xylene as their sole source of carbon in comparison to benzene and toluene. It was concluded that only Gram-negative bacteria can effectively metabolize benzene with more than one alkyl substituents. [116] The mineralization of benzene has been confirmed by oxidizing benzene to carbon dioxide with ferric iron as the terminal electron acceptor in the presence of the anaerobic *Geobacter* , shown by Anderson et al. (1998), summarized by Meckenstock et al. (2016). [100,117] However, as it was noticed in this and published studies, anaerobic microbial degradation was not observed in a wide variety of aquifer materials. [117] Some materials exhibited lag times of over 140 to at least 400 days under laboratory conditions before benzene was removed. [118,119]

A better correlation of such anaerobic microbial effects can be established with a reliable, *in-situ* contamination monitoring method without questioning the applicability of the obtained results. The additional monitoring of ferrous ions in combination with a microbial count may be particularly helpful in evaluating novel remediation techniques (i.e. OxyTech membrane).

The gas-water separation APPI-FAIMS in this case was used to initially investigate and differentiate the short term effect of oxygen in anoxic aquifers on the contamination with aromatic VOCs. Long-time monitoring, more suiting in the cases involving microbial activity, was also possible.

4.3.3. Possibility of oxygen enhanced remediation

The supposed effect of the OxyTech membrane is shown for one of the monitoring/sanitation wells in Fig. 41, courtesy of Fabricius Pro Terra. The difference in the conversion of OxyTech showed a significant effect on toluene, which was further investigated.

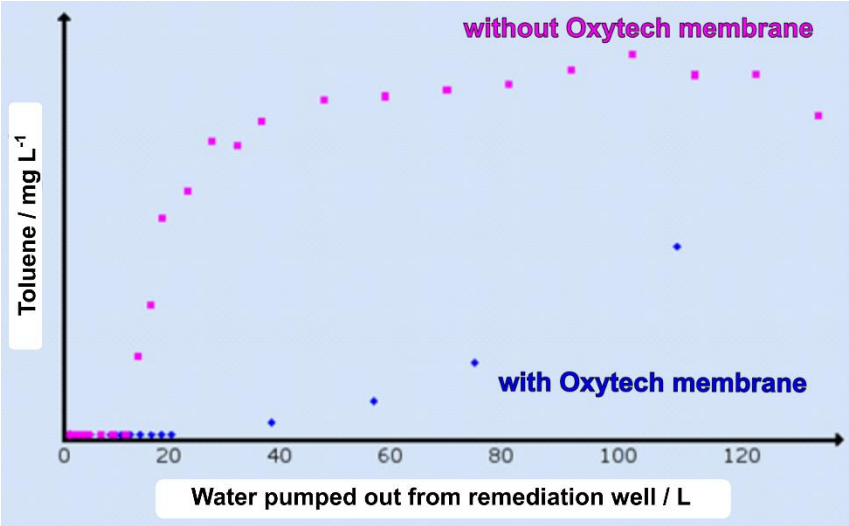

Fig. 41: Effect of OxyTech membrane on toluene concentration in a sampling groundwater well (courtesy of Fabricius Pro Terra).

Such changes in the concentration could involve an enrichment of the non-polar membrane with the non-polar aromatic VOCs like toluene. This could immediately lower the concentration until saturation of the silicone membrane occurs. After that, the concentration begins to increase with the simultaneous inflow of contaminated groundwater.

The influence of groundwater stagnation in a monitoring/remediation well is also not negligible. Different sub-zones of high or low concentrations of the contaminants can be formed. To avoid such bias a continuous monitoring of multiple parameters should be applied. If the effect of OxyTech, i.e. O_2, is confirmed, the question of

degradation kinetics arises. In contrast to microbial degradation, an immediate effect is observed here. This idea shifts the focus to chemically induced oxidation by the addition of O_2 under anaerobic groundwater conditions.

In addition to Fig. 41 initial results of TOC analysis from the Pump & Treat site are shown in Fig. 42. The location of the sample points is described in Fig. 43. Contaminated groundwater was collected from "Collector 1" for the P&T unit from the low oxygen anaerobic zone (i.e. below the water table), and from "Collector 2" for the SVE unit from the vadose zone (i.e. zone with elevated oxygen content). The "Oxidation tank" sample is actually the groundwater sample from "Collector 1" with increased O_2 content for intended Fe^{2+} precipitation.

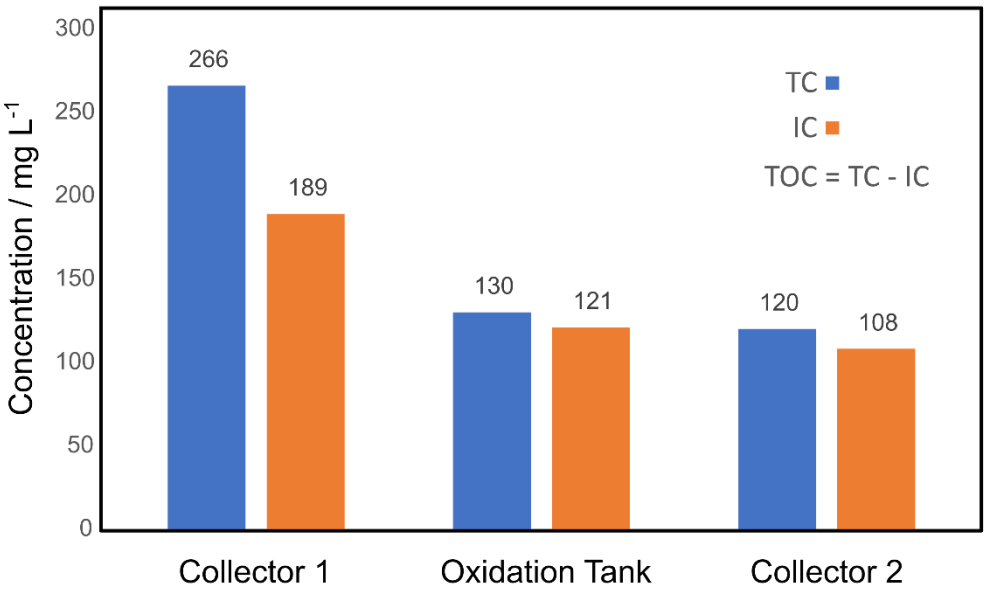

Fig. 42: Comparing TC and IC results of groundwater contamination site between P&T-collector (1), SVE-collector (2) and the oxidation tank.

The TOC values, i.e. the differences between TC (Total Carbon) and IC (Total Inorganic Carbon), seem to follow a trend related to the oxygen concentration and conductivity of the samples. The “Collector 1” sample was collected immediately after pumping. The dissolved oxygen (DO) content was lower than the detection limit of the optical sensor and the conductivity (1015 µS cm^{-1}) higher compared to the other two samples. “Oxidation tank” and especially “Collector 2” samples were close to oxygen saturation and the conductivity was 920 µS cm^{-1} and 878 µS cm^{-1}, respectively. The O2 content of the “Oxidation tank” sample was 8.36 mg L^{-1} at groundwater temperature of 13.5 °C, corresponding to an O_2 saturation of 80.4% [120], similar to “Collector 2”.

The lower conductivity of the samples where the DO value was increased was due to the lower Fe^{2+} concentration as a result of subsequent oxidation and precipitation.

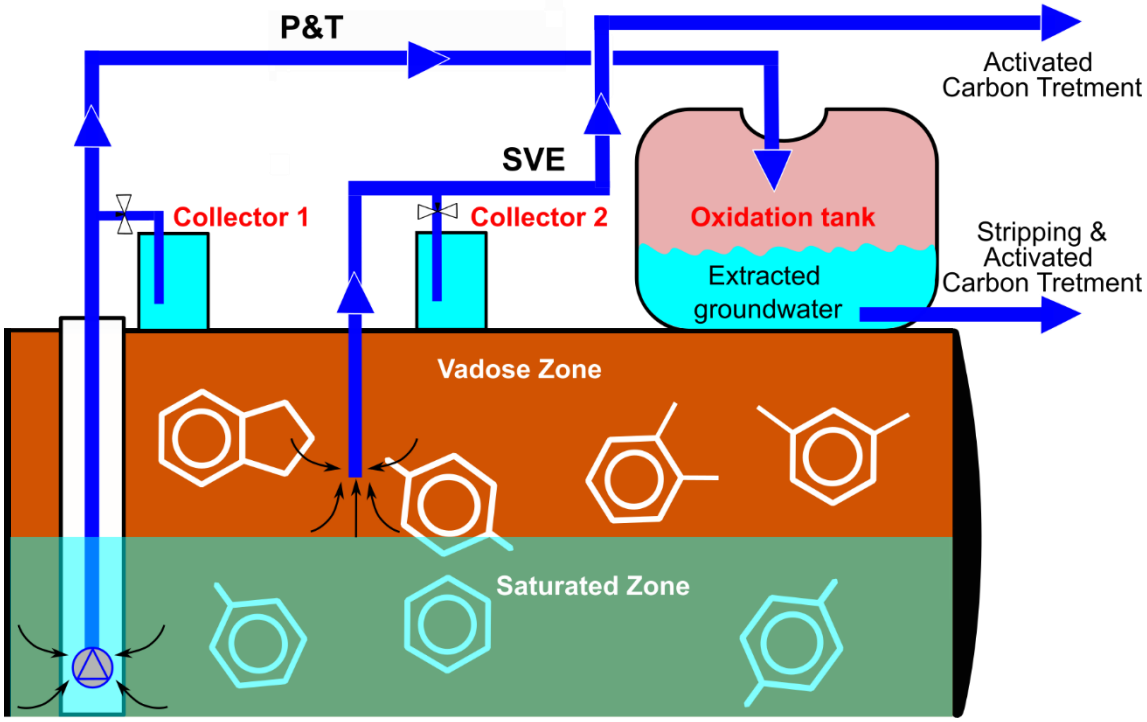

Fig. 43: Sample points (Collector 1, Collector 2 and Oxidation tank) from Fig. 42 (P&T - Pump & Treat; SVE - Soil Vapor Extraction).

The difference in the TC / IC ratio between “Collector 1” and the “Oxidation tank” could be a part of oxygen initiated degradation or, more likely, of evaporation of VOCs. The difference in IC could indicate a dilution effect.

A similar effect with a probable relationship between the concentrations of aromatic VOCs to the Fe^{2+} oxidation is shown in the Appendix (App. 1). It is noted that the signal intensity of the BTEX in the groundwater samples decreased with storage time for the samples that were not preserved (50% H_2SO_4 not added). Lowering the pH in the samples (< 2) prevented the oxidation of Fe^{2+} and thus the potential effects on the contaminants.

On-site monitoring of the contamination processes could contribute for better elucidation of the potential impact of oxygen in such cases through the use of the OxyTech membrane, especially in cases where O_2 is the limiting factor for ferrous oxidation (i.e. in anoxic conditions). In this case, a characterization of the OxyTech membrane should be performed as a first step.

4.3.4. Characteristics of an oxygen-permeable membrane (OxyTech®) for groundwater remediation

To clarify the mechanism of groundwater remediation using the OxyTech membrane, firstly the characteristics of such slow, continuous, oxygen-permeation membrane were investigated, its impact on the well conditions and chemical/biological processes. Unlike some other common techniques with rapid and intense O_2 infusion (e.g., air sparging), the slow introduction of oxygen could (potentially) support conditions enabling further growth of facultative / anaeobic bacteria.

Depending on site characteristics (e.g., well volume capacity, groundwater flow, groundwater composition, etc.), prolonged use of OxyTech at membrane pressures >1 bar (O_2) results in a complete change in redox conditions and favours the growth of aerobic bacteria that require an adaptation period. Such change in the well conditions (oxygen level) for aquifers with >20 mg L^{-1} Fe^{2+} is not recommended. [5,121] The rapid increase of DO in aquifers with high Fe^{2+} concentration leads to clogging and reduction of the aquifer permeability, which can dramatically minimize the success of an extended remediation. In addition, there can be an enormous impact from the pH change on the microbes that assist in the biodegradation of the contaminants.

Due to the slow oxygen supply with the OxyTec membrane, large pH changes are avoided. Fe^{3+} reducing bacteria are tolerable to wide pH ranges (e.g. *Geobacter sp.* CdA-3, pH range 5.5 - 8.1) [122,123] making them generally a suitable pairing with the OxyTech membrane.

In this study, the O_2 (slow infusion) reacted rapidly with the ferrous ion present (pH~ 7), thereby not able to significantly affect the anaerobic conditions and microorganisms. High pH changes were additionally avoided because the capacity of the groundwater was high (~10 mM HCO_3^-).

As shown in Fig. 44b oxygen bubbles initially form and adhere to the membrane where O_2 diffusion and reaction occur. The produced ferric iron species due to oxidation can serve as electron acceptors for the anaerobe iron-reducing bacteria (e.g. *Geobacter sp*.). Successful studies with graphite electrodes as electron acceptors for the *Geobacter metallireducens* instead of the Fe^{3+} species in the degradation of hydrocarbon-contaminated sediments have been published. [124] In comparison, OxyTech was intended to be more of a link to a Fe-cycling method with the use of iron-reducing microorganisms, but there was another potential chemical remediation aspect that was addressed in 5.3.

With the migration of the contamination plume comes the migration/”development” of the redox zones (e.g. Fe^{2+}/Mn^{2+} red. zone). This depends strongly on the size and strength of the contamination source, groundwater flow velocity and the geochemistry of the aquifer. [125] The natural change in redox conditions over time toward aerobic conditions would be supported and accelerated by O_2 introduction. For these cases, more intense infusion of oxygen with the OxyTech membrane is also possible and the established aerobic conditions should be maintained throughout. [24]

Variations of dissolved iron and manganese concentration in groundwater can occur with the season i.e. can be dependent on the amount of precipitation and the inflow of oxygen rich water into the aquifer. Oxidation of iron and manganese decreases the concentration of the available O_2. Returning back to previous anaerobic conditions is highly possible if the anaerobic conditions are dominant in the area.

Fig. 44 shows the 10 cm long OxyTech membrane used in the experimental setup from Fig. 37 for determining the oxygen permeability of the membrane (OD=10 mm, ID=8 mm, reinforced with nylon fibers (Fig. 44c,e)). The nylon fibers with average diameter of 10 µm are tight nets around the membrane, decreasing the permeability (providing areas smaller than 1 mm^2), but increasing stability when higher pressures are applied.

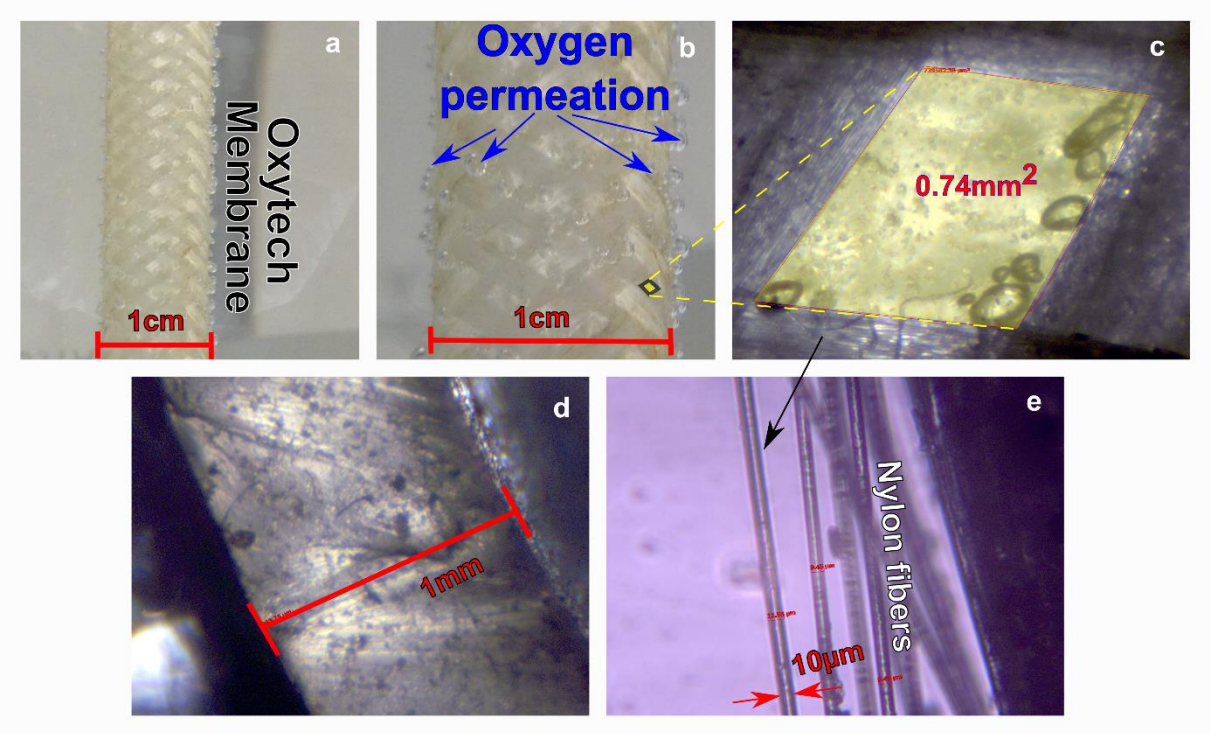

Fig. 44: (a) Oxytech membrane; (b) Pressurized (1bar) permeation of oxygen through the Oxytech membrane into water; (c) Silicon part of the membrane not covered with nylon fibers; (d) Cross-sectional view and thickness of the membrane; (e) Nylon fibers used for reinforcement of the membrane.

As a first step to determine permeability, a slow purge of O_2 with N_2 was done until the O_2 concentration in water was under the detection limit of the electrode. At this point the N_2 purging was stopped and the vessel was sealed. The O_2 supply was turned on at one of the desired pressures (0.6 - 2 bar) for the membrane and multiple measurements (at least 4) were performed. The procedure is described in part 4.2.3.

The generated permeation results (extrapolated) are shown for 1 m membrane length. The results of Tab. 12 are presented graphically in Fig. 45 where the O_2 inflow flux is shown for one day of membrane activity at a given pressure, as well as the theoretical saturation limit of a typical groundwater well. It could be noticed, there is

not a linear relation with the increase of membrane pressure and the permeate flux. When the inner pressure exceeds 1 bar the membrane starts slowly to expand, thus decreasing the initial membrane thickness to less than 1 mm (Fig. 44d). Differences in permeability in-between OxyTech membranes can originate from the impurities and bubble-like irregular shapes like in Fig. 44c.

Tab. 12: Extrapolated O_2 permeation rate of 1m long OxyTech membrane from Fig. 44 and Fig. 37 at different pressures in water (24 ±1 °C).

Membrane Pressure (bar)	**0.6**	**0.8**	**1**	**1.5**	**2**
Permeation flux (mg O_2/h)	**1.99**	**2.45**	**2.83**	**4.99**	**6.88**
Permeation RSD (%)	4.65	4.94	3.87	6.1	2.57

Considering the previously determined Fe^{2+} concentration of 3.7 mg L^{-1}, a pressure of 0.6 bar and a daily influx of 47.7 mg O_2 were used to reduce the possibility of clogging the well when using the OxyTech membrane on site. The groundwater temperature of 13 - 15 °C has maximum oxygen capacity of 10.1 - 10.5 mg L^{-1} (at 1

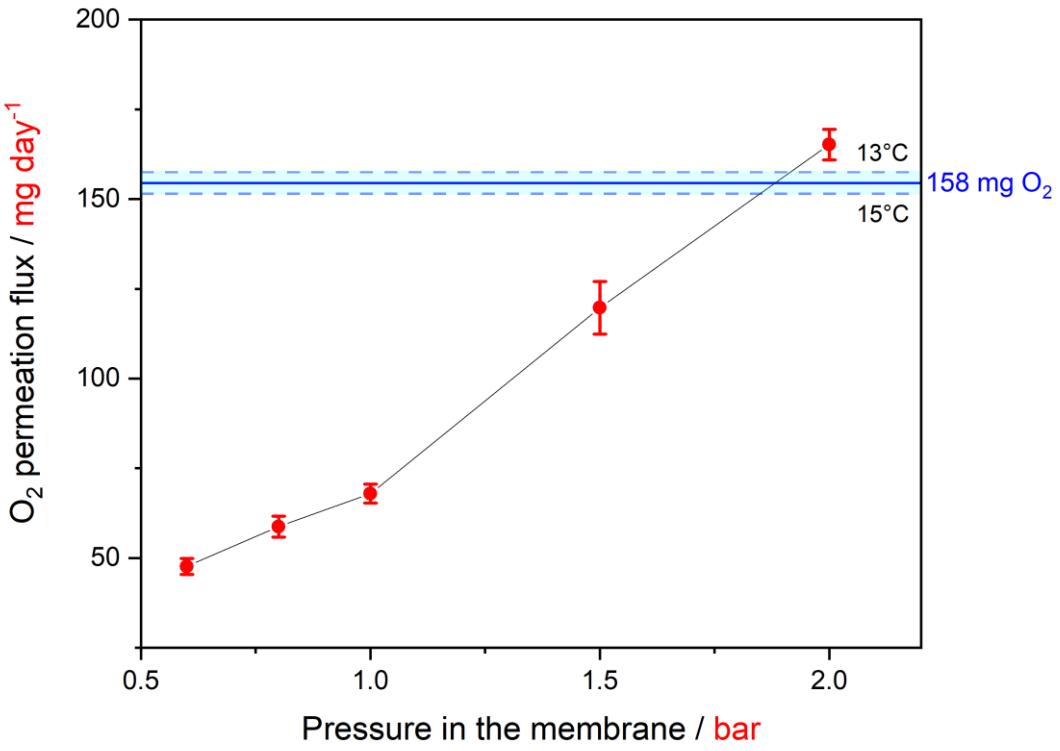

Fig. 45: Extrapolated daily (24 h) permeability flux increase with relative membrane pressure from (red); Theoretical O_2 saturation limit of an average remediation well with 3m water column (groundwater temperature 13 – 15 °C) (blue).

bar atmospheric pressure). The maximum depth of a remediation / monitoring well (i.e., the height of the water column) was around 5 m. More than 90% of the groundwater monitoring wells had a water column of 2.5 to 3 m, which corresponds to about 20 to 30 L of water. A constant membrane pressure of about 2 bar for one day reaches about 50% (158 mgO_2 L^{-1}) of the theoretical saturation of a well (Fig. 45), assuming no groundwater flow and the absence of Fe^{2+}, as the dominant reductive species. In this study, a groundwater flow of 8 m per day was reported, which classifies this aquifer as one with medium to high hydraulic conductivity according to various aquifer materials. [5] In a milder approach, a pressure of 0.6 bar was selected as a membrane pressure to investigate the effects on groundwater contamination.

4.3.5. On-site preparation for implementation of the OxyTech® membrane

After an initial assessment of the groundwater contamination site, determination of the properties of the OxyTech membrane for its use for *in situ* remediation, a new sampling effort was conducted prior to the start of gas-water separation APPI-FAIMS contamination monitoring.

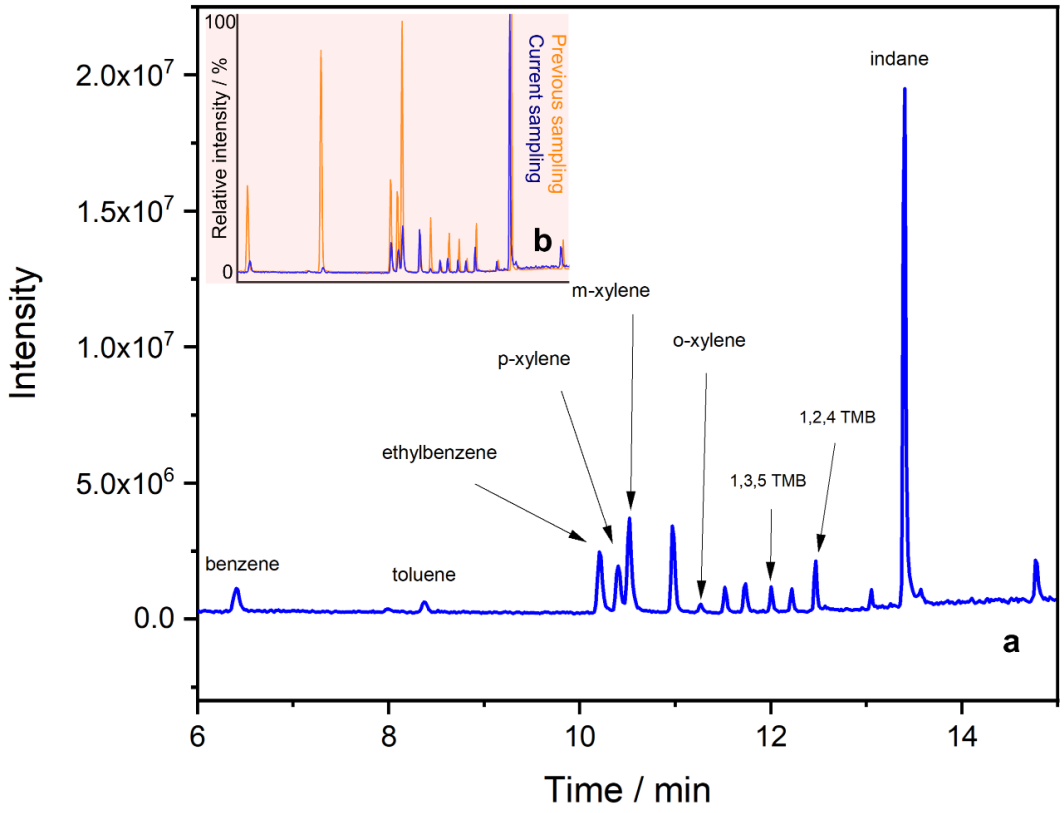

Fig. 46: a) Well sampling and subsequent HS-GC/MS analysis (blue) prior to deployment of the OxyTech membrane and initiation of on-site monitoring with the gas-water separation APPI-FAIMS; b) Overlay of previous (orange, Fig. 38) and current (blue) groundwater contamination profile.

Chronologically, the current sample Fig. 46a was taken 13 months after the initial survey (Fig. 38) of the same contamination area. An overlay relative to the indane intensity in both cases is shown in Fig 46b which shows the relative changes in the contamination profile. There can be more major phenomena contributing to this difference, such as the spatial spread of the plume over time and the remediation effects of the P&T and SVE units deployed on site.

The migration of the contamination plume is different for different types of contaminants. Generally, the higher the K_d value (soil/water partitioning coefficient) for a specific contaminant, the greater the sorption to soil and the slower the pollutant migrates compared to groundwater flow (i.e. it will have a higher retardation factor - R_f). [24] K_d values can greatly vary on the organic content in the soil since sorption occurs predominantly by partition into the soil organic matter, therefore K_{oc} (organic carbon - water partition coefficient) is used. Both, K_d or K_{oc} are considered soil adsorption coefficients and express how strongly a given contaminant is sorbed onto soil and organic matter.

Based on the decreased contaminant concentration in the water (Fig. 46b, Tab. 13) and the remaining contamination profile from the previous on-site sampling of the plume development, a clear trend can be seen along the log K_{oc} values (Tab. 13). Indane, as the contaminant with the highest log K_{oc} value, is also one of the

Tab. 13: The determined concentrations of aromatic VOC in groundwater (external calibration) before starting the APPI-FAIMS monitoring on-site and the appropriate log K_{oc} values of the contaminants.

AVOC	Conc. in groundwater (mg L^{-1})	log K_{oc}[a]
Benzene	**0.28** ±0.25	2.164
Toluene	**0.13**[b]	2.369
Ethylbenzene	**1.26** ±0.32	2.649
***p*-Xylene**	**1.37** ±0.3	2.574
***m*-Xylene**	**1.6** ±0.25	2.574
***o*-Xylene**	**0.15**[b]	2.583
1,3,5 TMB	**0.34**[b]	2.78
1,2,4 TMB	**1.22** ±0.34	2.788
Indane	**5.1** ±0.25	2.928

[a] - estimated from US EPA software [126] using Sabljić and Protić molecular connectivity method with improved correction factors [127].

[b] - under the LOD limit of the method

contaminants with the lowest decrease of ~ 30%. This high retardation i.e. soil adsorption also influences the partitioning of indane in water, thereby decreasing the effectivity of the physical remediation processes involved (P&T and SVE).

The application of surfactant and co-solvent flushing methods should be considered to additionally increase the remediation effectiveness in the case of indane. [24] According to its density, Indane is not considered a DNAPL (< 1 g mL^{-1}) [24], but the aforementioned techniques typically used for DNAPLs may shorten the time frame for remediation or contribute to more rapid spread of contamination in uncontrolled environments.

In the same time characterization of redox processes in the chosen remediation well was done for the whole monitoring process as shown in Fig. 47. Knowledge of redox conditions can be beneficial for interpretation of field observations, evaluation of plume development or assessment of natural attenuation and the engineering of remediation processes. [125] This field evidence suggests which situ bioremediation may be employed for different electron acceptors at various locations throughout a given site. Desimone (2009) concluded that the oxidation-reduction status and the degree of the aquifer confinement are the most important factors affecting the occurrence of contaminants in carbonate aquifers. [4] The red-ox status controls the fate of certain contaminants and is an indicator of frequent water recharge (i.e. the groundwater age). Redox reactions are also considered to be microbial mediated, thus enabling electron transfer to occur.

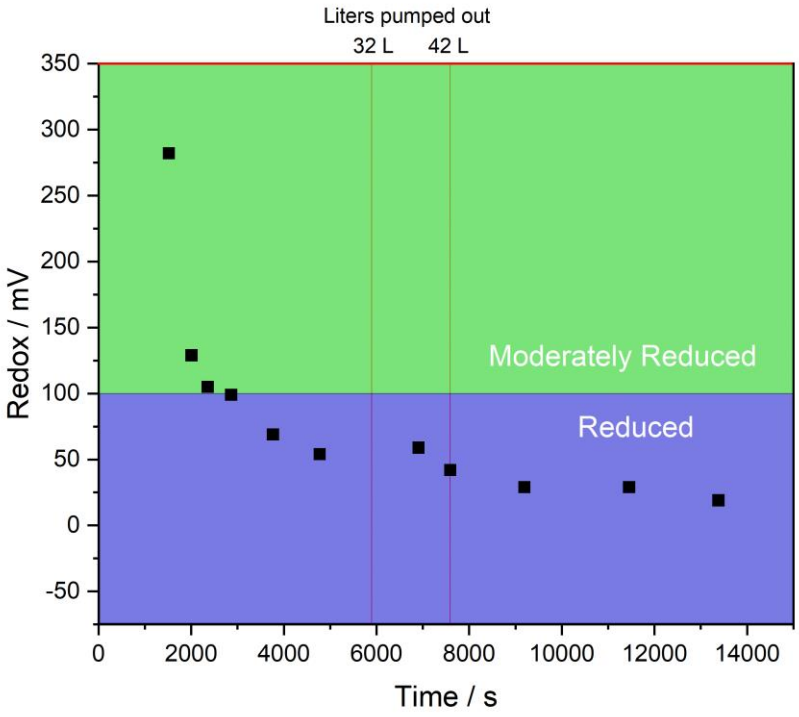

Fig. 47: On-site determination of the redox voltage development of the used specified monitoring well when OxyTech membrane was applied (pressure 0.6 bar). Redox (E_h) ranges according to [128].

Due to the absence of general internal redox equilibrium, it was previously advised to use the measured master Eh (redox or mixed potential) with a reserve in predicting the equilibrium chemistry of redox reactions in groundwater. [129]

The reducing conditions were confirmed (Fig. 47). The established 50 - 0 mV range after pumping out the possible stagnant groundwater in the well has confirmed the reducing, anaerobic conditions from this part of the aquifer. According to Hillel und Hatfield (2005) redox potential of 0 mV indicates that oxygen and nitrate are not likely present and that the iron and manganese compounds are in a reduced state. [128] The on-site oxygen concentration (0 - 0.01 mg L^{-1}) confirmed this hypothesis, although the concentration of Fe_{total} i.e. Fe^{2+} was decreased from the last sampling (< 1 mg L^{-1}).

It should be mentioned that the redox potential was taken in the same time when the OxyTech membrane was applied. According to Fig. 47, moderately reducing conditions were formed in the well, but the O_2 concentration was not increased (0 - 0.01 mg L^{-1}). Pumping out the water has shown that the membrane was not able to compensate for the high water turnover and the change in conditions was obvious. Taking this into account, the membrane pressure applied (0.6 bar) showed good characteristics by not inverting the monitoring well conditions to aerobic and thus influencing the microbial activity in a great way, but more importantly avoiding clogging of the well.

The relative pressure of 0.6 bar in the membrane in this case and under this reducing conditions and concentrations was considered appropriate.

4.3.6. Deployment of a gas-water separation APPI-FAIMS for on-site monitoring groundwater contamination and the effects of the OxyTech membrane

This part is focused on the implementation of the on-site monitoring analyses by the developed gas-water separation APPI-FAIMS for the short term deployment and application of the OxyTech membrane. The starting on-site parameters are discussed in 3.2.3.

Fig. 48 shows the construction of the stainless steel lance system by Fabricius ProTerra GmbH involving a perforated part for better membrane activity. The lance is connected on the spot and lowered into the monitoring / remediation well. It has an oxygen supply (blue tube) connected to the membrane, a sampling tube (white / grey) with a small immersion pump at the end for continuous sampling.

In Fig. 49a the lance system is already positioned in the monitoring / remediation well with the OxyTech membrane and the sampling tube; b) shows the deployment of the gas-water separation APPI-FAIMS with N_2 as a carrier gas without the multiparameter sampling unit; and c) shows the aromatic VOC signal during the monitoring process.

A simplified schematic diagram of the abovementioned monitoring gas-water separation APPI-FAIMS and remediation system is shown in Fig. 50. Nitrogen as

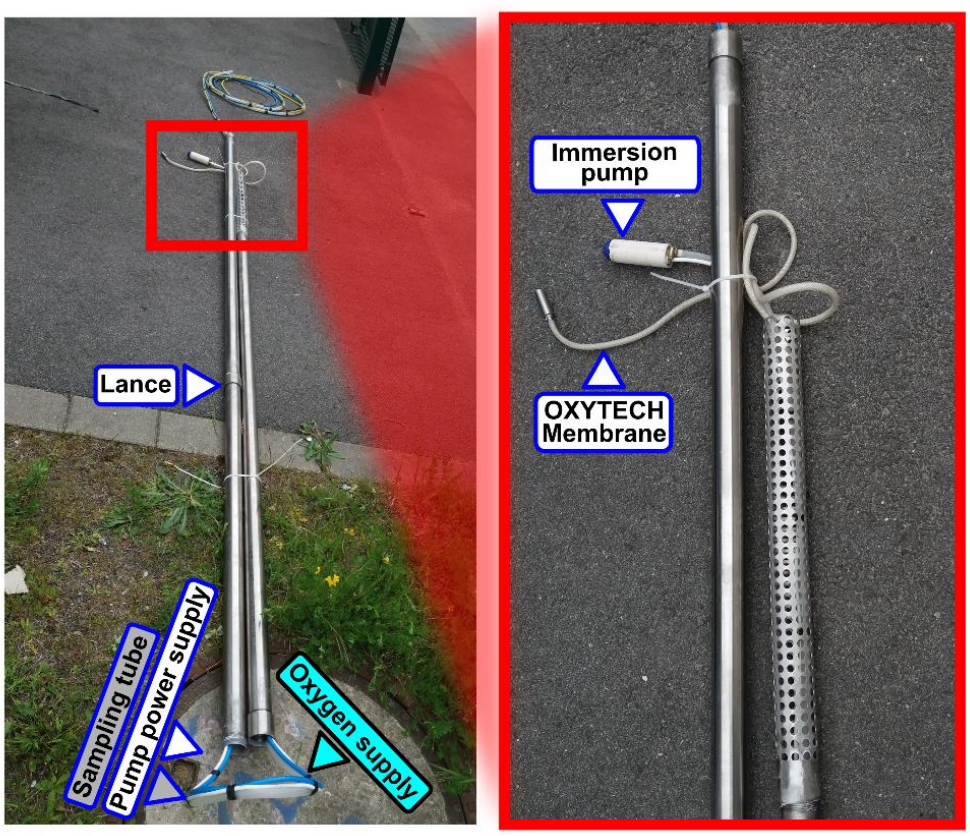

Fig. 48: Depiction of the lance with the OxyTech membrane and the sampling line system later inserted into the groundwater monitoring well.

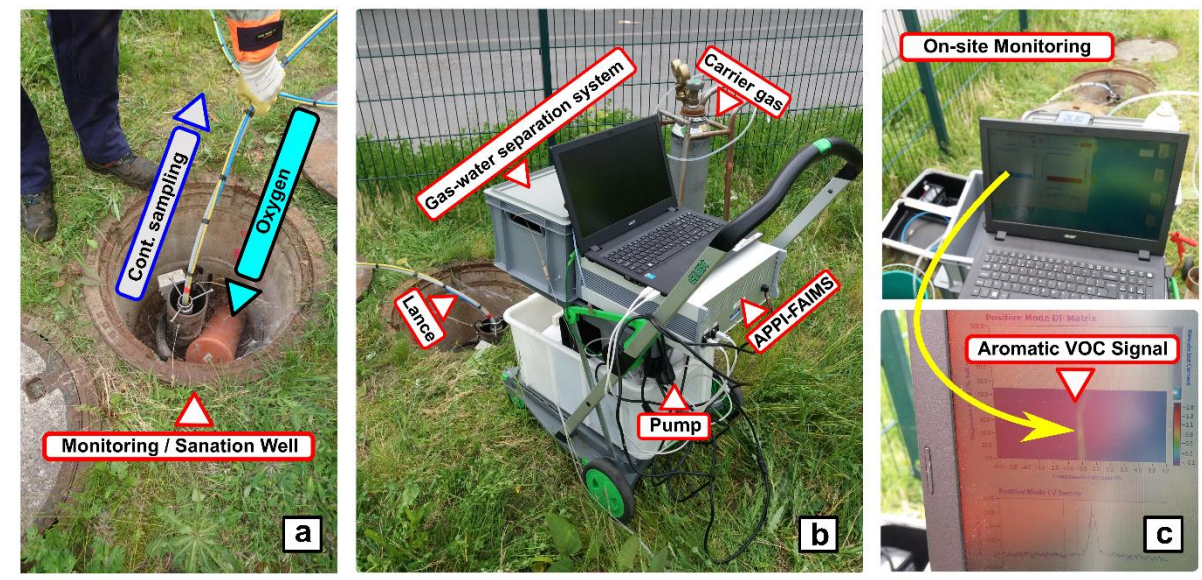

Fig. 49: (**a**) On-site application of the lance with simultaneous probing and inserting oxygen via OxyTech in the groundwater contamination site; (**b**) deployment of the gas-water separation APPI-FAIMS system; (**c**) production of a specific aromatic VOC signal for monitoring purposes.

carrier gas for the monitoring was used in order to avoid ferrous ion oxidation in the separation unit (SU) and successive scaling on the microporous PTFE membrane. Iron scaling of the membrane can greatly influence the aromatic VOC monitoring signal which could be prevented by the developed system. Nevertheless, reference solutions should be used to periodically test the performance of the membrane during extended periods of operation.

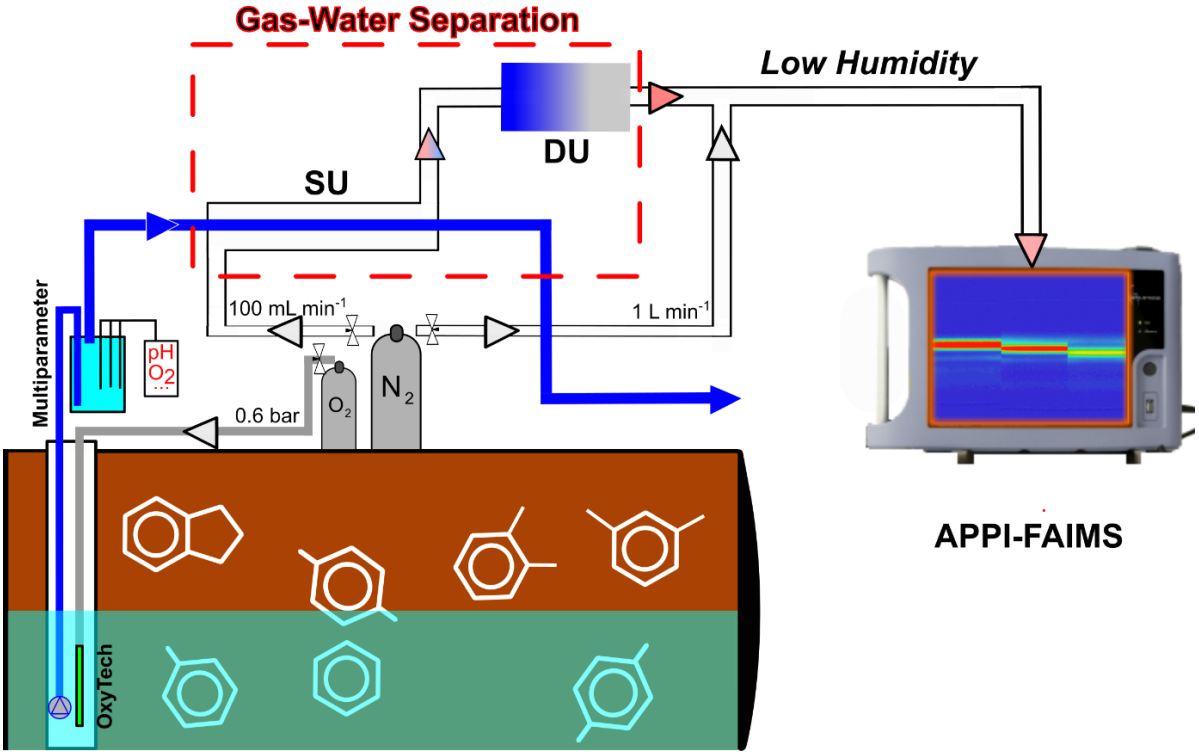

Fig. 50: Schematic depiction of the on-site monitoring system including gas-water separation APPI-FAIMS, multiparameter monitoring (e.g. pH, T, O_2 conc., Conductivity) and implementation of the OxyTech membrane.

4.3.7. Evaluation of the on-site application of gas-water separation APPI-FAIMS for monitoring purposes

The gas-water separation APPI-FAIMS system was used on-site for real-time groundwater monitoring of the previously addressed groundwater well over an extended period of time (~ 5 h). The application of pressure to the membrane (relative pressure 0.6 bar) had started at the ~ 2 h mark. Only the immediate effect of applying oxygen to the anoxic groundwater is considered in the relative short period of time. The chemical remediation aspect of oxygen in carbonate water in presence of ferrous iron is discussed in detail in part 3.3. The procedure and the results of the feasibility

study in application of on-site APPI-FAIMS monitoring at low humidity are shown as follows.

First, the presence of VOCs in the groundwater was confirmed by a DF fingerprint signal (Fig. 51). Different signal intensities were observed at 0% DF (CV_{max} N^{-1} = 0 Td) and 36% DF (CV_{max} N^{-1} = -0.016 Td) (Fig. 51b). Comparison of the CV_{max} N^{-1} of different aromatic VOCs, e.g., toluene (-0.178 Td) and indane (-0.061 Td), with the field determined CV_{max} N^{-1} (-0.016 Td) indicated that a larger aromatic VOC monomer was present that acts as a charge receiver. A larger aromatic VOC has a higher relative molar ionization response, i.e., a lower IE [33], and thus act as a receiver of the dopant charge. Considering this and the selectivity of the APPI source for aromatic VOCs, as well as the increased likelihood of the presence of a larger, unidentified species, the intensity of the sum signal at CV_{max} N^{-1} = -0.016 Td was used as a parameter for monitoring groundwater contamination with aromatic VOCs at this well (Fig. 52).

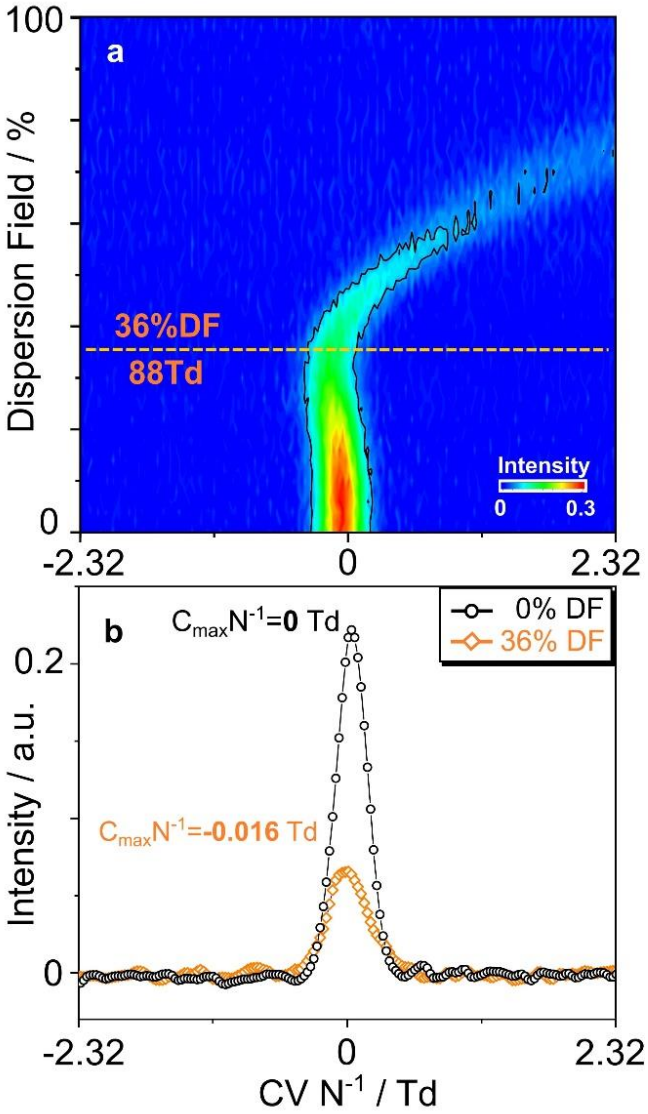

Fig. 51: (a) On-site dispersion field (DF) fingerprint of aromatic VOCs sum-signal in contaminated groundwater by gas-water separation APPI-FAIMS and (b) Intensity comparison of extracted signals at 0% DF and 36% DF.

After determination of CV_{max} N^{-1} (-0.016 Td), continuous contamination monitoring was performed at 36% DF and at 0% DF (CV_{max} N^{-1} = 0 Td) (Fig. 52a,b). The intensity at 0% DF was used as a more sensitive signal for continuous contamination monitoring with periodic change to 36% DF (Fig. 52a).
As seen in both cases, almost the same trend of intensity decrease was observed. A 31-39% decrease in VOCs intensity at CV_{max} N^{-1} values (0 Td and -0.016 Td) was determined between extracted sampling data in approximately 5 hours of continuous monitoring by the gas-water separation APPI-FAIMS (Fig. 52b). At the same time, in parallel with the on-site monitoring, control samples were regularly collected according to the previously established standard sampling procedures [130] for HS-GC/MS to confirm the trend observed in Fig. 52b. Under laboratory conditions, a similar trend in aromatic VOCs concentration was observed, with a 37.4% decrease in cumulative abundance (i.e., total intensity) (Fig. 52d) and a 36% decrease in total peak area.

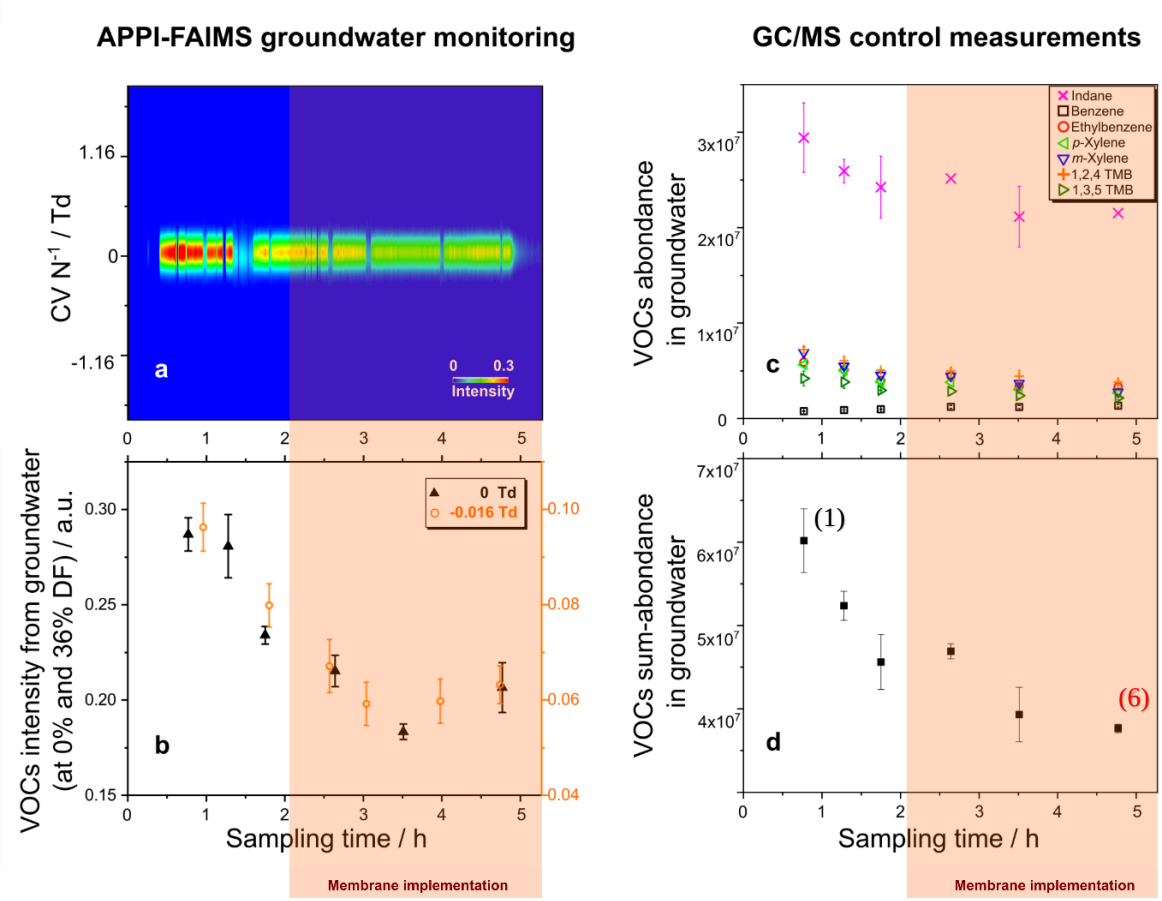

Fig. 52: APPI-FAIMS and HS-GC/MS monitoring data before and after applying the Oxytech membrane. (a) On-site monitoring of aromatic VOCs sum-signal in groundwater: at 0% DF (and periodically at specific 36% DF) in positive mode. (b) Signal intensity at CV_{max} N^{-1}=0 Td (for 0% DF) and at CV_{max} N^{-1}= -0.016 Td (for 36% DF) at different time points (data acquisition: 1 min signal average). (c) HS-GC/MS control measurements of samples taken at the same time as CV_{max} N^{-1}= 0 Td (0% DF) for: indane, benzene, ethylbenzene, *p*-xylene, *m*-xylene, 1,2,4 TMB and 1,3,5 TMB separately. (d) As a sum-abundance of aromatic VOCs in groundwater.

4.3.8. Summarizing the on-site results from the FAIMS-monitoring / membrane application and the multiple parameter analysis

The observed decrease in the concentration of aromatic VOCs indicates the probable difference in contaminant concentration in groundwater due to a stagnant monitoring well. After the well was completely purged (at the 2-hour mark), a relative stabilization of the trend in aromatic VOCs concentration was observed in both cases (Fig. 52b,d). The abrupt change in water conductivity (1340 to 1290 µS cm^{-2}) at the same time (Fig. 53a) also indicated possible purge. The timing of the conductivity drop occurred at a pumping volume of 20 - 30 L, which is consistent with the approximate volume of the well which depends mainly on the groundwater level (table).

These results could be somewhat ambiguous if we consider the fact that the application of the OxyTech membrane started around the same time.

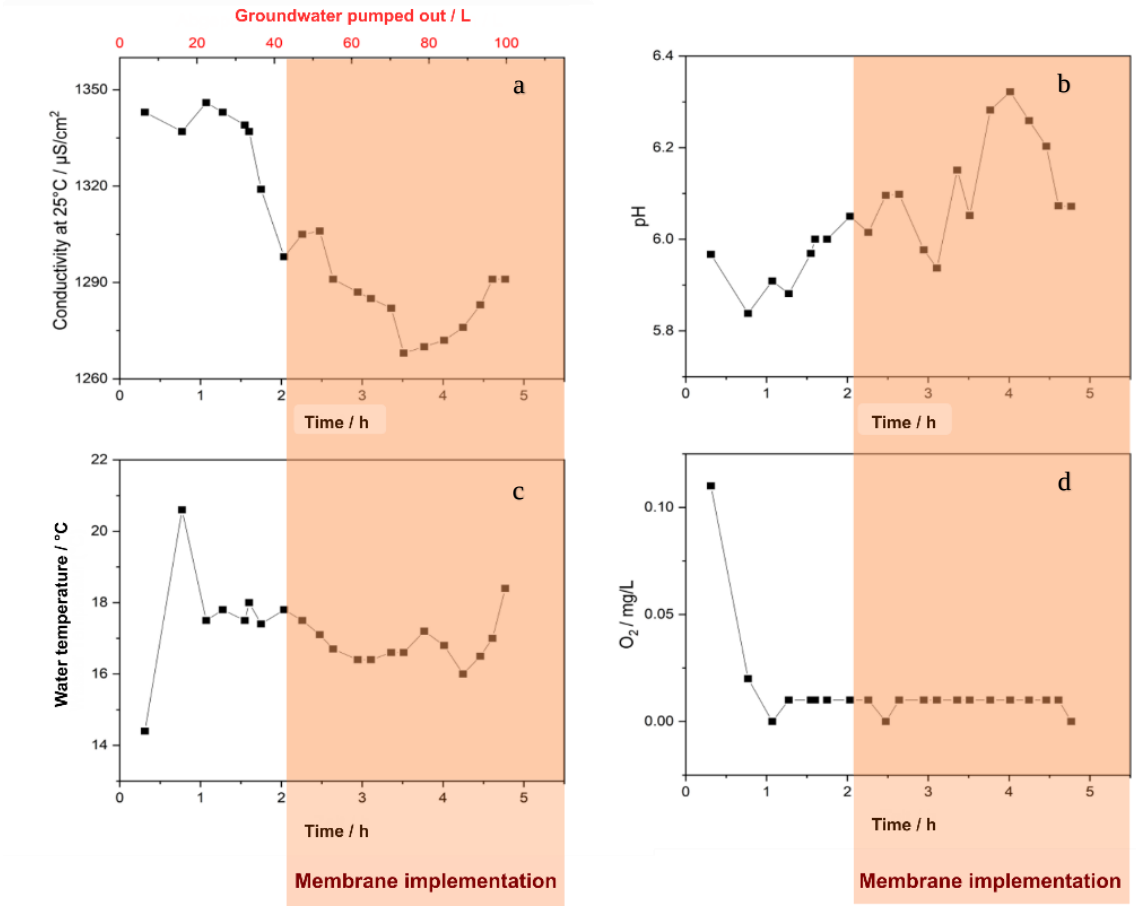

Fig. 53: Simultaneous monitoring of parameters (**a**) conductivity, **b**) pH, **c**) temperature of water, **d**) oxygen concentration in water) during gas-water separation APPI-FAIMS data acquisition from Fig. 52.

This general trend is possibly caused by the decrease in contaminant intensity due to well purging, provided that the concentration in the well is higher than the concentration of the surrounding groundwater (stagnant groundwater). The US EPA

recommends removing three well volumes prior to collecting a representative groundwater sample. [5] Discarding three well volumes is taken as an innsurance of the representative conditions manifested through relatively constant parameters (conductivity, temperature, redox potential, DO (dissolved oxygen), turbidity).

As the concentrations of the aromatic VOC contaminants have changed since the first sampling, the concentration in Fe_{tot} has also changed as part of the progressive evolution of the redox zones in the contamination plume, leading to iron depletion. [125] The initially reported Fe_{tot} (3.8 mg L^{-1}) decreased to 0.68 mg L^{-1} (ICP-OES) and 0.8 mg L^{-1} (AAS), respectively. Iron concentration may influence the initial (oxidation) effect of the OxyTech membrane, as explained later in part 5.3. Considering the anoxic conditions (Fig. 53d) it was supposed: $[Fe_{total}] \sim [Fe^{2+}]$ (see Tab. 11). At the end of monitoring/membrane application, after 5 hours, the total Fe concentration in groundwater was 0.27 mg L^{-1} (ICP-OES) i.e. 0.24 mg L^{-1} (AAS). The decrease of total Fe (i.e. the decrease as soluble Fe^{2+}) was also corresponding to the conductivity decrease (Fig. 53a).

Groundwater temperature played a significant role in generating reproducible aromatic VOC sum-signals. The relatively high atmospheric temperature fluctuations over the course of the year have little to no influence on the temperature of the groundwater in the aquifer. Pumped groundwater, on the other hand, is affected by atmospheric conditions at the surface. This effect is shown in Fig. 53c. Therefore, the monitoring of the groundwater temperature upon surface extraction is of great importance for the pervaporation of aromatic VOCs in SU. The higher ambient temperature increased the groundwater temperature for approx. 5 degrees after extraction, but more importaintly, the temperature was kept relatively constant at 17 °C before entering the SU. The instanation of a temperature controller at the SU with an adjustible temperature (in our case 30 °C) additionally helped in keeping the separation conditions constant. Investigations of the temperature effect on the specific sum signal of water with the gas-water separation APPI-FAIMS showed a maximum variance of 22% for a 10 °C difference in groundwater inflow temperature.The investigation was done on real groundwater sample.

The pH value increased to the previously reported value of ~6.2 (Fig. 53b), after the well was purged and anoxic conditions were established in the multiparameter vessel where pH, conductivity and DO were monitored. The lower pH value was mostly a result of the initial oxidation of Fe^{2+} with O_2 in the multiparameter container due to the increased initial oxygen content (Fig. 53d). After stabilization the DO remained constant throughout.

The consistently low DO content (0 - 0.01 mgO_2 L^{-1}) reconfirms the moderately-reducing groundwater conditions despite the application of the membrane. This also decreases the possibility of colging the well in cases of higher concentration presence of the ferrous iron. Constant pumping-out of small amounts of groundwater (in our case 250 mL min^{-1}) could further secure high permeability of the well under increasing oxidative conditions. The effect of the membrane at a lower groundwater flow rate would require correction of the membrane pressure or only periodic application of the membrane.

To summarize the difference of contaminant intensity at the start (1) and at the end (6) of the monitoring / remediation process (see Fig. 52d) an overlay of the average three chromatograms for both cases is shown in Fig. 54. The decrease in overall contaminant signal is evident. The only exception is the increase in benzene, whose concentration/intensity almost doubles (89.3%).

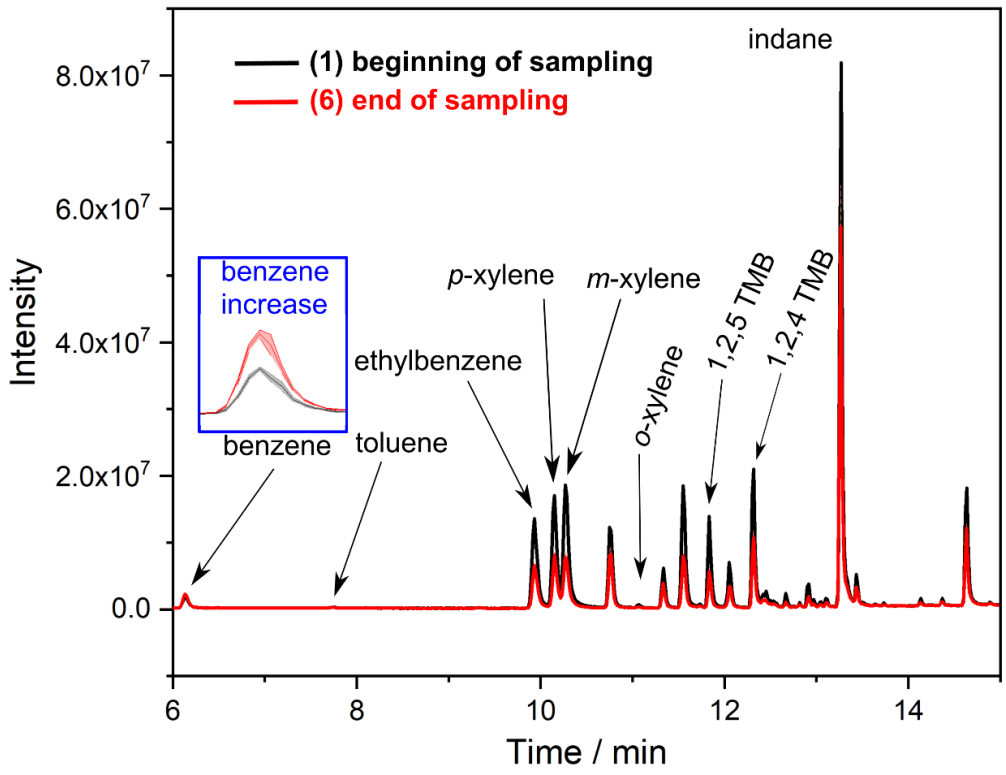

Fig. 54: Difference in intensity at the beginning (probe (1) Fig. 52 d) and at the end of 5 hour application of OxyTech membrane (probe (6) Fig. 52 d). The chromatograms in both cases are an average of triplets.

The inflow of groundwater in the well changed the concentration profile (Tab. 14), which may correspond to the actual surrounding concentration, possibly masking the effect of the OxyTech membrane.
This additional information indicates that there is no general equilibrium between the contaminated soil/groundwater or/and the groundwater in and around the well.
There can be various reasons including well ageing (clogging), which can have biological (e.g Fe^{2+} oxidizing bacteria) and chemical (Fe, Mn oxides and hydroxides) origin. Deterioration of the well construction material could also affect performance. PVC or stainless steel are the first choice for such well casings. [131] The use of PVC material as in the presented study and the inclusion of BTEX as impurities can accelerate the deterioration process and increase the adsorptive interaction.

Tab. 14: The determined concentrations of aromatic VOC in groundwater (external calibration) at the end of the APPI-FAIMS on-site monitoring Fig. 54 (red chromatogram).

AVOC	**Conc. in groundwater** (mg L^{-1})	Conc. difference of the initial and final sample in Fig. 54 (%)
Benzene	**0.53** ±0.24	↑ **89.3**
Toluene	N/A	↓ **N/A**
Ethylbenzene	**0.57** ±0.35	↓ **55**
***p*-Xylene**	**0.53** ±0.34	↓ **61**
***m*-Xylene**	**0.58** ±0.28	↓ **64**
***o*-Xylene**	N/A	↓ **N/A**
1,3,5 TMB	**0.06**[a]	↓ **82**
1,2,4 TMB	**0.57** ±0.36	↓ **53**
Indane	**3.7** ±0.18	↓ **27**

[a] - under the LOD limit of the method

The whole procedure involving the gas-water separation APPI-FAIMS monitoring, including the sampling procedure of the same well, was repeated after 4 days. Input of atmospheric water (e.g. rain) did not occur in this time period. The concentrations of the contaminants were very similar to those at the beginning of the previously described on site sampling (Fig. 54 (1), Tab. 13) and did not differ more than 9% in intensity, except for benzene (22% increase).

The APPI-FAIMS monitoring and successive sampling showed the same sum-signal and HS-GC/MS trend like in Fig. 52 (cf. Appendix (App. 2)). Nevertheless, the concentration of total Fe decreased for more than 25% in comparison to 4 days ago during which the membrane was active (O_2 pressure 0.6 bar). This could be awarded to the effect of the membrane.

The similar trend development, for the second time, under constant Oxytech activity was more indicative of general well purging, still the decrease in concentration of most contaminants (up to 9%) prior to the well purging before and after using the Oxytech (within a 4 day activity) was detected. Despite this indication, the effects of the ferrous ion oxidation on the aromatic VOC contaminants, i.e., the chemical effect of the OxyTech membrane and the slow permeation of oxygen in an anoxic, ferrous environment, were not confirmed. This aspect was addressed in more detail in the following part.

4.4. Conclusion

The focus of this part involved the immediate, chemical effects in implementation of an oxygen permeable silicone membrane (OxyTech) as a support of standard groundwater remediation treatments. With the application of OxyTech, relatively slow and pressure-dependant permeation of oxygen occurred. This gave the possibility of rather slow, gradual switching of the redox conditions in the monitoring well to occur (which also influences indigenous microbial species); more important, it prevents clogging of the well when high Fe^{2+}-concentration is present. It was shown, constant pumping of contaminated groundwater (like in the case of P&T) can provide the retaining of relatively constant conditions (steady state). In this work case the moderate-reducing conditions in the monitoring well were maintained during implementation of OxyTech.

Previously applied analysis of the groundwater revealed increased presence of indane next to the BTEX, which was confirmed through analytical standards and further taken into consideration.

At the same time, the APPI-FAIMS system with gas-water separation was used on site to monitor the contamination as described in Part 3. The monitoring system used was able to successfully monitor the intensity of aromatic VOC contamination in the groundwater well. In this case, a specific aromatic VOC sum signal with C_{max} N^{-1} of -0.016 Td successfully reflected the decreasing trend provided by static HS-GC/MS from strategically taken control samples. The on-site use of the gas-water separation APPI-FAIMS monitoring system was consistent with the time frame and appropriate to demonstrate the potential short-term effects (Fe^{2+}-oxidation) of the OxyTech membrane. Increase of the drying unit (DU) dimensions and periodical sampling could provide a basis for long-term monitoring possibility.

Nevertheless, the benefit of the application of OxyTech for remediation purposes remained inconclusive, despite the successful on-site monitoring method. The significant decrease of aromatic VOC and application of OxyTech coincided with the assumed volume needed for the groundwater well to be purged. The same monitoring procedure was done once again and showed almost identical development of the contamination trends, mostly independent from the start-time of OxyTech application. Unfortunately the current decreased presence of ferrous iron (< 1mg L^{-1}) in the well was seen as a crucial factor in the oxidation of the contaminants. Further analysis of the effect of ferrous oxidation in anoxic water with addition of dioxygen was carried out separately in order for the oxidation potential of ferrous containing groundwater to be confirmed.

5. The effects of oxygen-induced oxidation of ferrous iron in carbonate-rich water on aromatic volatile organic compounds

5.1. Introduction

Iron, iron oxides and carbonate rocks such as limestone, dolomite, marl and other carbonate minerals are omnipresent in the earth's crust and therefore in the groundwater as dissolved ferrous iron (in anoxic conditions) and as carbonate/bicarbonate ions. [5] Ferrous iron ions/salts/minerals are used in different ways when it comes to environmental applications, including reductive or oxidative removal of various water contaminants.

Fe^{2+} has a part in reducing organic and metal pollutants and thereby altering their toxicities. [132–134] Simultaneously, the efficiency of the contaminant transformation via reduction is positively affected by the carbonate presence [132], although other studies show the siderite lattice ($FeCO_3$) as a poor promoter of an electron transfer. [134]

The carbonate / bicarbonate equilibrium has also a prominent role in oxidation reactions supported by ferrous iron (e. g. Fenton's reactions). [27,135,136] The role of Fe^{2+} as a catalyst in production of different reactive species was always met with interest in consideration of advanced oxidation processes (AOPs). Fe^{2+} activation of alternative chemical oxidants such as percarbonate ($H_3CO_6^{2-}$) and persulphate ($S_2O_8^{2}$) *in situ* is considered important when considering the chemical properties of groundwater. However, both show low efficiency in carbonate-rich water with only low rates of organic matter (BTEX) degradation. The presence of bicarbonate / carbonate ions is crucial as they can scavenge reactive species such as $^{\bullet}OH$ radicals regardless of the initial chemical oxidant. [137]

Possible increased generation of reactive species was noticed in the presence of different ligands including the carbonate / bicarbonate system. Baudish and Welo (1924) discussed the mechanism for the oxidation of inorganic or organic compounds in presence of ferrous iron and activated oxygen, but with a small emphasis on the involvement of carbonate / bicarbonate ions. [138] The oxidation of ferrous iron in water, in presence of dioxygen, showed formation of reactive species (e.g. $^{\bullet}OH$) when specific ligands were present. This was the case with the reagent of Udenfriend (1953) containing EDTA and ascorbate. [139,140] More recently, several other studies discuss the same possibility of stimulated reactive species formation in the presence of various ferrous complexing agents and buffers including carbonate / bicarbonate ions. [141–143] The use of ferrous-activated oxygen in carbonate-rich water was not considered as such for remediation purposes, but the effects were noted. King et al. (1998) mentioned a trend and possible radical/H_2O_2 formation at oxic-anoxic interfaces in groundwater. [144]

In this work, the detection of possible $^{\bullet}OH$ radical formation in carbonate rich water, during Fe^{2+} oxidation (i.e. O_2 activation) was investigated in relation to the aromatic VOC and the application of the OxyTech membrane. The possible formation

of •OH radicals were monitored through the subsequent reaction with coumarin by producing fluorescent species with high quantum yield (e.g. 7-hydroxycoumarin).
GC/MS detection of the possible oxidation products of the previously mentioned groundwater contaminants (BTEX and indane) in reaction with the generated •OH radicals was carried out. The ferrous iron was oxidized in anoxic water rich in carbonate / bicarbonate by adding O_2 (simulating groundwater conditions) or in already O_2 saturated water.
This hypothesis related to the possibility of using oxygen as a small but simple additional step in groundwater remediation.

5.2. Experimental

5.2.1. Chemicals

For the experiments the following chemicals were used: benzene >99% (AppliChem GmbH, Germany); toluene >99.5% and indane ≥95% analytical standard (Sigma-Aldrich, Germany); ethylbenzene ≥99% (Fluka Analytical, Switzerland). MTBE ≥98% used for product extraction and liquid injection (Sigma-Aldrich, Germany). Iron (II) chloride tetrahydrate ≥98% from Bernd Kraft, Germany was used as ferrous species.

Buffer solutions used for calibration of the pH electrode: pH 7.00 (20 °C) phosphate mixture and pH 4.00 (20 °C) citric acid/NaOH/NaCl from Bernd Kraft, Germany. pH 9 (20 °C) VWR chemicals, USA. HCl (~37%) from Fisher, USA for glassware cleaning. Nitrogen (5.0; 99.999 % Air Liquide, Germany) was used for oxygen purging.

Coumarin-3-carboxylic acid, 99%, used as •OH scavenger, umbelliferone (7-hydroxycoumarin), 99% for calibration purposes and Piperazin-N,N′-bis-(2-ethanesulfonic acid) or PIPES ≥99% all purchased from Sigma-Aldrich, Germany.

$NaHCO_3$ ≥99.7% Riedel-de Haën, Honeywell (USA). 0.1 M solutions from NaOH (pellets for analysis) from Bernd Kraft, Germany and HCl 37% (analytical reagent grade) from Fisher, USA were used for adjusting the pH. In addition, tri-sodium citrate dehydrate ≥99% (Sigma-Aldrich, Germany) was used instead of $NaHCO_3$ for Fe^{2+} oxidation.

For the preparation of solutions, Milli-Q water > 18 MΩ was used from a Milli-Q Plus water purification system (Millipore, USA). Home-made 2 L vessel (from duran glass) was used for continuous measurement of temperature, pH and oxygen content (Fig. 55).

5.2.2. Instruments and methods

Fluorescence flow-through cuvette (QS), UV/VIS range (200-2500 nm) with optical path 10 x 2.5 mm from Hellma, Germany was used in all fluorescence applications if not stated otherwise.
Before the MTBE extraction the pH was adjusted by using 780 pH Metre from Metrohm, Switzerland; pH continuous monitoring was done by portable WTW multi 3420 Optical Oxygen Sensor FDO 925 and by Hach HQ30d portable multimeter. Peristaltic Pump Reglo Analog (Ismatec, Germany) was used to pump the solution through filter (SCAT HPLC suction filter, pore size 20 µm, Fisher Scientific) and the flow-through cuvette.
OEM Research Scale Type-R 200 D Sartorius, Germany was used for making solution and adding $FeCl_2 \cdot 4H_2O$ (i.e. Fe^{2+}). PTFE coated magnet agitator in combination with RCT basic magnetic stirrer from IKA, Germany. The overhead shaker (Reax 20 from Heidolph, Germany) was used at the end for better extraction 30 min, 13 rpm. Parallel evaporator Büchi Syncore Polyvap Q-101 R-12 from Büchi Labortechnik GmbH, Germany with MZ 2C Vacuum Pump Vacuubrand, Germany.
Spectrofluorophotometer RF-6000 from Shimadzu, data interval 1 nm, 5 nm excitation and emission bandwidth with high sensitivity (if not stated otherwise) was used for fluorescence determination. Excitation Wavelength 332 nm, scan speed 6000 nm/min, the sensitivity was set high or low depending on the signal.

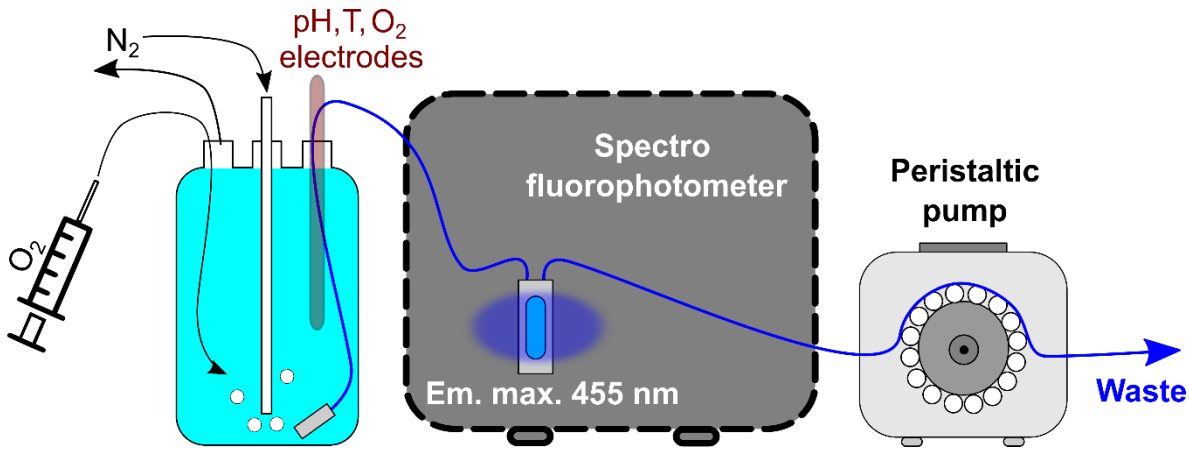

Fig. 55: Scheme of the experimental setup for determination of formation of •OH radicals with coumarin (from left to right: home-made, 2 L glass reaction vessel; spectrofluorophotometer; peristaltic pump).

For the detection and validation of the oxidation products a GC/MS system was used. GC: Trace GC/Ultra (Thermo) and MS: DSQ II from Thermo Electron Corporation USA, EI, 70 eV; Full scan mode: 50-350 m/z (single quadrupole); Column: Zebron ZB-SemiVolatiles (Phenomenex, Germany) 30 m x 0.25 mm ID x 0.25 µm film thickness. The temperature program was set to 40 °C (hold time 2 min) to 220 °C with 20 °C/min

and hold time of 2 min. Helium (>99.999% from Air Liquide, France) was used as carrier gas with a gas flow of 1 mL min^{-1}. The injection of the sample was carried out by automatic injection HTX PAL Autosampler (CTC Analytics AG, Switzerland). The 1.5 mL short thread screw vials 32 x 11.6mm (amber) were filled with sample and direct injection (DI) (3.5 µL) was used with splitless injection mode (splitless liner) and splitless time 1 min, at 250 °C injector temperature. The transfer line temperature was set to 250 °C. NIST/EPA/NIH Mass Spectral Library Version 2.0 from 2008 was used for mass search. [145]

Determination of formation of reactive species (•OH radicals) with oxidation of Fe in bicarbonate containing water and with coumarin as •OH scavenger (Fig. 55): the 2 L home-made vessel was filled with Milli-Q water and purging of N_2 was performed until oxygen was not detectable. The analytes were added under N_2 with a concentration of: 10 mM $NaHCO_3$, 0.1 mM Fe^{2+}, 20 µM coumarin. O_2 was added with a syringe (6 mL) after coumarin was fully dissolved and confirmed by spectrophotometric measurement (USB4000 spectrometer with ISS UV/VIS light source, Ocean Optics, USA).

Fe-oxidation was carried out with O_2 - saturated water (250 mL) in the presence of 10 mM $NaHCO_3$ and aromatic VOCs (benzene, toluene, ethylbenzene, indane) with a starting concentration ~35 mg L^{-1}. Approximately 15 mg $FeCl_2 \cdot 4H_2O$ were added four consecutive times to the solution (end pH~ 7). The pH was then lowered to 5 (1 M HCl); additionally 40 - 50 mL of MTBE were added and the Schott bottle was shaken with an overhead shaker for 30 min. The organic part was separated and reduced through evaporation with the parallel evaporator (30 min, 60°C). If needed, re-solvation with MTBE was performed to a final volume of 1 - 1.5 mL and injected. Experiments were performed in the dark to avoid induced photooxidation.

Ibuprofen sodium salt ≥98% (GC) from Sigma-Aldrich, Germany was used as a different contaminant and underwent a similar procedure as the AVOC previously. Six schott bottles (250 mL) were filled with Milli-Q water and $NaHCO_3$ (10 mM) was added to all. The pH was adjusted to 8 (1 M NaOH) and 15 mg of ibuprofen sodium salt (60 mg L^{-1}) was added to all six. In the first bottle no Fe^{2+} was added, in the second bottle only 10 mg of Fe^{2+}. Portions of ~10 mg were added and increased successively ending up with bottle 6 having ~50 mg Fe^{2+} in total. In-between the pH was adjusted to 8 before the next portion of Fe^{2+} was added. At the end the pH of all bottles was lowered to 5 and 20 mL of MTBE (organic phase) was added for extraction (1 h) in the overhead shaker. The organic portion was separated and reduced through evaporation (30 min, 60°C). An aliquot was taken for further analysis. The same procedure was used for the determination of the primary and secondary oxidation products of benzene and their relationship to each other.

Determination of the possible oxidation products of ibuprofen was done with HPLC (Agilent 1200) and single quadrupole mass spectrometer (Agilent 6120B). An eluent with a composition of 20% methanol (with 0.1% formic acid) and 80% water (with 0.1% formic acid) was used up to 4 min, flow gradient ratio change occurred till 10 min (80% methanol, 20% water). A “reversed-phase” separation column (Kinetex® 5 µm EVO C18 100 Å, 100 × 3.0 mm) was used at a flow rate of 0.5 mL min^{-1} and a

column temperature of T = 30 °C. The injection volume was 10 µL and the sequence time was 10 min. Ionization of the analytes was performed by electrospray ionization (ESI) in negative mode. The following settings were selected for this. A capillary voltage of 2500 V, Drying Gas (N_2) 10.5 L min^{-1}, Drying Gas Temperature 250 °C and Nebulizer Pressure 35 psig and additionally a solvent delay of 2.5 min were used.

For the single quadrupole mass spectrometer and the samples of ibuprofen oxidation with a scan mass range 50 - 300 m/z (100 % cycle time) in negative mode was chosen.

5.3. Results and discussion

5.3.1. Detection of reactive species (•OH radicals)

Coumarin was used in order to confirm the formation of reactive species, i.e., the suspected formation of •OH radicals only by adding O_2 for the oxidation of Fe^{2+} in anoxic conditions, without application of H_2O_2. The use of coumarin for detection of •OH radicals have several advantages, it is rapid, sensitive, specific, utilizes standard instrumentation and it exclusively forms the monohydroxylated isomer 7-hydroxycoumarin (Fig. 56), a compound with high quantum yield. [146]

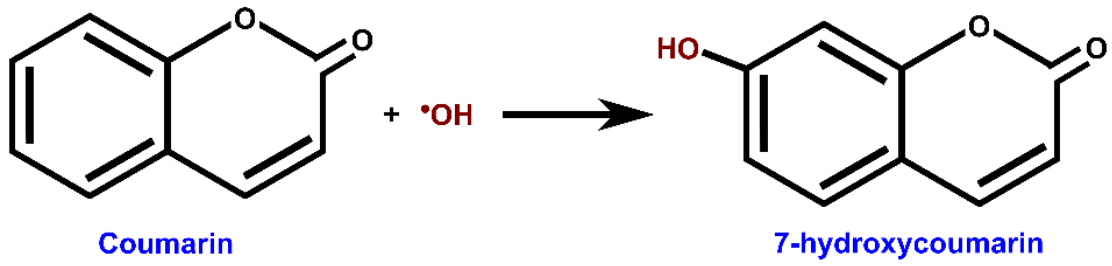

Fig. 56: Formation of 7-hydroxycoumarin (i.e. umbilliferone) by the reaction of coumarin and •OH radicals [147].

Coumarin itself is poorly fluorescent, it reacts with the hydroxyl radicals fast in a second order reaction limited only by diffusion ($k > 10^9\ M^{-1}\ s^{-1}$) and therefore it is utilized for detection/quantification in Fenton-type reactions. [148,149] Reaction rate constants differ slightly depending on the scientific source and are larger than the one listed in Tab. 15. Reaction rate constants of $6.4 \cdot 10^9\ M^{-1}\ s^{-1}$ and $8.2 \cdot 10^9\ M^{-1}\ s^{-1}$ are also reported by [149] and [146] respectively. The produced 7-hydroxycoumarin is highly fluorescence stable, allowing indirect quantitative analytical correlation with the presence of •OH radicals. Other hydroxycoumarin isomers could possibly be produced, but their fluorescence emission is negligible compared to 7-hydroxycoumarin. [148]

The hydroxyl radical is a neutral free radical with a relatively short lifetime in water, behaves like a weak acid, has a pK_a of 11.9 ±0.2 and an estimated electron affinity of 5.8 eV in water. [150]

Spectrophotometric, the •OH has a low absorbance in water that starts at 300 nm and increases at shorter wavelengths. [150] Unfortunately, this is the same region where iron oxidation ($Fe^{2+} \rightarrow Fe^{3+}$) is most evident.
The fluorescence of 7-hydroxycoumarin (7-HO-COU) has an emission maxima of 450-455 nm and is much more sensitive than the aforementioned spectrophotometric method.

Tab. 15: Reactivity of •OH radical in aqueous solution with various species as summed from Dorfman (1973) [150] and *Buxton et al. (1988) [151].

Analyte	***k* (M^{-1} s^{-1})**	**pH**
Benzene	7.80E+09	7
Phenol	1.40E+10	7.4-7.7
Toluene	3.00E+09	3
m-Xylene *	7.50E+09	~7
o-Xylene *	6.70E+09	~7
p-Xylene *	7.00E+09	~7
Ethylbenzene*	7.50E+09	7
Coumarin*	**2E+09**	***I***
o-Cresol*	1.10E+10	9
p-Cresol*	1.20E+10	5.5
Fe^{2+} *	3.20E+08	7
Fe^{2+}	>1E+8	0.1
Mn^{2+}	>1.4E+8	7
CO_3^{2-}	4.20E+08	10.8; or < 11.6
HCO^{3-}	15000000	6.5

5.3.1.1. Fluorescence intensity of umbelliferone as a function of pH

The majority of the methods utilizing coumarin as •OH radical scavengers were performed at a constant pH and did not explicitly address the dependence of the umbelliferone (7-hydroxycoumarin) fluorescence intensity on pH. Pereira et al. (2018) addressed this issue. [152] Initially, 322 nm was used as the excitation wavelength,

which represents the excitation maximum under acid-neutral conditions (Fig. 57). Changes occurred when $NaHCO_3$ was added to simulate carbonate-rich groundwater as in a large number of aquifers. [153]

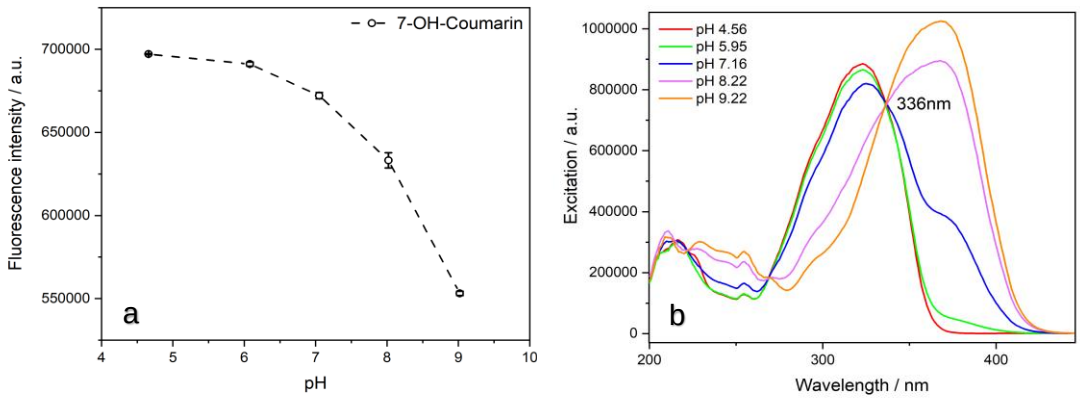

Fig. 57: Influence of pH on the fluorescence parameters of umbelliferone (7-hydroxycoumarin). a) Change of fluorescence intensity for 20 µM 7 –hydroxycoumarin with change of pH (parameters: excitation at 322 nm, emission at 455 nm); b) Excitation spectra of 7-hydroxycoumarin at the maximum emission point (455 nm) and determination of the isosbestic point at 336 nm.

The fluorescence intensity of umbelliferone was significantly influenced by the change in pH, especially in the range from 7 to 9 (Fig. 57a). Decrease of around 20% was observed from pH 4.7 - 9. This was due to the increased deprotonation of umbelliferone with increasing pH, knowing its pK_a is 7.7. [152]
Deprotonation of umbelliferone stabilizes the π→π* transition as it increases the conjugation of the system. Pereira et al. (2018) [152] established an isosbestic point at 336 nm with an UV-VIS spectrophotometer, which was also confirmed in our case with an excitation spectrum (Fig. 57b). The isobestic point was crucial for measurements in which pH changes were caused by Fe^{2+} oxidation.

After confirming the isosbestic point of umbelliferone (7-hydroxycoumarin) with respect to pH (336 nm), additional effects of bicarbonate/carbonate anions on the fluorescence signal were considered because of the known high concentrations in groundwater. For this purpose a fluorescence calibration of 7-hydroxycoumarin in water was performed (Fig. 58, green). $NaHCO_3$ was added to the same calibration solutions to achieve a final concentration of 10 mM and pH 8.4 - 8.5 (Fig. 58, blue). The new calibration values were almost identical with the previous, thus dismissing any effects (e.g. inner filter effect) that could have been caused by$NaHCO_3$.
Therefore, the formation of umbelliferone (i.e. 7-hydroxycoumarin) was further used as a reliable indirect method to detecting possible formation of •OH radicals in the carbonate-rich water.

The presence of an increased amount of Ca^{2+} cations (4.2 - 6.9 mM) in groundwater with high alkalinity (expressed as 10 mM HCO_3^-) indicates an actual

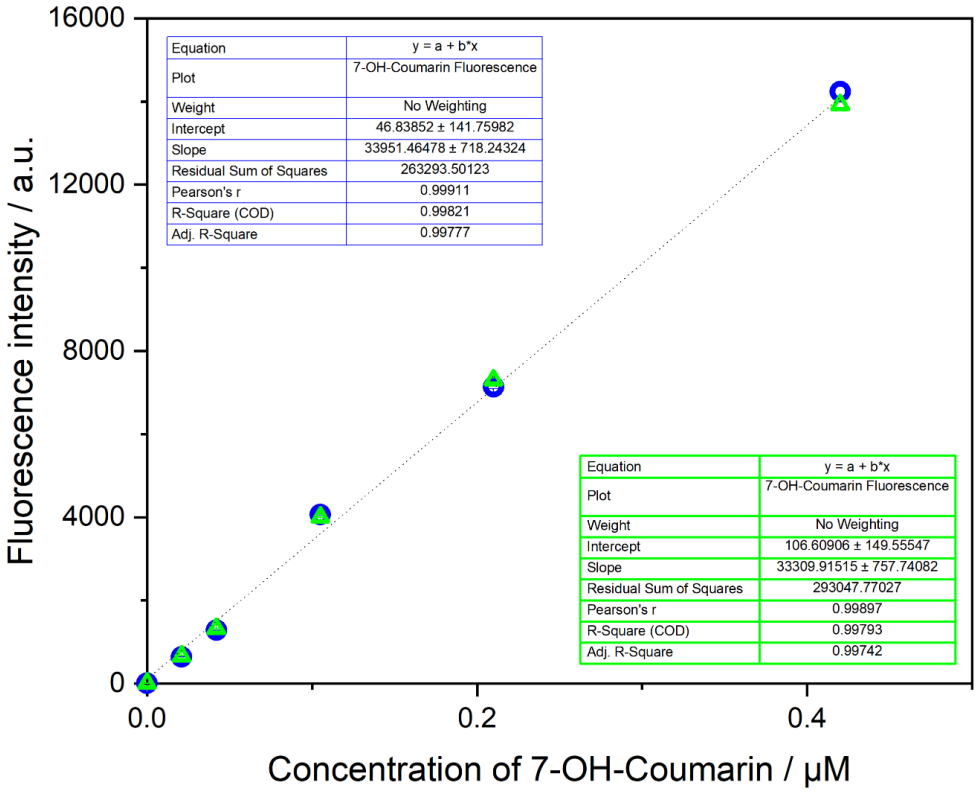

Fig. 58: Calibration of 7-hydroxycoumarin (7-OH-Coumarin) with excitation at 336 nm (isosbestic point) and emission at 455 nm in the case with (green) and without (blue) the presence of 10 mM $NaHCO_3$ and at different pH.

increased presence of carbonate/bicarbonate ions in the groundwater. According to the carbonate mass balance for surface waters (eq. 29), $2[Ca^{2+}] \sim [HCO_3^-]$ generally holds, which approximately explains for the determined alkalinity and Ca^{2+} concentration. [154]

$$CaCO_3\,(s) + CO_2\,(aq) + H_2O \leftrightarrows Ca^{2+} + 2HCO_3^- \qquad \text{eq. 29}$$

In addition, an increase of CO_2 in groundwater causes a shift in equilibrium, a decrease in pH, and dissolution of $CaCO_{3\,(s)}$ ($K_{sp} = 3.36 \cdot 10^{-9}$) present in the marlstone or limestone, contributing to the increased carbonate concentration in groundwater. [16] It should be noted that high carbonate / bicarbonate concentrations in water are possible in closed systems such as groundwater.
Groundwater CO_2 could originate from previous microbial activities (respiration / oxidation) under anoxic and oxic groundwater conditions [109], which could be enhanced by organic contaminants.

Since the pH range of the groundwater is between 6.2 - 7, and considering the speciation diagram of carbonic acid (Bjerrum plot), bicarbonate and carbonate, it is expected for HCO_3^- to be the predominant carbonate species in the aquifer. This changes with the presence of metal cations such as iron as described later.

5.3.1.2. Formation and detection of possible •OH radicals upon ferrous oxidation with oxygen in carbonate-rich water (oxygen-induced oxidation)

The detection of •OH radicals was performed as previously described using coumarin (20 µM) in presence of Fe^{2+} (final concentration 0.2 mM) and $NaHCO_3$ (10 mM), similar to the values determined in the field.

In this case (i.e., Fig. 59a), a fluorescence signal with emission maxima at 455 nm, typical for 7-hydroxycoumarin, has proven the formation of •OH radicals.

Another observation was made in Fig. 59b where absence, or only a possible weak fluorescence was noticed.

In both cases, the same amount of Fe^{2+} in the form of $FeCl_2 \cdot 4H_2O$ was added to the solution in two separate portions. After the addition of the first amount of Fe^{2+}, 6

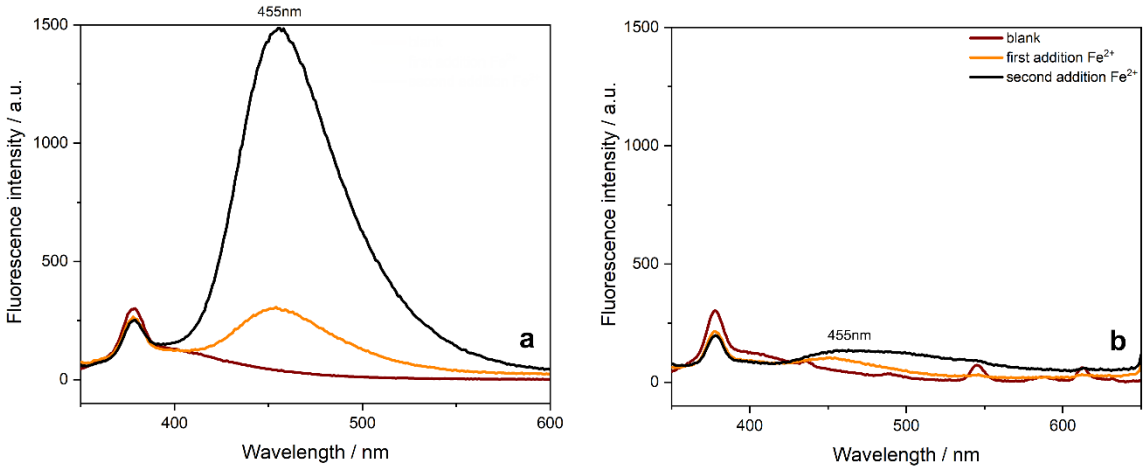

Fig. 59: Fluorescence intensity increase with addition of Fe^{2+} in O_2 saturated water in presence of 20 µM Coumarin. (a) with HCO_3^- (b) without HCO_3^-.

mL of O_2 was successively added to the anoxic water solution for controlled ferrous iron oxidation. The signal in Fig. 59a occurred only after the addition of oxygen. The only difference between Fig. 59a and Fig. 59b is the presence/absence of $NaHCO_3$. The addition of $NaHCO_3$ increased the pH of the solution and enabled oxidation ($Fe^{2+} \rightarrow Fe^{3+}$) to occur. In the second case, Fig. 59b, the oxidation of Fe^{2+} in Milli-Q water lowered the pH thereby slowing the reaction. Addition of 1 M NaOH increased the pH, allowing complete and rapid oxidation of Fe^{2+}, as was the case with the previous addition of $NaHCO_3$, yet no fluorescence was observed.

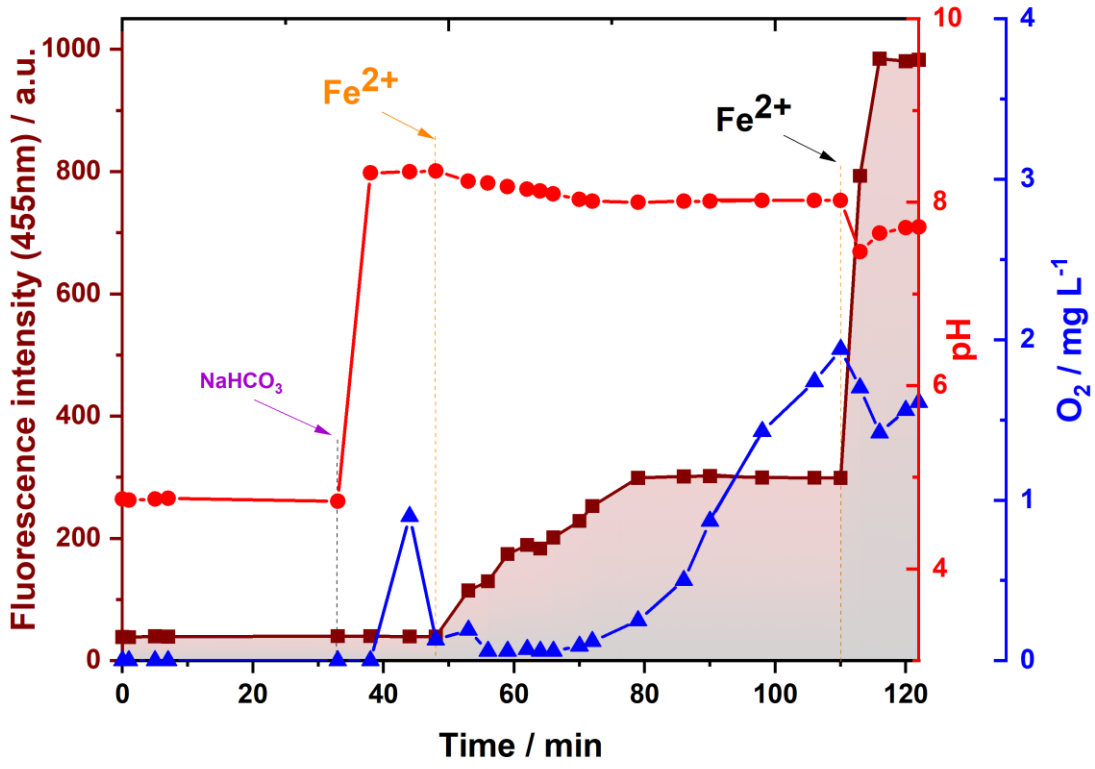

Fig. 60: Continuous observation of fluorescence intensity at 455 nm, pH and DO (dissolved oxygen) for the Fe^{2+}- oxidation in water with $NaHCO_3$ in presence of coumarin (20 µM) as hydroxyl radical scavenger.

Fig. 60 and Fig. 61 show the results of the two separate Fe^{2+}-oxidation processes with simultaneous monitoring of fluorescence, pH and dissolved oxygen content.

In both cases similar conditions were set. The oxidation of the ferrous iron in presence of bicarbonate proved the formation of •OH radicals through the increase of the fluorescence intensity at 455 nm. The increase in fluorescence intensity after the initial addition of $FeCl_2 \cdot 4H_2O$ and O_2 was slower due to the O_2 deficit. After opening the vessel and gradually increasing the DO content to 2 mg L^{-1}, Fe^{2+} was added for the second time. The fluorescence intensity increased and reached a plateau almost immediately, simultaneously the oxygen content dropped below 1.5 mg L^{-1} and the pH decreased from 8.02 to 7.72. Similar pH decrease (from 8.34 to 8.02) was recorded for the first time when Fe^{2+} was added. The only difference was the disproportionate increase in fluorescence intensity.

Taking the variables into account, an overall increase in fluorescence intensity of 28% was registered for the same amount of Fe^{2+} which was added for the second time (Fig. 60). This supposed difference in quantum yield is thought to be a product of the aqueous equilibrium between bicarbonate and carbonate ions, i.e. their different •OH radical scavenging potential. The reaction rate constant of •OH with HCO_3^- is significantly (42 times) slower compared to the reaction rate constant of •OH with CO_3^-

(Tab. 15). Therefore, the increasing presence of CO_3^{2-}, mainly as $^{\bullet}OH$ radical scavenger, is considered to be the main reason for the decrease of fluorescence intensity of 7-hydroxycoumarin. In addition, CO_3^{2-} could form $FeCO_3$ with ferrous iron ($K_{sp} = 3.13 \cdot 10^{-11}$), thus reducing its availability.

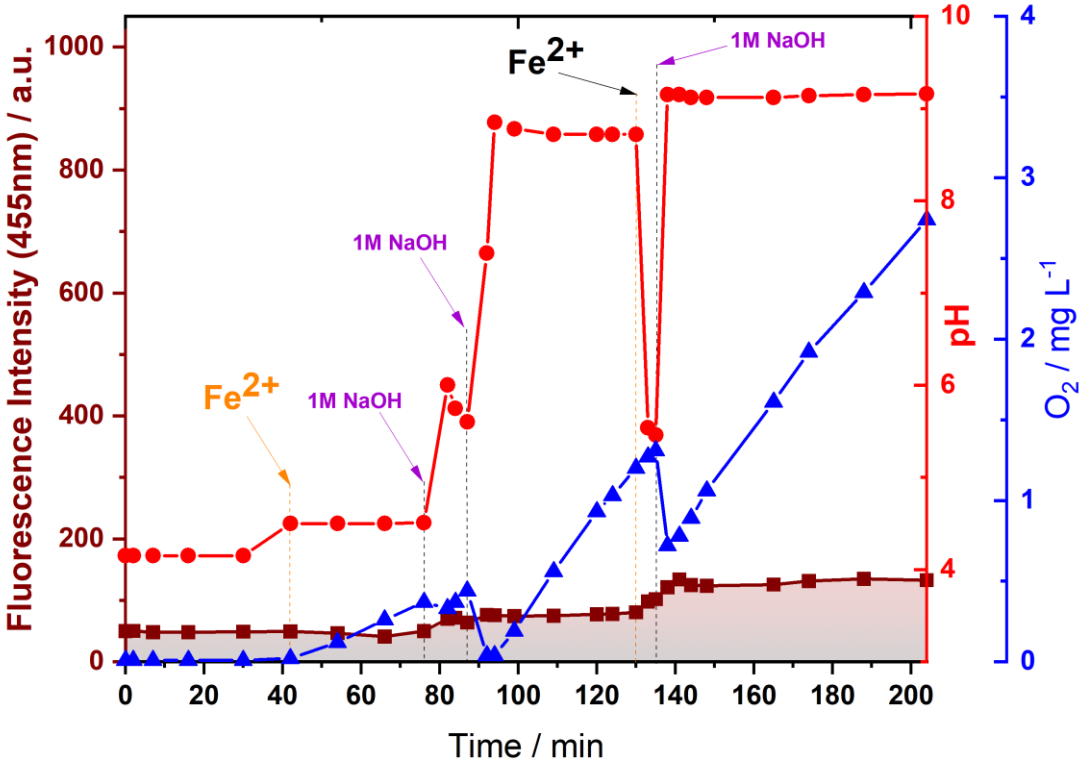

Fig. 61: Continuous observation of fluorescence intensity at 455 nm, pH and DO (dissolved oxygen) for the Fe^{2+}-oxidation in water with addition of NaOH in presence of coumarin (20 µM) as a hydroxyl radical scavenger.

There is also an inhibitory effect of $[Cl^-]$ on $^{\bullet}OH$ radicals, which was previously studied by Lou and Lee (1995) using the Fenton process of BTX removal (pH 4) as an example. [155] They concluded that the effect was not significant even at high $[Cl^-]$ 0 - 900 mg L^{-1}. Therefore, the effect of the presence of Cl^- (5 - 22 mg L^{-1}), as $FeCl_2 \cdot 4H_2O$, was considered negligible in this investigation. More recent studies, e.g., Wu et al. (2014) have suggested otherwise, especially for $[Cl^-] > 1$ mM. [156] This limit was not exceeded during our experiments, even by several successive $FeCl_2 \cdot 4H_2O$ additions, as will be shown later.

To further minimize the possible influence of Cl^- activity on the results, the same counter-ion (Na^+) was used in both cases for $NaHCO_3$ (Fig. 60) and NaOH (Fig. 61).

It could be concluded that the presence of bicarbonate ions at a pH range between 6.5 and 8 favours the formation of reactive species, possibly $^{\bullet}OH$ radicals in Fe^{2+} oxidation with dioxygen. This pH range fits most aquifers, including the

groundwater studied in this work. With decreasing of the pH < 5, the oxidation of the ferrous iron becomes much slower (Fig. 62) and was therefore not considered.

The stoichiometry between Fe^{2+} oxidation and consumed oxygen was determined from the amount of Fe^{2+} added and the approximate decrease of the projected oxygen content. In both cases when oxygen reacted, a similar stoichiometry of 4:1 was found for Fe^{2+}:O_2. This is consistent with eq. 30 [157] and the formation of iron oxide-hydroxide.

However, the stoichiometry of 5:1 for Fe^{2+} : O_2 was also detected with the reactions in Fig. 60 and Fig. 61, as they were repeated several times.

$$2\,Fe^{2+} + 0.5\,O_2 + 3H_2O \rightarrow 2\,FeOOH + 4H^+ \qquad \text{eq. 30}$$

In the case when $NaHCO_3$ was not present (Fig. 61) the production of •OH radicals upon Fe^{2+} oxidation in water was not confirmed. The small increase in fluorescence could be due to various marginal factors. The oxidation in (Fig. 61) was carried out with O_2, supported by addition of NaOH. The Fe^{2+} : O_2 stoichiometry followed the same ratio.

In order to confirm the presence of reactive species shown in Fig. 59a and Fig. 60, BTEX and Indane were added as contaminants. The same contaminants were detected previously at the groundwater contamination site. The possible formation of oxidation products during oxygen-induced oxidation of natural pollutants and their detection as confirmation of the coumarin-based method for the detection of •OH radicals are presented (5.3.2).

5.3.2. Detection of possible oxidation products of BTEX and indane in water upon ferrous oxidation with oxygen in carbonate-rich water

As seen previously, the pH range has a defining role in groundwater chemistry. In the presented study the pH varied between 6.2 and 7 depending on the sampling place and included relative high buffer capacity. Therefore, the oxidation of Fe^{2+} had relatively slower kinetic (Fig. 62a) and the half-life of the Fe^{2+} oxidation in oxygen saturated water for the lowest detected pH 6.2 was around 50 min.

Hence, the on-site use of the APPI-FAIMS monitoring system (part 4.3.7.) was consistent with the time frame and appropriate to demonstrate the potential short-term effects of the OxyTech membrane, i.e., Fe^{2+} oxidation.

Ferrous iron is generally present as hydrated Fe^{2+} which is the dominant form at pH 6 - 8 when no carbonate / bicarbonate is present. In the previous case the working pH was between 7.7 and the starting pH of 8.5 (established from $NaHCO_3$) with an

increased presence of $FeOH^+$ (Fig. 62b), $FeHCO_3^+$ complex and mostly $FeCO_3$ (siderite). According to King (1998), with the exception of siderite, $Fe(CO_3)_2^{2-}$ and $FeCO_3OH^-$ are dominating the speciation of Fe^{2+} in natural waters containing more than 1 mM carbonate alkalinity, where the $Fe(CO_3)_2^{2-}$ complex is most kinetically active for pH > 6. [144]

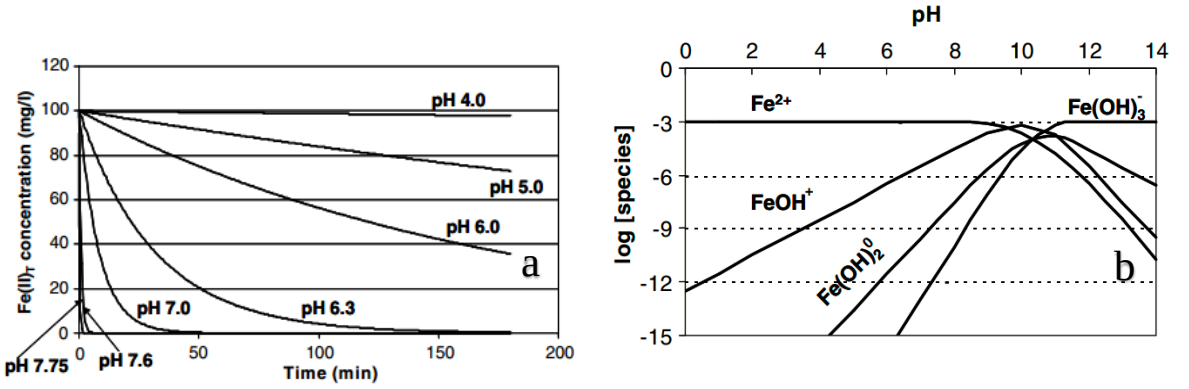

Fig. 62: (a) Oxidation rate model of soluble Fe^{2+} in a batch test as a function of pH (assumptions: infinite dilution, oxygen saturated water at 25 °C); (b) Log species-pH diagram of soluble ferrous hydroxide species at infinite dilution. Both adopted from [158].

This highlights an important role in the possible involvement of carbonate/bicarbonate anions in the natural remediation of the contaminants.

For the detection of BTEX oxidation products the same conditions like previously were applied (5.3.1.). The concentration of the analyte (benzene, toluene or ethylbenzene) in water was increased to > 30 mg L^{-1}. The water was saturated with oxygen, and contained $NaHCO_3$ (10 mM) with a starting pH in the range of 8.5 - 8.7. Ferrous iron ($FeCl_2 \cdot 4H_2O$) was added successively four times gradually reaching 0.3; 0.6; 0.9; 1.2 mM concentration. At the end the products were extracted and analysed with GC/MS (5.2. Experimental).

Provided, $^{\bullet}OH$ radicals are formed upon the immediate addition of Fe^{2+} in the oxygen saturated water (> 8 mg L^{-1}), rapid interaction with aromatic compounds is expected including formation of different isomers from substituted aromatic compounds. The reactions of $^{\bullet}OH$ radicals in water are divided into four different reaction types: addition, hydrogen abstraction, electron transfer and reactions between radicals. [150] BTEX contaminants are oxidized by addition of an OH group on the benzene ring, thus forming cyclohexadienyl radical. The addition reaction is a second order reaction in the range ~10^9 M^{-1} s^{-1} (Tab. 15) controlled from the rate defining diffusion of the neutral $^{\bullet}OH$ radical ($2.3 \cdot 10^{-5}$ cm^2 s^{-1}). The role of the pH influence on the oxidation kinetics should be also considered. [150]

In Fig 63, an overlay of an extracted organic phase (GC/MS, liquid injection) shows possible oxidation products of toluene. The same procedure was applied for all three solutions with toluene in oxygen-saturated water. Two of them had different

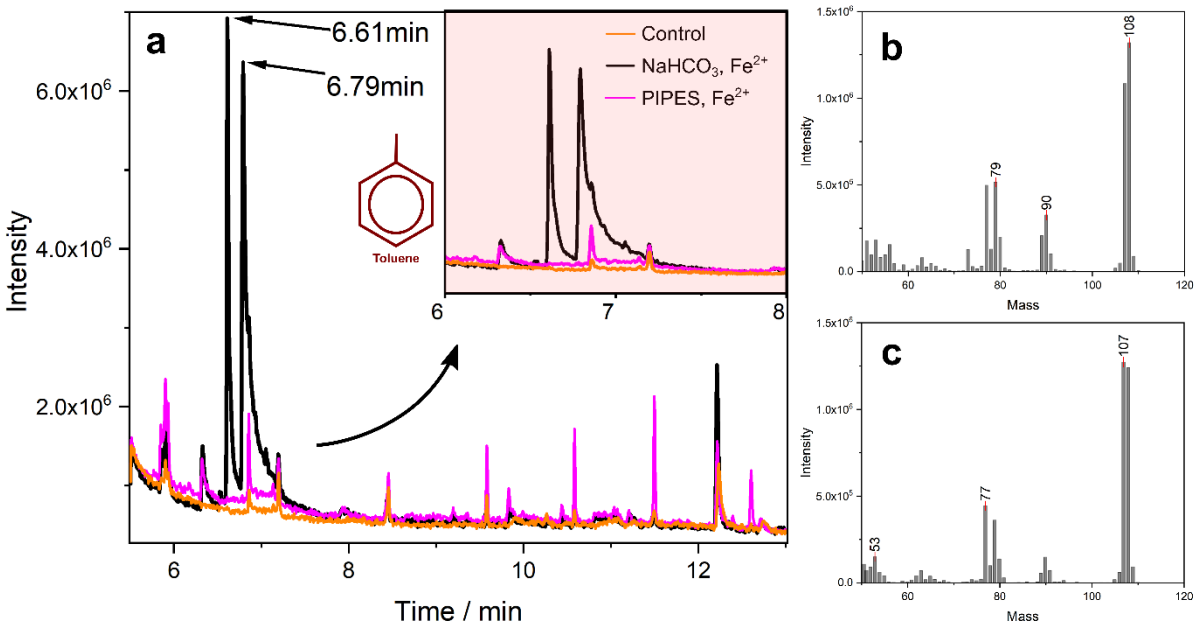

Fig. 63: Overlay of GC/MS chromatograms from the liquid injection (3.5 µL) of the extracted organic phase involved in oxidation of toluene in water (35 mg L^{-1} or 0.38 mM); a) Chromatograms from the three separate water solutions: orange (toluene), black (toluene, 10 mM $NaHCO_3$, Fe^{2+} with *I*= 20 mM) and pink (toluene, 1.13 mM PIPES, Fe^{2+} with *I* = 4.5 mM) were done in triplets; b) and c) mass spectrum of the supposed toluene oxidation products, peak at 6.61 min and at 6.79 min respectively.

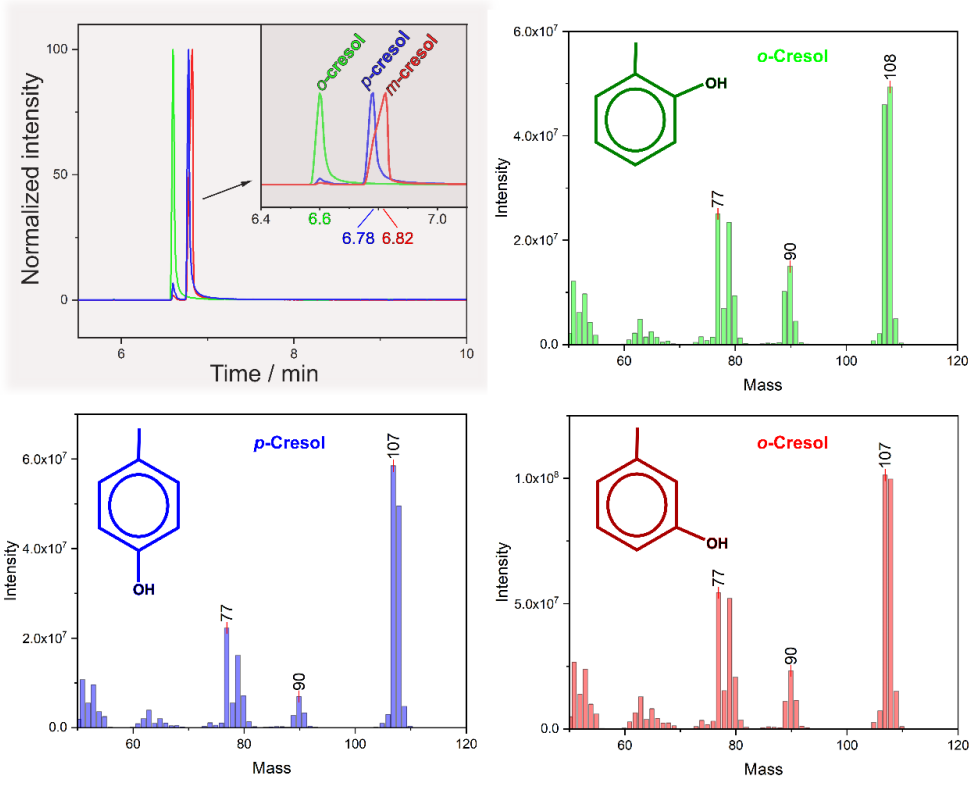

Fig. 64: Overlay of chromatograms produced by separate gas-phase (50 µL) injection of cresol standards (*o*-cresol, *m*-cresol, *p*-cresol) and their respective mass spectra.

buffers, with the same amount of Fe^{2+} added. Immediate Fe^{2+} oxidation took place in both buffer solutions. The third one had only toluene and served as a control (pH 5). After adjusting the pH to 5, extraction with MTBE (methyl tertiary butyl ether) was performed for all three. The chromatograms with two possible product peaks are shown in Fig. 63a with the characteristic mass spectra (b) for the peak at 6.61 min and (c) at 6.79 min. The possible intense toluene peak was avoided with a solvent cut.

The buffer solution containing 20 mM $NaHCO_3$ (pH 8.5) was the only sample that showed the above peaks (Fig. 63a, black chromatogram). However, this was not the case with the PIPES buffer (1,4-piperazine bis(ethanesulfonic acid)) and with the control solution.

PIPES is mostly used as a biological buffer, belongs to the Good buffers and is classified as a non-complexing buffer. [159] Nevertheless, PIPES affected the formation of reactive species, although it enabled Fe^{2+} oxidation. Interaction between the ferrous iron and the two sulfonic groups is possible, but it is more likely that the presence of two hydroxyl groups acts as an effective radical scavenger. PIPES is present in lower concentration than the carbonate buffer, so the lower ionic strength (I= 4.5 mM) should have a positive effect on the formation of Fe^{2+} complexes. [160] However, the bicarbonate/carbonate could have special complex formation that promotes oxygen activation.

The mass spectra of both peaks (Fig. 63b,c) were almost identical with the one of the separate cresol isomers (Fig. 64), thereby confirming the previous findings. The

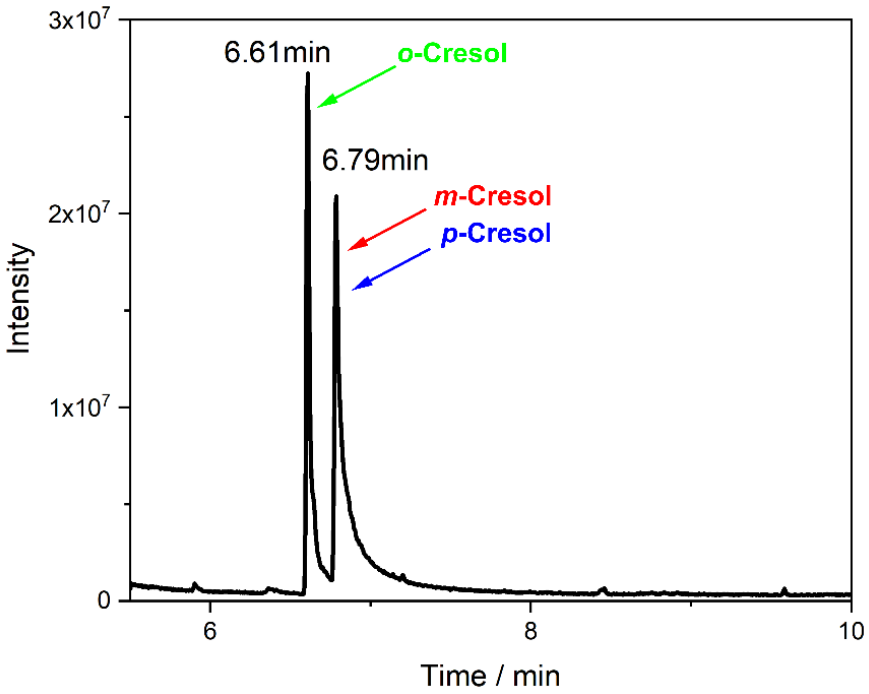

Fig. 65: GC/MS chromatogram from a liquid injection (3.5 µL) of cresol standards mix in MTBE. The concentration of all three Cresols separately was ~7 mg L^{-1}.

isomers were expected to be the most likely products of the •OH addition reactions with toluene, which further confirmed the previous fluorescence results.
For the cresols, identical retention times as in Fig. 63 were observed when analysed together in the same MTBE matrix (Fig. 65). *m*-cresol and *p*-cresol were detected as one peak with 3.4% lower intensity than the *o*-cresole peak, although all three substances were present in the same concentration.

The same products have been reported in the literature for Fenton oxidation of toluene (only in different ratios), including known products (benzyl alcohol, benzaldehyde, benzoic acid, bibenzyl, etc.). [161] Evidence for the presence of benzyl alcohol and benzaldehyde, as in [161], for the carbonate buffer solution was provided by the mass spectra library [145], but due to the negligible trace presence, these were not confirmed with external standards.

In the same manner the products of benzene oxidation by an •OH radical attack, originating from the ferrous ion oxidation in water, were identified (Fig. 66). The carbonate/bicarbonate buffer system i.e. $NaHCO_3$ (10 mM) was used in both cases

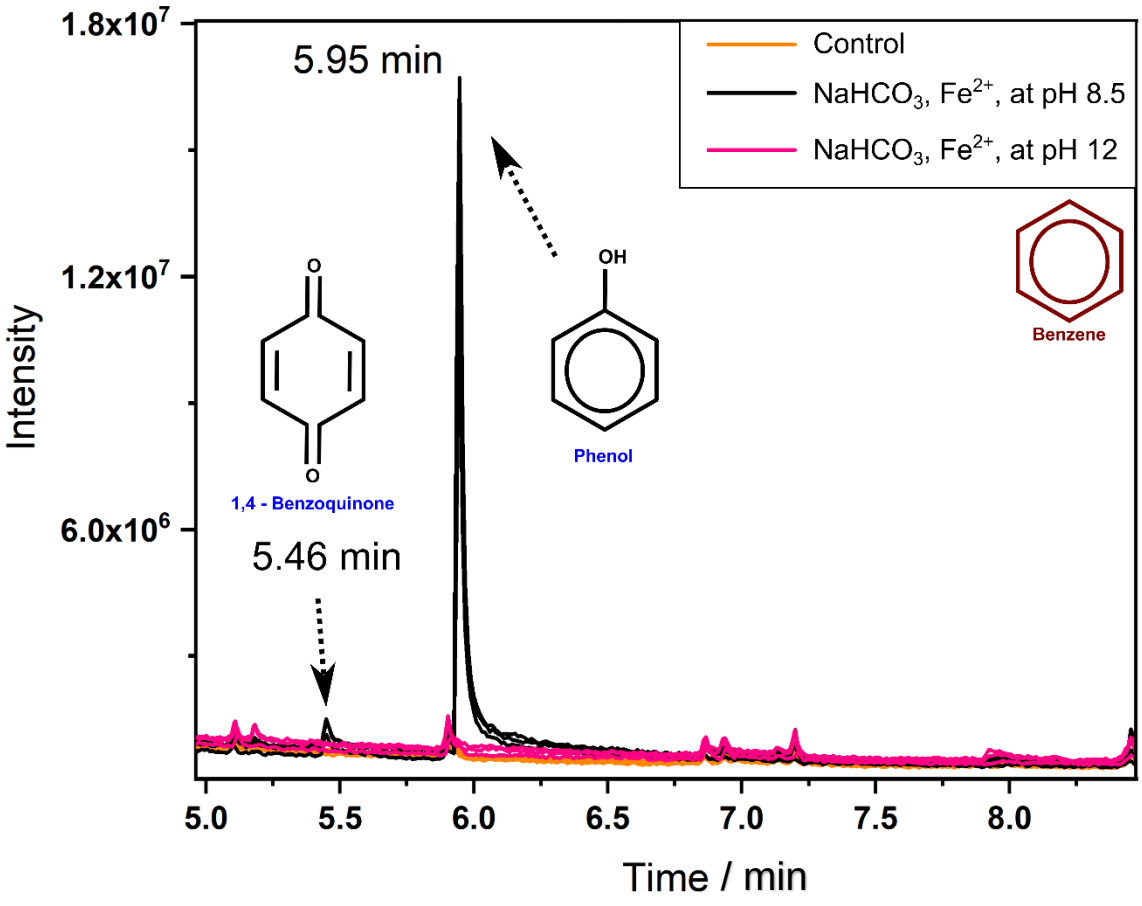

Fig. 66: Overlay of GC/MS chromatograms from the liquid injection (3.5 µL) of the extracted organic phase involved in the oxidation of benzene in water (70 mg L^{-1} or 0.9 mM); orange (benzene); black (benzene, 10 mM $NaHCO_3$, Fe^{2+} with *I*= 10 mM) starting pH 8.5; pink (benzene, 10 mM NaHCO3, Fe^{2+} with *I*= 45,5 mM) starting pH 12, adjusted with NaOH.

instead of PIPES. The ionic strength and concentration of $NaHCO_3$ was lowered for a half than in the previous case. No pH adjustments were made for the first case (pH 8.5), but NaOH was added for the second (pH 12). The expected phenol peak appeared only at pH of 8.5, as shown in Fig. 64. The detection of phenol was confirmed by analytical standards.

1,4-Benzoquinone (*p*-benzoquinone) (CAS: 106-51-4) was another product of the oxidation of benzene, although with a lower intensity than phenol (Fig. 66). In previous studies in the field of pulse radiolysis of water to form $^{\bullet}OH$ radicals and their interaction with benzene, hydroquinone and cyclohexa-2,5-diene-1,4-diol were detected as oxidation products. [162] Nevertheless, no hydroquinones (e.g. *p*-hydroquinone, pK_a 9.85, K_{ow} 0.59) were detected, although they had similar extraction-relevant parameters (e.g. pK_a, log K_{ow}) as the other oxidation products. [16,126]
In contrast to the radiolytic studies, Kunai et al. (1986) detected phenol and benzoquinone (10:1 molar ratio, respectively) as the main products of benzene oxidation with the Fenton's reagent. [163] The same Fenton's reagent products and the same ratio (intensity) was seen in this study (Fig. 66).
After further addition of ferrous iron and its subsequent oxidation, a decrease in phenol is observed, with a corresponding but relatively small increase in *p*-benzoquinone intensity. This suggests *p*-benzoquinone as a possible product of the secondary oxidation of phenol and should be further investigated (5.3.5). It should also be noted that the reaction constant of $^{\bullet}OH$ radicals with phenol is greater than the reaction constant of the primary oxidation of benzene (Tab. 15). This further complicates the determination of the reaction kinetics and stoichiometry.

For the same reaction at an elevated pH of 12, no benzene oxidation products were detected. This could be due to the increased presence of CO^{3-} at pH 12 in carbonate-rich water, which acts as an $^{\bullet}OH$ scavenger; and/or the dissociation of the $^{\bullet}OH$ radical (pK_a 11.9), resulting in $O^{-\bullet}$, which has a much lower chemical reactivity compared to $^{\bullet}OH$. [150]

The case of ethylbenzene (Fig. 67) is reminiscent of the case of toluene. Two product peaks are detected in the $NaHCO_3$ -containing solution to which ferrous iron ($FeCl_2 \cdot 4H_2O$) was added.
The corresponding NIST mass spectra library for the two new peaks provided three products with high probability. [145,164] This included all ethylbenzene isomers formed by oxidative addition of a hydroxyl group: 2-ethyl-phenol (2-EP) (CAS: 90-00-6), 3-ethyl-phenol (3-EP) (CAS: 620-17-7) and 4-ethyl-phenol (4-EP) (CAS: 123-07-9). In this case confirmation with analytical standards was not carried out. The same oxidation products of ethylbenzene have been detected in modified Fenton processes or reactions with $^{\bullet}OH$ radicals in general. [165]

The same characteristic peaks but with lower intensity were observed in Fig. 67 (pink chromatogram) for the solution containing Fe^{2+} without $NaHCO_3$.
Before the addition of iron, the pH of water (Milli-Q) was 6 - 5 because a gas-water CO_2 -equilibrium had been established. The slow oxidation of Fe^{2+} at pH < 6 was enhanced by the addition of NaOH, resulting in complete iron oxidation ending at pH_{max} 10.7. The induced dynamic pH increase combined with the presence of CO_2 (i.e. HCO_3^-

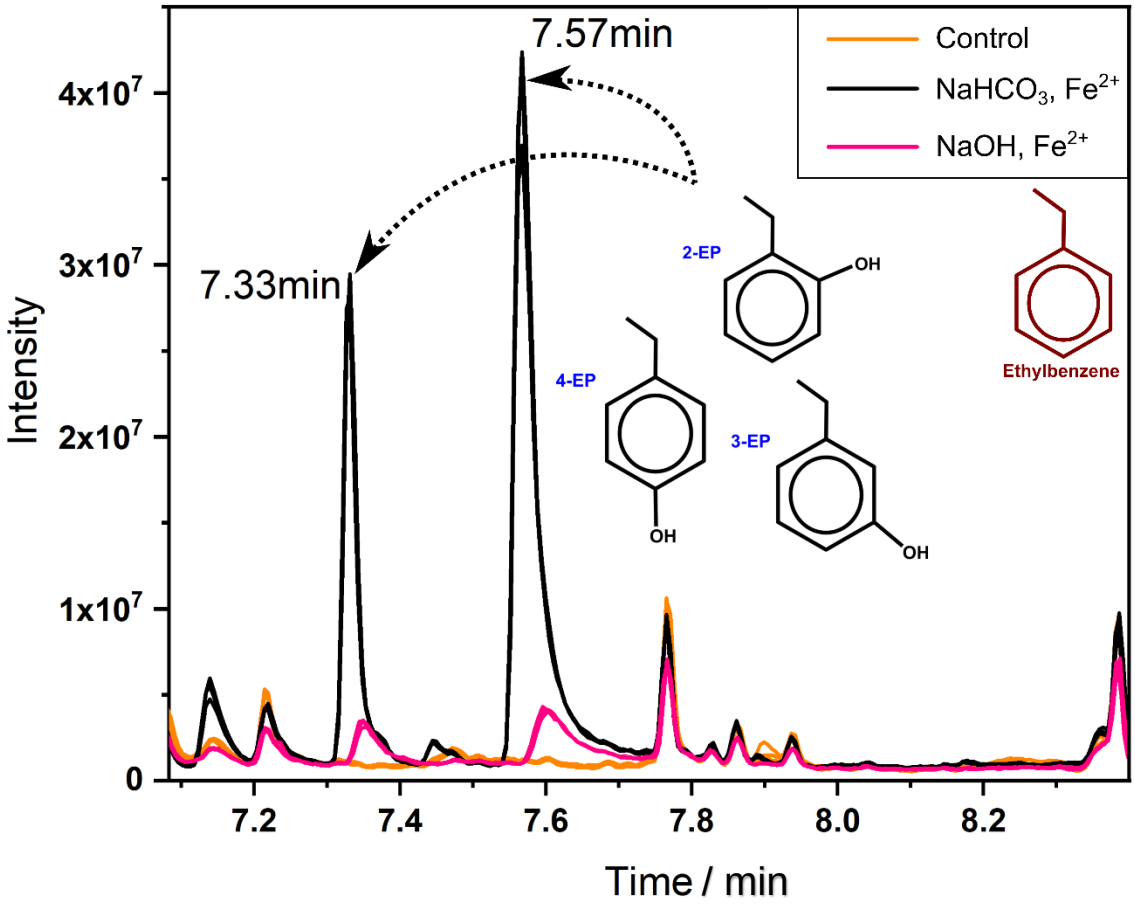

Fig. 67: Overlay of GC/MS chromatograms from the liquid injection (3.5 µL) of the extracted organic phase involved in the oxidation of ethylbenzene in water (70 mg L^{-1} or 0.66 mM); orange (ethylbenzene, 10 mM $NaHCO_3$ with *I*= 10 mM), black (ethylbenzene, 10 mM $NaHCO_3$, 1.2 mM Fe^{2+} with *I*= 10 mM), pink (ethylbenzene, 1 M NaOH, 1.2 mM Fe^{2+} with *I*= 1 mM).

/ CO_3^{2-}) resulted in a short prevalence of the bicarbonate ion, which could explain the occurrence of the same, but less intense ethyl-phenol peaks.

Peaks of other reported products involved in the oxidation of the aliphatic side chain of ethylbenzene to acetophenone (CAS: 98-86-2) and benzenemethanol (CAS: 98-85-1) [165] were detected (mass spectra) in trace amount in all three solutions. This could be explained by a prior autoxidation of ethylbenzene when exposed to O_2 [166] and the subsequent presence of Fe^{3+}, which could act as a catalyst in cases where ferric iron is present. [167]

Xylenes as a part of the BTEX contaminants were also oxidized in water upon oxidation of ferrous iron with oxygen in the presence of carbonate/bicarbonate ions (not shown). Dimethylphenoles (xylenols) as oxidation products were detected with the oxidation of *m*- and *o*-xylene.

Autoxidation of indane represents a larger issue than for ethylbenzene, especially knowing the ability of dioxygen to initiate a spontaneous autoxidation reaction for slightly different cyclopentane rings (i.e. indene). [168] Indane is slightly

soluble in water (100 mg L^{-1}, Tab. 1) which indirectly affects the accessibility for direct autoxidation at the water surface.

Fig. 68 shows two particularly intense peaks for 2-indanol (CAS: 4254-29-9) and 2-indanone (CAS: 615-13-4). Both could be products of •OH radicals, as indicated in the NIST data library. [145] Indanone is already registered in literature as one of the products of the •OH reaction (i.e. H_2O_2) with indane. [169] These peaks occurred in all samples containing indane, indicating previous autoxidation or contamination of the analytical standard (≥ 95% purity).

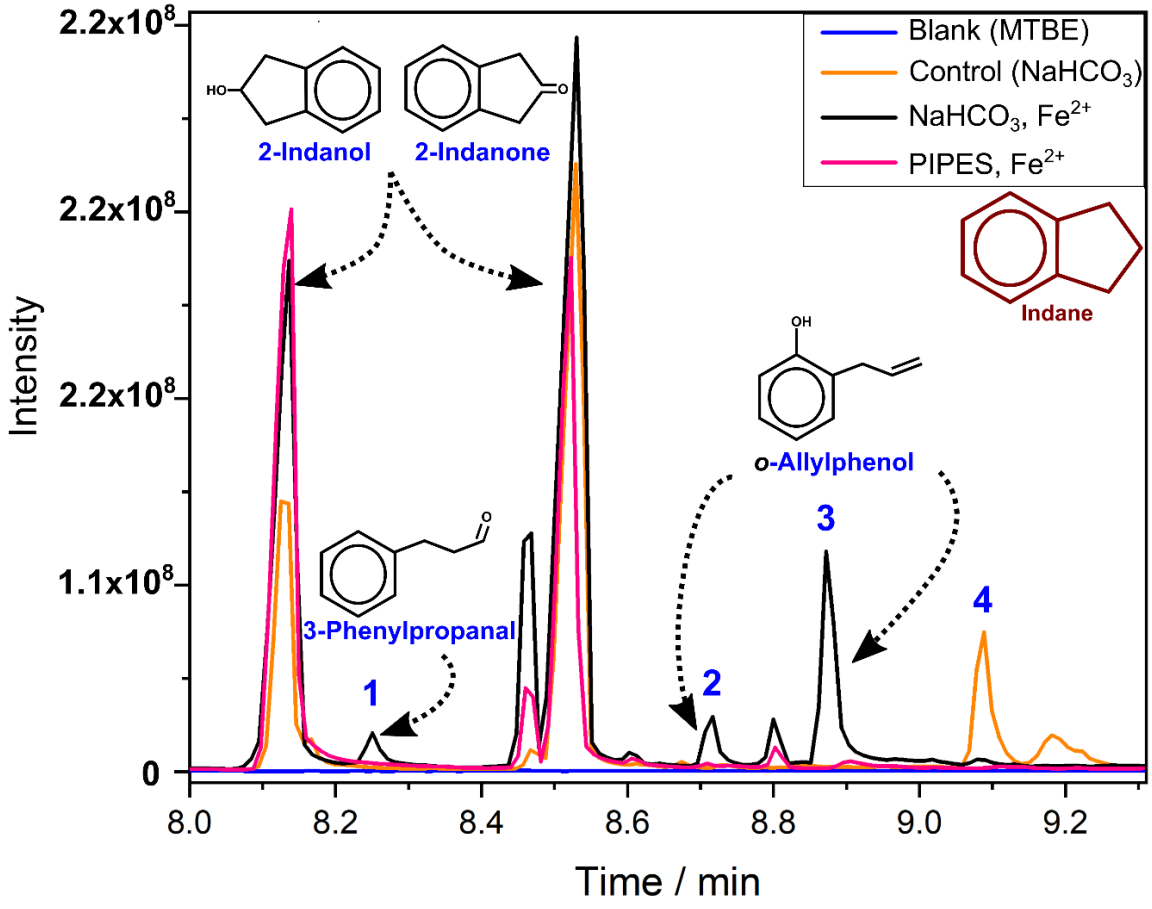

Fig. 68: Overlay of GC/MS chromatograms from the liquid injection (3.5 µL) of the extracted organic phase involved in the oxidation of indane in water (77 mg L^{-1} or 0.65 mM); blue (MTBE), orange (indane, 10 mM $NaHCO_3$ with *I*= 10 mM), black: (indane, 10 mM $NaHCO_3$, Fe^{2+} with *I*= 10 mM) and pink (indane, 1.13 mM PIPES, Fe^{2+} with *I*= 4.5 mM).

Only peaks 1,2, and 3 were detected exclusively upon addition of $FeCl_2 \cdot 4H_2O$ to the indane/$NaHCO_3$ aqueous solution and all of them suggested Fe^{2+}-supported oxidative opening of the cyclopentane ring probably via 2-indanol and 2-indanone or independently. *o*-Allylphenol (CAS: 1745-81-9) and its structural isomers were determined as peaks 2 and 3. Peak 1 hinted at the presence of 3-Phenylpropanal

(CAS: 1335-10-0). The confirmation of the products was done for at least two separate processes and in triplets. Additional indane oxidation products due to •OH-radical activity were not excluded.
Peak 4 appeared only once when the pH was lowered from 8.5 to 5 with 1 M HCl (3.62 mL), before the extraction step.

In Tab. 16 selected determined products of the ferrous iron supported oxidation in bicarbonate-rich water are listed with the relative increase of solubility compared to the respected precursor contaminant. In all cases an increase of solubility is shown. This can produce advantages and disadvantages for the contamination remediation of the aromatic VOCs.
The increased solubility contributes to indirect increase in contaminant migration through the aquifer, thereby possibly increasing the reach of the contamination plume. This is especially important when the oxidation product has higher toxicity or increased carcinogenic effects than the starting contaminant precursor.
On the other hand, the increased solubility could potentially shorten the duration of site remediation under controlled conditions. By promoting oxygen-induced oxidation (e.g., with OxyTech membrane) as a support to another standard remediation method, such as the pump-and-treat method, an increase in remediation efficiency could be achieved.
In general, the toxicity of BTEX contaminants is reduced or it is categorized as the same after oxidation. For instance, benzene is a known human carcinogen, but the

Tab. 16: Solubility of some oxidation products from the aromatic VOCs (benzene, toluene, xylenes and ethylbenzene).

Oxidation Product	**CAS No.**	**Mol. Weight**	**Solubility** [a]	**Relative increase in solubility** [b]
		g/mol	**g/kg H_2O**	**%**
Phenol	108-95-2	94	92	520
1,4 Benzoquinone	106-51-4	108	13.8	78
***o*-Cresol**	95-48-7	108	31.8	613
***m*-Cresol**	108-39-4	108	25.7	495
***p*-Cresol**	106-44-5	108	23.1	445
Xylenols	---	122	3.5-7.9	205-462
4-Ethyl-phenol	123-07-9	122	5.9	366

[a] - solubility values from [16]
[b] - compared to the solubility of the corresponding precursor (Tab. 1) relative small differences depending on the ref. can occur

previously determined oxidation products (phenol and 1,4-benzoquinone) are not treated as one, or at least the evidence are inconclusive. [170] In the case of toluene and xylene as precursors and cresols and xylenols as their oxidation products,

respectively, no significant increase in toxicity was reported as well as no mutagenic activity. Both products are considered as readily biodegradable. [171]

Considering all, there is a justification in applying oxygen-induced oxidation as a support to a major remediation method (e.g. P&T).

5.3.3. Formations of specific iron oxide-hydroxides

Different results of ferrous iron oxidation in the cases from 5.3.2. were evident not only in the presence or absence of oxidation products, but also in the different solution colors at the end of the reaction. The typical example shown in Fig. 69a shows water contaminated with ethylbenzene after oxidation of Fe^{2+} at initial pH 8.5 (bottle 2) and at pH 12 (bottle 3) (cf. Fig. 67). Bottle (2) contained Fe^{2+}, which was oxidised to Fe^{3+} in carbonate-rich water and had a lighter colour than the iron in bottle (3), which was oxidised by adding NaOH. After precipitation, the supernatant from bottles (2) and (3) was subjected to UV-Vis spectrophotometric analysis. No specific absorption bands were measured for the solution in bottle (3). In contrast, specific maxima between 283-285 nm and at 359 nm were obtained for the solution in bottle (2) (Fig. 69b). The wavelengths 285 nm and 359 nm are typical UV-Vis absorption bands for goethite and lepidocrocite, respectively. Goethite (α-FeOOH) and lepidocrocite (γ-FeOOH) are oxide-hydroxides with orthorhombic structure and yellow-brown and orange color, respectively. [172] In addition, lepidocrocite is dimorphic with goethite, and its occurrence is usually accompanied by goethite, as both are naturally occurring iron oxide-hydroxides. [173,174]

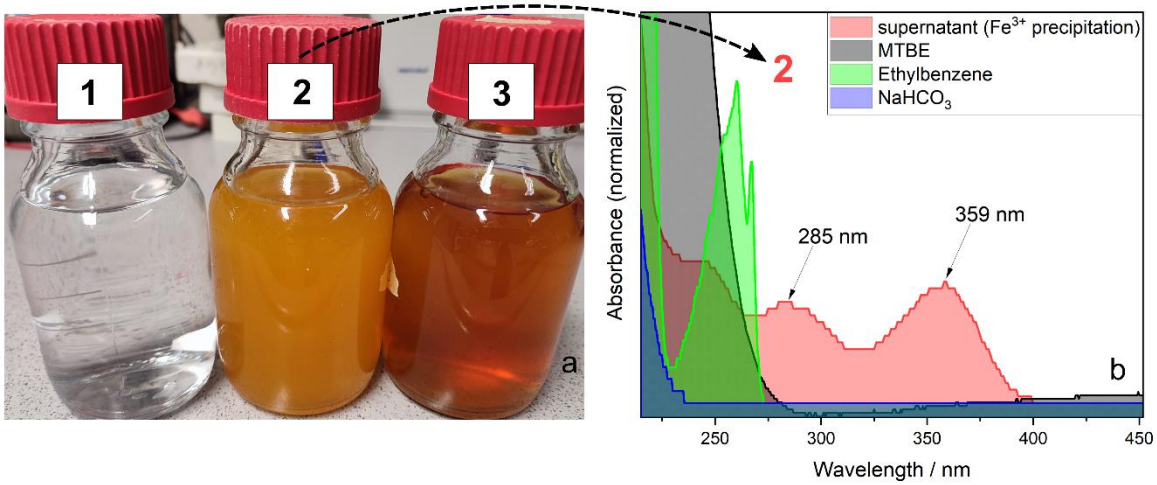

Fig. 69: Colour differences of solutions after oxidation of Fe^{2+} in the presence of ethylbenzene: bottle (1) blank ($NaHCO_3$, ethylbenzene); bottle (2) $NaHCO_3$, Fe^{2+}, ethylbenzene; bottle (3) NaOH, Fe^{2+}, ethylbenzene; b) UV-Vis spectra from supernatant of bottle 2. The pure spectra of known analytes in the solution (MTBE, ethylbenzene and $NaHCO_3$) have been added for clarity.

This was consistent with the colour seen in bottle (2) prior to precipitation (Fig. 69a). Sample coloration attributable to goethite and lepidocrocite could possibly serve as a rough indicator for •OH radical formation when O_2 is introduced under anoxic (groundwater) conditions in the presence of ferrous iron and carbonate/bicarbonate ions. Other studies have confirmed that the presence of carbonate enhances goethite aggregation, both involved in •OH radical production. [132] In presence of siderite ($FeCO_3$), goethite nanoparticles form after 2h of ferrous ion oxidation. [175]

A similar colour, indicating the presence of both oxide-hydroxides, was found in the samples taken on site, especially when no sample preservation was applied.

Given the concentration range and ubiquitous occurrence of carbonate species, especially bicarbonate, in natural waters (Tab. 17) there is an opportunity to investigate remediation potential in natural waters (i.e. groundwater) as a support for other remediation processes in general. As a general rule the concentration of inorganic ligands like HCO_3^- is higher than that of organic ligands, which are usually reported as a collective (sum) parameter. [153] However, as shown (5.3.4.), the activation of dioxygen in presence of HCO_3^- and Fe^{2+} could possibly be influenced from other ligands present.

Tab. 17: Concentration range of some ligands in natural waters [153].

Ligand	Concentration log (mol L^{-1})
HCO_3^-	-4 to -2.3
Cl^-	-5 to -3
SO_4^{2-}	-5 to -3
HS^-/S^{2-} (anoxic conditions)	-6 to -3
CO_3^{2-}	-6 to -4
F^-	-6 to -4
Organic acids	-6 to -4
Particle surface groups	-8 to -4
Amino acids	-7 to -5

5.3.4. Citrate and glutamic acid as the dominant ligands instead of bicarbonate / carbonate in ferrous-supported oxygen induced oxidation i.e. •OH radical production

Some organic ligands in combination with ferrous iron could positively influence the activation of oxygen and the formation of reactive species without any involvement of an activator like H_2O_2 or UV-light. [176–180]

Additionally, the influence of organic ligands (e.g. carboxylic acid) has been investigated in other studies, including the photo-Fenton process. Baba et al. (2015) showed that he formation of Fe^{2+}-containing carboxylic ligands had a positive effect on

•OH radical formation with the Fenton reaction and the photo-Fenton process in general. [181]

To determine the possible role of the carboxyl group, another ligand was used instead of bicarbonate. The detection of •OH radical involving coumarin (5.3.1.) was performed in presence of citric acid (pK_a values 3.13, 4.76, 6.4 [182]) i.e tri-sodium citrate dihydrate salt instead of sodium bicarbonate.

The formation of •OH radical was confirmed by the appearance/increase in fluorescence, similar to the cases where bicarbonate was present (Fig. 70). A simultaneous decrease in oxygen and pH was also observed. In this case, the initial pH was slightly above 8, which contributed to only a negligible presence of a protonated carboxylic group from the tricarboxylic citric acid. [183] Compared to the kinetics of •OH radical formation with sodium bicarbonate, the kinetic with tri-sodium citrate dihydrate was considerably slower, probably due to the involvement of the three carboxyl groups in a polydental metal-ligand interaction. This could sterically hinder the oxidation of the iron, as shown in Fig. 71 for different time points.

Furthermore, only a slight colour change without precipitation was observed, in contrast to the case where bicarbonate was used (Fig. 69).

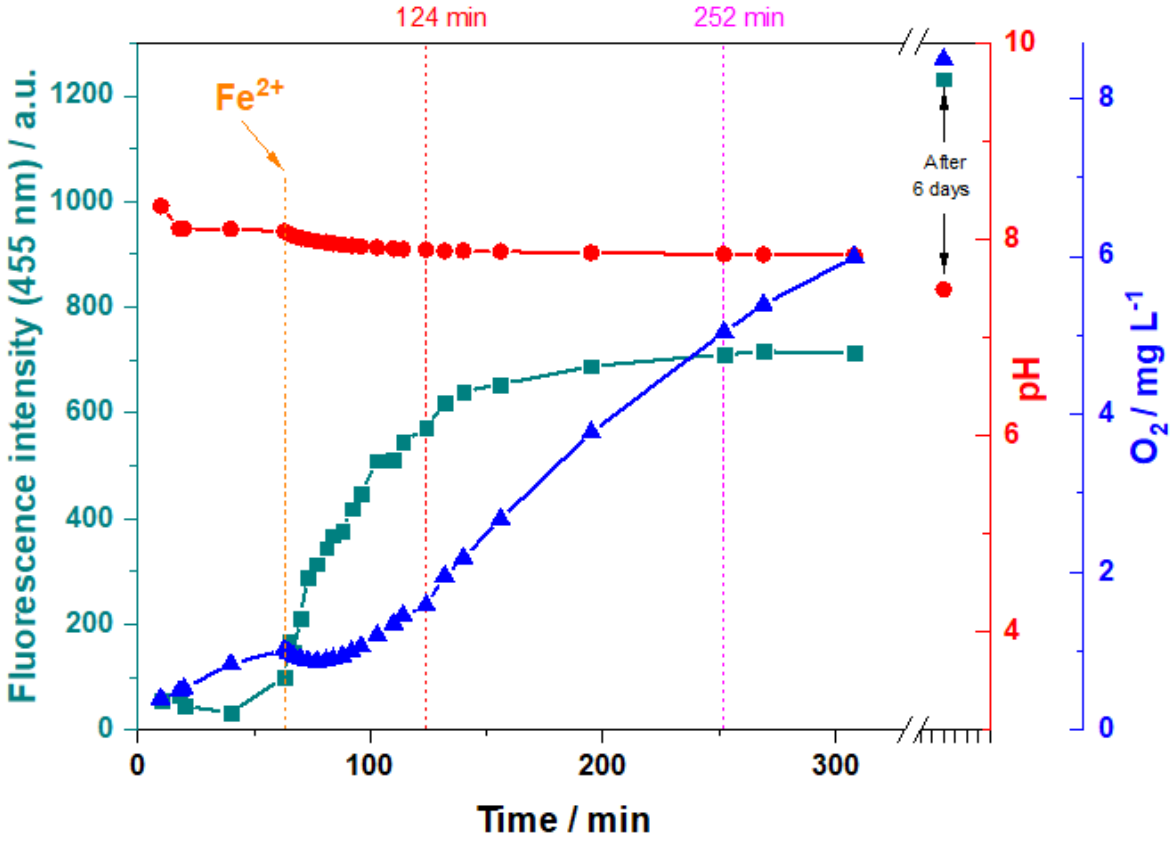

Fig. 70: Continuous observation of fluorescence intensity at 455 nm, pH and DO (dissolved oxygen) for the Fe^{2+}-oxidation in water (0.1mM Fe^{2+}) in presence of tri-sodium citrate dihydrate (10 mM) and coumarin (20 µM) as a hydroxyl radical scavenger.

The absorption bands in the case of citrate in Fig. 71 (274 nm and 312 nm) were also different from those in the case of bicarbonate, including the significant colour difference. Nevertheless, the formation of •OH radicals was indirectly confirmed in both cases.

After six days, an increase of more than 40% from •OH radical was observed with a corresponding decrease in pH, with minimal change in the colour of the solution.

It was evident, the presence of protonated or deprotonated carboxylic group as a ligand (e.g., bicarbonate and citrate) enabled the activation of ferrous iron when dioxygen was added or present.

Recent studies done by Škarohlíd et al. (2020) involving citric acid-chelated ferrous ions have confirmed their role in the degradation of chlorinated volatile organic compounds (CVOCs), which occurred without any additional activation. [184] Moreover, contrary to the authors' expectations, the degradation efficiency of this system was comparable to that with peroxydisulfate ($S_2O_8^{2-}$) as activator. In both cases artificially prepared groundwater was used, which contained $NaHCO_3$, $KHCO_3$ and had a pH of 7.5, similar to the conditions in our case. This suggests that the carboxylic group of citric acid may also be involved in the oxygen-activated oxidation of AVOCs, similar to the bicarbonate / carbonate ions.

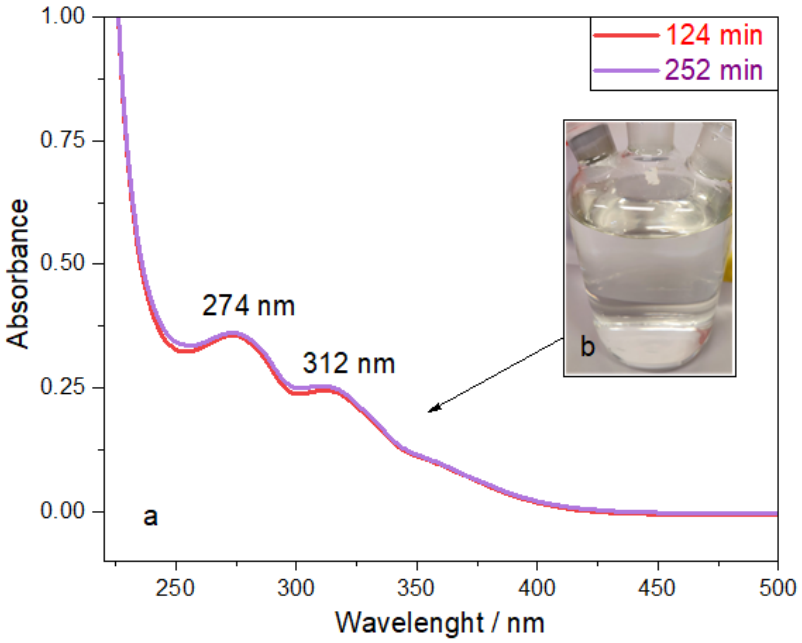

Fig. 71: a) Overlay of UV-Vis spectra of the solution from Fig. 70 at two different time points (124 and 252 min); b) Color of the solution in the reaction vessel from the same solution (Fig. 70).

This was not the case when different kinds of ligand were used instead of citrate (i.e. tri-sodium citrate dihydrate). L-Glutamic acid (146 g mol^{-1}; solubility 4.46 g kg^{-1}) was added in the same amount as tri-sodium citrate dihydrate before (10 mM). pH of the solution (8.5) was adjusted by adding 1M NaOH (10 mM). The absence of the fluorescence signal confirmed that •OH radicals are not detected despite the presence

of two carboxyl groups of the glutamic acid. The presence of other types of ligands (e.g. hydroxyl anion, amino group) can greatly influence the production of reactive species. Other studies have shown that the presence of nitrogen-containing ligands stabilizes Fe^{2+} ions, thus inhibiting the oxidation process. [142]
This underscores the importance of determining the possible ligands and their concentration in groundwater before any type of induced iron oxidation is performed. Besides other parameters (e.g. pH, reaction kinetics), the presence of different ligands can strongly influence the outcome of •OH radical-formation in groundwater.

5.3.5. Oxygen-induced oxidation of ibuprofen as a typical water contaminant in the presence of ferrous iron in carbonate-rich water and the difficulties in indirect quantification of the produced •OH radicals

Hydroxyl radicals show high rate reactivity ($k \geq 10^8$ M^{-1} s^{-1}) with almost all organic moieties including C-H bonds. [185] In this sense the oxygen-activated oxidation in bicarbonate presence was additionally tested on another known water contaminant - ibuprofen ($C_{13}H_{18}O_2$, 206 g mol^{-1}, pK_a 4.9). [16] In this work ibuprofen was used in the form of ibuprofen sodium salt with considerably higher solubility in water (~3.8 g L^{-1} at 25°C). [186] Several additions of Fe^{2+} contributed to the partial oxidation of ibuprofen. The reaction between the generated hydroxyl radicals and ibuprofen proceeds rapidly with a reaction rate constant of $7.4 \cdot 10^9$ M^{-1} s^{-1}, in the similar range as for coumarin. [187]

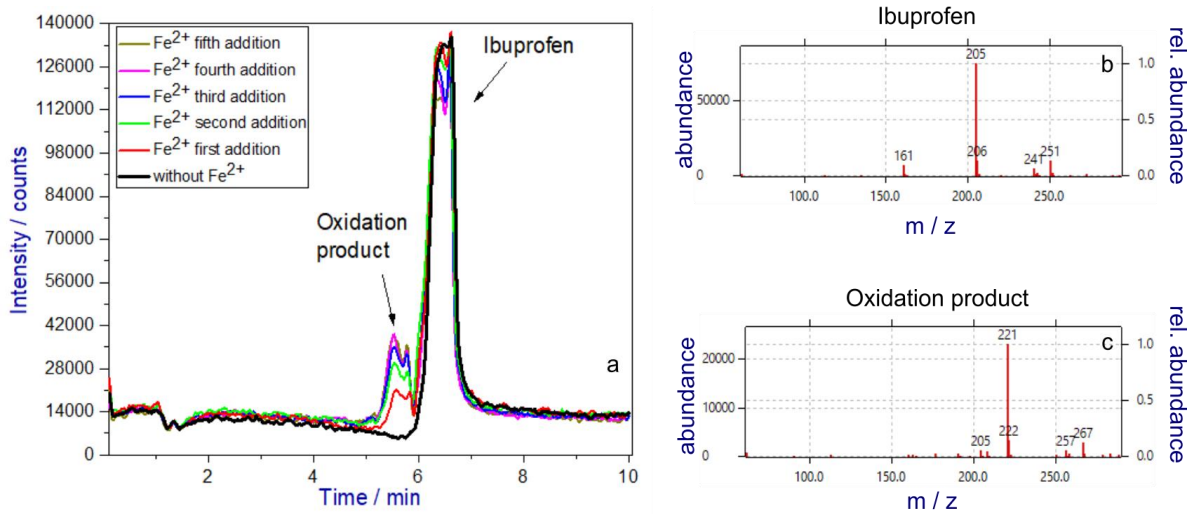

Fig. 72: **a**) ESI-HPLC/MS chromatogram overlay (negative mode) of an ibuprofen oxidation in the presence of $NaHCO_3$ upon successive addition of multiple Fe^{2+} portions (10 - 11 mg) at pH 8; **b**) mass spectrum of the ibuprofen peak in (a); **c**) mass spectrum of the possible oxidation product peak (a).

In Fig. 72a an overlay of chromatograms in negative mode showed the presence of ibuprofen (parent ion $(M-H)^-$ with 205 m/z, Fig. 72b) and formation of an oxidation product ($(M-H)^-$ with 221 m/z, Fig. 72c), both manifesting an unresolved double peak typical for the two enantiomers of ibuprofen. [188]

The presence of an oxidation product was confirmed by the appearance of a new peak signal with a shorter retention time than ibuprofen, due to the ‘‘reversed-phase’’ column. 2-[4-(1-hydroxy isobutyl)phenyl]propionic acid (with m/z of 221 $(M-H)^-$, Fig. 72c) is a possible monohydroxylated oxidation product of ibuprofen and probably responsible for the oxidation product peak in Fig. 72a. [189]

Upon further addition of Fe^{2+} ($FeCl \cdot 4H_2O$), a separate increase in mass intensity was observed for 237 m/z. The same mass-to-charge ratio was reported by Madhavan et al. (2010) for the degradation of ibuprofen. [189] It involved a di-hydroxylated product (negative mode, $(M-H)^-$) which was a result of a possible secondary •OH radical oxidation of 2-[4-(1-hydroxy isobutyl)phenyl]propionic acid (Fig. 73). The intensity of the signal (237 m/z) as a selected ion was significantly lower compared to the primary oxidation product, but showed the expected, albeit only slightly increasing trend, which was considered inconclusive.

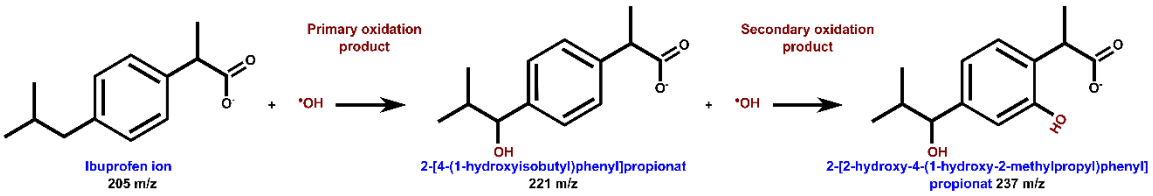

Fig. 73: Stages of ibuprofen oxidation and representatives of possible primary and secondary oxidation products at pH 8 with matching mass-to-charge ratios.

In Fig. 74 the increase in signal of the primary oxidation product from Fig. 72a was graphically presented. It was clear that the signal area of the product did not increase proportionally with the amount of Fe^{2+} added. There could be several reasons for this, including the enhanced presence of primary oxidation products and Fe^{3+}, which contributes to their separate reaction with the generated •OH radicals.

The reaction between the primary oxidation product and the generated •OH radicals was more obvious in the case of benzene and involved the same process of successive Fe^{2+} addition as in the case of ibuprofen.

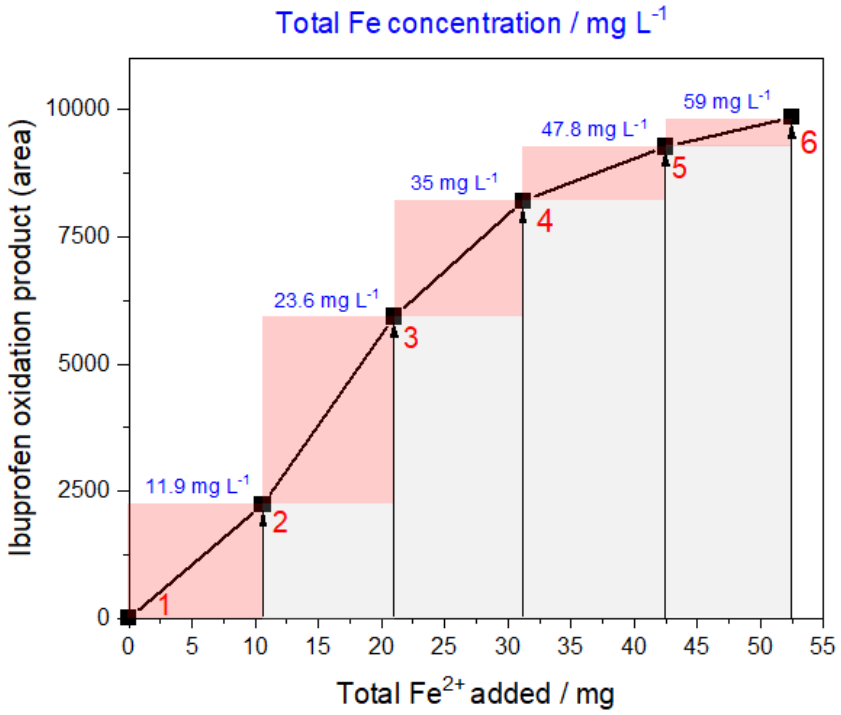

Fig. 74: Increase of the oxidation product peak area of ibuprofen (from Fig. 72a) with a successive addition of Fe^{2+} in multiple portions (10 - 11 mg) at pH 8. Shown in red is the last addition of Fe^{2+} for the respective vessel (1 - 6) and the corresponding increase in peak area.

As previously discussed, phenol and 1,4-benzoquinone (*p*-benzoquinone) are detected as primary and secondary oxidation products of benzene, respectively (Fig. 74). Both reactions occur at a fast rate. The literature shows an even higher rate for the secondary oxidation, taken both reactions are not limited by the diffusion rate of the •OH radicals in water. [150]

Therefore, as the phenol concentration increases, the yield of 1,4-benzoquinone also increases steadily, especially after the third consecutive addition of Fe^{2+} (Fig. 76). In turn, the presence of redox-active quinone moieties can reduce ferric iron, but at a much lower rate, creating a possible redox cycle. [190]

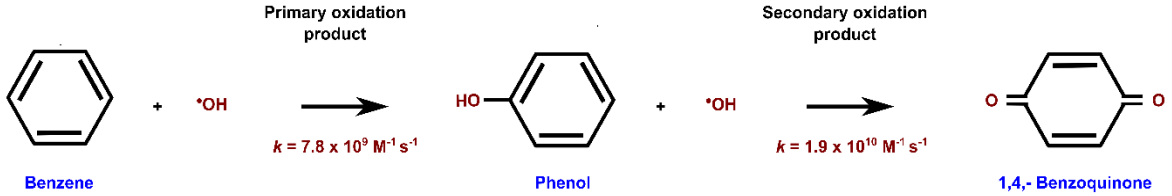

Fig. 75: Stages of benzene oxidation and the primary and secondary oxidation products with the corresponding reaction rate constants from Tab. 15.

Fig. 76 merely confirms the results previously obtained for the primary oxidation product of ibuprofen. The amount of produced •OH radicals can only be approximated after the first two or three additions of Fe^{2+} when little to no secondary oxidation was detected.

The low estimated vapour pressure (VP) of ibuprofen (0.025 Pa), unlike AVOCs such as benzene ($1.16 \cdot 10^4$ Pa) [126], was used for more reliable, indirect approximation of the oxidation yield i.e. produced •OH radicals. On average, the first three Fe^{2+} additions

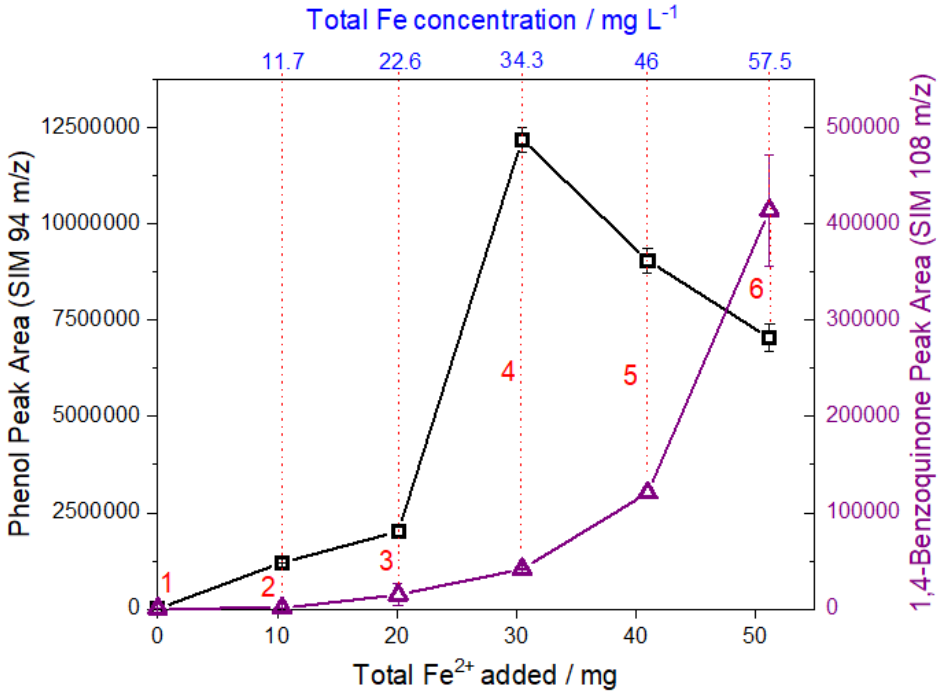

Fig. 76: Formation of phenol (black) as a primary and 1,4-benzoquinone (blue) as a secondary oxidation product of oxygen-activated oxidation of benzene with multiple successive additions (2 - 6) of Fe^{2+} (10 - 11 mg) at pH 8. The procedure for extraction and reduction of the sample volume was the same as for ibuprofen (5.2.2.). Detection was done by liquid injection GC/MS as previously described for benzene (cf. Fig. 66).

contributed to a decrease of the total ibuprofen signal area of about 5%. Rough approximation of the Fe^{2+} : •OH stoichiometry gave a ratio close to 4:1, similar to the stoichiometry for the oxidation of Fe^{2+} in water with O_2 (cf. eq. 30). This possibility should be further investigated and confirmed, given ibuprofen itself has a carboxyl group similar to other suitable organic ligands (e.g. EDTA, citrate).

The previous spectrofluorophotometric determination of •OH radicals, indirectly via coumarin oxidation (5.3.1.), greatly underestimated the production of •OH radicals relative to the ibuprofen case. The probable reason for this difference is the overlap of

the excitation wavelength of coumarin (336 nm) with the absorption range of the increasing Fe^{3+} concentration, despite filtration. The small pH difference of 0.5 units could also contribute to the differences to some extent.

5.3.6. Reasons involved in the production of •OH reactive species upon ferrous iron oxidation by oxygen in carbonate-rich water

The generation of •OH radicals in advanced oxidation processes (AOPs) like different Fenton processes (including Fenton, photo-Fenton and Fenton-like reactions), exhibit a great potential in water contamination treatment. [181] A common denominator in these processes remains to be the activation step mainly in the form of hydrogen peroxide and/or light energy source.

The Udenfriend's reagent was one of the first examples of biomimetic production of •OH radicals without the typical activation of the ferrous/ferric ion, as in the Fenton processes mentioned above. [191]

Similar to the Udenfriend's reagent, production of •OH radicals was seen in this work upon input of oxygen in anoxic, ferrous ion-rich groundwater. The direct participation of dioxygen in oxidation of the aromatic VOCs via the involvement of transition metals complexes is referred to as oxygen activation or metal-activated oxygen. [168]

The oxidation of organic compounds is hindered by the spin limitation of oxygen in the ground state (triplet), but metal complexes can be used to overcome this spin limitation. Barton et al. (1993) and Cornell et al. (2003) stated that such metal-dioxygen complexes could possibly be very useful in the discovery of novel remediation processes. [172,191]

The presence of organic ligands (e.g., EDTA, DTPA, bipyridine) was already seen as a contributor to the activation of oxygen and the formation of reactive species [176–180], still the involvement of inorganic species such as carbonate/bicarbonate in context of groundwater remediation has not been fully considered.

The bicarbonate anion has already shown different effects in the application of advanced oxidation processes (AOPs). For example, in some cases of H_2O_2 application it significantly increased the oxidation efficiency [192], while in the case of Fe^{2+}-activated persulfate [156] it had a negative effect connected to radical scavenging. H_2O_2 scavenging from bicarbonate led to the formation of peroxy mono carbonate ions (HCO_4^-) with a peroxide-like structure providing ''bicarbonate-activated peroxide oxidations'' of thiols. [192]

As already shown in the Bjerrum plot of carbonic acid [110], the bicarbonate ion is the dominant species at neutral and slightly basic pH, nevertheless, $FeHCO_3^+$ (log*K* 1.47) was not the most dominant iron-carbonate complex. In contrast, according to King (1998) and Fig. 77, siderite ($FeCO_{3(aq)}$ with log*K* 5.69) was the most dominant iron species along with the presence of non-complexed Fe^{2+} (i.e. $Fe(H_2O)_6^{2+}$) under slightly acidic and reducing conditions. $Fe(CO_3)(OH)^-$ (log*K* 9.97) was significantly present under slightly basic conditions. [144,193]

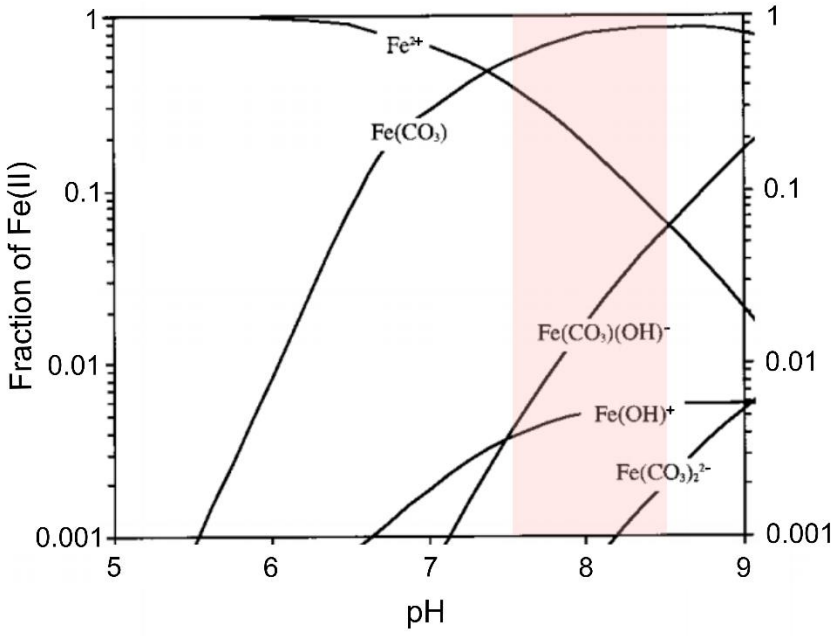

Fig. 77: Fe^{2+} speciation in pure water with 2.3 mM of $NaHCO_3$ and 0.03 atm of pCO_2 adopted from [144] with the pH range in use (red).

The double-bidentate carbonate complex $Fe(CO_3)_2^{2+}$, as the largest contributor to the overall oxidation reaction rate in the pH 6 - 8.5, had a low presence under pH 8.5. Other such bidentate chelating complexes like 2,2'-bipyridine i.e. $Fe(bpy)_2^{2+}$ were involved in oxygen activation and production of reactive species. [194]

The aforementioned pH effect plays a major role on complex speciation from Fig. 77. The increase in the total concentration of 7-hydroxycoumarin i.e. $^{\bullet}OH$ radicals (Fig. 60) was accompanied by the decrease in pH from 8.4 to 7.7. There are several explanations for this.

Firstly, the already mentioned and very probable decrease of $[CO_3^{2-}]$ and its scavenging effect with the pH decrease;

Secondly, the increase in concentration of any from the following ion species: Fe^{2+}, $FeHCO_3^{2+}$, $Fe(OH)_2$ (with pH decrease);

And thirdly, the possible joint effect of the first two.

The possibility of $FeCO_3$ involvement is also not excluded. Recently a study on the involvement of siderite in $^{\bullet}OH$ radical production with and without involving organic acids and thiols was published, but the whole oxidation process of siderite is still relatively poorly understood. [195]

The reaction of oxygen with iron(II) complexes is irreversible and rapid [168], with possible additional side reactions. In Fig. 78 the ferrous iron oxidation in presence of HCO_3^- and CO_3^{2-} was shown with several important oxygen activation pathways (1, 2, 2b) that could lead to the formation of different reactive species.

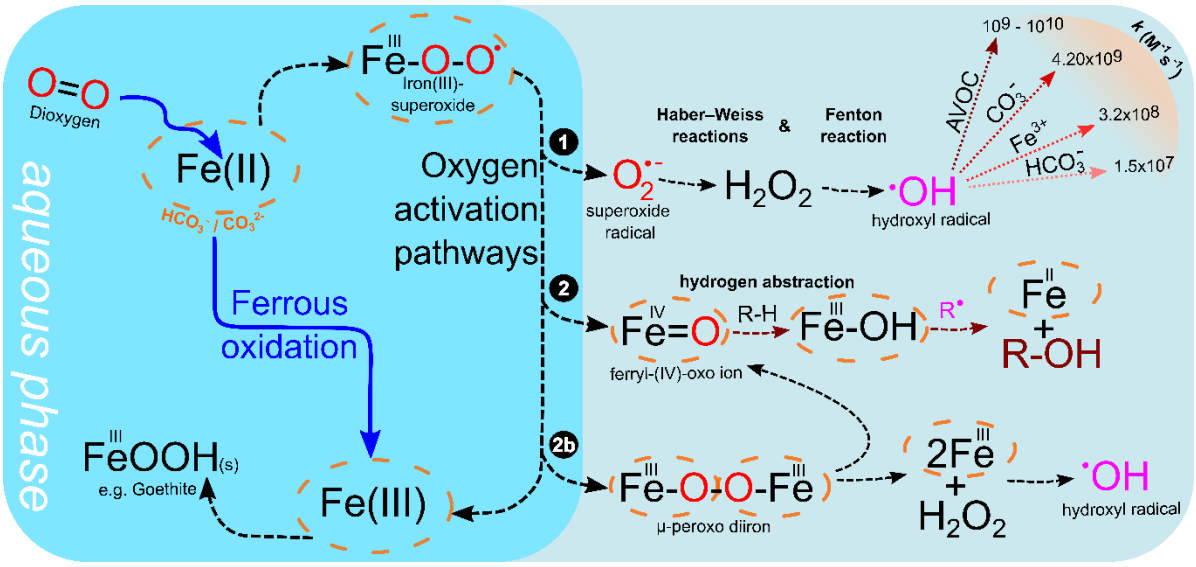

Fig. 78: Oxidation of ferrous iron in aqueous phase in the presence of bicarbonate/carbonate system. Possible oxygen activation pathways involving organic ligands (1, 2, 2b) [176–178,196]. Reaction rate constants of •OH radicals with the major participants in the solutions including AVOC as contaminants [150].

(i) One of them (pathway 1) is the successive formation of a superoxide ($O_2^{-\bullet}$) and H_2O_2 in slightly acidic to neutral waters with the initial oxidation of $FeOH^+$. [153] $O_2^{-\bullet}$ is the ‘‘initiator’’ for the Haber-Weiss reactions, [197] the Fenton reaction [29] and thus for the production of •OH radicals.

$O_2^{-\bullet}$ is also a reactive species and can be responsible for the oxidation of contaminants, but the reaction rate of $O_2^{-\bullet}$ with coumarin, for example, is more than 10-times slower than the reaction rate of •OH.

(ii) The ferryl-(IV)-oxo ion $(Fe^{IV}=O)^{2+}$ is a reactive species with lesser oxidizing power than the •OH radical. As roughly shown in the oxidation activation pathway (2) the initial oxidation of Fe^{2+} to Fe^{4+} via Fe(III) superoxide (O_2 coordination) is followed by the subsequent reduction, i.e., proton abstraction (H^+) with formation of reactive radicals (R•). [198,199]

$(Fe^{IV}=O)^{2+}$ could be also formed when a ferrous ion abstracts oxygen from previously formed peroxide (e.g. from pathway 1) and forms a coordinate double bond. [198] One difference between •OH and $(Fe^{IV}=O)^{2+}$ reactive species is that reducing agents do not interfere with ferryl-(IV)-oxo ion oxidation as with •OH-induced oxidation.

(iii) The possible pathway (2b) of oxygen activation involves the formation of μ-peroxo diiron. The reaction of oxygen with ferrous-carbonate complexes proceeds rapidly, initially leading to the formation of Fe(III) superoxide, which may be followed by further rapid attachment and successive oxidation of another ferrous-carbonate complex, thus producing μ-peroxo diiron. [168] This peroxo-bridged species could undergo a homolytic cleavage, producing ferryl-(IV)-oxo ion following pathway (2) or rapidly dissociate into two Fe^{3+}-complexes and H_2O_2, generating •OH radicals by the Fenton reaction. [177]

In this work, the formation of reactive species via all three oxygen activation pathways is possible through the O_2 oxidation of Fe^{2+} complexes in the presence of bicarbonate/carbonate, yet it was suspected that the majority involves the production of •OH radicals. In contrast to (1) and (2b), pathway (2) (Fig. 78) is not directly involved in the formation of hydroxyl radicals. The ferryl-(IV)-oxo ion has a lower oxidizing power and is therefore more specific (regio- and stereoselective) than the hydroxyl radical. [198] Its oxidizing power is approximately equal to the C-H bond strength of benzene (431 kJ mol^{-1}) [168], which affects the efficiency of benzene oxidation, i.e., the formation of phenol. The formation of cresols instead of benzaldehyde in the case of toluene argues for the presence of •OH radicals, since the methyl group of toluene has an average C-H bond strength of 356 kJ mol^{-1}. [168]
Therefore, the formation of reactive species is observed mainly through the hydroxyl radicals and their reactions, also in view of the fact that the AVOC oxidation products, to a greater extent, are identical to the oxidation products of the Fenton reaction.

The activation of dioxygen by the formation of •OH radicals via pathway 2b was found to be potentially relevant. The pH shift has shown an influence on the specification of ferrous iron in bicarbonate/carbonate systems like previously shown in Fig. 77. With the increased presence of Fe^{2+} i.e. $Fe(H_2O)_6^{2+}$ a positive trend in •OH radicals was observed. One possibility is that the μ-peroxo diiron i.e $[(ligand)Fe\text{-}O_2^{2-}\text{-}Fe(ligand)]^{2-}$ from pathway (2b) favours the formation of H_2O_2 by incorporating two different ligands (CO_3^{2-} and H_2O) i.e. the most dominant species $FeCO_3$ and $Fe(H_2O)_6^{2+}$ at circumneutral pH value. The rapid dissociation of the dimer and formation of H_2O_2 is shown in eq. 31 for the case of EDTA as ligand (L). The rate of H_2O_2 production increases with decreasing of the pH. [177]

$$[(L)Fe^{3+}(O_2^{2-})Fe^{3+}(L)\,]^{2-} \xrightarrow[fast,\ pH\ 6]{} 2[Fe^{3+}(L)H_2O] + H_2O_2 \qquad \text{eq. 31}$$

Replacing of O_2^{2-} i.e. O^{2-} with H_2O after the dissociation of the dimer is due to the increased stability of the complex. Both ligands are weak field ligands, but the crystal field splitting power (Δ_o) of the Fe-complex with the H_2O-ligand is higher and therefore more stable complex is formed (cf. ‘‘spectrochemical’’ series). [153]

In general, the role of the ligands (organic carboxylic groups or inorganic HCO_3^-/CO_3^{2-}) is crucial in the oxygen activation process. This is evident in our systems where little or no HCO_3^-/CO_3^{2-} is present. The ferrous oxidation in the presence of dioxygen with $^-$OH groups as ligands (1mM and pH ~ 11) had no significant production of reactive species (Fig. 61). No oxidation products were detected even in the presence of HCO_3^-/CO_3^{2-}, at pH 12 in the case of benzene (Fig. 66), as previously mentioned.

The formation of the μ-peroxo diiron is especially favoured when ferrous ions are present in excess compared to oxygen. According to Seibig et al. (1997), the peroxo-bridged complex cannot be formed when there is an excess of oxygen. [177] Therefore, the typically anoxic groundwater with increased Fe^{2+} and

carbonate/bicarbonate content could enhance the formation of reactive species when small amounts of dioxygen are added. The effects of different reactive species and the presence of other oxidation-quenching species / scavengers could be crucial.

5.4. Conclusion

The possibility for formation of reactive oxidation species in carbonate-rich water or groundwater with metal-activated oxygen or oxygen activation processes was confirmed in the case of ferrous iron and AVOCs as contaminants. Primary oxidation products and in some cases, secondary oxidation products of AVOC were detected in water. The formation of the reactive species ($^{\bullet}$OH radicals) was additionally confirmed by the fluorescence detection of 7-hydroxycoumarin during the oxidation of coumarin. It was confirmed that the quantitative signal of 7-hydroxycoumarin and indirectly of the formed $^{\bullet}$OH radicals are independent of the high bicarbonate / carbonate concentration in water (no quenching interaction noticed).

The initial idea involved the possibility of using oxygen (i.e. dioxygen) in oxygen-induced oxidation of AVOC in anoxic groundwater as a side reaction to the oxidation of ferrous to ferric iron. The activation was supported by the presence of carbonates as ligands, typical of groundwater conditions. Oxygen containing ligands e.g., organic acids, have already been shown to be successful promoters of oxygen activation (citric acid). The same was confirmed here for inorganic oxygen-containing carbonate ligands at slightly basic pH values. The rapid reaction rates of the AVOC with $^{\bullet}$OH radicals, in contrast to the reaction rates with bicarbonate (dominant species at pH 6.5 - 8.3) as a potential radical scavenger, have also enabled the oxidation of AVOCs to take place.

The products from the oxygen activation of benzene, toluene, *m*- and *o*-xylene and ethylbenzene resemble the products from the corresponding Fenton reactions, suggesting a mechanism based on reaction with $^{\bullet}$OH radicals. The oxidation of ibuprofen (as non-AVOC) and indane was carried out under similar conditions.

Assumptions were made about the mechanisms involved in the formation of $^{\bullet}$OH radicals and, based on these, a prioritization of the possible significant pathways was made. A stronger involvement of the superoxide radical (Haber-Weiss reactions) and µ-peroxo diiron in comparison to the ferryl-(IV)-oxo ion as reactive species was assumed. The role of µ-peroxo-diiron in oxygen-depleted water with excess ferrous presence was highlighted.

Indirect quantitative determination of total $^{\bullet}$OH radicals formed was difficult due to secondary oxidation products, increased presence of Fe^{3+} or other pH dependent scavengers (CO_3^{2-}).

6. General conclusion and outlook

The primary aim of this work was to develop a cost-effective, reliable FAIMS method for on-site assessment of groundwater contamination/remediation with aromatic organic volatile compounds (AVOCs). The potential impact of an oxygen-based remediation method using an oxygen-permeable membrane (OxyTech) under anoxic groundwater conditions was also investigated and confirmed.

Both, APCI (^{63}Ni) and APPI ion sources were tested and showed different characteristics and signal inconsistency upon increased humidity in the FAIMS. Depending on the ion source used, a significant influence on the generated AVOCs signals was observed. Even low humidity (~ 2 ppm_v) was responsible for the suppression of the analyte signal (e.g., toluene and benzene) due to the increased proton affinity of the growing water cluster when using ^{63}Ni-FAIMS. In contrast, with APPI-FAIMS, the effects of humidity during APP-ionization and post-ionization increased the complexity, but more importantly, the intensity of the different AVOC signals to varying degrees. The formation of benzene and toluene water clusters ($M(H_2O)_n$) prior to ionization was confirmed as a probable reason for the increased APP-ionization efficiency (by decrease of the ionization energy). The toluene ionization efficiency in presence of high humidity (~ 400 ppm_v) increased by about 30%. The post-ionization effect of the field strength (88 Td) on the ionized clusters ($M^+(H_2O)_n$) resulted in additional fragmentation of the toluene-water or benzene-water clusters. This fragmentation was also the probable cause of the partial dissociative ionization of the water clusters and their subsequent detection (i.e. indirect ionization). This was observed with the non-polar analytes that have a relative stronger interaction with water molecules (e.g. benzene, toluene).
For indane, TMBs and other more non-polar contaminants that have a weaker interaction with water molecules, the signal change with increasing humidity was much smaller and in some cases (e.g. TMB) was not observed at all. The photoionization signal of the xylenes, such as *p*-xylene, was slightly affected and its intensity increased with the increase of humidity in the FAIMS.
Increasing the humidity by more than 400 ppm_v resulted in a significant decrease in the sensitivity of the APPI-FAIMS method for the detection of all analytes.

The use of the gas-water separation system in combination with APPI-FAIMS for more efficient water separation provided stable moisture content and AVOC signals. With the gas-water separation system the humidity was successfully reduced to < 1.6 ppm_v and maintained. This minimized the increase and the inconsistency of the signal intensity for all aromatic contaminants and minimized the effects of humidity on the charge transfer reactions between multiple analytes (the dopant effect) by simplifying the gas-phase ion-chemistry in the FAIMS. As a result a site specific AVOC sum-signal was formed, which is crucial for the trend monitoring of organic contaminants in groundwater. Validation of the AVOC sum-signal was performed for several analyte combinations with the gas-water separation APPI-FAIMS at low humidity (< 1.6 ppm_v). In the same time the unit showed relatively fast cleaning times

(2 - 3 min) for higher AVOCs concentrations, although greatly dependant from the analyte.
The efficiency of the gas-water separation process was also confirmed for the case of ^{63}Ni-FAIMS.

Prior to the application of the Oxytech membrane and the FAIMS monitoring system, an initial standard sampling and analysis of the groundwater revealed, in addition to BTEX, an increased presence of indane, high basicity (10 mM HCO_3^- equivalents), anoxic conditions and presence of ferrous iron (3.7 mg L^{-1}). The application of OxyTech resulted in a relatively slow and pressure-dependent input of oxygen (1.99 mg h^{-1}) into the contaminated groundwater. This allowed for a rather slow, gradual change in redox conditions in the monitoring well and possibly influenced the migration of the Fe^{2+} plume; more importantly, it prevented the well from clogging when a higher Fe^{2+} concentration was present. In this case, the initial moderately reducing conditions in the monitoring well were maintained during the use of OxyTech. At the same time, the APPI-FAIMS system with gas-water separation was deployed on-site to monitor the contamination and the OxyTech application. The monitoring system used was able to monitor the intensity of aromatic VOC contamination in the groundwater well almost in real time until the breakthrough of the drying unit occurred (4-5 h). A characteristic AVOC sum-signal with C_{max} N^{-1} = -0.016 Td successfully reflected the decreasing trend of contaminants in the monitoring well. This trend was confirmed by static HS-GC/MS analyses of samples taken at the same time.

The significant decrease in AVOCs with the application of the OxyTech membrane was coinciding with the purging the groundwater well. The same monitoring procedure was carried out again and showed an almost identical development of the contamination trends, which were mostly independent of the time when the OxyTech application started. It was assumed that the current low ferrous iron concentration (< 1 mg L^{-1}) in the well was the decisive factor for the oxidation of the contaminants. A further analysis of the effects of Fe^{2+} oxidation in anoxic water with the addition of dioxygen was conducted separately to confirm the oxidation potential of ferrous-rich groundwater.

The possibility of the formation of reactive oxidation species in carbonate-rich water or groundwater with metal-activated oxygen or oxygen activation processes was confirmed in the case of ferrous iron and AVOCs as contaminants. The role of oxygen (i.e. dioxygen) in oxygen-induced oxidation of AVOCs in anoxic water as a side reaction to the oxidation of ferrous to ferric iron was confirmed.
Primary oxidation products and in some cases secondary oxidation products of AVOC were detected in the water. The formation of the reactive species ($^{\bullet}$OH radicals) was additionally confirmed by the fluorescence detection of 7-hydroxycoumarin during the oxidation of coumarin. It was confirmed that the quantitative signal of 7-hydroxycoumarin and indirectly of the formed $^{\bullet}$OH radicals is independent of the high bicarbonate/carbonate concentration in water.

The activation was supported by the presence of carbonates as ligands, typical of groundwater conditions. Oxygen containing ligands such as organic acids (i.e. -COOH groups), have already been shown to be successful promoters of oxygen activation (e.g. citric acid). The same was confirmed here for inorganic oxygen-containing carbonate ligands at slightly basic pH values. The faster reaction rates of $^{\bullet}OH$ radicals with AVOCs compared to the reaction rates with bicarbonate as a dominant species (at pH 6.5 - 8.3) and a potential radical scavenger, have also contributed to the oxidation of AVOCs.

The products from the oxygen activation of benzene, toluene, *m*- and *o*-xylene and ethylbenzene were similar to the products from the corresponding Fenton reactions, indicating a similar mechanism based on the reaction with $^{\bullet}OH$ radicals. The oxidation of ibuprofen (as non-AVOC) and indane was successfully carried out under similar conditions.

Assumptions were made about the mechanisms involved in the formation of $^{\bullet}OH$ radicals and on this basis a prioritization of the possible significant pathways was made. A stronger involvement of the superoxide radical (Haber-Weiss reactions) and µ-peroxo-diiron in comparison to the ferryl-(IV)-oxo ion as reactive species was assumed. The possibility of µ-peroxo-diiron formation in oxygen-depleted water with excess of ferrous ion presence was highlighted.

Indirect quantitative determination of total $^{\bullet}OH$ radicals formed was difficult due to secondary oxidation products, increased presence of Fe^{3+} and pH dependent scavengers (CO_3^{2-}).

Considering the results, oxygen-induced oxidation in anoxic waters containing Fe^{2+} and carbonates (e.g. groundwater) close to circumneutral pH may occur by incremental addition of O_2. Still the effects could be minor, which is why it could be regarded more as a supporting remediation method. The effectiveness of oxygen-induced oxidation in groundwater is considered to be site specific and should be additionally investigated via site specific parameters (pH, Fe^{2+}, HCO_3^-/CO_3^{2-} etc.) and presence of scavengers prior to application.

These results were used to highlight the hidden potential of slowly permeating oxygen in support to groundwater remediation without the use of activators like H_2O_2, and to demonstrate the feasibility of using the simplified ‘‘stand-alone’’ FAIMS or IMS-based analytical methods for on-site contamination monitoring.

However, the problem of the humidity influence on these analytical methods remains and should be also adequately addressed in the up-and-coming FAIMS/IMS systems.

7. Appendix

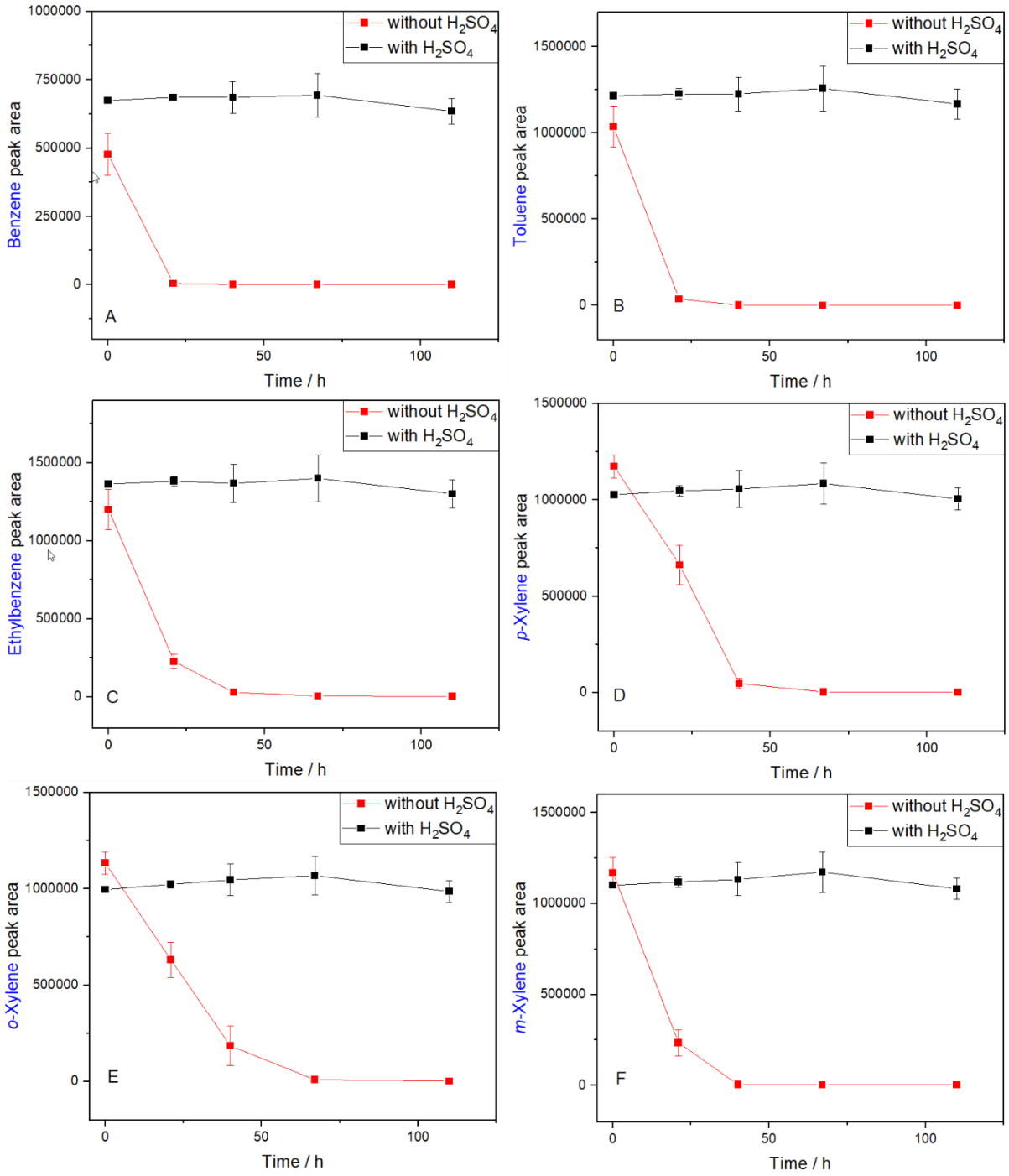

App. 1: Change in peak area of unpreserved (red) and preserved (black) real groundwater samples containing BTEX as contaminants (Examination method: static HS-GC/MS). For both cases, 1.1% of the vessel volume was made up with distilled water (unpreserved) or 50% H_2SO_4 (pH 1-2) (preserved) [200]. Samples were collected, tested, and stored for a period of 5 days (max. 6°C).

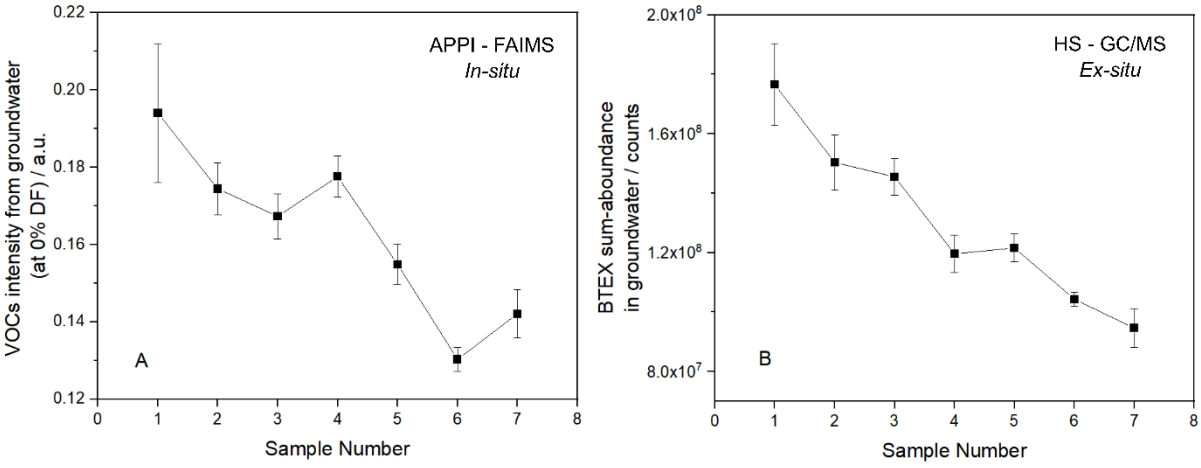

App. 2: A) On-site monitoring of the total VOC intensity signal (sum-signal) over a 4 h period at 0% DF; B) Sum-signal of BTEX from samples taken during the acquiring of (A) by static HS-GC/MS in laboratory conditions. Decrease in sum-signal in (A) and (B) was 33% and 46% respectively. OxyTech membrane was in operation (0.6 barg) before the start of the monitoring and during the 4 h period.

7.1. List of figures

7.2. List of tables

7.3. List of publications, presentations, posters and awards

Publications

(2022) ‘‘Atmospheric pressure photoionization - High-field asymmetric ion mobility spectrometry (APPI-FAIMS) studies for on-site monitoring of aromatic volatile organic compounds (VOCs) in groundwater’’
S. Joksimoski, K. Kerpen, U. Telgeder (Talanta);

(2021) ‘‘Development and comparison of direct immersion solid phase micro extraction Arrow-GC/MS for the determination of selected pesticides in water’’
S. M. S. Khademi, A. Salemi, M.Jochmann, **S.Joksimoski**, U. Telgeder (Microchemical Journal);

(2016) ‘‘Analysis of gasoline contaminated water samples by means of dopant-assisted atmospheric pressure photoionization differential ion mobility spectrometry’’
A. Kuklya, **S. Joksimoski**, K. Kerpen, F. Uteschil, R. Marks, U. Telgeder (International Jurnal for Ion Mobility Spectrometry).

Presentations

(2019) ‘‘Gas-water separation unit for direct monitoring of BTEX contaminated groundwater with FAIMS’’
Joksimoski, S., Kerpen, K., Marks, R., Telgheder, U.
29. Doktorandenseminar Hohenroda, 6 - 8 January 2019, Hohenroda, Germany;

(2018) ‘‘Gas-water separation unit for direct monitoring of BTEX contaminated groundwater with FAIMS’’
Joksimoski, S., Kuklya, A., Kerpen, K., Marks, R., Telgheder, U.
7. Anwendertreffen Ionenmobilitätsspektrometrie, 6 - 7 March 2018 Reutlingen, Germany.

Posters

(2021) ‘‘Groundwater monitoring with APPI-FAIMS in combination with a gas/water separation system’’
Joksimoski, S., Kerpen, K., Uteschil, F., Marks, R., Telgheder, U.
8. Anwendertreffen Ionenmobilitätsspektrometrie, 17 – 19 March 2021 Reutlingen, Germany (on-line);

(2019) ‘‘Gas-water separation unit for direct monitoring of BTEX contaminated groundwater with FAIMS’’
Joksimoski, S., Kerpen, K., Marks, R., Telgheder, U.
28th Annual ISIMS conference, July 28th – August 2nd 2019, Hannover, Germany;

(2019) ‘‘Gas-water separation unit for direct monitoring of BTEX contaminated groundwater with FAIMS’’
Joksimoski, S., Kerpen, K., Marks, R., Telgheder, U.
ANAKON 2019, 25 - 28 March 2019, Münster, Germany;

(2018) ‘‘Gas-water separation unit for direct monitoring of BTEX contaminated groundwater with FAIMS’’
Joksimoski, S., Kerpen, K., Marks, R., Telgheder, U.
3. Wasseranalytisches Seminar (MWAS 2018): 12. bis 13. September 2018, Mülheim an der Ruhr, Germany.

Awards

Part of this work was a cooperation with a partner company (Fabricius Pro Terra GmbH). This cooperation project was approved from ZiM (Zentrale Innovationsprogramm Mittelstand) under the original title:

„Entwicklung eines kombinierten In-situ-Sanierungs- und Monitoringverfahrens für die Behandlung von Grundwasserschäden (Luft-Untergrund-Kontamination-Erfassung "LUKE")“.

The AiF (Arbeitsgemeinschaft industrielle Forschungsvereinigungen) anounced this cooperation as a successful project example and was subsequently nominated for the German Environmental Award 2021.

This part of the scientific work was funded by BMWI (Bundesministerium für Wirtschaft und Klimaschutz) with the funding reference number ZF4265101SA6.

7.4. Statement

Hiermit versichere ich, dass ich die vorliegende Arbeit mit dem Titel:

‘‘High-field asymmetric ion mobility spectrometry (FAIMS) study for on-site monitoring of aromatic volatile organic compounds in groundwater and their degradation in the presence of ferrous iron and carbonate’’

Selbst verfasst und keine außer den angegebenen Hilfsmittel und Quellen benutzt habe, und dass die Arbeit in dieser oder ähnlicher Form noch bei keiner anderen Universität eingereicht wurde.

Krefeld, im Mai 2023

8. References

[1] P. Quevauviller, Groundwater monitoring, Wiley-Blackwell, Oxford, 2009.

[2] J. Margat, J. van der Gun, Groundwater around the world: A geographic synopsis, CRC, Boca Raton, Fla., 2013.

[3] A. Gil, L.A. Galeano, M.Á. Vicente (Eds.), Applications of Advanced Oxidation Processes (AOPs) in Drinking Water Treatment, Springer International Publishing, Cham, 2019.

[4] L.A. Desimone, Geological Survey Scientific Investigations: Quality of water from domestic wells in principal aquifers of the United States, 1991-2004, Reston, VA, 2009.

[5] C. Zhang, Soil and groundwater remediation: fundamentals, practices, and sustainability, John Wiley & Sons, 2019.

[6] Weidemeier T., Approximation of biodegradation rate constants for monoaromatic hydrocarbons (BTEX) in groundwater, 1996.

[7] C.M. Vitale, S. Gutovitz, Aromatic Toxicity, StatPearls Publishing, Treasure Island (FL), 2021.

[8] Research and Markets, The world's largest market research store, Benzene-Toluene-Xylene (BTX) Market - Growth, Trends, COVID-19 Impact, and Forecasts (2021 - 2026), https://www.researchandmarkets.com/reports/5514218/benzene-toluene-xylene-btx-market-growth?utm_source=GNOM&utm_medium=PressRelease&utm_code=qj6kc5&utm_campaign=1639828+-+Global+Benzene-Toluene-Xylene+Market+(2021+to+2026)+-+Growth%2c+Trends%2c+COVID-19+Impact+and+Forecasts&utm_exec=jamu273prd#, 2021 (accessed 7.03.2022).

[9] A. Bhandari (Ed.), Remediation technologies for soils and groundwater, ASCE, Reston, Va., 2007.

[10] G.A. Eiceman, E.G. Nazarov, B. Tadjikov, R.A. Miller, Monitoring volatile organic compounds in ambient air inside and outside buildings with the use of a radio-frequency-based ion-mobility analyzer with a micromachined drift tube, Field Analyt. Chem. Technol. 4 (2000) 297–308. 10.1002/1520-6521(2000)4:6<297:AID-FACT50>3.0.CO;2-H.

[11] G. Walendzik, J.I. Baumbach, D. Klockow, Coupling of SPME with MCC/UV-IMS as a tool for rapid on-site detection of groundwater and surface water contamination, Analytical and bioanalytical chemistry 382 (2005) 1842–1847. 10.1007/s00216-005-3362-6.

[12] H.I. Essaid, B.A. Bekins, I.M. Cozzarelli, Organic contaminant transport and fate in the subsurface: Evolution of knowledge and understanding, Water Resour. Res. 51 (2015) 4861–4902. 10.1002/2015WR017121.

[13] C.L. Yaws, Thermophysical properties of chemicals and hydrocarbons, Andrew, Norwich, NY, 2008.

[14] D. Mackay, Handbook of physical-chemical properties and environmental fate for organic chemicals, 2nd ed., CRC/Taylor & Francis, Boca Raton, FL, 2006.

[15] R. Sander, Compilation of Henry's law constants (version 4.0) for water as solvent, Atmos. Chem. Phys. 15 (2015) 4399–4981. 10.5194/acp-15-4399-2015.

[16] W.M. Haynes (Ed.), CRC handbook of chemistry and physics: A ready-reference book of chemical and physical data, 97th ed., CRC Press, Boca Raton, London, New York, 2017.
[17] W.-Y. Shiu, K.-C. Ma, Temperature Dependence of Physical–Chemical Properties of Selected Chemicals of Environmental Interest. I. Mononuclear and Polynuclear Aromatic Hydrocarbons, Journal of Physical and Chemical Reference Data 29 (2000) 41–130. 10.1063/1.556055.
[18] D.G. Shaw (Ed.), Hydrocarbons with water and seawater: [überwiegend Tab.], 1st ed., Pergamon Pr, Oxford, 1989.
[19] C. Wan, P.B. Harrington, D.M. Davis, Trace analysis of BTEX compounds in water with a membrane interfaced ion mobility spectrometer, Talanta 46 (1998) 1169–1179. 10.1016/S0039-9140(97)00363-9.
[20] A.B. Kanu, H.H. Hill, M.M. Gribb, R.N. Walters, A small subsurface ion mobility spectrometer sensor for detecting environmental soil-gas contaminants, Journal of environmental monitoring JEM 9 (2007) 51–60. 10.1039/b610493b.
[21] E.K. Nyer, J. Bedessem, Groundwater treatment technology, 3rd ed., Wiley; Chichester John Wiley [distributor], Hoboken, N.J., 2009.
[22] F.-G. Simon, T. Meggyes, C. McDonald, Advanced groundwater remediation: Active and passive technologies / edited by F.-G. Simon, T. Meggyes, C. McDonald, Telford, London, 2002.
[23] J.T. Albergaria, M.C.M. Da Alvim-Ferraz, C. Delerue-Matos, Remediation of sandy soils contaminated with hydrocarbons and halogenated hydrocarbons by soil vapour extraction, Journal of environmental management 104 (2012) 195–201. 10.1016/j.jenvman.2012.03.033.
[24] R.L. Siegrist, M. Crimi, T.J. Simpkin (Eds.), In situ chemical oxidation for groundwater remediation, Springer, New York NY, 2011.
[25] S.G. Huling, B.E. Pivetz, In-situ chemical oxidation, 2006.
[26] J. Hoigné, H. Bader, The role of hydroxyl radical reactions in ozonation processes in aqueous solutions, Water Research 10 (1976) 377–386. 10.1016/0043-1354(76)90055-5.
[27] T. Umschlag, H. Herrmann, The Carbonate Radical (HCO3·/CO3-·) as a Reactive Intermediate in Water Chemistry: Kinetics and Modelling, Acta hydrochim. hydrobiol. 27 (1999) 214–222. 10.1002/(SICI)1521-401X(199907)27:4<214:AID-AHEH214>3.0.CO;2-6.
[28] R.J. Watts, A.L. Teel, Chemistry of modified Fenton's reagent (catalyzed H2O2 propagations-CHP) for in situ soil and groundwater remediation, Journal of environmental engineering 131 (2005) 612–622.
[29] H.J.H. Fenton, Oxidation of tartaric acid in presence of iron, Journal of the Chemical Society, Transactions 65 (1894) 899–910.
[30] D.H. Kampbell, T.H. Wiedemeier, J.E. Hansen, Intrinsic bioremediation of fuel contamination in ground water at a field site, Journal of Hazardous Materials 49 (1996) 197–204. 10.1016/0304-3894(96)01753-0.
[31] E. Jindrová, M. Chocová, K. Demnerová, V. Brenner, Bacterial aerobic degradation of benzene, toluene, ethylbenzene and xylene, Folia microbiologica 47 (2002) 83–93. 10.1007/BF02817664.

[32] D.R. Lovley, M.J. Baedecker, D.J. Lonergan, I.M. Cozzarelli, E.J.P. Phillips, D.I. Siegel, Oxidation of aromatic contaminants coupled to microbial iron reduction, Nature 339 (1989) 297–300. 10.1038/339297a0.
[33] C. Zhang, G.N. Bennett, Biodegradation of xenobiotics by anaerobic bacteria, Applied microbiology and biotechnology 67 (2005) 600–618. 10.1007/s00253-004-1864-3.
[34] H.-W. Wang, C.-L. Chen, Y.-J. Liu, X.-T. Zhang, D.-Y. Kong, X.-Z. Wang, J.-K. Luo, Humidity effects on resolution and sensitivity of UV-FAIMS in VOCs detection, Anal. Methods 7 (2015) 1401–1406. 10.1039/c4ay02167c.
[35] ISO 11423-1:1997-06, Water quality - Determination of benzene and some derivatives - Part 1: Head-space gas chromatograhic method.
[36] DIN 38407-39:2011-09, German standard methods for the examination of water, waste water and sludge - Jointly determinable substances (group F) - Part 39: Determination of selected polycyclic aromatic hydrocarbons (PAH) - Method using gas chromatography with mass spectrometric detection (GC-MS) (F 39).
[37] ISO 11423-2:1997-06, Water quality - Determination of benzene and some derivatives - Part 2: Method using extraction and gas chromatography.
[38] DIN EN ISO 17943:2016-10, Water quality - Determination of volatile organic compounds in water - Method using headspace solid-phase micro-extraction (HS-SPME) followed by gas chromatography-mass spectrometry (GC-MS).
[39] S. Joksimoski, K. Kerpen, U. Telgheder, Atmospheric pressure photoionization - High-field asymmetric ion mobility spectrometry (APPI-FAIMS) studies for on-site monitoring of aromatic volatile organic compounds (VOCs) in groundwater, Talanta 247 (2022) 123555. 10.1016/j.talanta.2022.123555.
[40] H. Borsdorf, G.A. Eiceman, Ion Mobility Spectrometry, Applied Spectroscopy Reviews 41 (2006) 323–375. 10.1080/05704920600663469.
[41] G.A. Eiceman, Z. Karpas, H.H. Hill, Ion mobility spectrometry, 3rd ed., CRC Press, Boca Ration, Fla., 2014.
[42] T. Mayer, H. Borsdorf, Accuracy of ion mobility measurements dependent on the influence of humidity, Anal. Chem. 86 (2014) 5069–5076. 10.1021/ac5007393.
[43] A.A. Shvartsburg, Differential ion mobility spectrometry: Nonlinear ion transport and fundamentals of FAIMS, CRC Press, Boca Raton, 2009.
[44] G.A. Eiceman, E.G. Nazarov, R. Miller, A Micromachined Field Asymmetric-Ion Mobility Spectrometer for Detecting Volatile Organic Chemicals in Ambient Air, in: SAE International400 Commonwealth Drive, Warrendale, PA, United States, 2000.
[45] R.A. Miller, E.G. Nazarov, G.A. Eiceman, A. Thomas King, A MEMS radio-frequency ion mobility spectrometer for chemical vapor detection, Sensors and Actuators A: Physical 91 (2001) 301–312. 10.1016/S0924-4247(01)00600-8.
[46] B.M. Kolakowski, Z. Mester, Review of applications of high-field asymmetric waveform ion mobility spectrometry (FAIMS) and differential mobility spectrometry (DMS), The Analyst 132 (2007) 842–864. 10.1039/b706039d.
[47] E.G. Nazarov, S.L. Coy, E.V. Krylov, R.A. Miller, G.A. Eiceman, Pressure effects in differential mobility spectrometry, Anal. Chem. 78 (2006) 7697–7706. 10.1021/ac061092z.

[48] R. Guevremont, High-field asymmetric waveform ion mobility spectrometry: A new tool for mass spectrometry, Journal of chromatography. A 1058 (2004) 3–19. 10.1016/j.chroma.2004.08.119.
[49] I.A. Buryakov, E.V. Krylov, E.G. Nazarov, U. Rasulev, A new method of separation of multi-atomic ions by mobility at atmospheric pressure using a high-frequency amplitude-asymmetric strong electric field, International Journal of Mass Spectrometry and Ion Processes 128 (1993) 143–148. 10.1016/0168-1176(93)87062-W.
[50] A.A. Shvartsburg, R.D. Smith, A. Wilks, A. Koehl, D. Ruiz-Alonso, B. Boyle, Ultrafast differential ion mobility spectrometry at extreme electric fields in multichannel microchips, Anal. Chem. 81 (2009) 6489–6495. 10.1021/ac900892u.
[51] A. Wilks, M. Hart, A. Koehl, J. Somerville, B. Boyle, D. Ruiz-Alonso, Characterization of a miniature, ultra-high-field, ion mobility spectrometer, Int. J. Ion Mobil. Spec. 15 (2012) 199–222. 10.1007/s12127-012-0109-x.
[52] E. Hoffmann, V. Stroobant, Mass spectrometry: Principles and applications, 3rd ed., Wiley, Chichester, 2011.
[53] C. Chen, D. Jiang, H. Li, UV photoionization ion mobility spectrometry, Analytica chimica acta 1077 (2019) 1–13. 10.1016/j.aca.2019.05.018.
[54] J. Ševčik, S. Krýsl, A photoionization detector, Chromatographia 6 (1973) 375–380. 10.1007/BF02270573.
[55] E.G. Nazarov, R.A. Miller, G.A. Eiceman, J.A. Stone, Miniature differential mobility spectrometry using atmospheric pressure photoionization, Anal. Chem. 78 (2006) 4553–4563. 10.1021/ac052213i.
[56] T.J. Kauppila, T. Kuuranne, E.C. Meurer, M.N. Eberlin, T. Kotiaho, R. Kostiainen, Atmospheric pressure photoionization mass spectrometry. Ionization mechanism and the effect of solvent on the ionization of naphthalenes, Anal. Chem. 74 (2002) 5470–5479. 10.1021/ac025659x.
[57] X. Jia, D. Hou, L. Wang, D. O'Connor, J. Luo, The development of groundwater research in the past 40 years, Journal of Hydrology 587 (2020) 125006. 10.1016/j.jhydrol.2020.125006.
[58] H.H. Hill, G. Simpson, Capabilities and limitations of ion mobility spectrometry for field screening applications, Field Analyt. Chem. Technol. 1 (1997) 119–134. 10.1002/(SICI)1520-6521(1997)1:3<119:AID-FACT2>3.0.CO;2-S.
[59] A. Kuklya, F. Uteschil, K. Kerpen, R. Marks, U. Telgheder, Effect of the humidity on analysis of aromatic compounds with planar differential ion mobility spectrometry, Int. J. Ion Mobil. Spec. 18 (2015) 67–75. 10.1007/s12127-014-0162-8.
[60] J. Langejuergen, M. Allers, J. Oermann, A. Kirk, S. Zimmermann, Quantitative detection of benzene in toluene- and xylene-rich atmospheres using high-kinetic-energy ion mobility spectrometry (IMS), Anal. Chem. 86 (2014) 11841–11846. 10.1021/ac5034243.
[61] L. Arce, M. Menéndez, R. Garrido-Delgado, M. Valcárcel, Sample-introduction systems coupled to ion-mobility spectrometry equipment for determining compounds present in gaseous, liquid and solid samples, TrAC Trends in Analytical Chemistry 27 (2008) 139–150. 10.1016/j.trac.2008.01.001.

[62] S. Holopainen, M. Nousiainen, M.E. Sillanpää, O. Anttalainen, Sample-extraction methods for ion-mobility spectrometry in water analysis, TrAC Trends in Analytical Chemistry 37 (2012) 124–134. 10.1016/j.trac.2012.03.014.
[63] Y. Du, W. Zhang, W. Whitten, H. Li, D.B. Watson, J. Xu, Membrane-extraction ion mobility spectrometry for in situ detection of chlorinated hydrocarbons in water, Anal. Chem. 82 (2010) 4089–4096. 10.1021/ac100162d.
[64] H. Borsdorf, A. Rämmler, Continuous on-line determination of methyl tert-butyl ether in water samples using ion mobility spectrometry, Journal of chromatography. A 1072 (2005) 45–54. 10.1016/j.chroma.2004.12.041.
[65] S. Holopainen, M. Nousiainen, M. Sillanpää, Determination of fuel ethers in water by membrane extraction ion mobility spectrometry, Talanta 106 (2013) 448–453. 10.1016/j.talanta.2013.01.026.
[66] J.I. Baumbach, S. Sielemann, Z. Xie, H. Schmidt, Detection of the gasoline components methyl tert-butyl ether, benzene, toluene, and m-xylene using ion mobility spectrometers with a radioactive and UV ionization source, Anal. Chem. 75 (2003) 1483–1490. 10.1021/ac020342i.
[67] DIN 32645:2008-11, Chemical analysis - Decision limit, detection limit and determination limit under repeatability conditions - Terms, methods, evaluation.
[68] E. Krylov, E.G. Nazarov, R.A. Miller, B. Tadjikov, G.A. Eiceman, Field dependence of mobilities for gas-phase-protonated monomers and proton-bound dimers of ketones by planar field asymmetric waveform ion mobility spectrometer (PFAIMS), The journal of physical chemistry. A 106 (2002) 5437–5444. 10.1021/jp020009i.
[69] L.A. Viehland, E. Mason, Gaseous ion mobility and diffusion in electric fields of arbitrary strength, Annals of Physics 110 (1978) 287–328. 10.1016/0003-4916(78)90034-9.
[70] E.A. Mason, E.W. McDaniel, Transport properties of ions in gases, Wiley, New York, 1988.
[71] E.V. Krylov, S.L. Coy, E.G. Nazarov, Temperature effects in differential mobility spectrometry, International journal of mass spectrometry 279 (2009) 119–125. 10.1016/j.ijms.2008.10.025.
[72] X. An, G.A. Eiceman, J.A. Stone, A determination of the effective temperatures for the dissociation of the proton bound dimer of dimethyl methylphosphonate in a planar differential mobility spectrometer, Int. J. Ion Mobil. Spec. 13 (2010) 25–36. 10.1007/s12127-010-0037-6.
[73] Florian S., Wie Funktionieren GORE-TEX® Membranen?, https://www.bergfreunde.de/blog/gore-tex-membran/ (accessed 05/30/2022).
[74] E.P.L. Hunter, S.G. Lias, Evaluated Gas Phase Basicities and Proton Affinities of Molecules, Journal of Physical and Chemical Reference Data 27 (1998) 413–656. 10.1063/1.556018.
[75] Sharon G. Lias, Ionization Energy Evaluation in NIST Chemistry WebBook, NIST Standard Reference Database Number 69, Eds. P.J. Linstrom and W.G. Mallard, National Institute of Standards and Technology, Gaithersburg MD, 20899. 10.18434/T4D303, (retrieved March 5, 2022).
[76] L. Klasinc, B. Kovac, H. Gusten, Photoelectron spectra of acenes. Electronic structure and substituent effects, Pure and Applied Chemistry 55 (1983) 289–298. 10.1351/pac198855020289.

[77] J.O. Howell, J.M. Goncalves, C. Amatore, L. Klasinc, R.M. Wightman, J.K. Kochi, Electron transfer from aromatic hydrocarbons and their .pi.-complexes with metals. Comparison of the standard oxidation potentials and vertical ionization potentials, J. Am. Chem. Soc. 106 (1984) 3968–3976. 10.1021/ja00326a014.
[78] J.P. Maier, D.W. Turner, Steric inhibition of resonance studied by molecular photoelectron spectroscopy. Part 2.—Phenylethylenes, J. Chem. Soc., Faraday Trans. 2 69 (1973) 196–206. 10.1039/F29736900196.
[79] H. Back, W. Kaim, H.E. Rohwer, Radikalionen, XX, Chem. Ber. 111 (1978) 3573–3584. 10.1002/cber.19781111106.
[80] C. Köppel, H. Schwarz, F. Bohlmann, Elektronenstossinduzierte Fragmentierung von Acetylenverbindungen—VIII, Org. Mass Spectrom. 8 (1974) 25–29. 10.1002/oms.1210080104.
[81] J.E. Reutt, L.S. Wang, Y.T. Lee, D.A. Shirley, Molecular beam photoelectron spectroscopy and femtosecond intramolecular dynamics of H 2 O + and D 2 O +, The Journal of Chemical Physics 85 (1986) 6928–6939. 10.1063/1.451379.
[82] H. Borsdorf, P. Fiedler, T. Mayer, The effect of humidity on gas sensing with ion mobility spectrometry, Sensors and Actuators B: Chemical 218 (2015) 184–190. 10.1016/j.snb.2015.04.102.
[83] C. Hop, T.B. McMahon, G.D. Willett, Determination of bond dissociation energies via energy-resolved collision induced dissociation in a fourier transform ion cyclotron resonance spectrometer, International Journal of Mass Spectrometry and Ion Processes 101 (1990) 191–208. 10.1016/0168-1176(90)87011-5.
[84] R.G. Keesee, A.W. Castleman, Thermochemical Data on Gas-Phase Ion-Molecule Association and Clustering Reactions, Journal of Physical and Chemical Reference Data 15 (1986) 1011–1071. 10.1063/1.555757.
[85] N.F. Dalleska, K. Honma, P.B. Armentrout, Stepwise solvation enthalpies of protonated water clusters: collision-induced dissociation as an alternative to equilibrium studies, J. Am. Chem. Soc. 115 (1993) 12125–12131. 10.1021/ja00078a059.
[86] M. Meot-Ner, P. Hamlet, E.P. Hunter, F.H. Field, Bonding energies in association ions of aromatic compounds. Correlations with ionization energies, J. Am. Chem. Soc. 100 (1978) 5466–5471. 10.1021/ja00485a034.
[87] D.J. Goebbert, P.G. Wentold, Water dimer proton affinity from the kinetic method, European journal of mass spectrometry (Chichester, England) 10 (2004) 837–846. 10.1255/ejms.684.
[88] S. Klee, S. Albrecht, V. Derpmann, H. Kersten, T. Benter, Generation of ion-bound solvent clusters as reactant ions in dopant-assisted APPI and APLI, Analytical and bioanalytical chemistry 405 (2013) 6933–6951. 10.1007/s00216-013-7114-8.
[89] S. Li, E.R. Bernstein, Toluene–water clusters, The Journal of Chemical Physics 97 (1992) 792–803. 10.1063/1.463181.
[90] B. Ernstberger, H. Krause, A. Kiermeier, H.J. Neusser, Multiphoton ionization and dissociation of mixed van der Waals clusters in a linear reflectron time-of-flight mass spectrometer, The Journal of Chemical Physics 92 (1990) 5285–5296. 10.1063/1.458603.
[91] G.N. Gerasimov, B.E. Krylov, O.N. Kononova, R. Hallin, A. Morozov, F. Heijkenskjold, A. Arnesen, E.V. Zhukova, The effect of short-wavelength

discharge radiation on the transmission of a magnesium fluoride window, J. Opt. Technol. 69 (2002) 158. 10.1364/JOT.69.000158.
[92] P.G. Wilkinson, Oscillator strengths of the resonance lines of the rare gases—I. Krypton, Journal of Quantitative Spectroscopy and Radiative Transfer 5 (1965) 503–510. 10.1016/0022-4073(65)90083-X.
[93] M. Miyazaki, A. Fujii, T. Ebata, N. Mikami, Electronic spectroscopy of benzene–water cluster cations, [C6H6–(H2O)n]+ (n=1–4): spectroscopic evidence for phenyl radical formation through size-dependent intracluster proton transfer reactions, Chemical Physics Letters 399 (2004) 412–416. 10.1016/j.cplett.2004.10.036.
[94] DIN 32645:2008-11, Chemical analysis - Decision limit, detection limit and determination limit under repeatability conditions - Terms, methods, evaluation.
[95] J. Mandel, The statistical analysis of experimental data, Dover Publ, New York, 1984.
[96] St. Sielemann, J.I. Baumbach, H. Schmidt, P. Pilzecker, Quantitative analysis of benzene, toluene, and m-xylene with the use of a UV-ion mobility spectrometer, Field Analyt. Chem. Technol. 4 (2000) 157–169. 10.1002/1520-6521(2000)4:4<157:AID-FACT2>3.0.CO;2-#.
[97] A. Kuklya, S. Joksimoski, K. Kerpen, F. Uteschil, R. Marks, U. Telgheder, Analysis of gasoline contaminated water samples by means of dopant-assisted atmospheric pressure photoionization differential ion mobility spectrometry, Int. J. Ion Mobil. Spec. 19 (2016) 121–130. 10.1007/s12127-016-0194-3.
[98] S. Mitra, P. Roy, BTEX, Research J. of Environmental Sciences 5 (2011) 394–398. 10.3923/rjes.2011.394.398.
[99] G. Bitton, Encyclopedia of environmental microbiology, Wiley, New York, Chichester, 2002.
[100] R.U. Meckenstock, M. Boll, H. Mouttaki, J.S. Koelschbach, P. Cunha Tarouco, P. Weyrauch, X. Dong, A.M. Himmelberg, Anaerobic Degradation of Benzene and Polycyclic Aromatic Hydrocarbons, Journal of molecular microbiology and biotechnology 26 (2016) 92–118. 10.1159/000441358.
[101] J.G. Hering, W. Stumm, CHAPTER 11. OXIDATIVE AND REDUCTIVE DISSOLUTION OF MINERALS, in: M.F. Hochella, A.F. White (Eds.), Mineral-Water Interface Geochemistry, De Gruyter, 1990, pp. 427–466.
[102] W. Davison, Conceptual models for transport at a redox boundary, 1985.
[103] T.L. Gibson, A.S. Abdul, P.D. Chalmer, Enhancement of In Situ Bioremediation of BTEX-Contaminated Ground Water by Oxygen Diffusion from Silicone Tubing, Groundwater Monitoring & Remediation 18 (1998) 93–104. 10.1111/j.1745-6592.1998.tb00606.x.
[104] E.M. Godsy, E. Warren, I.M. Cozzarelli, B.A. Bekins, R.P. Eganhouse, Determining BTEX biodegradation rates using in situ microcosms at the Bemidji site, Minnesota: trials and tribulations, in: US Geological Survey Toxic Substances Hydrology Program. Proceedings of the Technical Meeting. US Geological Survey, Reston, VA, pp. 159–167.
[105] DIN EN ISO 9963-1:1996, Water quallty — Determination of alkalinity — Part 1: Determination of total and composite alkalinity.

[106] Harvey Jr AE, Smart JA, Amis ES., Simultaneous spectrophotometric determination of iron (II) and total iron with 1, 10-phenanthroline, Anal. Chem. (1955) 26–29.
[107] D.R. Lovley, E.J. Phillips, Novel mode of microbial energy metabolism: organic carbon oxidation coupled to dissimilatory reduction of iron or manganese, Applied and environmental microbiology 54 (1988) 1472–1480. 10.1128/aem.54.6.1472-1480.1988.
[108] ISO 5667-3:2012, Water quality — Sampling — Part 3: Preservation and handling of water samples.
[109] C.A.J. Appelo, D. Postma, Geochemistry, groundwater and pollution, 2nd ed., Balkema, Leiden, New York, 2005.
[110] W.J. Weber, W. Stumm, Mechanism of Hydrogen Ion Buffering in Natural Waters, Journal - American Water Works Association 55 (1963) 1553–1578. 10.1002/j.1551-8833.1963.tb01178.x.
[111] M.M. Fortune WB, Determination of iron with O-phenanthroline: a spectrophotometric study. Industrial & Engineering, Analytical chemistry (1938) 60–64.
[112] Harvey Jr AE, Smart JA, Amis ES., Simultaneous spectrophotometric determination of iron (II) and total iron with 1, 10-phenanthroline, Analytical chemistry (1955) 26–29.
[113] H.J. Albrechtsen, T.H. Christensen, Evidence for microbial iron reduction in a landfill leachate-polluted aquifer (Vejen, Denmark), Applied and environmental microbiology 60 (1994) 3920–3925. 10.1128/aem.60.11.3920-3925.1994.
[114] K. Kapoor, Illustrated dictionary of microbiology, Oxford Book Co, Jaipur, India, 2010.
[115] J. Damborsky, M. Damborska, S. Stipek, A. Jesenska, L. Trantirek, V. Sklenar, Effect of the carbon source on assessment of degrading bacteria with the spread-plating technique during in situ bioremediation, Folia microbiologica 45 (2000) 35–40.
[116] E. Lang, Diversity of bacterial capabilities in utilizing alkylated benzenes and other aromatic compounds, Letters in applied microbiology 23 (1996) 257–260. 10.1111/j.1472-765X.1996.tb00078.x.
[117] R.T. Anderson, J.N. Rooney-Varga, C.V. Gaw, D.R. Lovley, Anaerobic Benzene Oxidation in the Fe(III) Reduction Zone of Petroleum-Contaminated Aquifers, Environ. Sci. Technol. 32 (1998) 1222–1229. 10.1021/es9704949.
[118] J. Kazumi, M.E. Caldwell, J.M. Suflita, D.R. Lovley, L.Y. Young, Anaerobic Degradation of Benzene in Diverse Anoxic Environments, Environ. Sci. Technol. 31 (1997) 813–818. 10.1021/es960506a.
[119] B.H. Wilson, G.B. Smith, J.F. Rees, Biotransformations of selected alkylbenzenes and halogenated aliphatic hydrocarbons in methanogenic aquifer material: a microcosm study, Environ. Sci. Technol. 20 (1986) 997–1002. 10.1021/es00152a005.
[120] U.S. Geological Survey, Techniques and Methods, 2020.
[121] D. Lorenz, Auswertung internationaler Fachliteratur zu In-Situ-Anwendungen in der gesättigten Zone bei der Altlastenbearbeitung, 2008.
[122] D.E. Cummings, A.W. March, B. Bostick, S. Spring, F. Caccavo, S. Fendorf, R.F. Rosenzweig, Evidence for microbial Fe(III) reduction in anoxic, mining-

impacted lake sediments (Lake Coeur d'Alene, Idaho), Applied and environmental microbiology 66 (2000) 154–162. 10.1128/AEM.66.1.154-162.2000.
[123] K. Küsel, M. Blöthe, D. Schulz, M. Reiche, H.L. Drake, Microbial reduction of iron and porewater biogeochemistry in acidic peatlands, Biogeosciences 5 (2008) 1537–1549. 10.5194/bg-5-1537-2008.
[124] T. Zhang, S.M. Gannon, K.P. Nevin, A.E. Franks, D.R. Lovley, Stimulating the anaerobic degradation of aromatic hydrocarbons in contaminated sediments by providing an electrode as the electron acceptor, Environmental microbiology 12 (2010) 1011–1020. 10.1111/j.1462-2920.2009.02145.x.
[125] T.H. Christensen, P.L. Bjerg, S.A. Banwart, R. Jakobsen, G. Heron, H.-J. Albrechtsen, Characterization of redox conditions in groundwater contaminant plumes, Journal of Contaminant Hydrology 45 (2000) 165–241. 10.1016/S0169-7722(00)00109-1.
[126] US EPA, Estimation Programs Interface Suite™, US EPA, United States Environmental Protection Agency, Washington, DC, USA, 2012.
[127] A. Sabljić, M. Protić, Molecular connectivity: A novel method for prediction of bioconcentration factor of hazardous chemicals, Chemico-Biological Interactions 42 (1982) 301–310. 10.1016/0009-2797(82)90074-6.
[128] D. Hillel, J.L. Hatfield, Encyclopedia of soils in the environment, Academic, Amsterdam, London, 2005.
[129] R.D. Lindberg, D.D. Runnells, Ground water redox reactions: an analysis of equilibrium state applied to eh measurements and geochemical modeling, Science (New York, N.Y.) 225 (1984) 925–927. 10.1126/science.225.4665.925.
[130] ISO 11423-1:1997-06, Water quality - Determination of benzene and some derivatives - Part 1: Head-space gas chromatograhic method.
[131] W.J. Seevers, J.H. Lehr, Handbook of complex enviromental remediation problems, McGraw-Hill, New York, London, 2001.
[132] G. Chen, T.B. Hofstetter, C.A. Gorski, Role of Carbonate in Thermodynamic Relationships Describing Pollutant Reduction Kinetics by Iron Oxide-Bound Fe2, Environ. Sci. Technol. 54 (2020) 10109–10117. 10.1021/acs.est.0c02959.
[133] L.E. Eary, D. Rai, Chromate removal from aqueous wastes by reduction with ferrous ion, Environ. Sci. Technol. 22 (1988) 972–977. 10.1021/es00173a018.
[134] M. Elsner, R.P. Schwarzenbach, S.B. Haderlein, Reactivity of Fe(II)-bearing minerals toward reductive transformation of organic contaminants, Environ. Sci. Technol. 38 (2004) 799–807. 10.1021/es0345569.
[135] A. Mizrahi, D. Meyerstein, Plausible roles of carbonate in catalytic water oxidation, in: Water Oxidation Catalysts, Elsevier, 2019, pp. 343–360.
[136] E. Illés, A. Mizrahi, V. Marks, D. Meyerstein, Carbonate-radical-anions, and not hydroxyl radicals, are the products of the Fenton reaction in neutral solutions containing bicarbonate, Free radical biology & medicine 131 (2019) 1–6. 10.1016/j.freeradbiomed.2018.11.015.
[137] J. Lemaire, V. Croze, J. Maier, M.-O. Simonnot, Is it possible to remediate a BTEX contaminated chalky aquifer by in situ chemical oxidation?, Chemosphere 84 (2011) 1181–1187. 10.1016/j.chemosphere.2011.06.052.

[138] O. Baudisch, L.A. Welo, On the Mechanism of the Catalytic Action of Salts I, Journal of Biological Chemistry 61 (1924) 261–274. 10.1016/S0021-9258(18)85173-0.
[139] S. Udenfriend, C.T. Clark, J. Axelrod, B.B. Brodie, ASCORBIC ACID IN AROMATIC HYDROXYLATION, Journal of Biological Chemistry 208 (1954) 731–739. 10.1016/S0021-9258(18)65598-X.
[140] B.B. Brodie, J. Axelrod, P.A. Shore, S. Udenfriend, ASCORBIC ACID IN AROMATIC HYDROXYLATION, Journal of Biological Chemistry 208 (1954) 741–750. 10.1016/S0021-9258(18)65599-1.
[141] U. Kunapuli, C. Griebler, H.R. Beller, R.U. Meckenstock, Identification of intermediates formed during anaerobic benzene degradation by an iron-reducing enrichment culture, Environmental microbiology 10 (2008) 1703–1712. 10.1111/j.1462-2920.2008.01588.x.
[142] K.D. Welch, T.Z. Davis, S.D. Aust, Iron autoxidation and free radical generation: effects of buffers, ligands, and chelators, Archives of biochemistry and biophysics 397 (2002) 360–369. 10.1006/abbi.2001.2694.
[143] A.V. Kachur, S.W. Tuttle, J.E. Biaglow, Autoxidation of Ferrous Ion Complexes: A Method for the Generation of Hydroxyl Radicals, Radiation Research 150 (1998) 475. 10.2307/3579668.
[144] D.W. King, Role of Carbonate Speciation on the Oxidation Rate of Fe(II) in Aquatic Systems, Environ. Sci. Technol. 32 (1998) 2997–3003. 10.1021/es980206o.
[145] S. Stein, Y. Mirokhin, D.Tchekhoskoi, G. Mallard, NIST MS Search 2.0, National Institute of Standards and Technology, 2008.
[146] K. Ishibashi, A. Fujishima, T. Watanabe, K. Hashimoto, Detection of active oxidative species in TiO2 photocatalysis using the fluorescence technique, Electrochemistry Communications 2 (2000) 207–210. 10.1016/S1388-2481(00)00006-0.
[147] M. Wojtoniszak, B. Zielinska, R.J. Kalenczuk, E. Mijowska, Photocatalytic performance of titania nanospheres deposited on graphene in coumarin oxidation reaction, Mater Sci-Pol 30 (2012) 32–38. 10.2478/s13536-012-0008-1.
[148] G. Louit, S. Foley, J. Cabillic, H. Coffigny, F. Taran, A. Valleix, J.P. Renault, S. Pin, The reaction of coumarin with the OH radical revisited: hydroxylation product analysis determined by fluorescence and chromatography, Radiation Physics and Chemistry 72 (2005) 119–124. 10.1016/j.radphyschem.2004.09.007.
[149] T.S. Singh, B. Madhava Rao, H. Mohan, J.P. Mittal, A pulse radiolysis study of coumarin and its derivatives, Journal of Photochemistry and Photobiology A: Chemistry 153 (2002) 163–171. 10.1016/S1010-6030(02)00272-1.
[150] L.M. Dorfman, Reactivity of the hydroxyl radical in aqueous solutions, Washington, DC, 1973.
[151] G.V. Buxton, C.L. Greenstock, W.P. Helman, A.B. Ross, Critical Review of rate constants for reactions of hydrated electrons, hydrogen atoms and hydroxyl radicals (·OH/·O − in Aqueous Solution, Journal of Physical and Chemical Reference Data 17 (1988) 513–886. 10.1063/1.555805.
[152] T. Pereira, D. Franco, F. Vitório, R. Amaral, A. Ponzoni, A. Kümmerle, Microwave-assisted synthesis and pKa determination of umbelliferone, Quim. Nova (2018). 10.21577/0100-4042.20170262.

[153] W. Stumm, J.J. Morgan, Aquatic chemistry: Chemical equilibria and rates in natural waters / Werner Stumm, James J. Morgan, 3rd ed., Wiley, New York, Chichester, 1996.
[154] D.C. Harris, Quantitative chemical analysis, 8th ed., W.H. Freeman and Co, New York, 2010.
[155] J.C. LOU, S.S. LEE, Chemical Oxidation of BTX Using Fenton's Reagent, Hazardous Waste and Hazardous Materials 12 (1995) 185–193. 10.1089/hwm.1995.12.185.
[156] X. Wu, X. Gu, S. Lu, M. Xu, X. Zang, Z. Miao, Z. Qiu, Q. Sui, Degradation of trichloroethylene in aqueous solution by persulfate activated with citric acid chelated ferrous ion, Chemical Engineering Journal 255 (2014) 585–592. 10.1016/j.cej.2014.06.085.
[157] V.V. Tikhomirov, Hydrogeochemistry fundamentals and advances. Volume 1, Groundwater composition and chemistry, Wiley, Beverly, Massachusetts Scrivener Publishing, Hoboken, New Jersey, 2016.
[158] B. Morgan, O. Lahav, The effect of pH on the kinetics of spontaneous Fe(II) oxidation by O2 in aqueous solution--basic principles and a simple heuristic description, Chemosphere 68 (2007) 2080–2084. 10.1016/j.chemosphere.2007.02.015.
[159] Q. Yu, A. Kandegedara, Y. Xu, D.B. Rorabacher, Avoiding interferences from Good's buffers: A contiguous series of noncomplexing tertiary amine buffers covering the entire range of pH 3-11, Analytical biochemistry 253 (1997) 50–56. 10.1006/abio.1997.2349.
[160] A.G. Aslamkhan, A. Aslamkhan, G.A. Ahearn, Preparation of metal ion buffers for biological experimentation: a methods approach with emphasis on iron and zinc, The Journal of experimental zoology 292 (2002) 507–522. 10.1002/jez.10068.
[161] J.R.L. Smith, R.O.C. Norman, 539. Hydroxylation. Part I. The oxidation of benzene and toluene by Fenton's reagent, J. Chem. Soc. (1963) 2897. 10.1039/jr9630002897.
[162] X.-M. Pan, M.N. Schuchmann, C. von Sonntag, Oxidation of benzene by the OH radical. A product and pulse radiolysis study in oxygenated aqueous solution, J. Chem. Soc., Perkin Trans. 2 (1993) 289. 10.1039/P29930000289.
[163] A. Kunai, S. Hata, S. Ito, K. Sasaki, The role of oxygen in the hydroxylation reaction of benzene with Fenton's reagent. Oxygen 18 tracer study, J. Am. Chem. Soc. 108 (1986) 6012–6016. 10.1021/ja00279a057.
[164] S.E. Stein, NIST/EPA/NIH Mass Spectral Library-PC Version, NIST Standard Reference Database 1A, NIST, 1977.
[165] Y. Xue, S. Lu, X. Fu, V.K. Sharma, I. Mendoza-Sanchez, Z. Qiu, Q. Sui, Simultaneous removal of benzene, toluene, ethylbenzene and xylene (BTEX) by CaO2 based Fenton system: Enhanced degradation by chelating agents, Chemical Engineering Journal 331 (2018) 255–264. 10.1016/j.cej.2017.08.099.
[166] G.A. Russell, Deuterium-isotope Effects in the Autoxidation of Aralkyl Hydrocarbons. Mechanism of the Interaction of PEroxy Radicals 1, J. Am. Chem. Soc. 79 (1957) 3871–3877. 10.1021/ja01571a068.
[167] S. Evans, J.R. Lindsay Smith, The oxidation of ethylbenzene and other alkylaromatics by dioxygen catalysed by iron(III)

tetrakis(pentafluorophenyl)porphyrin and related iron porphyrins, J. Chem. Soc., Perkin Trans. 2 (2000) 1541–1552. 10.1039/B000967I.
[168] R.A. Sheldon, J.K. Kochi, Metal-catalyzed oxidations of organic compounds: Mechanistic principles and synthetic methodology including biochemical processes / Roger A. Sheldon, Jay K. Kochi, Academic Press, New York, London, 1981.
[169] J. Muzart, A. N'ait Ajjou, G.V. Nizova, G.B. Shul'pin, Oxygenation of cyclohexane, indan, and styrene with hydrogen peroxide in the presence of chromium trioxide or the chromium complex (Bu3SnO)2CrO2 (1991) 1454–1457.
[170] R.P. Pohanish, Sittig's handbook of toxic and hazardous chemicals and carcinogens, William Andrew, Norwich, 2017.
[171] Ullmann's Encyclopedia of Industrial Chemistry, Wiley, 2000.
[172] R.M. Cornell, U. Schwertmann, The iron oxides: Structure, properties, reactions, occurences and uses / R.M. Cornell, U. Schwertmann, 2nd ed., Wiley-VCH, Weinheim, Cambridge, 2003.
[173] J.R. Duffield, J.R. Johns, F. Marsicano, D.R. Williams, Chemical speciation modelling and thermodynamic database compilation—III. Modelling solid formation and dissolution, Polyhedron 10 (1991) 1121–1129. 10.1016/S0277-5387(00)81379-0.
[174] D. LANGMUIR, D.O. WHITTEMORE, Variations in the Stability of Precipitated Ferric Oxyhydroxides, in: J.D. Hem (Ed.), Nonequilibrium Systems in Natural Water Chemistry, AMERICAN CHEMICAL SOCIETY, WASHINGTON, D. C., 1971, pp. 209–234.
[175] L.C. Füllenbach, J.P.H. Perez, H.M. Freeman, A.N. Thomas, S. Mayanna, J.E. Parker, J. Göttlicher, R. Steininger, J. Radnik, L.G. Benning, E.H. Oelkers, Nanoanalytical Identification of Siderite Dissolution-Coupled Pb Removal Mechanisms from Oxic and Anoxic Aqueous Solutions, ACS Earth Space Chem. 4 (2020) 1966–1977. 10.1021/acsearthspacechem.0c00180.
[176] M.J. Burkitt, B.C. Gilbert, Model studies of the iron-catalysed Haber-Weiss cycle and the ascorbate-driven Fenton reaction, Free radical research communications 10 (1990) 265–280. 10.3109/10715769009149895.
[177] S. Seibig, R. van Eldik, Kinetics of [Fe II (edta)] Oxidation by Molecular Oxygen Revisited. New Evidence for a Multistep Mechanism, Inorg. Chem. 36 (1997) 4115–4120. 10.1021/ic970158t.
[178] I.L. Yurkova, H.-P. Schuchmann, C. von Sonntag, Production of OH radicals in the autoxidation of the Fe(II)–EDTA system, J. Chem. Soc., Perkin Trans. 2 (1999) 2049–2052. 10.1039/A904739E.
[179] U.R. Pillai, E. Sahle-Demessie, V.V. Namboodiri, R.S. Varma, An efficient and ecofriendly oxidation of alkenes using iron nitrate and molecular oxygen, Green Chem. 4 (2002) 495–497. 10.1039/B204300A.
[180] A. Sobkowiak, D. Naróg, D.T. Sawyer, Iron(III, II)-induced activation of dioxygen for the oxygenation of cyclohexene and related unsaturated hydrocarbons, Journal of Molecular Catalysis A: Chemical 159 (2000) 247–256. 10.1016/S1381-1169(00)00198-9.
[181] Y. Baba, T. Yatagai, T. Harada, Y. Kawase, Hydroxyl radical generation in the photo-Fenton process: Effects of carboxylic acids on iron redox cycling, Chemical Engineering Journal 277 (2015) 229–241. 10.1016/j.cej.2015.04.103.

[182] A.M.N. Silva, X. Kong, M.C. Parkin, R. Cammack, R.C. Hider, Iron(III) citrate speciation in aqueous solution, Dalton transactions (Cambridge, England 2003) (2009) 8616–8625. 10.1039/b910970f.
[183] S. Krukowski, M. Karasiewicz, W. Kolodziejski, Convenient UV-spectrophotometric determination of citrates in aqueous solutions with applications in the pharmaceutical analysis of oral electrolyte formulations, Journal of food and drug analysis 25 (2017) 717–722. 10.1016/j.jfda.2017.01.009.
[184] R. Škarohlíd, L. McGachy, M. Martinec, Z. Rošková, Removal of PCE/TCE from groundwater by peroxydisulfate activated with citric acid chelated ferrous iron at 13 °C, Environmental Technology & Innovation 19 (2020) 101004. 10.1016/j.eti.2020.101004.
[185] Y. Lee, U. von Gunten, Oxidative transformation of micropollutants during municipal wastewater treatment: comparison of kinetic aspects of selective (chlorine, chlorine dioxide, ferrate VI, and ozone) and non-selective oxidants (hydroxyl radical), Water Research 44 (2010) 555–566. 10.1016/j.watres.2009.11.045.
[186] P. Bustamante, M.A. Pena, J. Barra, The modified extended Hansen method to determine partial solubility parameters of drugs containing a single hydrogen bonding group and their sodium derivatives: benzoic acid/Na and ibuprofen/Na, International journal of pharmaceutics 194 (2000) 117–124. 10.1016/s0378-5173(99)00374-9.
[187] M.M. Huber, S. Canonica, G.-Y. Park, U. von Gunten, Oxidation of pharmaceuticals during ozonation and advanced oxidation processes, Environ. Sci. Technol. 37 (2003) 1016–1024. 10.1021/es025896h.
[188] M.A. Zayed, M.F. Hawash, M.A. Fahmey, A.M.M. El-Gizouli, Investigation of ibuprofen drug using mass spectrometry, thermal analyses, and semi-empirical molecular orbital calculation, J Therm Anal Calorim 108 (2012) 315–322. 10.1007/s10973-011-1876-z.
[189] J. Madhavan, F. Grieser, M. Ashokkumar, Combined advanced oxidation processes for the synergistic degradation of ibuprofen in aqueous environments, Journal of Hazardous Materials 178 (2010) 202–208. 10.1016/j.jhazmat.2010.01.064.
[190] C.K. Remucal, D.L. Sedlak, The Role of Iron Coordination in the Production of Reactive Oxidants from Ferrous Iron Oxidation by Oxygen and Hydrogen Peroxide, in: P.G. Tratnyek, T.J. Grundl, S.B. Haderlein (Eds.), Aquatic Redox Chemistry, AMERICAN CHEMICAL SOCIETY, Washington, DC, 2011, pp. 177–197.
[191] D.H.R. Barton, Arthur E. Martell, Donald T. Sawyer, The Activation of Dioxygen and Homogeneous Catalytic Oxidation, Springer US, Boston, MA, 1993.
[192] C.A.S. Regino, D.E. Richardson, Bicarbonate-catalyzed hydrogen peroxide oxidation of cysteine and related thiols, Inorganica Chimica Acta 360 (2007) 3971–3977. 10.1016/j.ica.2007.05.020.
[193] Texas A&M University, College Station, TX, Database 46: NIST Critically Selected Stability Constants of Metal Complexes, NIST.
[194] J.P. Hage, J.A. Powell, D.T. Sawyer, Iron(II)-Induced Activation of Dioxygen for Oxygenation of Cyclohexene and Methyl Linoleate and Initiation of the

Autoxidation of 1,4-Cyclohexadiene, J. Am. Chem. Soc. 117 (1995) 12897–12898. 10.1021/ja00156a043.
[195] H. Yu, P. Zhang, J. Liu, Y. Zheng, N.A. Mustapha, Effects of low-molecular-weight organic acids/thiols on hydroxyl radical production from natural siderite oxidation, Chemical Geology 584 (2021) 120537. 10.1016/j.chemgeo.2021.120537.
[196] V. Zang, R. van Eldik, Kinetics and mechanism of the autoxidation of iron(II) induced through chelation by ethylenediaminetetraacetate and related ligands, Inorg. Chem. 29 (1990) 1705–1711. 10.1021/ic00334a023.
[197] F. Haber, J. Weiss, The catalytic decomposition of hydrogen peroxide by iron salts, Proc. R. Soc. Lond. A 147 (1934) 332–351. 10.1098/rspa.1934.0221.
[198] R. Ovalle, A History of the Fenton Reactions (Fenton Chemistry for Beginners), in: R. Ahmad (Ed.), Reactive Oxygen Species, IntechOpen, 2022.
[199] S. Sahu, D.P. Goldberg, Activation of Dioxygen by Iron and Manganese Complexes: A Heme and Nonheme Perspective, J. Am. Chem. Soc. 138 (2016) 11410–11428. 10.1021/jacs.6b05251.
[200] DIN EN ISO 5667-3:2018, Water quality - Sampling - Part 3: Preservation and handling of water samples.